Naturfareprosjektet DP.6 Kvikkleire

Effekt av progressiv bruddutvikling for utbygging i områder med kvikkleire: Tilbakeregning av Vestfossenskredet

56
2014

RAPPORT

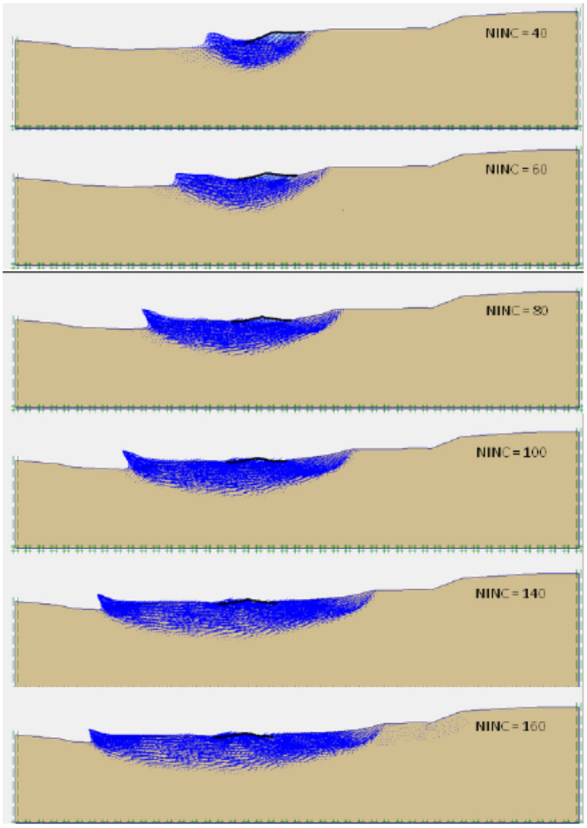

Utvikling av inkrementelle forskyvninger (hastighet) i løpet av analysen

NIFS
NATURFARE
INFRASTRUKTUR - FLOM - SKRED

Naturfareprosjektet: Delprosjekt Kvikkleire

Effekt av progressiv bruddutvikling for utbygging i områder med kvikkleire: Tilbakeregning av Vestfossenskredet

Norges vassdrags- og energidirektorat i et samarbeid med Statens vegvesen og Jernbaneverket

2014

Rapport nr. 56/2014
Effekt av progressiv bruddutvikling for utbygging i områder med kvikkleire: Tilbakeregning av Vestfossenskredet

Utgitt av: Norges vassdrags- og energidirektorat i et samarbeid med Statens vegvesen og Jernbaneverket
Utarbeidet av:
Petter Fornes, Gustav Grimstad, Hans Petter Jostad v/NGI

Dato: 12.05.2014
Opplag: P.O.D.
ISBN: 978-82-410-1008-8

Avrop:

Denne rapporten er en del av et samarbeidsprosjekt mellom Statens Vegvesen Vegdirektoratet (SVV), Norges Vassdrags og Energidirektorat (NVE) og NGI. Overordnet mål for samarbeidsprosjektet er å etablere et forbedret beregningsgrunnlag for etablering av sikkerhetsfaktorer og prosedyrer for prosjektering av bygg, anlegg og samferdsel i områder med kvikkleire eller meget sensitiv leire. Denne rapporten viser bruken av NGI-ADPSoft-modellen med ikke-lokal tøyning i forbindelse med tilbakeregning av Vestfossenskredet i 1984. NGI-ADPSoft-modellen er beskrevet i NIFS rapport 55/2014.

Emneord: sprøbruddmateriale, skred, progressivbrudd, strain softening, NGI-ADP soft

NGI Rapport / Report

Effekt av progressiv bruddutvikling for utbygging i områder med kvikkleire

A2 Tilbakeregning av skred

20092128-00-5-R
12. mai 2014
Rev. nr.: 0

Hovedkontor:
Pb. 3930 Ullevål Stadion
0806 Oslo

Avd Trondheim:
Pb. 1230 Sluppen
7462 Trondheim

T 22 02 30 00
F 22 23 04 48

Kontonr 5096 05 01281
Org. nr 958 254 318 MVA

ngi@ngi.no
www.ngi.no

Prosjekt

Prosjekt:	Effekt av progressiv bruddutvikling for utbygging i områder med kvikkleire
Dokumenttittel:	A2 Tilbakeregning av skred
Dokumentnr.:	20092128-00-5-R
Dato:	12. mai 2014
Rev. nr.:	0

Oppdragsgiver

Oppdragsgiver:	Statens Vegvesen Vegdirektoratet Norges Vassdrags og Energidirektorat
Kontaktperson:	Roald Aabøe (SVV) Odd Are Jensen (NVE)
Kontraktreferanse:	Oppdragsbekreftelser datert 25. (SVV) og 10. (NVE) november 2010

For NGI

Prosjektleder:	Hans Petter Jostad
Utarbeidet av:	Petter Fornes / Gustav Grimstad
Kontrollert av:	Hans Petter Jostad

Sammendrag

Dette er et samarbeidsprosjekt mellom Statens Veivesen Vegdirektoratet (SVV), Norges Vassdrags og Energidirektorat (NVE) og NGI. Overordnet mål for prosjektet er å etablere et forbedret grunnlag for valg av sikkerhetsfaktorer og prosedyrer for prosjektering av bygg, anlegg og samferdsel i områder med kvikkleire eller meget sensitiv leire.

Denne rapporten viser bruken av NGI-ADPSoft-modellen med ikke-lokal tøyning i forbindelse med tilbakeregning av Vestfossenskredet i 1984. I tillegg er det vist et tilfelle hvor modellen er brukt i tilbakeregning av skredet ved Smårød i 2006 (Bonadies, 2012). NGI-ADPSoft-modellen er beskrevet i Aktivitet 1 (NGI, 2012).

Sammendrag (forts.)

Hovedkonklusjonene fra denne aktiviteten er:

- Et ”beste estimat” av input parametere og antagelser gir en bruddlast som samsvarer meget godt med aktuell oppfylling som initierte skredet i 1984.
- Input parametrene er basert på skjærspenning-tøyningskurver inkludert softening fra udrenerte skjærforsøk på prøver tatt i et borehull (litt utenfor skredområdet), målt vanninnhold i et profil, estimering av opprinnelig (historisk) terrengnivå fra vingeborprofil, ekstrapolering av skjærstyrkeprofiler ved hjelp av NGIs blokk-database for SHANSEP parametere og CPTU-tester fra et annet område langs Vestfosseneleva.
- Bruddlasten fører til en progressiv bruddutvikling som (under konstant last) forplanter seg, i tilnærmet horisontalt terreng, helt fram til den andre siden av Vestfosselva tilsvarende som for skredet i 1984.
- Likevekt under den progressive bruddutviklingen er oppnådd ved geometriendringer (setning av fyllingen og en propagerende terrengheving av den passive sonen). Beregnet terrengendring samsvarer meget godt med oppmålinger etter skredet.
- Effekten av softening/sprøbrudd i forbindelse med initiering av skredet er i dette tilfellet estimert til å være i størrelsesorden 10 %.
- Usikkerheten i bruddlasten er i dette tilfellet først og fremst knyttet til styrken og deformasjonsegenskapene til tørrskorpen, initialspenningene under fyllingen, tidligere terreng (skjærstyrkeprofilet), og skjærbåndtykkelsen like etter mobilisering av maks udrenert aktiv skjærstyrke.
- Modellering av den progressive bruddutviklingen er følsom på valg av elementnett og parametere til løsningsalgoritmen i kombinasjon med skjærbåndtykkelse og softeningoppførsel. Men en sannsynlig bruddmekanisme hvor endelig terrenggeometri samsvarer meget godt med innmålt topografi etter skredet er oppnådd med realistiske input parametere.
- Effekten av den indre lengden og sprøheten til kvikkleira er i størrelsesorden lik effekten av usikkerhetene til de andre input parametrene. Resultatene kan derfor ikke benyttes til si noe om forventet skjærbåndtykkelse idet bruddet initieres.
- I grenselikevektsbetraktningene er det vist at effekten av tøyningskompatibilitet er mindre enn 10 % i form av minkning i sikkerhetsfaktor.

NGI-ADPSoft anses, basert på dette studiet, å være velegnet for videre bruk i dette prosjektet, og vil derfor bli benyttet til å kvantifisere sannsynlig effekt av softening/sprøbrudd i forbindelse med geoteknisk prosjektering i områder med meget sensitiv leire.

Innhold

1 Innledning

Dette prosjektet er et samarbeidsprosjekt mellom Statens Vegvesen Vegdirektoratet (SVV), Norges vassdrags og energidirektorat (NVE) og NGI. Overordnet mål for prosjektet er å etablere et forbedret grunnlag for valg av sikkerhetsfaktorer og prosedyrer for prosjektering av bygg, anlegg og samferdsel i områder med kvikkleire eller meget sensitiv leire.

Prosjektet som startet i 2010 og vil bli avsluttet i 2012, er delt opp i følgene hovedaktiviteter:

1. Ferdigstille implementeringen av en numerisk metode
2. Tilbakeregning av skred
3. Sensitivitetsanalyse
4. Sannsynlighetsanalyse
5. Kalibrering av sikkerhetsfaktorer
6. Effekt av tøyningshastighet
7. Implementering av ny kunnskap

Denne rapporten dokumenterer resultatene fra Aktivitet 2: Tilbakeregning av skred. Skredet ved Vestfossen i 1984 ble vurdert som mest egnet for dette studiet. Hovedmålet med aktiviteten er å demonstrere hvor egnet den numeriske modellen som er beskrevet i Aktivitet 1 (NGI, 2012) er for denne type analyser. I dette tilfellet er modellen benyttet både til å studere initieringen av skredet og den progressive bruddutviklingen etter initieringen. Resultatene er sammenlignet med en mer konvensjonell grenselikevektsmetode og elementmetodeanalyser uten effekt av softening.

1.1 Bakgrunn

Ved stabilitetsberegninger for fyllinger, skjæringer og skråninger i områder med kvikke eller sensitive leirer benyttes grenselikevektsmetoden (f. eks. GeoSuite Stability eller Slope W) i standard prosjektering. Grenselikevektsmetoden som benyttes i disse programmene er basert på en antagelse om perfekt plastisk (duktil) oppførsel, mens meget sensitive og kvikke leirer defineres å ha en sprø oppførsel. Det er kjent (for eksempel Janbu, 1970; Bernander, 2000 & 2011; Andresen et al., 2002; Andresen og Jostad, 2004 & 2007) at sprøbruddoppførsel slik vi har i kvikkleirer kan føre til lavere bruddverdi og en annen type bruddmekanisme enn for perfekt plastiske leirer.

Det er gjort mye arbeid i Norge på kartlegging av kvikkleireområder og etterregning av skred ved bruk av tradisjonelle grenselikevektsmetoder. Imidlertid har det i løpet av de siste tjue årene internasjonalt og nasjonalt, innen geomekanikk og andre mekanikkfag, blitt forsket mye for å bedre forståelsen av mekanismer knyttet til progressive brudd. Nasjonalt kan vi nevne grunnleggende studier på effekten av lokal drenasje fra tynne bruddsoner også kalt skjærbånd utført av Thakur (2007) og pågående arbeid av Ph.D. student Gylland (Gylland, 2009).

I tillegg har det ved NGI i løpet av de siste 10 årene blitt utviklet materialmodeller og analyseprogrammer som kan benyttes for å regne på brudd i sensitive leirer (Andresen et al., 2002; Jostad et al., 2006, Grimstad et al., 2010, Jostad og Grimstad, 2011). Grunnleggende innhold i disse beregningsmodellene er:

- Kompatibilitet i forskyvninger med tilhørende tøyninger, og likevekt mellom drivende krefter og stabiliserende spenninger beregnet ved hjelp av et elementmetodeprogram, for eksempel Plaxis (www.plaxis.nl)
- Sammenheng mellom tøyninger og stabiliserende spenninger bestemt ved hjelp av en anisotrop elastoplastisk materialmodell, for eksempel NGI-ADPSoft (Grimstad et al. 2010)
- Problemet med nettavhengige resultater, hvor bruddoppførselen blir mer og mer sprø ved gjentatt forfining av elementnettet er for eksempel unngått ved å benytte en såkalt ”ikke-lokal” skjærtøyningsformulering som beskrevet i Grimstad et al. (2010) og Jostad og Grimstad (2011), i stedet for den klassiske skjærtøyningen gitt av gradientene til forskyvningsfeltet
- Kontinuerlig oppdatering av geometrien i forbindelse med den progressive bruddutviklingen etter at skråningen har blitt ustabil er tatt hensyn til ved å benytte en stordeformasjonsformulering som for eksempel den som er tilgjengelig i Plaxis

Disse punktene vil bli studert nærmere i de neste kapitelene i forbindelse med tilbakeregning av et skred.

1.2 Mulige skred for tilbakeregning med kjent pålastning som mest sannsynlig årsak

Tabell 1.1 gir en oversikt over noen skred i meget sensitive materialer som er antatt å være utløst av en fylling og som deretter har utviklet seg til et progressivt brudd.

Tabell 1.1 Progressive brudd som mest sannsynlig er utløst av en fylling

	År	**L [m]**	**A [m^2]**	**V [m^3]**
Bekkelaget	1953	160	16E3	100E3
Sem	1974	120	-	-
Vestfossen	1984	150	15E3	150E3
Balsfjord	1988	-	45E3	450E3
Finneidfjord	1996	-	-	1E6
Leistad, Malvik	2002	-	25E3	-
Smårød	2006	230	100E3	750E3
Fauske	2007	-	-	-

1.3 Valgt skred

Basert på tilgjengelig informasjon for de forskjellige skredene i Tabell 1.1 er skredet ved Vestfossen, 11. september 1984 funnet å være mest hensiktsmessig for dette

studiet. Skredet var mest sannsynlig initiert av pågående fyllingsarbeider i forbindelse med etablering av et nytt idrettsanlegg. Skredet omfattet et område på ca. 100 m x 150 m, og dybden av skredet var i størrelsesorden 10 m under terreng. Figur 1.1 viser et oversiktskart over skredet, mens Figur 1.2 viser et snitt gjennom området med fyllingsarbeider og detaljer av opprinnelig beregnet kritisk mekanisme etter klassisk grenselikevektsmetode.

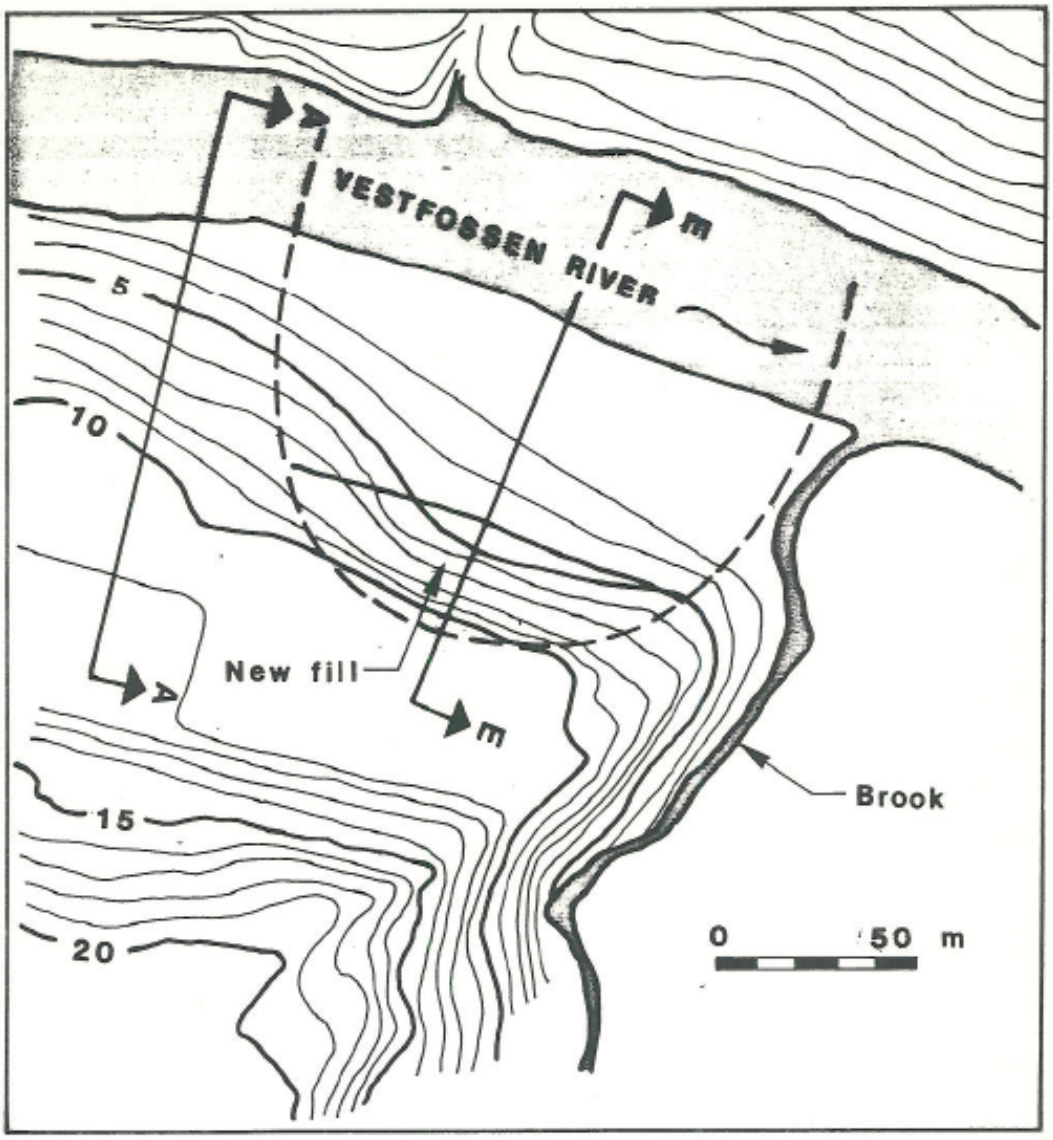

Figur 1.1 Oversikt over skredområdet ved Vestfossen i 1984 (Karlsrud, 1984)

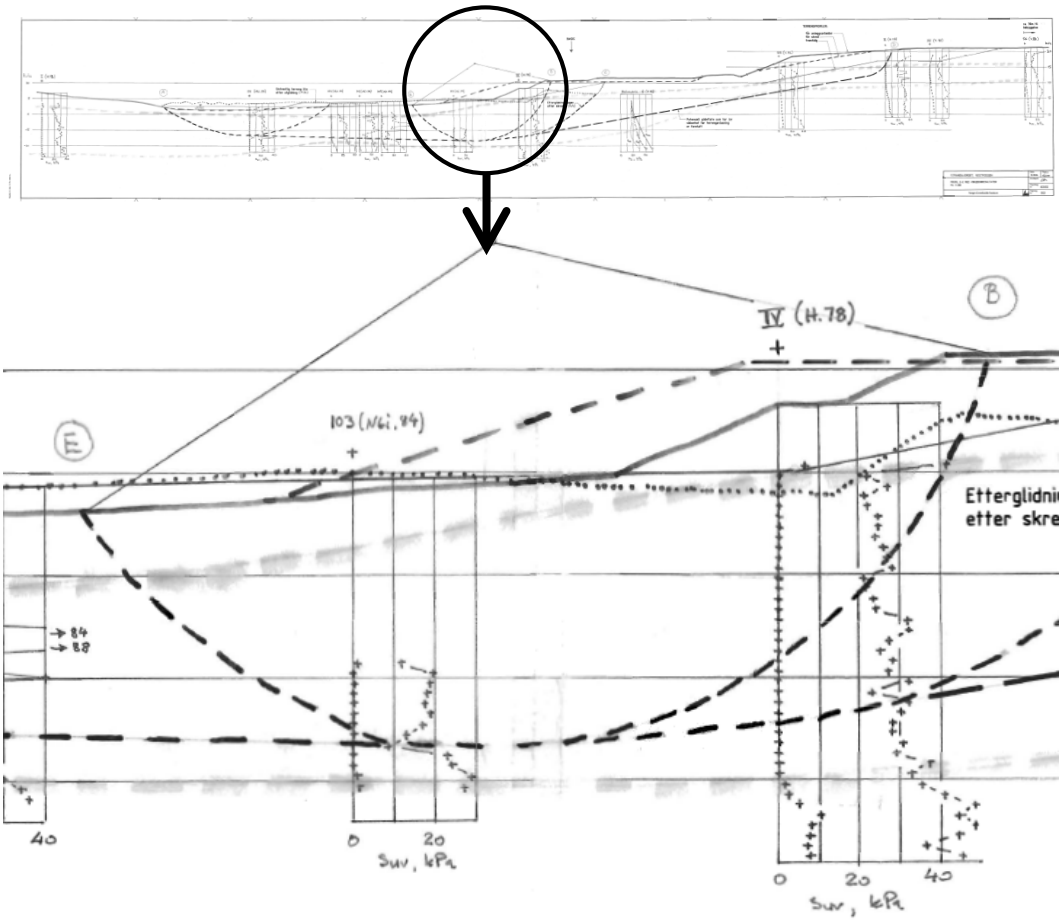

Figur 1.2 Snitt gjennom skråningen hvor skredet skjedde med detalj av beregnet kritisk sirkulærsylindrisk bruddflate

Karlsrud (1984) oppgir at sikkerheten for den lokale sirkulærsylindriske bruddmekanismen er 1.1 til 1.2. Videre oppgir han at sikkerheten for den endelige mekanismen er 1.8 til 2.0. Basert på dette konkluderer han at man ikke kan forklare mekanismen ved Vestfossen uten å henvise til en progressiv bruddmekanisme. Sammenlignet med for eksempel skredet ved Bekkelaget i 1953 (NGI, 1955) og ved Sem i 1974 (NGI, 1974) så skiller skredet ved Vestfossen seg ut ved at sikkerheten for den endelige mekanismen er veldig høy og at sikkerheten mot brudd ved utlegging av fyllingen var beregnet til å være større enn 1.0. Den høye sikkerheten for den endelige mekanismen ved Vestfossen skyldes til dels at skredet ved Vestfossen propagerte særdeles langt inn i et tilnærmet flatt område.

Når det gjelder skredet ved Bekkelaget kan man stille spørsmål ved riktigheten av det udrenerte skjærstyrkeprofilet som ble brukt ved tilbakeregningen. Med dagens prøvemetoder/korrelasjoner ville man antagelig ha beregnet en høyre sikkerhet også der.

Skredet ved Smårød i Sverige i 2006 er tilbakeregnet med NGI-ADPSoft-modellen i en mastergradsoppgave i samarbeid med NTNU (Bonadies, 2012). Resultatene fra arbeidet er vist i seksjon 7, og oppgaven er gitt som Vedlegg A.

2 Grunnlagsdata for Vestfossen

2.1 Historie

Terrengarbeid som skulle gi plass for et nytt idrettsanlegg på Vestfossen ble i 1982 prosjektert av NGI (1982). Det ble gjort grunnundersøkelser i området, og likevektsberegninger av skråningen ga tilstrekkelig sikkerhetsfaktorer. I etterkant av skredet ble det gjort tilleggsundersøkelser, hovedsaklig vingebor men også poretrykksmålinger for å finne glideflaten til bruddet (NGI, 1984). Basert på NGI (1982 og 1984) kan det se ut som om den lokal glideflate ved fyllingen ikke ble undersøkt før etter skredet. Dette var kanskje fordi geometrien i seg selv ikke ble mer kritisk (brattere) etter terrengendringene. Men den kritiske forskjellen er at geometriendringen er udrenert, det vil si at spenningstilstanden går fra å være drenert til å bli i en udrenert tilstand.

2.2 Grunnundersøkelser

I skredområdet ble det gjort grunnundersøkelser med vingebor, dreiesonderinger, dreietrykksonderinger og poretrykksmålinger. Det ble tatt en prøveserie, som ble benyttet til rutineundersøkelser og udrenerte skjærforsøk (3 CAUC og 3 DSS forsøk).

Figur 2.1 viser en oversikt over det prosjekterte idrettsanlegget på Vestfossen, med alle grunnundersøkelsene og skredområdet.

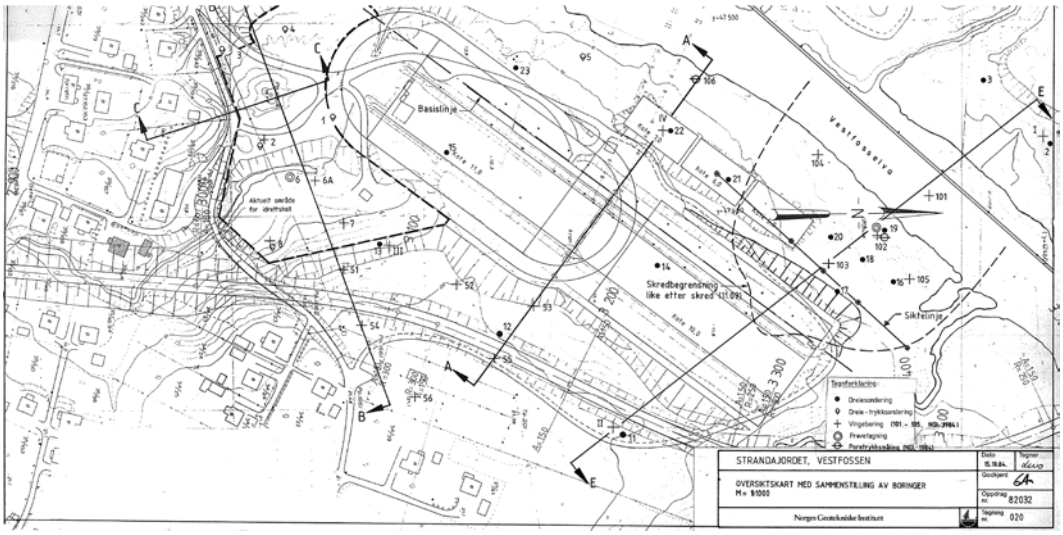

Figur 2.1 Borplan med oversikt over grunnundersøkelser og skredområdet (NGI, 1984)

Figur 2.2 viser et vertikalsnitt fra prosjekteringen. Snittene er merket i Figur 2.1. Som vist på snitt A-A ble det i prosjekteringen antatt et historisk terreng (sjøbunn) med jevn helning. Snitt B-B viser at det dermed må ha vært betydelig overlagring (ca. 11 m) der hvor prøveserien har blitt tatt. Prøveserien ble tatt i en grop, hvilket betyr at det sannsynligvis er et poreovertrykk i leira der prøven ble tatt.

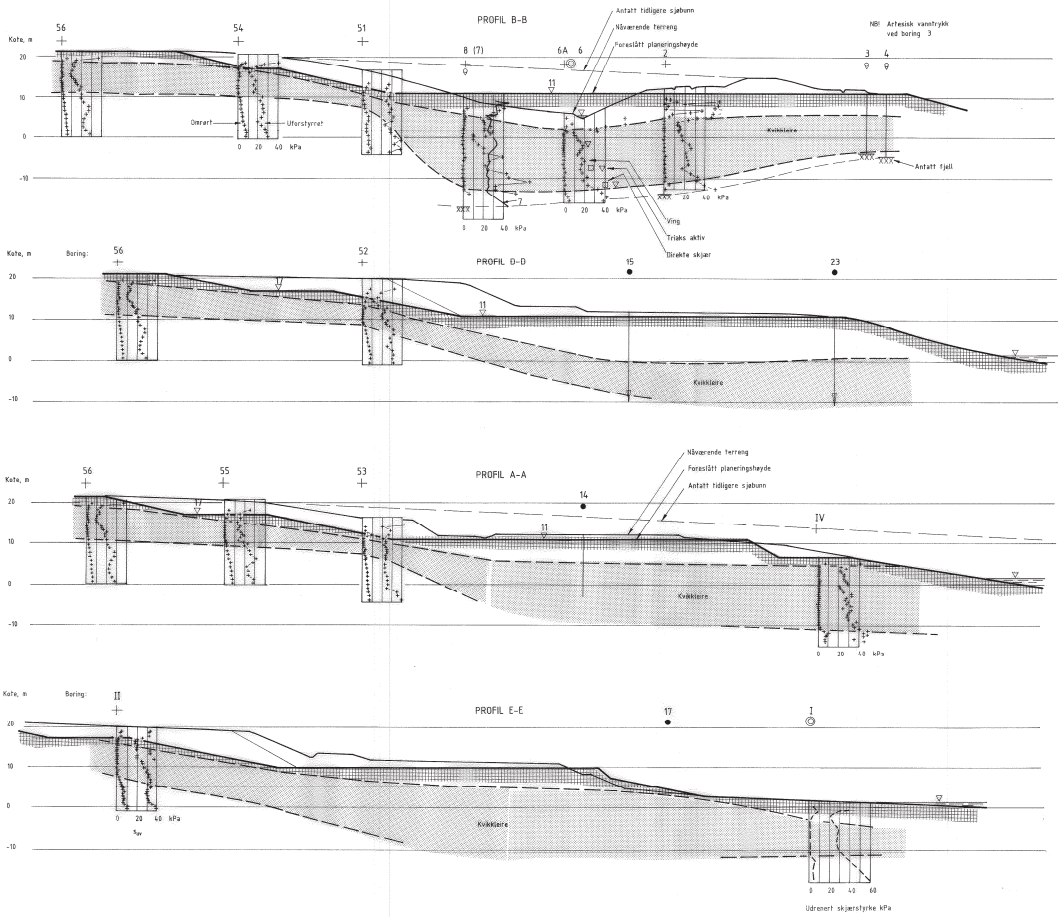

Figur 2.2 Snitt fra prosjekteringen i 1982 (NGI, 1982)

Figur 2.3 viser snitt E-E av glideflaten til skredet. Vingeborforsøk er tegnet inn i snittet, og triaksforsøkene er flyttet inn i snittet. Se Figur 2.1 for hvor prøveserien egentlig er tatt. I etterkant av skredet ble supplerende vingeborforsøk gjort for å lokalisere bruddflaten.

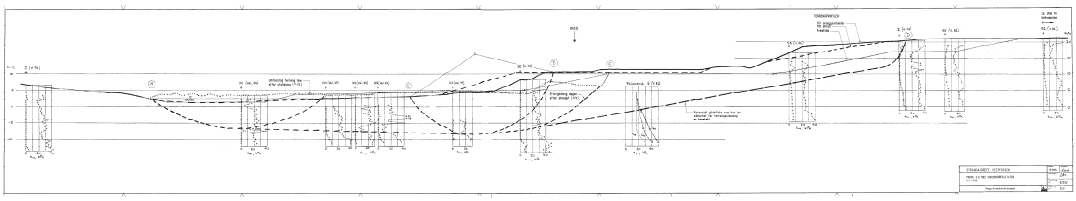

Figur 2.3 Estimert bruddflate og vingeborforsøk (NGI, 1984)

Figur 2.4 viser resultatene (rutineundersøkelser og 3 CAUC- og 3 DSS-forsøk) fra prøveserien. Ved ca. 12 m dybde endres vanninnholdet fra ca. 45 % til 35 %, og romvekten fra ca. 18.0 til 19.4 kN/m^3. Konusforsøk på intakt og omrørt leire viser at leira er meget sensitiv (kvikk). De øverste 2 meterne ser ut til å ha stor skjærstyrke, og konusforsøk på intakt leire viser rimelig konstant styrke med dybden. Fra triaksforsøkene derimot ser styrken ut til å øke lineært fra null, som en normalkonsolidert leire.

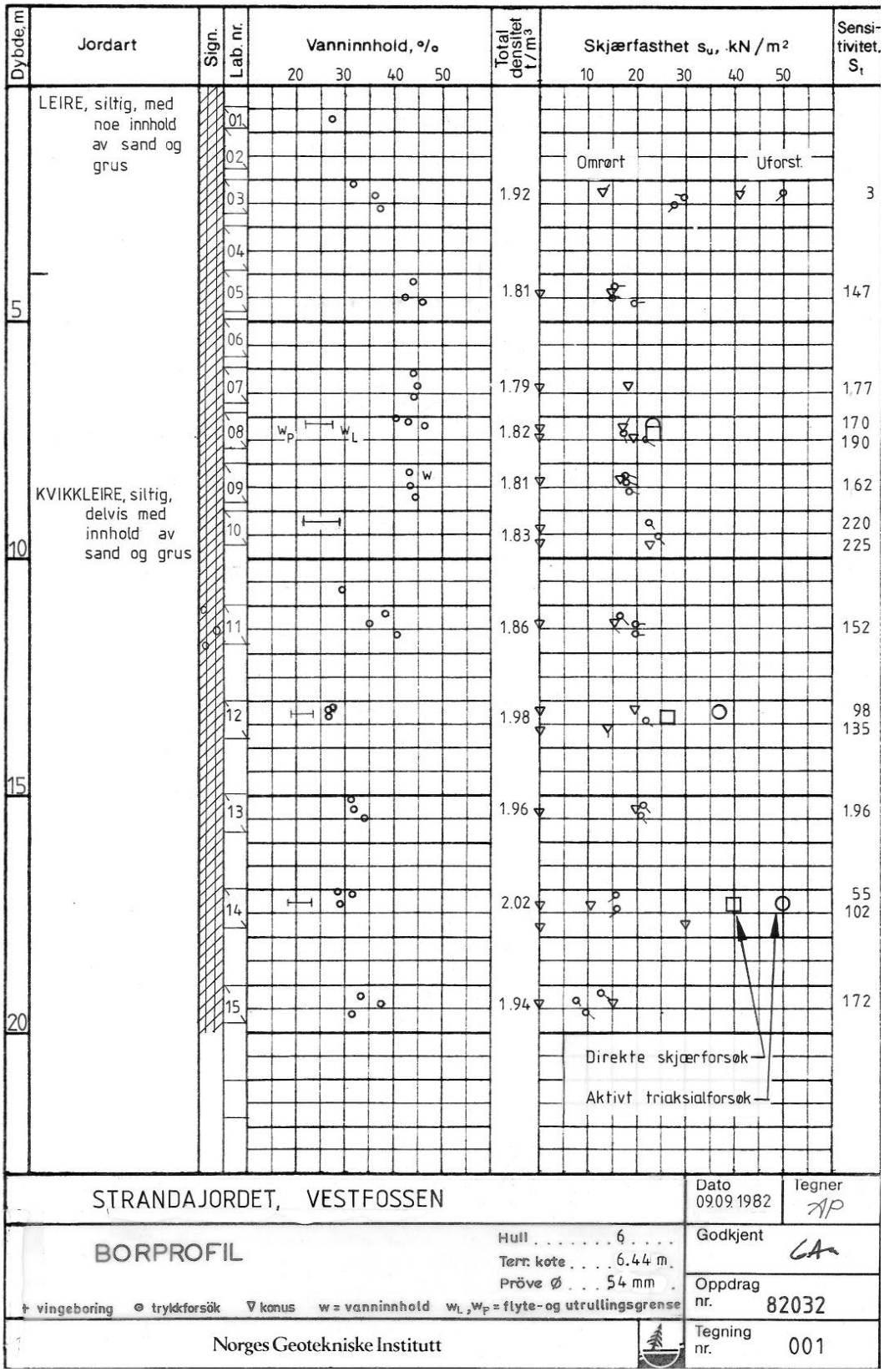

Figur 2.4 Labforsøk på prøveserie (NGI, 1982)

Figur 2.5 viser igjen snitt B-B hvor prøveserien er tatt. Figuren viser en sammenstilling av vingebor- og triaksforsøk som er gjort ved siden av hverandre. Figur 2.6 viser målte forhold mellom udrenert skjærstyrke og effektivt overlagringstrykk for aktiv, DSS og vingebor.

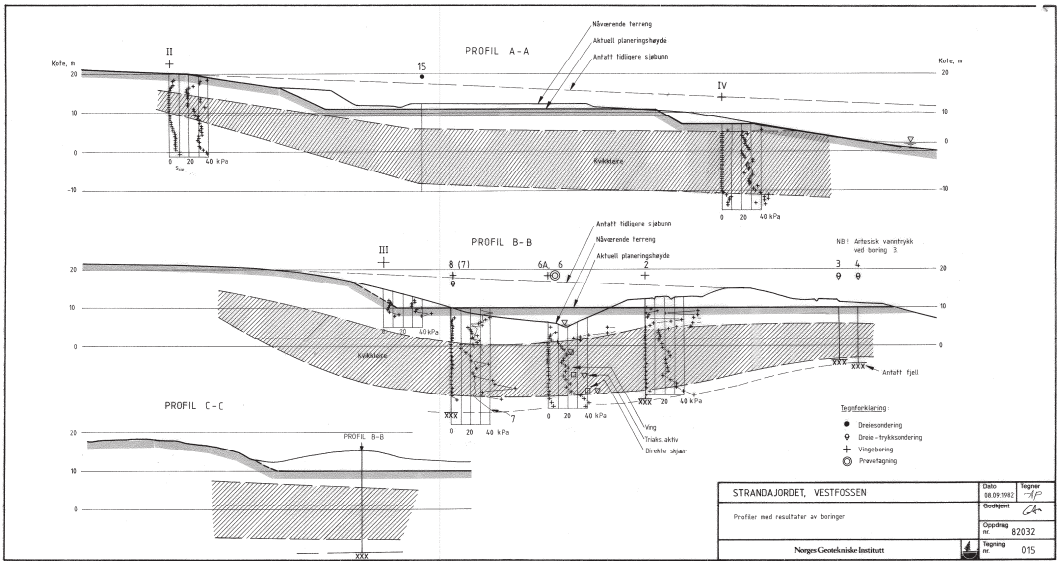

Figur 2.5 Vingebor og triaksforsøk (NGI, 1982)

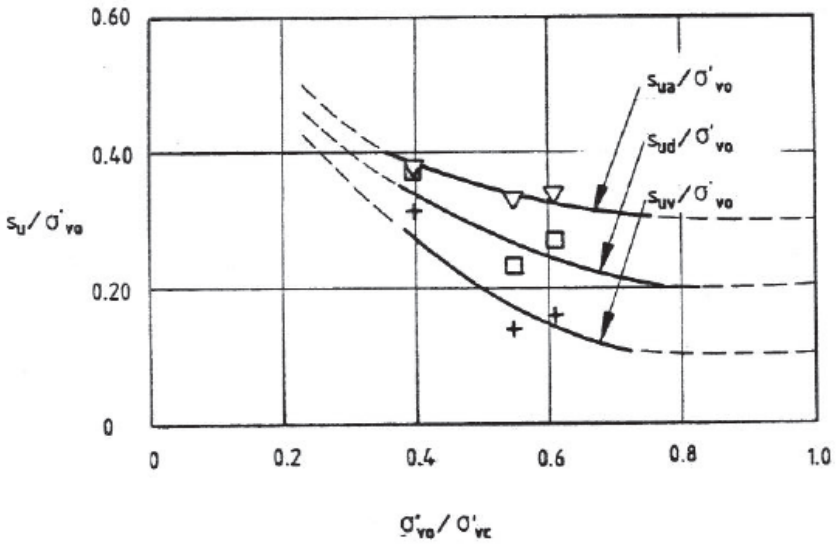

Figur 2.6 Målte forhold mellom udrenert skjærstyrke og effektivt overlagringstrykk (NGI, 1982)

Figur 2.7 viser resultatene fra triaksforsøkene. Det er tegnet inn hjelpelinjer som viser hva residualtøyningen er om man ekstrapolerer lineært, og hva den største verdien av skjærstyrken kan være om man tar hensyn til prøveforstyrrelse. Det antas her at spenningsstien i en fullstendig uforstyrret prøve kunne ha fulgt en udrenert spenningssti med helning 1:3 helt opp til bruddlinjen (Berre et al. 2007).

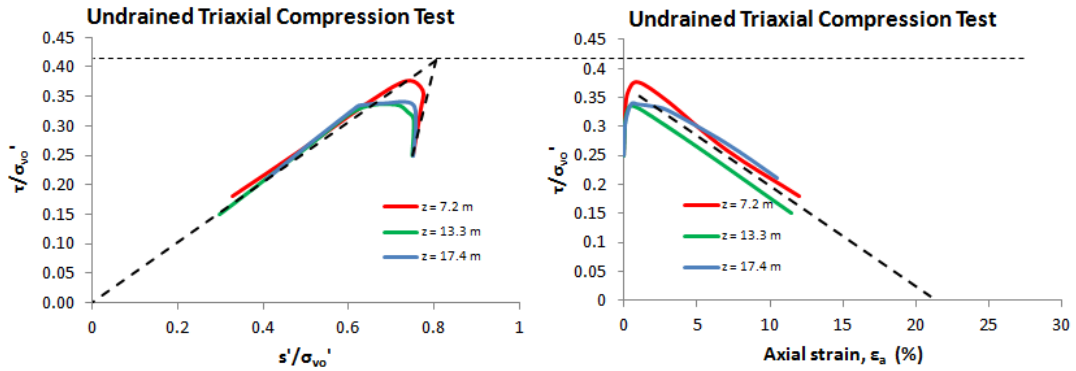

Figur 2.7 Normaliserte triaks spenningsstier og normalisert maksimum skjærspenning mot aksialtøyning.

2.3 Andre aktuelle grunnundersøkelser i området

I forbindelse med en planlagt utbygging av en gårdsbygning ca. 4 km oppstrøms elven er det blitt gjort grunnundersøkelser og stabilitetsberegninger. En kvikkleireskråning ble her instrumentert av NGI (2011b). Det ble blant annet gjort CPTU tester. Grunnforholdene her antas å være nokså representative for Vestfossen. Figur 2.8 viser Vestfossen idrettsanlegg (rød ring) og tomten som ble instrumentert (tegnestift).

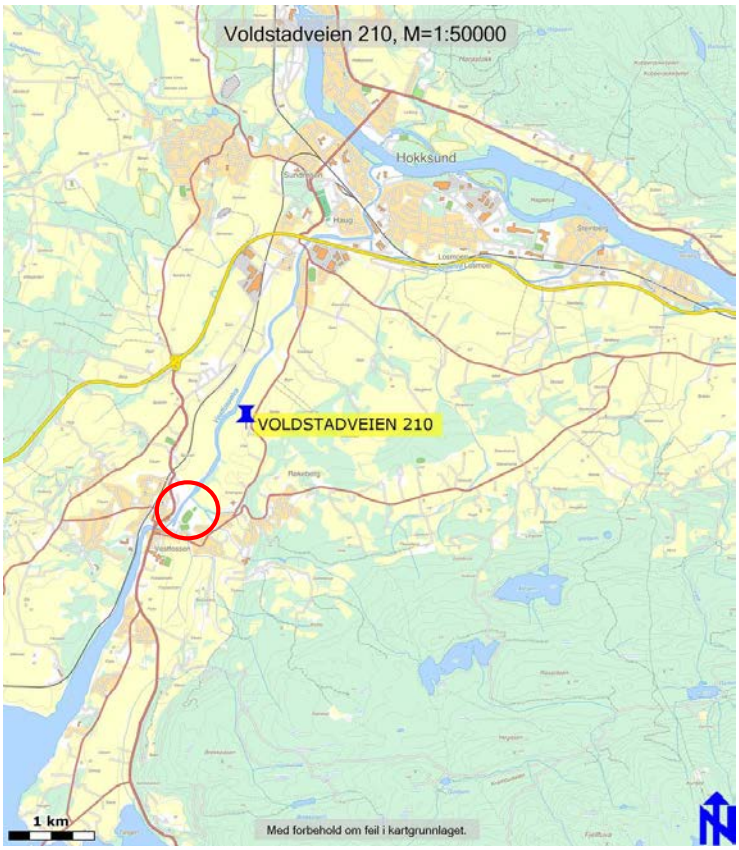

Figur 2.8 Oversiktskart over aktuell strekning langs Vestfossen

Tolkningen av CPTU i Figur 2.9, viser at det er noe tørrskorpe i toppen. Anbefalt s_u^A er ikke lavere enn 25 kPa. Videre ser man at det er en reduksjon i styrken (som ikke nødvendigvis er riktig) basert på tolkning av målt poretrykk ved 14 m dybde, som tilsvarer skille mellom to lag med forskjellig vanninnhold og romvekt. Ved bruk av vanninnholdsavhengige S- og m-parametre i SHANSEP-prosedyren som foreslått i Karlsrud et al. (2012) ser man en lignende reduksjon, se seksjon 3.3.

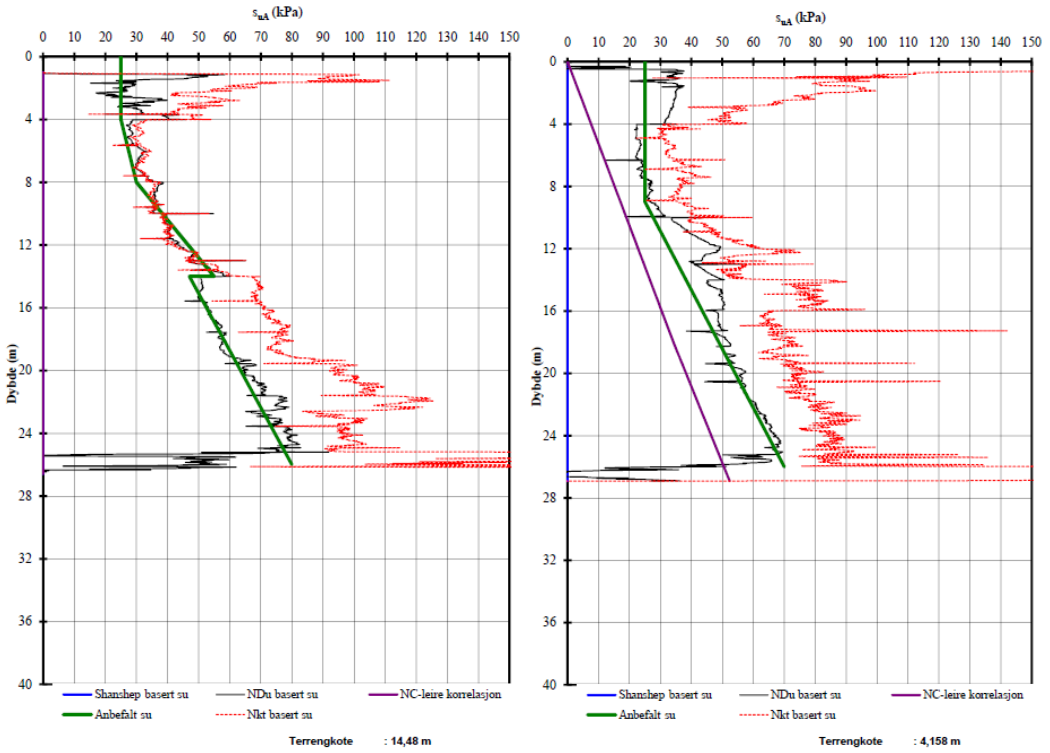

Figur 2.9 CPTU-tolkning for borhull 7 og 8 (NGI, 2011). Grønn strek er anbefalt s_u^A (basert på NΔu).

3 Jordparametre

3.1 Jorddata

I listen under finnes forutsetninger og anbefalinger i forbindelse med analysene av skredet ved Vestfossen:

- Skjærstyrkeprofil er etablert basert på grunnundersøkelser (vingebor og triaksforsøk), NGIs database for norske leirer (Karlsrud, 2012) kombinert med SHANSEP-prosedyren (Ladd & Foot 1974).
- Egenvekt av kvikkleira er satt til 18 kN/m^3. Denne er forenklet valgt konstant med dybden. Egenvekt er brukt både for beregning av udrenert skjærstyrke etter SHANSEP, og for beregning av vekten av jord.
- Friksjonsvinkel, φ, = 30°. Denne brukes kun for drenert tørrskorpe og beregning av K_0 og drenert tverrkontraksjonstall.

- Vanninnhold er valgt som funksjon av dybden som gitt av Figur 3.1. Figur 3.3 gir i tillegg valgt nivå for profil av vanninnhold.
- Overkonsolideringsgrad som skyldes historisk kryp, OCR_τ, er satt til 1.1.
- Antatt tidligere terrengnivå og nåværende grunnvannsnivå som vist på Figur 3.2.
- Figur 3.4 gir et typisk resultat fra et triaksforsøk som er brukt til å kalibrere materialoppførselen.

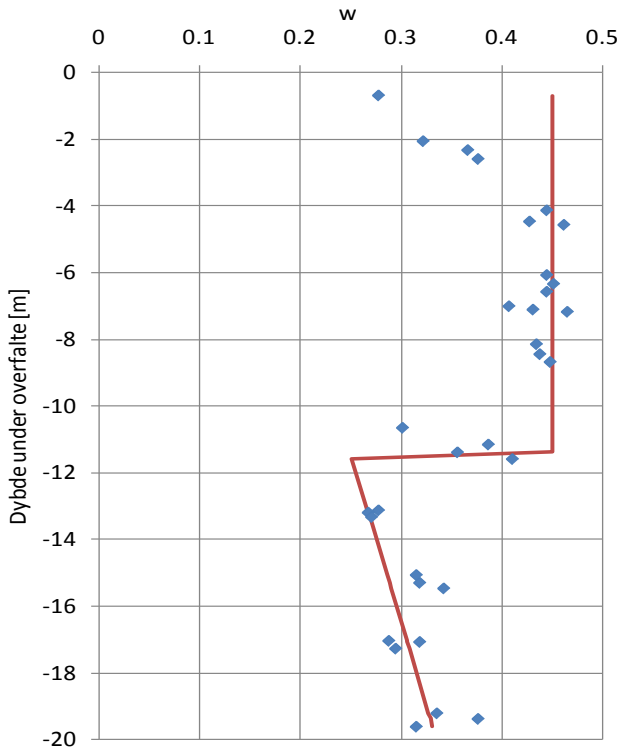

Figur 3.1 Vanninnhold ved Vestfossen (NGI 1982)

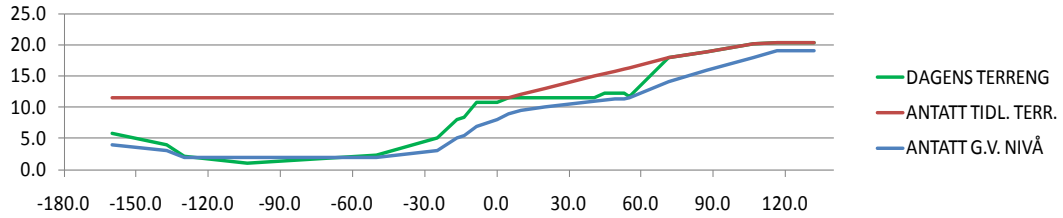

Figur 3.2 Antatt terreng, tidligere terreng og grunnvannsnivå for valgt tverrsnitt ved Vestfossen

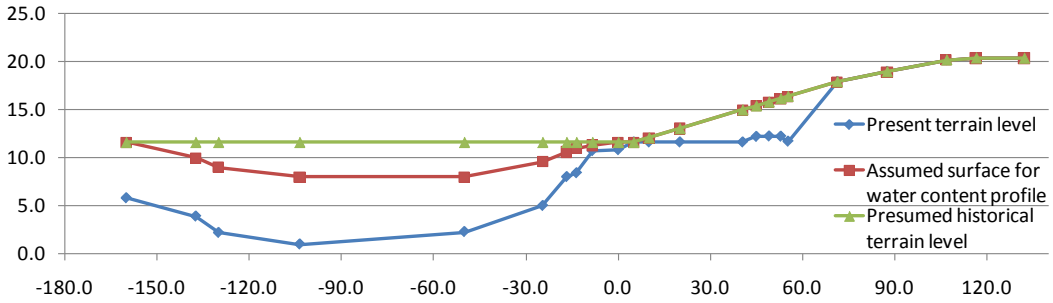

Figur 3.3 *Antatt terreng, tidligere terreng og nivå for bestemmelse av vanninnhold for valgt tverrsnitt ved Vestfossen*

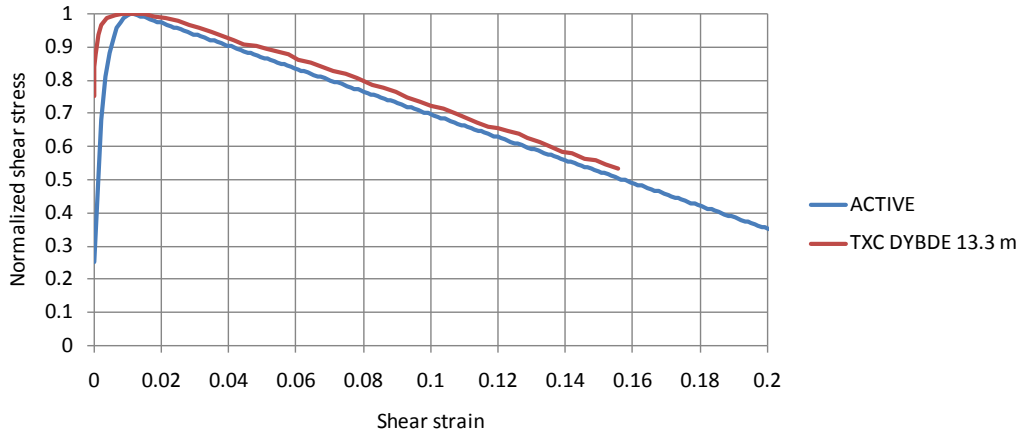

Figur 3.4 *Normalisert udrenert triaksforsøk (rød kurve) sammenlignet med respons av NGI-ADPSoft (blå kurve)*

3.2 SHANSEP-profil

I SHANSEP (”**S**tress **H**istory **A**nd **N**ormalized **S**oil **E**ngineering **P**roperties”) prosedyren korreleres udrenert skjærstyrke mot graden av overkonsolidering, OCR (Figur 3.5). Ved å dele OCR opp i en tidsavhengig del OCR_τ som skyldes historisk kryp og en som skyldes tidligere overlagring *POP*, kan skjærstyrken basert på SHANSEP skrives som:

$$s_u = \sigma'_{v0} \cdot S \cdot OCR^m = \sigma'_{v0} \cdot S \cdot \left(1 + \frac{POP}{\sigma'_{v0}}\right)^m \cdot {OCR_\tau}^m$$

Hvor: s_u er udrenert skjærstyrke (anisotropi etableres ved å bruke forskjellige parametere *S* og *m* avhengig av retningen for skjærdeformasjonen)
S er SHANSEP normalisering parameter
m er SHANSEP potens parameter
OCR er grad av overkonsolidering
POP er geologisk overlagring
OCR_τ er grad av overkonsolidering som skyldes kryp

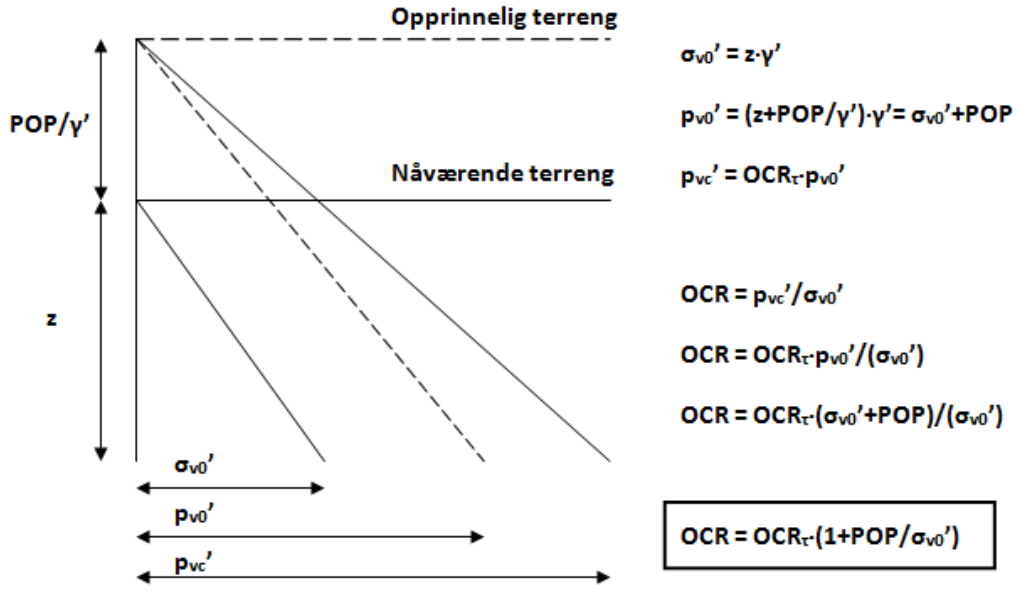

Figur 3.5 *OCR bestemt av tidligere overlagring POP* og historisk kryp OCR_τ

For aktiv tilstand foreslår Karlsrud et al. (2012) S = (0.27+0.10·w) og m = (0.58+0.33·w), hvor w er vanninnhold. For Vestfossen vil dette bety at S = 0.315 og m = 0.7285 (Figur 3.1) for w = 45 %.

Som vist i Figur 3.1 så er det et markant fall i vanninnhold ved en dybde på rundt 12 m. Ved bruk av de foreslåtte korrelasjoner fører dette til en reduksjon i udrenert skjærstyrke ved denne dybden.

Et profil over udrenert skjærstyrke for aktiv tilstand er etablert ved hjelp av Karlsruds SHANSEP-parametere basert på antagelser om tidligere geologisk overlagring, vanninnhold og romvekt, se Figur 3.1, Figur 3.2 og Figur 3.3. Minimum styrke i toppen av profilet for s_u^A satt til 31 kPa, og Figur 3.7 viser beregnet profil over s_u^A i aktuelt tverrsnitt ved Vestfossen.

3.3 Anisotropiforhold

I NGI-ADPSoft er skjærstyrken avhengig av retningen på skjærdeformasjonen. Inndata til modellen er udrenert styrke fra aktiv triaksforsøk og anisotropiforhold, se Figur 3.6. Forholdet mellom DSS og aktiv styrke, og mellom passiv og aktiv styrke, er konstant innen hvert lag.

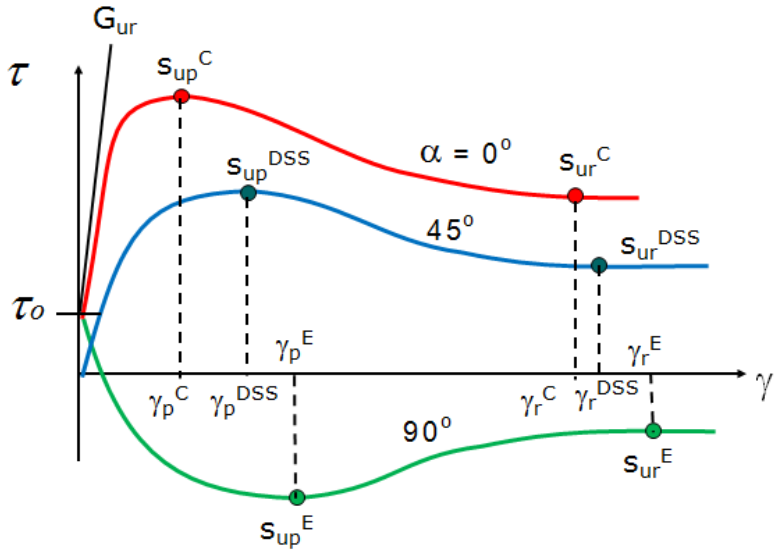

Figur 3.6 Inputparametre til NGI-ADPSoft

Grunnlaget for anisotropiforholdene for Vestfossen er tre CAUC- og tre DSS-forsøk, se Figur 2.6. Ved dybde 7.2 m, 13.3 m og 17.4 m er forholdet s_u^{DSS}/s_u^A henholdsvis tilnærmet lik 1.0, 0.7 og 0.8. Berre et al. (2007) viser at reduksjon i styrke på grunn av prøveforstyrrelse fra 54 mm-prøver forventes å være større for s_u^A enn s_u^{DSS}. Ved å ta hensyn til dette vurderes forholdet s_u^{DSS}/s_u^A til å være mellom 0.65 og 0.75. Siden det ikke er utført CAUE-forsøk, er det antatt at $s_u^P/s_u^A = 2 \cdot s_u^{DSS}/s_u^A - 1$.

Tilsvarende som for aktiv tilstand foreslår Karlsrud et al. (2012) vanninnholdsavhengige SHANSEP-parametre for passiv og DSS tilstand. For passiv tilstand foreslår Karlsrud at S = (0.0+0.26·w) og m = (0.86−0.30·w), og for DSS at S = (0.14+0.18·w) og m = (0.35+0.77·w).

Figur 3.8 og Figur 3.9 viser beregnet anisotropiforhold i aktuelt tverrsnitt. Merk at skift i vanninnholdet også får konsekvens for anisotropiforholdet. Som det fremgår av styrkeprofilene så medfører fallet i vanninnhold at det oppstår et fall i s_u^{DSS}/s_u^A. Dette indikerer, hvis korrelasjonene er riktig for dette materialet, at et sjikt med lavere direkte skjærstyrke kan eksistere her. Når man sammenligner dette resultatet med resultater fra vingebor (Figur 1.2) og CPTU (Figur 2.9), finner man dette sjiktet igjen som et sjikt med lavere tolket skjærstyrke. Dette gir støtte for at beregnet styrkeprofil er realistisk.

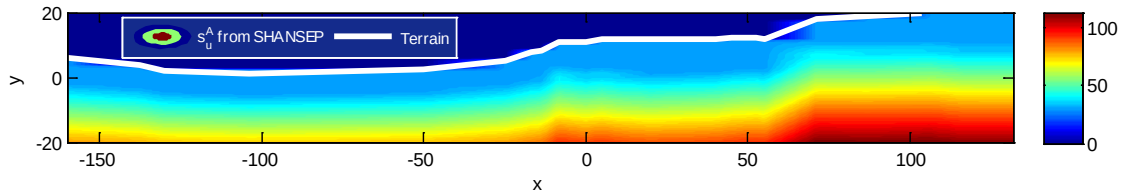

Figur 3.7 Profil over beregnet s_u^A [kPa] ved Vestfossen

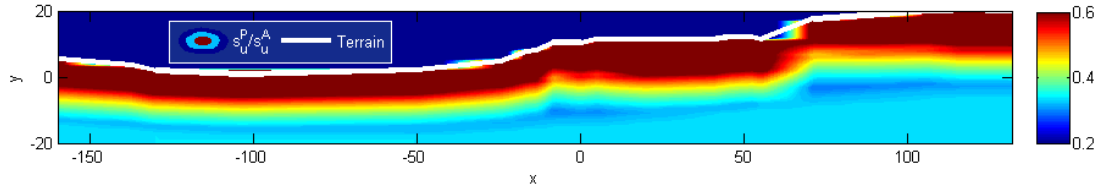

Figur 3.8 Profil over beregnet s_u^P/s_u^A ved Vestfossen

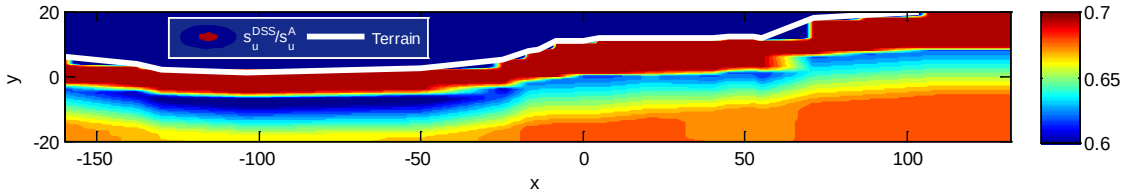

Figur 3.9 Profil over beregnet s_u^{DSS}/s_u^A ved Vestfossen

3.4 OCR$_\tau$ og POP – Opprinnelig terreng

Overkonsolideringsgrad som skyldes historisk kryp, OCR$_\tau$, er antatt lik 1.1. Dette er i samsvar med forsøk gjort på blokkprøver av Drammensleire (NGI, 2011). Triaksforsøkene i to dybder (Figur 2.7) ble benyttet til å vurdere usikkerheten i OCR$_\tau$ ved hjelp av SHANSEP-formelen i seksjon 3.2.

Figur 3.10 viser aktiv udrenert skjærstyrke fra SHANSEP sammen med skjærstyrken fra triaksforsøk, med og uten korreksjon for prøveforstyrrelse. POP og OCR$_\tau$ er kalibrert slik at SHANSEP-styrkeprofilet ligger innenfor usikkerheten i styrken fra triaksforsøkene. Knekken på kurvene ved 10 m dybde skyldes overgangen til lavere vanninnhold. For å få god tilpasning til triaksforsøkene må OCR$_\tau$ være mellom 1.0 og 1.5 og POP være mellom 0 og 20 kPa.

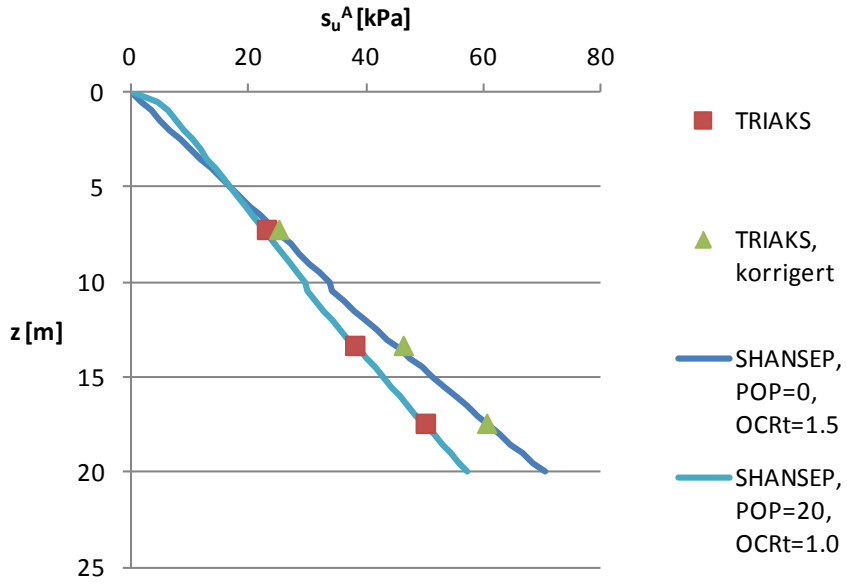

Figur 3.10 s_u^A *fra SHANSEP og fra triaks, med og uten korreksjon for prøveforstyrrelse*

Snitt B-B i Figur 3.11 viser at opprinnelig terreng sannsynligvis har vært minst 11 m over dagens terreng der boreprøven ble tatt. Med POP på grunn av 11 m overlagring blir styrke fra SHANSEP-prosedyren større enn i triaksforsøkene, vist på Figur 3.12. En mulig årsak til denne forskjellen kan være lokalt poreovertrykk der prøven ble tatt. Med en ekvivalent høyere egenvekt av vann, γ_w = 13 kN/m^3 blir effektivspenningene lavere, og dermed blir også styrken fra SHANSEP lavere og innenfor usikkerheten i styrke på grunn av prøveforstyrrelse, se Figur 3.12.

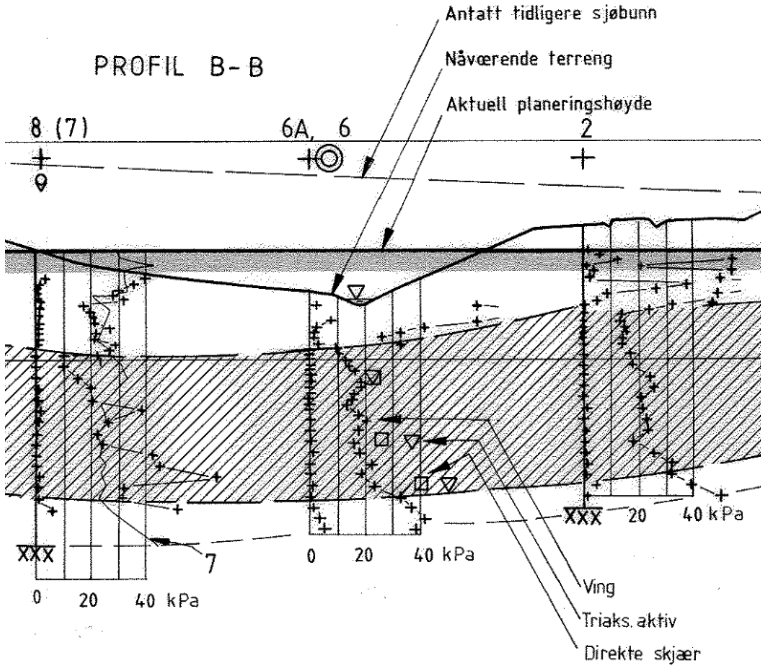

Figur 3.11 *Snitt B-B, vingebor, triaks, antatt opprinnelig terreng*

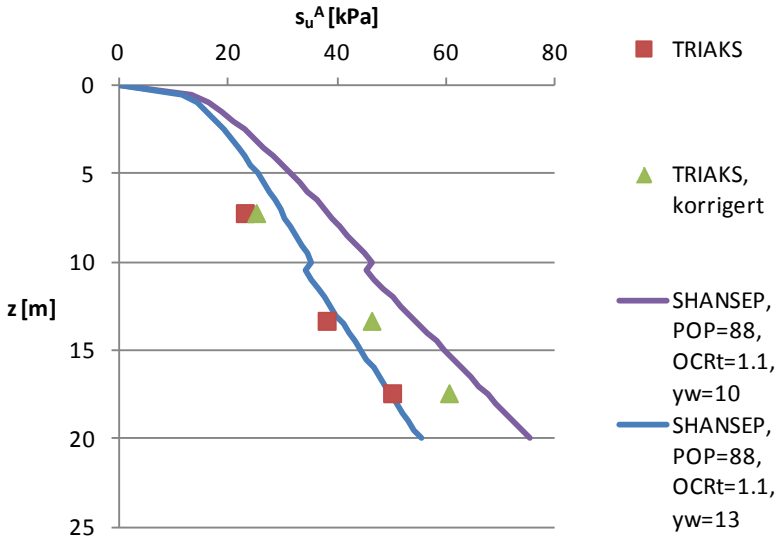

Figur 3.12 *SHANSEP for OCR_τ = 1.1, POP = 88 kN/m^3 og ekvivalent egenvekt for vann γ_w = 13 kN/m^3(poreovertrykk)*

Fordi leireprøvene er tatt utenfor skredsonen er triaksforsøkene kun benyttet til å vurdere OCR_τ. For å estimere POP er det antatt et plant hellende opprinnelig terreng, som i prosjekteringen fra 1982, se snitt A-A på Figur 2.2. Høydekurver for opprinnelig terreng er bestemt ved å kalibrere POP i SHANSEP mot styrke fra vingeborforsøk I på den andre sida av Vestfosselva, se Figur 3.13a.

Figur 3.13b viser skjærstyrken fra triaksforsøkene sammen med styrken fra vingebor på samme sted. Basert på vingeborstyrken i den mindre sensitive leira, og styrke fra triaksforsøk når man tar hensyn til prøveforstyrrelse, er styrkeforholdet s_{uv}/s_u^A antatt å være mellom 0.6 og 0.7.

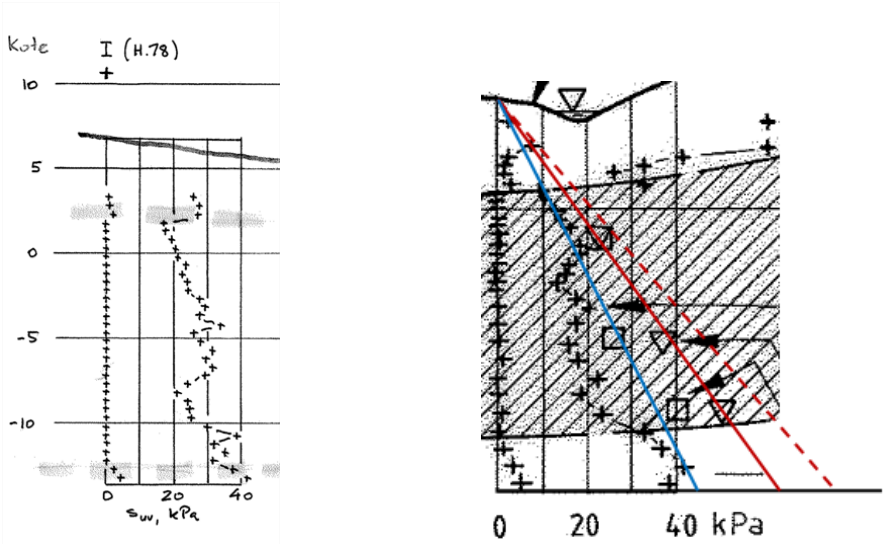

Figur 3.13 *Vingebor I fra snitt E-E (a), og triaksforsøk sammen med vingebor i snitt B-B (b)*

Figur 3.14 viser opprinnelig terreng etter å ha kalibrert POP med SHANSEP for s_{uv}/s_u^A lik 0.6, 0.65 og 0.7, og OCR_τ lik 1.1.

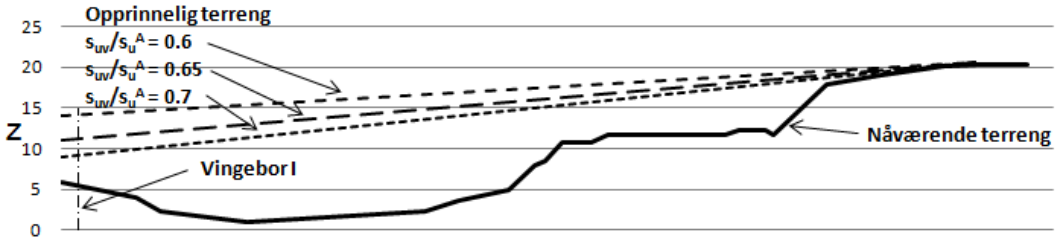

Figur 3.14 Opprinnelig terreng for OCR_τ = 1.1 med s_{uv}/s_u^A = 0.6, 0.65 og 0.7

3.5 K_0 beregning

Mayne og Kulhawy (1982) foreslår for horisontalt lagdelt jord følgende ligning for beregning av K_0:

$$K_0 = (1\text{-}\sin\varphi) \cdot OCR^{\sin\varphi}$$

Ved å dele opp OCR i en spennings- og tidsstyrt komponent gir dette:

$$= (1\text{-}\sin\varphi) \cdot (1+POP/\sigma_{v0}')^{\sin\varphi} \cdot OCR_\tau^{\sin\varphi}$$

Dette kan gi en noe for høy K_0 fordi kryp gir mindre endring i K_0 enn bidraget for avlastning.

Hvis man som en forenkling antar at materialet er elastisk under spenningsendringen, fra dette nivået til dagens nivå, kan man regne ut et tilhørende tverrkontraksjonstall ved å sette følgende relasjon lik den over:

$$K_0 = (1\text{-}\sin\varphi)\cdot(1+POP/\sigma_{v0}')\cdot OCR_\tau - \nu/(1\text{-}\nu)\cdot((1+POP/\sigma_{v0}')\cdot OCR_\tau\text{-}1)$$

Ved å løse ut for ν, finner man en typisk verdi på rundt 0.25. Dette betyr at en drenert tverrkontraksjon på 0.25 er en fornuftig antagelse. Denne blir brukt for etablering av initial likevektstilstand i FE beregningen.

3.6 Skjærbåndtykkelse

Sprøheten til leira styres av to ting. Det ene er softeningkurven, hvor mye tøyning som skal til for å komme ned til en valgt residualstyrke. Desto større helning, desto sprøere materiale. Den initielle delen av softeningkurven er tatt fra triaksforsøkene. Det er da antatt at prøvene deformeres tilnærmet homogent i denne fasen av forsøket.

Det andre som styrer sprøheten til leira er skjærbåndtykkelsen. Hvis skjærdeformasjonen konsentreres i et tynt bånd blir materialoppførselen veldig sprø. Det er derimot knyttet stor usikkerhet til denne skjærbåndtykkelsen (som mest sannsynelig er styrt av lokal drenasje og tøyningshastighet).

I en klassisk elementmetodeformulering vil skjærbåndtykkelsen være gitt av elementstørrelsen. I NGI-ADPSoft kan derimot skjærbåndtykkelsen kontrolleres ved input av l_{int} til å være uavhengig av elementstørrelsen. For å modellere effekten av en skjærbåndtykkelse som er mindre enn elementstørrelsen er det lagt inn en parameter $1\text{-}l^*/l_{int}$ som øker graden av sprøhet ved å øke helningen på softeningkurven. Dette er en tilnærming som ikke tar hensyn til alle effektene av redusert skjærbåndtykkelse.

4 Grenselikevektsberegninger

Basert på den antatte udrenerte skjærstyrkefordelingen i forrige kapitel er stabiliteten først tilbakeregnet ved hjelp av en klassisk Fellenius stabilitetsmetode. Metoden baserer seg på momentlikevekt for en sirkulærsyllindrisk flate uten endeeffekt. Ligningen under gir beregning av sikkerhetsfaktoren:

$$F = \frac{R \cdot \int \tau_f dL}{W \cdot X} \approx \frac{R \cdot \sum \tau_f \Delta L}{\sum \Delta W_i \cdot \Delta X_i}$$

Hvor R er radien til sirkelflaten, X er horisontalavstanden fra sirkelsentrum til tyngdepunktet av jordmassen innenfor sirkelflaten, τ_f er skjærstyrken langs glideflaten og W er vekten av jordmassen også innenfor sirkelflaten.

4.1 Tøyningskompatibilitet

Beregninger med og uten idealisert tøyningskompatibilitet langs glideflaten er utført både på jordprofil med antatt konstant vanninnhold mot dybden og med jordprofil der variasjon i vanninnhold er inkludert.

Tøyningskompatibilitet er oppnådd ved å finne den største sikkerhetsfaktoren for forskjellige konstante skjærtøyninger langs en gitt potensiell bruddflate. Deretter minimeres sikkerhetsfaktoren ved å finne den flaten som gir lavest sikkerhet. Dermed vil flaten oppnådd ved hjelp av tøyningskompatibilitet ikke nødvendigvis være den samme som man oppnår uten tøyningskompatibilitet. For å kunne utføre tøyningskompatibilitets beregninger må man bestemme seg for en spenning-tøyningsoppførsel. Figur 4.1 viser den valgte oppførselen for aktiv, passiv og DSS tilstand i beregningene. Disse er oppnådd ved kalibrering mot utførte triaks- og DSS-forsøk (NGI, 1982). Skjærtøyningen ved maks udrenert skjærstyrke er $\gamma_p{}^C$ = 1 % for triaks-kompresjon, $\gamma_p{}^{DSS}$ = 5 % for DSS og $\gamma_p{}^E$ = 10 % for triaks-strekk forsøk.

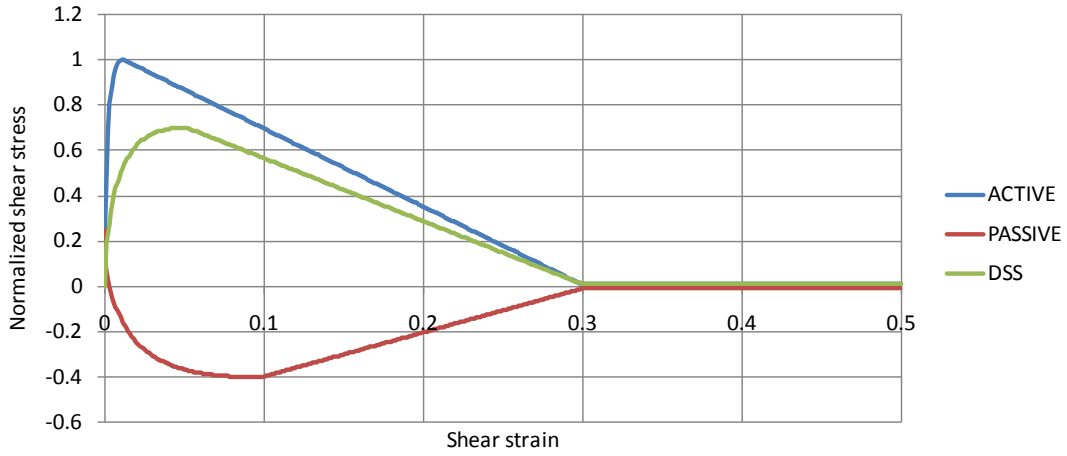

Figur 4.1 Valgt tøynings–spenningsrelasjon

4.2 Resultater

Figur 4.2 viser de mest kritiske sirkulærsylindriske bruddflatene, oppnådd med og uten tøyningskompatibilitet. Sikkerhetsfaktoren er henholdsvis 0.932 og 1.006 for beregning med og uten tøyningskompatibilitet. Effekten av tøyningskompatibilitet gir i dette tilfellet en reduksjon i sikkerheten på omtrent 7 %. Bruddflatene er nesten helt identiske, men den med tøyningskompatibilitet har litt større utstrekning. Den kritiske skjærtøyningen i analysen er tett på bruddtøyningen i DSS.

Beregnet sikkerhet og potensiell sirkulær bruddmekanisme uten fylling vises i Figur 4.3. Som figuren viser er den beregnede sikkerheten før fylling omtrent 1.19 (inklusiv krav til tøyningskompatibilitet). Figur 4.4 viser at den beregnede kritiske flaten for initialtilstanden får en økning i sikkerhet når fyllingen tas hensyn til. Forbedringen for denne flaten er på 9 %. Dette er dermed innenfor kravet til prosentvis forbedring som er krevd av NVE veilederen (NVE, 2011). I prosjekteringen i 1982 ble også dette tiltaket (fyllingen) sett på som et stabiliserende tiltak.

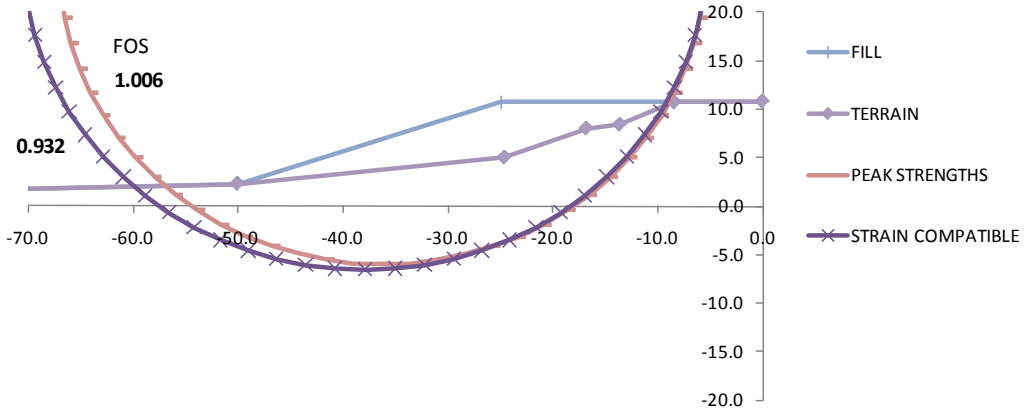

Figur 4.2 Kritiske sirkulære bruddmekanismer med og uten tøyningskompatibilitet

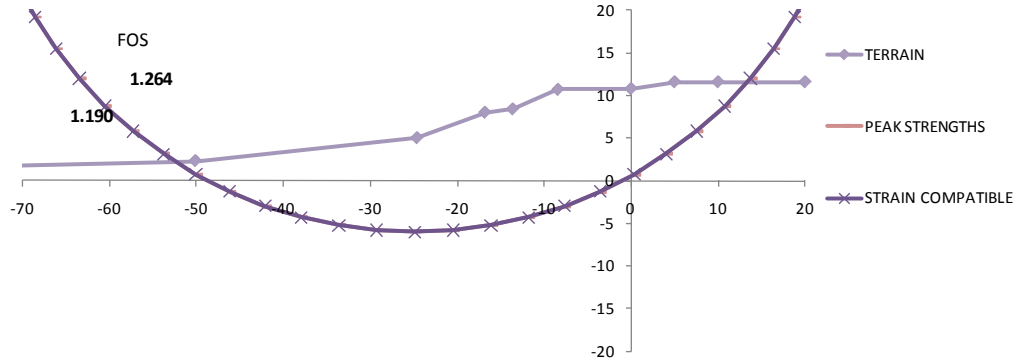

Figur 4.3 Kritiske sirkulære bruddmekanismer med og uten tøyningskompatibilitet for tilstanden uten fyllingen

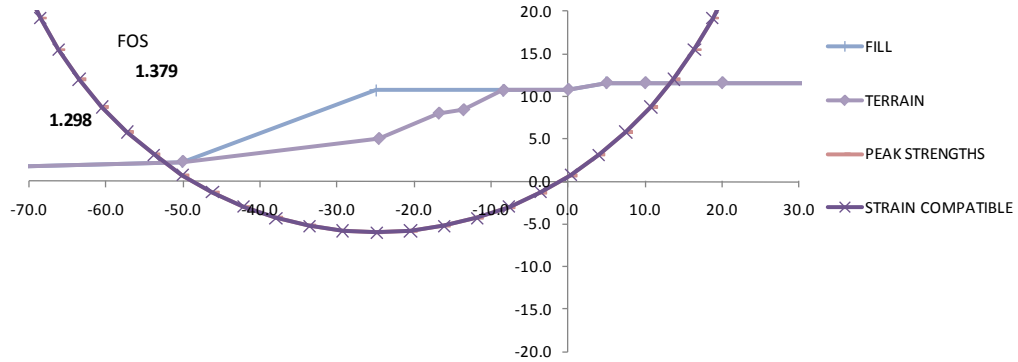

Figur 4.4 Beregnet sikkerhet etter oppfylling langs kritiske bruddflater (med og uten tøyningskompatibilitet) for tilstanden før oppfyllingen

4.3 Kommentarer til grenselikevektsberegningene

- Det er vist at sikkerhetsfaktoren som tidligere var beregnet for fyllingen ved Vestfossen (i størrelsesorden 1.2) sannsynligvis var for optimistisk. Dette skyldes blant annet valget av udrenert skjærstyrke i toppen av jordprofilet. Dette betyr at skredet ved Vestfossen havner i kategorien av skred som skyldes en pålastning, og hvor pålastningen har medført en reduksjon i beregnet lokal sikkerhet ned mot 1.0. Beregnet sikkerhet kan i dette tilfellet på grunn av neglisjering av sideskjær til og med være mindre enn 1.0.
- Ved å ta hensyn til tøyningskompatibilitet reduseres sikkerheten med ca. 7 %.
- Fyllingen medførte, som antatt i prosjekteringen, i en økning i sikkerheten for skråningen på oversiden av fyllingen. Fyllingen ble også prosjektert slik at helningen ikke var brattere enn opprinnelig terreng. Fyllingen som en kritisk drivende kraft ble derfor dessverre ikke undersøkt.

5 Elementanalyser - Initiell bruddlast

Hensikten med beregningene i dette kapittelet er å finne ut om tilbakeregning av Vestfossen kan brukes til å verifisere beregningsmodellen presentert i Aktivitet 1, NGI (2012). Dette inkluderer studie av sannsynlig skjærbåndtykkelse ved initiering av bruddet. Ved å ta hensyn til usikkerheten i skjærstyrkeprofilet vil man kunne beregne et variasjonsområde skjærbåndtykkelsen må ligge innenfor for at bruddet skal bli initiert under den aktuelle oppfyllingen.

5.1 Geometri

Figur 5.1 viser geometrien til elementmodellen som ble benyttet i beregningene. Det er inkludert en 2-4 m tykk tørrskorpe i toppen, og seks soner med leire. I de fleste beregningene ble et fint elementnett med 1251 15-noders elementer benyttet. I tillegg ble et meget fint nett med 2702 elementer brukt. Begge elementnettene er forfinet like under fyllingen hvor en har softening under maks belasting. Vekten av fyllingen er i alle tilfeller skalert til en verdi hvor fylling og leira under blir ustabil.

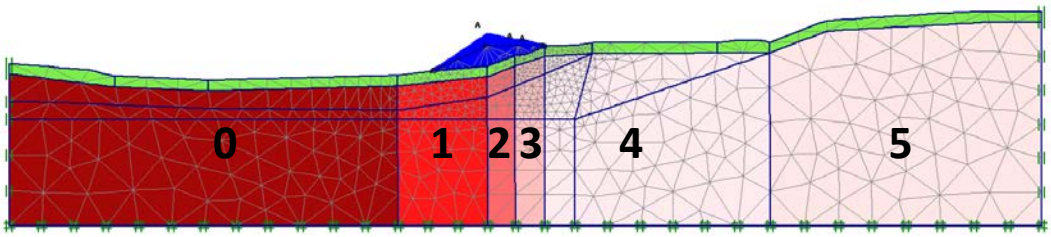

Figur 5.1 Elementnett med 1251 elementer

5.2 Inndata

Leira er modellert med NGI-ADPSoft (NGI, 2012). Den laterale variasjonen i det udrenerte skjærstyrkeprofilet ble idealisert ved å dele modellen inn i seks soner med hvert sitt materialsett, vist på Figur 5.1. SHANSEP-prosedyren ble benyttet i overgangen mellom sone 0, 1, 2, 3 og 4. For å oppnå et kontinuerlig s_u-profil i hele tverrsnittet ble det interpolert lineært mellom disse. Alle sonene har samme skjærstyrkegradient gitt av ${s_u}^A_{inc}$ mot dybden og minimums skjærstyrke ${s_u}^A_{ref}$ ved dybde y_{ref}. Dybden y_{ref} varier langs tverrsnittet, styrt av parameteren $\delta y_{ref}/\delta x$. Den er valgt slik at det er samme y_{ref} i overgangen mellom sonene. For sone 0 og 4 ble $\delta y_{ref}/\delta x$ forenklet valgt lik 0, og for sone 5 ble samme helning valgt som i den bratteste delen av skråningen i sonen.

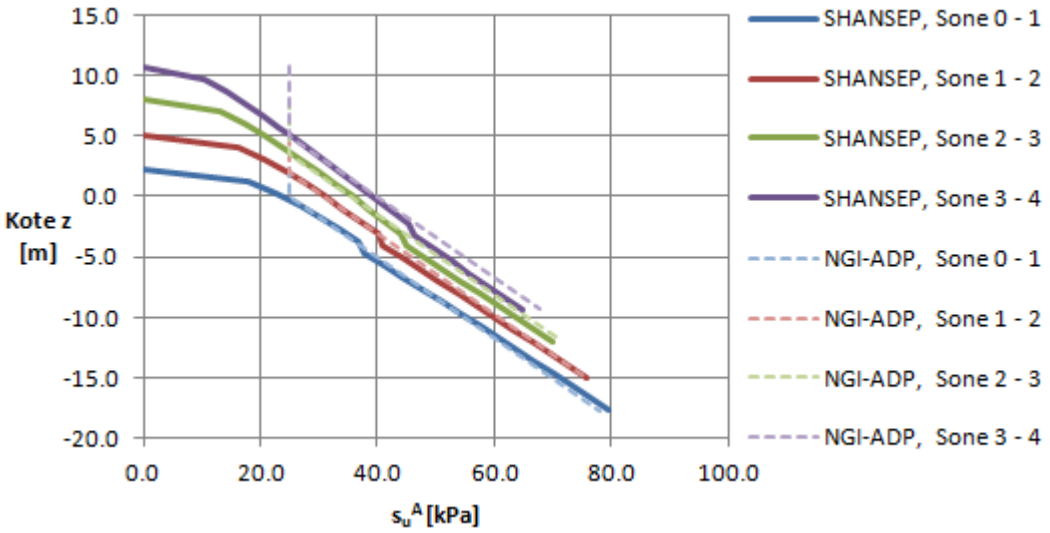

Figur 5.2 *Kote z mot aktiv skjærstyrke for 4 styrkeprofil beregnet med SHANSEP for s_{uv}/s_u^A = 0.65, og tilpasset NGI-ADPSoft*

Opprinnelig terreng som vist på Figur 3.14 ble brukt til å bestemme POP for de 4 styrkeprofilene vist på Figur 5.2, etablert med SHANSEP med OCR_τ lik 1.1. Figur 5.3 viser konturer av aktiv skjærstyrke i hele tverrsnittet, interpolert mellom de 4 styrkeprofilene.

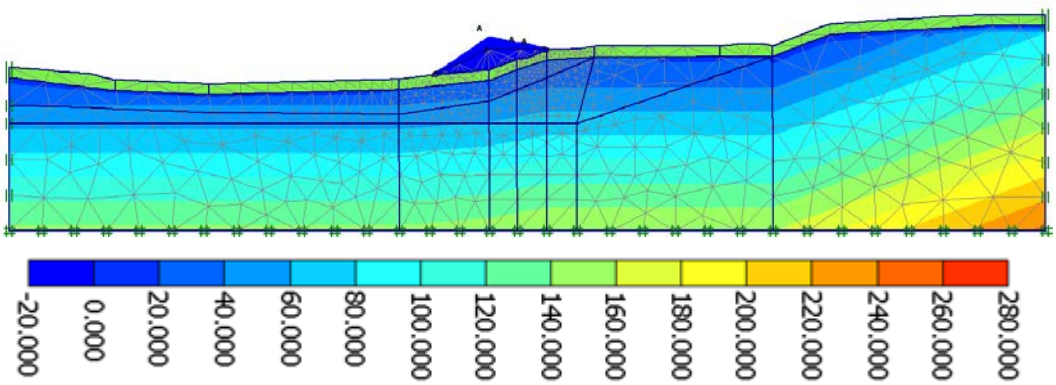

Figur 5.3 *Styrke s_u^A [kPa] for s_{uv}/s_u^A = 0.65*

Tørrskorpen ble modellert som Mohr Coulomb-materiale med friksjonsvinkel φ = 30 °. Basert på tolkningen av CPTU-testene i Figur 2.9 er det i tillegg antatt at aktiv skjærstyrke i leira ikke kan være lavere enn 25 kPa, se Figur 5.2.

Skjærtøyninger ved maks skjærstyrke er basert på DSS- og triaksforsøk fra Vestfossen (NGI, 1982) og NGIs blokkprøvedatabase (Karlsrud et al., 2012). Det ble antatt γ_p^C = 1 %, γ_p^{DSS} = 3 % og γ_p^P = 5 %. Skjærtøyning ved residualstyrke γ_r = 30 %, ble antatt for alle deformasjonsretninger. Figur 2.7 viser at en lineær ekstrapolering av softeningkurven gir ε_a lik 20 % ved en residualstyrke lik null. Selv

om skjærstyrken ikke kommer ned til residual ved global bruddlast er dette med og definerer graden av sprøhet.

Parameterne c_1 og c_2 styrer helningen av softeningkurven fra maks skjærstyrke og ned til residual. Figur 5.4 viser kurver for NGI-ADPSoft hvor $c_1 = c_2 = 1$, 1.5 og 2 er benyttet. Verdien 1 gir sprøere oppførsel like etter peak enn 2 som gir en mykere overgang til softeningen. Figuren viser også normaliserte kurver fra triaksforsøkene, som ikke er korrigert for prøveforstyrrelse. Softeningkurven av en uforstyrret prøve vil typisk være brattere, og derfor er $c_1 = c_2 = 1$ til 2 antatt å være ett mulig spenn av verdier. Initiell skjærstivhet $G_{ur}/s_u^A = 400$ ble benyttet i beregningene.

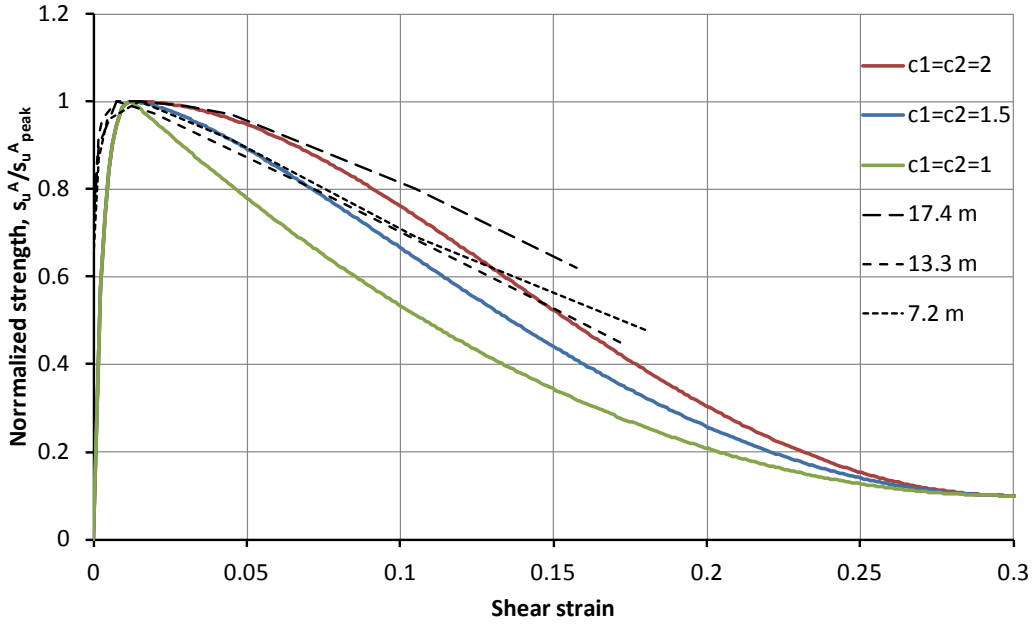

Figur 5.4 Normaliserte triakskurver og effekt av c_1 og c_2

Et "beste estimat" av inputparametere for NGI-ADPSoft ble valgt som utgangspunkt for beregningene, se Tabell 5.1. Følgende valg er da gjort for parametere med usikkerhet:

- Softeningkurven: $c_1 = c_2 = 1.5$
- Anisotropiforhold: $s_u^{DSS}/s_u^A = 0.7$, $s_u^P/s_u^A = 0.4$
- Opprinnelig terreng, POP: $s_{uv}/s_u^A = 0.65$
- Tørrskorpe:
  - Tykkelse 3 m
  - $s_u^A{}_{ref} = 25$ kPa (minimumsverdi)
  - Friksjonsvinkel $\varphi = 30$ °
- Skjærbåndtykkelse: $l^* = l_{int} = 0.3$ m

Tabell 5.1 Input parametere til NGI-ADPSoft, "Beste estimat"

Parameter	Sone 0	Sone 1	Sone 2	Sone 3	Sone 4	Sone 5
γ_{unsat} [kN/m^3]	18	18	18	18	18	18
γ_{sat} [kN/m^3]	18	18	18	18	18	18
k_x [m/s]	0	0	0	0	0	0
k_y [m/s]	0	0	0	0	0	0
K_0	0.75	0.75	0.75	0.75	0.75	0.75
G_{ur}/s_u^A	400	400	400	400	400	400
$s_u^A{}_{ref}$ [kPa]	25	25	25	25	25	25
$s_u^A{}_{inc}$[kPa]	3	3	3	3	3	3
x_{ref} [m]	-50.1	-50.1	-24.6	-16.8	-8.4	55.2
y_{ref} [m]	0	0	2	3.5	5	5
$\delta y_{ref}/\delta x$	0	0.079	0.192	0.179	0	0.373
s_u^{DSS}/s_u^A	0.7	0.7	0.7	0.7	0.7	0.7
s_u^P/s_u^A	0.4	0.4	0.4	0.4	0.4	0.4
τ_0/s_u^A	0.2	0.2	0.2	0.2	0.2	0.2
$s_u^A{}_r/s_u^A$	0.01	0.01	0.01	0.01	0.01	0.01
$s_u^{DSS}{}_r/s_u^A$	0.01	0.01	0.01	0.01	0.01	0.01
$s_u^P{}_r/s_u^A$	0.01	0.01	0.01	0.01	0.01	0.01
γ_p^C [%]	1	1	1	1	1	1
γ_p^{DSS}[%]	3	3	3	3	3	3
γ_p^P[%]	5	5	5	5	5	5
γ_r^C[%]	30	30	30	30	30	30
γ_r^{DSS}[%]	30	30	30	30	30	30
γ_r^P[%]	30	30	30	30	30	30
c_1	1.5	1.5	1.5	1.5	1.5	1.5
c_2	1.5	1.5	1.5	1.5	1.5	1.5
v	0.25	0.25	0.25	0.25	0.25	0.25
v_u	0.495	0.495	0.495	0.495	0.495	0.495
α	2	2	2	2	2	2
l_{int} [m]	0.3	0.3	0.3	0.3	0.3	0.3
$1\text{-}l^*/l_{int}$	0	0	0	0	0	0
Int.Type	0	0	0	0	0	0
GS-pl/tot	0	0	0	0	0	0

5.3 Beregninger

I beregningene ble grunnvannstand satt i bunnen av modellen, slik at profilet startet uten initielt poretrykk. Poretrykket er tatt hensyn til ved etablering av styrkeprofilene siden det påvirker effektivspenningstilstanden og dermed skjærstyrken. $K_0 = 0.75$ og $\tau_0/s_u^A = 0.2$ ble valgt for å gi best mulig tilpasning til initiell mobilisering i den aktive sonen under fyllingen idet fylling blir ustabil.

I første beregningsfase ble initialspenningene modifisert slik at de er i likevekt med grensebetingelsene (hellende terrengoverflate). I neste fase ble fyllingen med null

romvekt aktivert og 5 % av fyllingslasten påført som en fordelt last. I denne fasen og de påfølgende ble oppdatert elementnett benyttet. I neste fase ble fyllingslasten økt med "total multipliers" helt til maks last er oppnådd (global instabilitet).

For å få små nok lastinkrementer ble "desired minimum iterations" redusert fra 6 til 3 og toleransen redusert fra 0.01 til 0.001. Fordi fyllingen ble modellert med et lineært elastisk materiale, ble bruddet tvunget til å gå i bakkant av fyllingen, som observert etter skredet på Vestfossen.

På grunn av usikkerhet i parameterne er det i tillegg til analysen med "beste estimat"-parametere gjort et parameterstudie. For å se effekten av hver parameter er kun én variert om gangen. Følgende parametere og spenn av verdier er studert:

- Softeningkurven: $c_1 = c_2 = 1 – 2$
- Anisotropiforhold: $s_u^{DSS}/s_u^A = 0.65 – 0.75$
- Opprinnelig terreng, POP: $s_{uv}/s_u^A = 0.6 – 0.7$
- Tørrskorpe:
  - Tykkelse 2 – 4 m
  - $s_u^A{}_{ref} = 25 – 30$ kPa
  - Friksjonsvinkel $\varphi = 20 – 40$ °
- Skjærbåndtykkelse: $l^* = 0.075 – 0.6$ m

5.4 Resultater

I beregningene med "beste estimat"-parametere og fint elementnett gikk skråningen til brudd ved 94 % oppfylling, se Tabell 5.2. Med meget fint nett gikk den til brudd ved 93 % oppfylling. Avviket fra virkelig last er lite nok til å kunne forklares av 3D-effekt. Figur 5.5 viser oppfyllingsgrad mot forskyvning av fyllingen. Figuren viser også en beregning med perfekt plastisk oppførsel, uten softening. Fordi oppdatert nett er benyttet flater ikke kurven ut, men øker lineært etter oppfyllingsgrad 1.118.

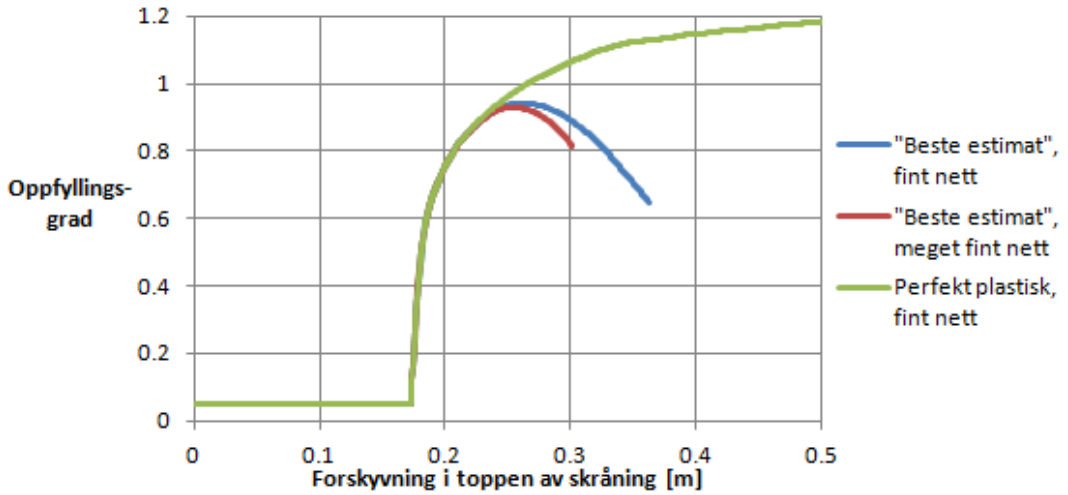

Figur 5.5 "Beste estimat", oppfyllingsgrad mot forskyvning

Tabell 5.2 *"Beste estimat"-parametere og varierende antall element. Avvik i forhold til referanse analyse VF_BC_01*

Filnavn	Beskrivelse	Antall element	Oppfyllingsgrad	Avvik
VF_BC_01	Fint nett	1251	0.942	-
VF_BC_61	Meget fint nett	2702	0.931	-1.2 %
VF_BC_71	Perfekt plastisk	1251	1.118	18.7 %

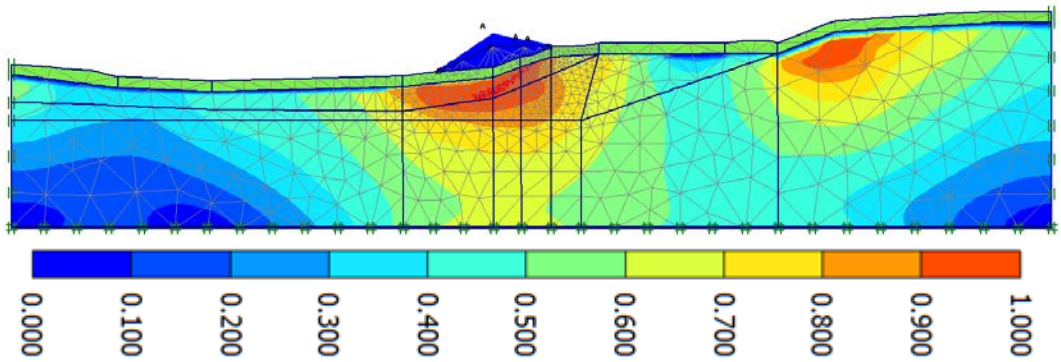

Figur 5.6 *"Beste estimat", κ_1-plot, mobilisering τ/s_u^A*

Figur 5.6 viser mobiliseringsgrad κ_1 ved maks last for "beste estimat"-parametere. Ved initiell skjærspenning τ_0 er $\kappa_1 = 0$, og ved maks udrenert skjærstyrke er $\kappa_1 = 1$. Det er de bratte skråningene som er høyest mobilisert, og nesten hele bruddflaten under fyllingen er fullt mobilisert ved maks last.

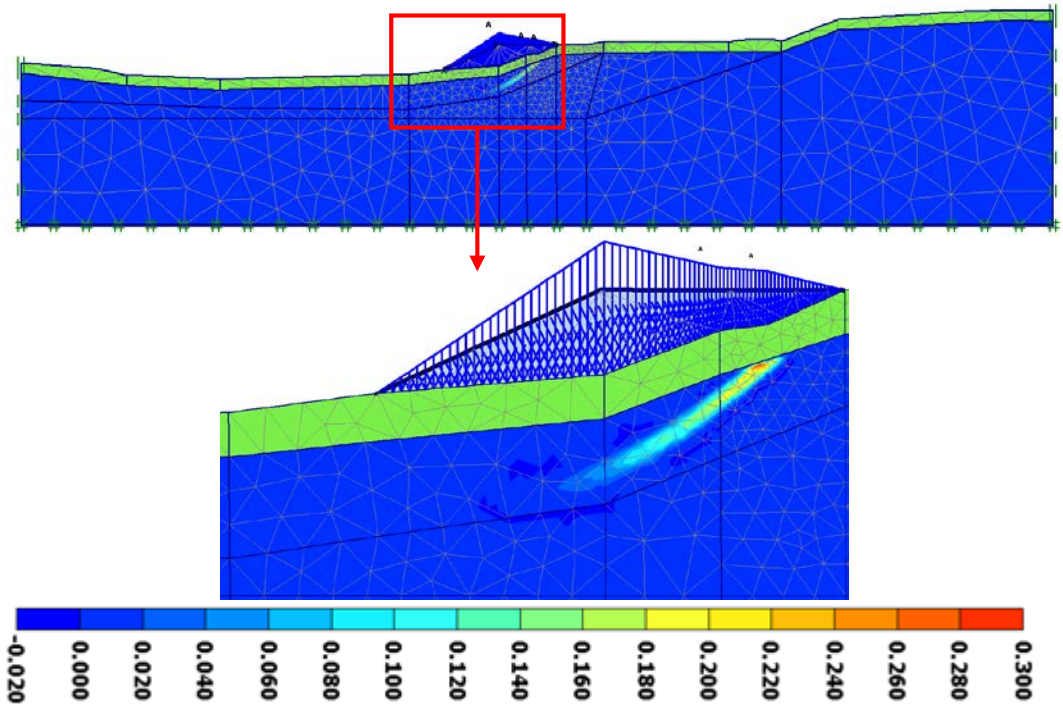

Figur 5.7 *"Beste estimat", κ_2-plot, største verdi er lik 0.3*

Figur 5.7 viser grad av softening uttrykt ved hjelp av κ_2 ved maks last. Ved maks styrke er $\kappa_2 = 0$ ($\kappa_1 = 1$) og ved residualstyrke er $\kappa_2 = 1$.

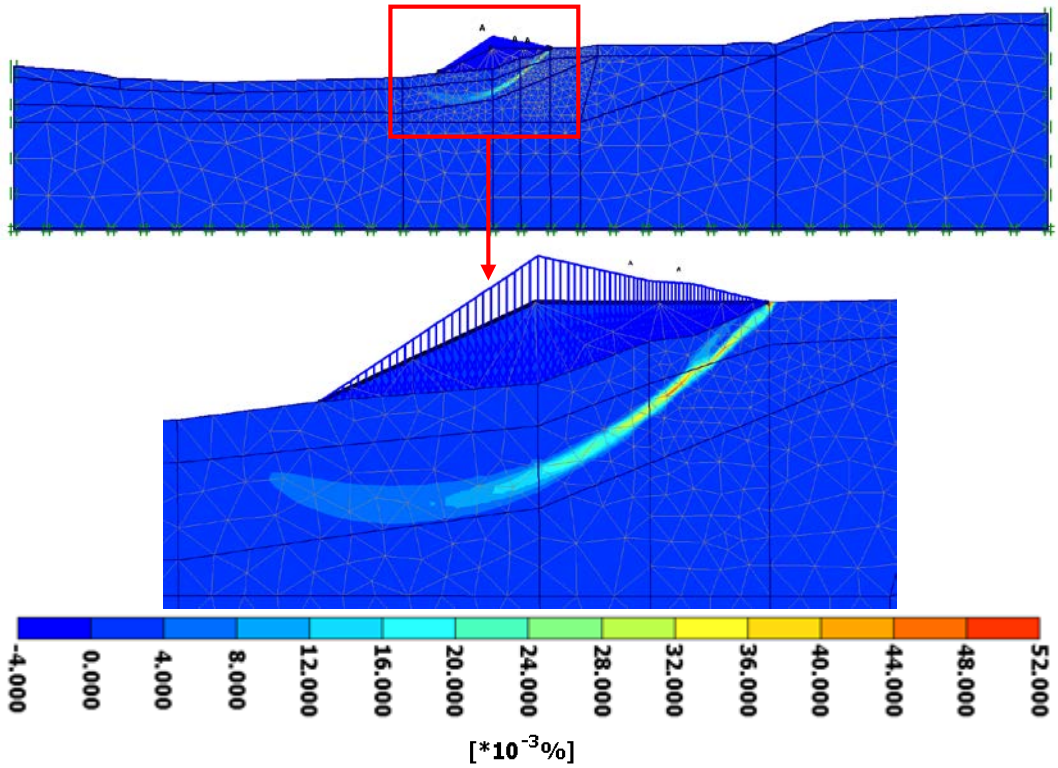

Figur 5.8 "Beste estimat", inkrementelle skjærtøyninger

Figur 5.8 viser inkrementelle skjærtøyninger ($1/2 \cdot d\gamma_{max}$) ved maks last. Man ser av figuren at bruddflaten starter i bakkant av fyllingen.

Tabell 5.3 Effekt av softeningkurven, c_1 og c_2

Filnavn	Beskrivelse	$c_1 = c_2$	Oppfyllingsgrad	Avvik
VF_BC_01	"Beste estimat"	1.5	0.942	-
VF_BC_11	Duktil softening	2	0.992	5.3 %
VF_BC_12	Sprø softening	1	0.869	-7.8 %

Tabell 5.3 viser at ved å gjøre softeningoppførselen sprøere, så reduseres bruddlasten. Usikkerhet i bruddlast på grunn av softeningkurven er opptil 7.8 %.

Tabell 5.4 Effekt av anisotropiforhold

Filnavn	Beskrivelse	s_u^{DSS}/s_u^{A}	Oppfyllingsgrad	Avvik
VF_BC_01	"Beste estimat"	0.7	0.942	-
VF_BC_41	Høyere DSS-styrke	0.75	1.003	6.5 %
VF_BC_42	Lavere DSS-styrke	0.65	0.887	-5.8 %

Tabell 5.4 viser at ved å øke eller redusere DSS (og passiv) styrke, så blir bruddlasten tilsvarende større eller mindre. Usikkerhet i bruddlast på grunn av anisotropiforhold er opptil 6.5 %.

Tabell 5.5 Effekt av opprinnelig terreng og styrkeprofil

Filnavn	Beskrivelse	s_{uv}/s_u^A	Oppfyllingsgrad	Avvik
VF_BC_01	"Beste estimat"	0.65	0.942	-
VF_BC_21	Høyere oppr. terreng	0.6	1.000	6.1 %
VF_BC_22	Lavere oppr. terreng	0.7	0.878	-6.7 %

Tabell 5.5 viser at jo høyere opprinnelig terreng SHANSEP-styrkeprofilet er basert på, desto høyere bruddlast. Usikkerhet i bruddlast på grunn av opprinnelig terreng er opptil 6.7 %.

Tabell 5.6 Effekt av tørrskorpe

Filnavn	Beskrivelse	t [m]	φ [°]	$s_u^A{}_{ref}$ [kPa]	Oppfyllingsgrad	Avvik
VF_BC_01	"Beste estimat"	3	30	25	0.942	-
VF_BC_31	Høy friksjonsvinkel	3	40	25	0.970	3.0 %
VF_BC_32	Lav friksjonsvinkel	3	20	25	0.880	-6.6 %
VF_BC_34	Høy $s_u^A{}_{ref}$ i leira	3	30	30	1.006	6.8 %
VF_BC_36	Tynn tørrskorpe	2	30	25	0.884	-6.1 %
VF_BC_37	Tykk tørrskorpe	4	30	25	1.017	7.9 %

Tabell 5.6 viser at bruddlasten blir høyere for økt tykkelse av tørrskorpe, økt friksjonsvinkel i tørrskorpe, og høyere $s_u^A{}_{ref}$ i leira. Usikkerhet i bruddlast på grunn av egenskaper til tørrskorpen er opptil 7.9 %.

Tabell 5.7 Effekt av skjærbåndtykkelse

Filnavn	Beskrivelse	l* [m]	l_{int} [m]	Oppfyllingsgrad	Avvik
VF_BC_01	"Beste estimat", 1251 elementer	0.3	0.3	0.942	-
VF_BC_51	1251 elementer	0.6	0.6	0.990	5.1 %
VF_BC_52	1251 elementer	0.3	0.6	0.922	-2.1 %
VF_BC_53	1251 elementer	0.15	0.3	0.877	-6.9 %
VF_BC_54	1251 elementer	0.075	0.15	0.851	-9.6 %
VF_BC_55	1251 elementer	0.15	0.15	0.911	-3.3 %
VF_BC_56	1251 elementer	0.075	0.075	0.896	-4.9 %
VF_BC_57	1251 elementer	0.075	0.3	0.842	-10.6 %
VF_BC_58	1251 elementer	0.15	0.6	0.874	-7.2 %
VF_BC_61	2702 elementer	0.3	0.3	0.930	-1.2 %
VF_BC_62	2702 elementer	0.15	0.15	0.886	-5.9 %
VF_BC_63	2702 elementer	0.15	0.3	0.870	-7.6 %

Tabell 5.7 viser hvordan oppfyllingsgraden varier avhengig av skjærbåndtykkelsen l* og l_{int}. For l* < l_{int} er softening kurven gjort brattere (sprøere) for å ta hensyn til en tynnere skjærbåndtykkelse enn det som oppnås med l_{int}. Ved å doble skjærbåndtykkelsen øker oppfyllingsgraden med omtrent 5 %, og ved å halvere skjærbåndtykkelsen reduseres den med omtrent 7 %. Figur 5.9 viser hvordan oppfyllingsgraden er påvirket av l*. Fordi l_{int} er begrenset av elementnettet er resultatene sortert etter hvilken korrigeringsfaktor 1-l*/l_{int} og hvilket elementnett som er benyttet.

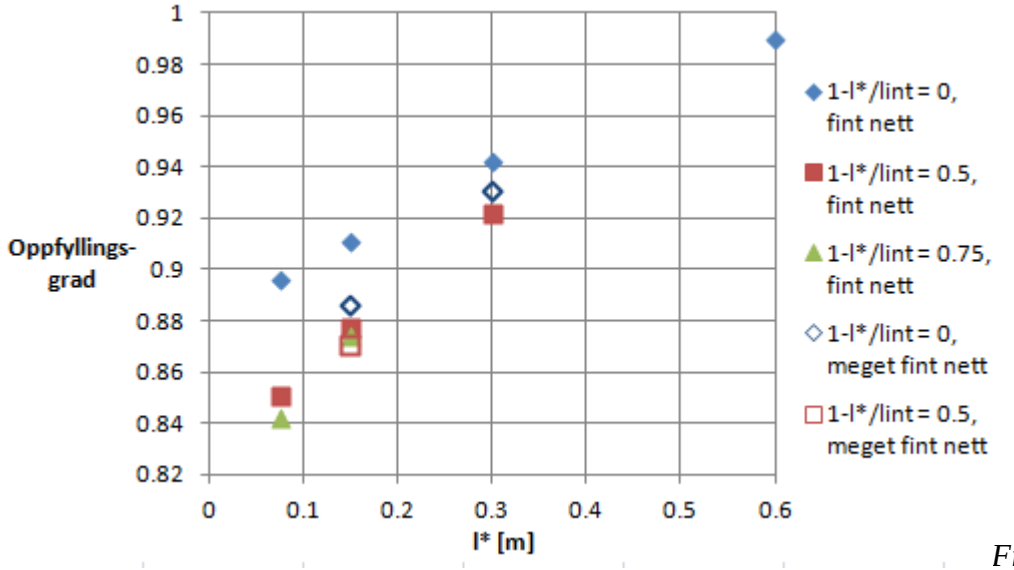

*Figur 5.9 Oppfyllingsgrad mot skjærbåndtykkelse l**

Usikkerheten i parameterne over tilsvarer omtrent en dobling eller halvering i skjærbåndtykkelsen. Fordi effekten av usikkerheten i material input parameterne er tilnærmet like stor som effekten av varierende skjærbåndtykkelse er det vanskelig å bruke Vestfossen til å kalibrere seg fram til riktig skjærbåndtykkelse ved initiering av et progressivt skred.

6 Elementanalyser – Progressiv bruddutvikling

I elementanalysene presentert i dette kapittelet er skjærstyrke- og K_0-profilet gitt i henholdsvis seksjon 3.2 og 3.5, importert til PLAXIS via en spesiell input prosedyre, utviklet spesielt for Vestfossen i dette prosjektet. NGI-ADPSoft er brukt i analysene med softening og NGI-ADP (Grimstad et al. 2011) i analysene uten softening. NGI-ADP tillater bruk av c/phi-reduksjon, og resultatene kan derfor sammenlignes med resultatene fra grenselikevektsanalysene.

6.1 Analyser med ”strain-softening”

Fremgangsmåten som er brukt i disse analysene går ut på å legge på en ekstra (meget liten) last i tillegg til fyllingen som er stor nok til å initiere en progressiv bruddutvikling. I analyse nr. 1 var nødvendig tilleggslast 1.14 kPa. Lasten blir deretter fjernet og bruddutviklingen opprettholdes ved å øke vekten ved bruk av ”total multipliers”. I analyse nr. 1 ble vekten da økt med kun 1.26 % for å opprettholde bruddutviklingen. Analysene er utført med oppdatert geometri. Toleransen er i den siste fasen redusert til 0.001 og ”arc-length” er skrudd av. PLAXIS er da tvunget til å oppnå likevekt ved økte forskyvninger og ikke ved lastreduksjon. Tabell 6.1 gir en liste over beregninger som er gjort for å tilbakeregne skredet ved Vestfossen. Den første analysen er en idealisert ”beste estimat” av input data. Input data er deretter noe endret for å få best samsvar med observert bruddutvikling.

Figur 6.1 viser utviklingen av bruddmoden (inkrementelle forskyvninger) for analyse nr. 1. Analysen kunne vært kjørt videre, men den har allerede propagert tilstrekkelig langt og begynner å involvere for stort område i bakkant av fyllingen i forhold til det som ble observert etter skredet. I denne analysen er all leiren modellert med samme grad av softening, noe som er urealistisk. Leiren lenger bak i skråningen er mindre sensitiv. I tillegg vil tørrskorpen redusere den drivende kraften fra skråningen, og dermed redusere nødvendig heving av den passive sonen og tilsvarende senkning av område bak.

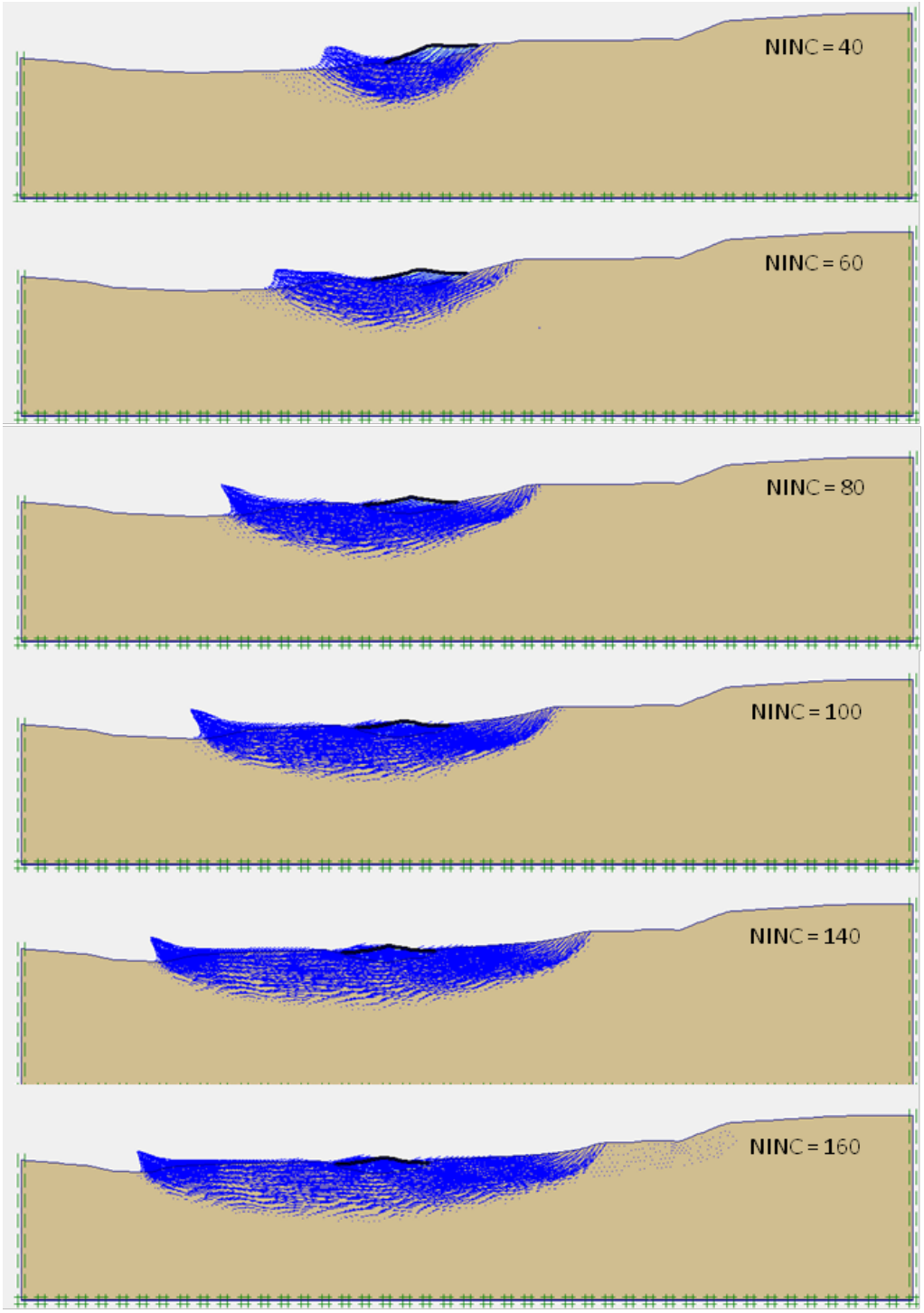

Figur 6.1 Utvikling av inkrementelle forskyvninger (hastighet) i løpet av analysen (økende antall inkrementer) for analyse nr. 1

Tabell 6.1 Liste over utførte analyser (varierende forutsetninger) i forbindelse med tilbakeregning av den progressive bruddutviklingen for skredet ved Vestfossen

Nr.	Antall elementer	Grad av "softening"		Lengde av bruddet	Senkning av fyllingen	Kommentar
		s_u^r/s_u^p	γ_{res}			
1	728	0.05	30%	150 m	4.0 m → 5.9 m	Idealisert tilfelle, l_{int} = 2 m, c1 = c2 = 1.0. Propagerer for langt bakover.
2	781	0.05	30%	129 m	4.0 m → 6.1 m	Lagt til "tørrskorpe med s_u^r/s_u^A = 0.3
3	2964	0.05	30%	-	-	Som nr. 2 med forfinet nett. Problemer med konvergens
4	3096	0.05	30%	-	-	Økt tykkelsen av tørrskorpen
5	942	0.1	30%	-	-	Lokalt forfinet nett, økt residual styrken til 0.1 (0.5 for tørrskorpen)
6	942	0.1	30%	145 m	4.0 m → 6.4 m	Endret softening kurven, $c_1 = c_2$ = 2.0

Figur 6.2 viser konturer av inkrementelle forskyvninger for analyse nr. 6. Som figuren viser er det i bakkant av fyllingen de største inkrementelle forskyvningene er konsentrert mot slutten av bruddmekanismen. Dette er i samsvar med observasjonene i felt, hvor skredet i bakkant skjedde påfølgende dag av hovedskredet.

Figur 6.3 viser konturer av vertikale forskyvninger for analyse nr. 6, plottet sammen med opprinnelig elementnett. Med kjøring nr. 6 oppnås den mekanismen som er nærmest den mekanismen som ble opplevd in-situ. Samsvaret er illustrert i Figur 6.4, som viser innmålt geometri på topp av beregnet vertikale forskyvninger.

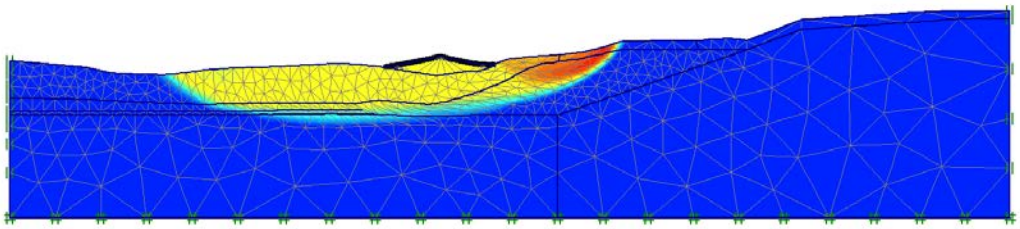

Figur 6.2 Konturplot av inkrementelle forskyvninger for analyse nr. 6.

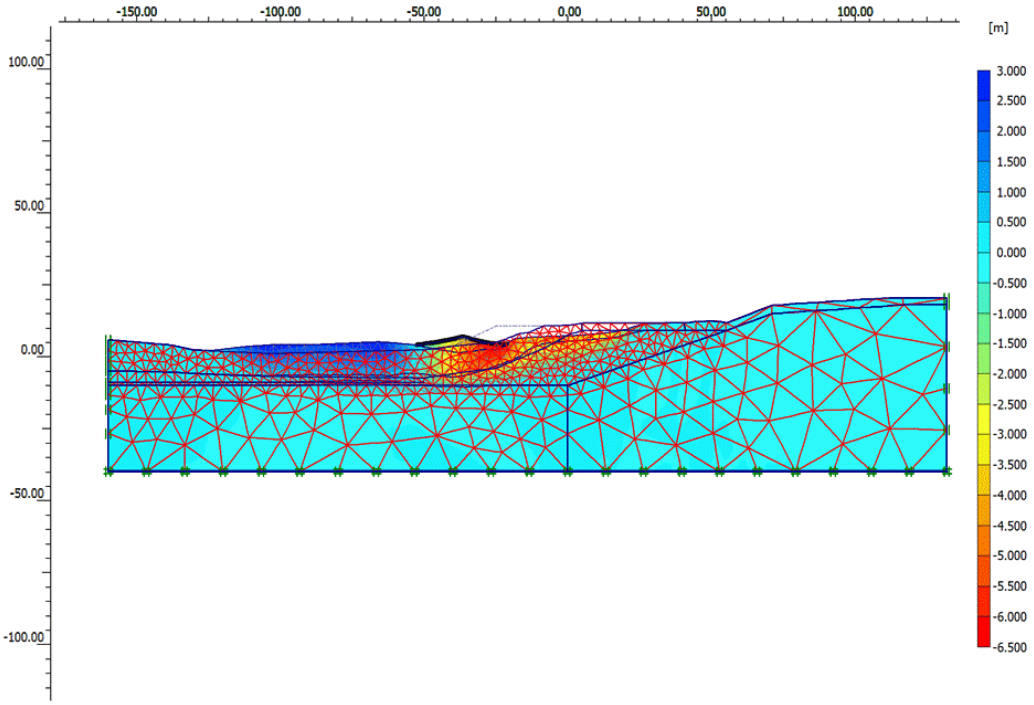

Figur 6.3 Plot av totale vertikale forskyvninger på originalt elementnett

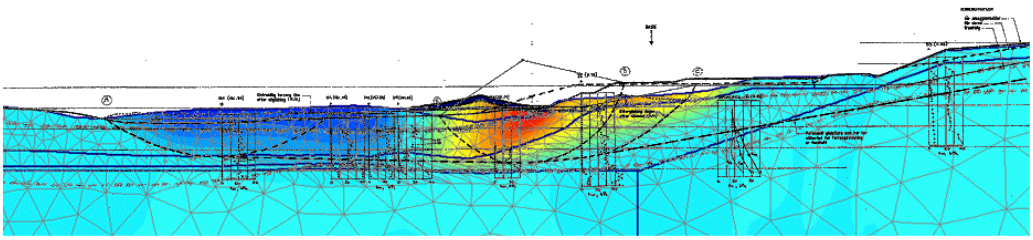

Figur 6.4 Plot av totale vertikale forskyvninger med opptegnet innmålt geometri

6.2 Analyser uten "strain-softening"

Hensikten med disse analysene er å kvantifisere effekten av softening. Først er initialtilstanden uten fylling (last) undersøkt. Et fint elementnett er brukt i denne analysen. Oppnådd sikkerhet er 1.28. Dette samsvarer godt med resultatet fra grenselikevektsmetoden uten tøyningskompatibilitet som ga en sikkerhet på 1.26. Kritisk bruddmekanisme er derimot forskjellig. Bruddmekanismen fra elementanalysen, vist i Figur 6.5, er en sammensatt flate som også involverer skråningen bakenfor fyllingen.

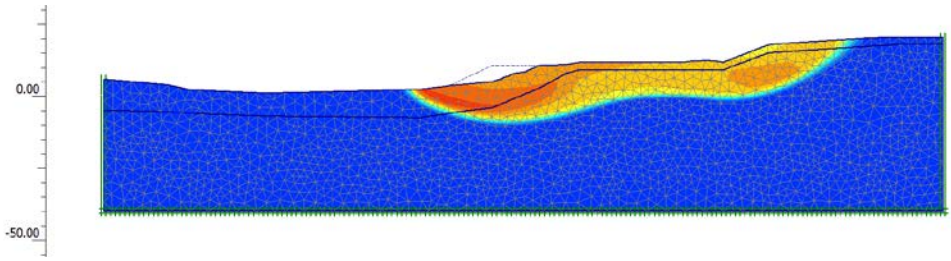

Figur 6.5 Konturer av totale forskyvninger etter c/phi-reduksjon, uten softening og fylling

For å undersøke effekten av softening for forskjellige antakelser, er først bruddlasten bestemt med NGI-ADPSoft. Vekten av fyllingen (påført som last) er skalert opp til maks last uavhengig av vekten til fyllingen. Sikkerheten er deretter for denne bruddlasten beregnet med c/phi-reduksjon for en perfekt plastisk oppførsel. For dette er det brukt en brukerdefinert modell som tillater samme input som før, men neglisjerer softening. Analysene er gjort uten bruk av oppdatert nett, noe som fører til lavere bruddlast enn med oppdatert nett. Men siden effekten av geometriendring er tilnærmet lik for tilfelle med og uten softening, antas effekten av softening å være lite påvirket av dette. Tabell 6.2 viser en sammenstilling av de analyser som er gjort på denne måten. Den oppnådde sikkerhetsfaktoren i analysene uten softening kan betraktes som en "korreksjonsfaktor" som tar hensyn til effekten av softening i analyser med et perfekt plastisk materiale. Faktoren tar hensyn til en kombinasjon av tøyningskompatibilitet (som for eksempel funnet i grenselikevektsanalysene med softening) og grad av progressivitet (lokale tøyningskonsentrasjoner og refordeling av spenninger på grunn av softening).

Figur 6.6 og Figur 6.7 viser henholdsvis konturer av κ_1 (et mål på mobilisering av maks skjærstyrke) og κ_2 (et mål på mobilisering av residual styrke) ved maks last. Man kan se fra konturene av κ_2 under maks last, at området som er i softening er veldig lite. I dette tilfellet vil maks last basert på "first yield" prinsippet, bare ført til marginalt høyere beregnet faktor.

Spesifikt for Vestfossen er det allikevel vist at det er sannsynlig at effekten av sprøbrudd/softening er mindre enn 10 %.

Tabell 6.2 Liste over simuleringer for beregning av effekten av softening

Nr.	Antall elem-enter	Grad av "softening"			Last-faktor [%]	Effekt av softening [%]	Kommentar
		s_u^r/s_u^p	γ_{res} [%]	l_{int} [m]			
7	942	0.1	30	1.5	88.9	4	Som analyse nr. 6
8	823	0.1	30	1.5	90.0	4	Nytt nett, fint kun under fylling
9	823	0.1	30	0.5	82.5	5	Mindre l_{int}
10	823	0.1	30	0.1	78.5	5	Mindre l_{int}
11	823	0.1	30	0.5	74.6	5	Ingen "tørrskorpe", l_{int} = 0.5 m
12	823	0.1	15	0.5	83.2	6	Ingen "tørrskorpe", Økt sprøhet av materialet, γ_{res} =15%
13	823	0.1	15	0.5	73.2	9	Ingen "tørrskorpe", c_1=c_2=1.0 (→ økt sprøhet)
14	823	0.1	15	0.5	76.1	8	Ingen "tørrskorpe", c_1=c_2=1.0, τ_0/s_u^A = 0.0 og K_0 = 1 (isotrop initialtilstand)
15	823	0.1	15	0.5	**48.8**	**15**	Ingen "tørrskorpe", c_1=c_2=1.0, τ_0/s_u^A = 0.7 (konstant med dybden)

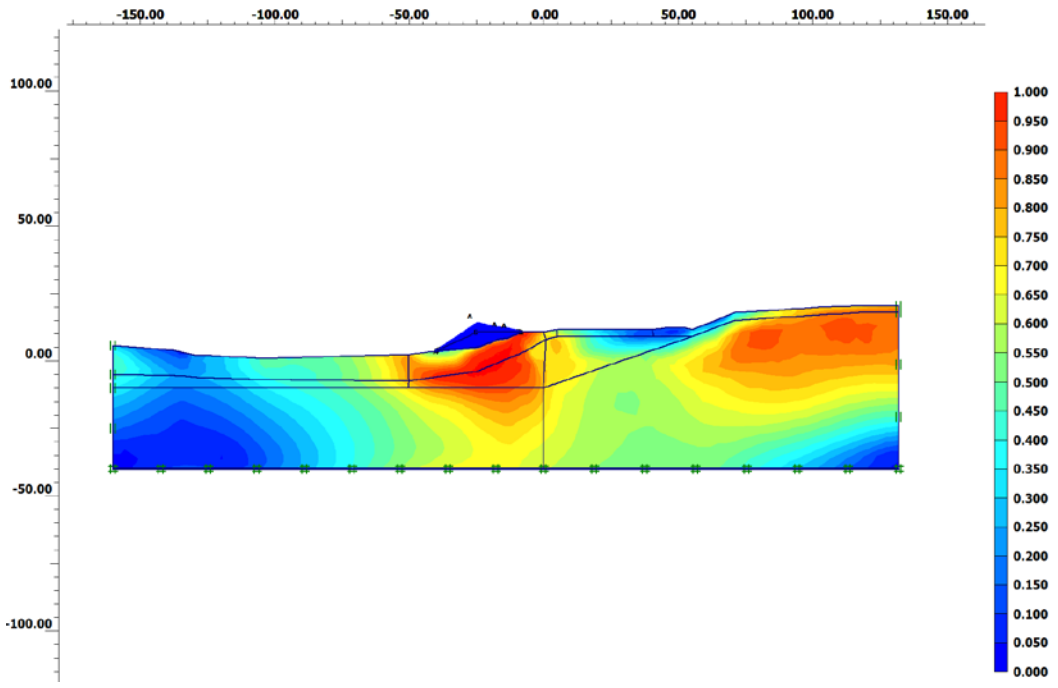

Figur 6.6 Konturer av κ_1 under maks last for nr. 12

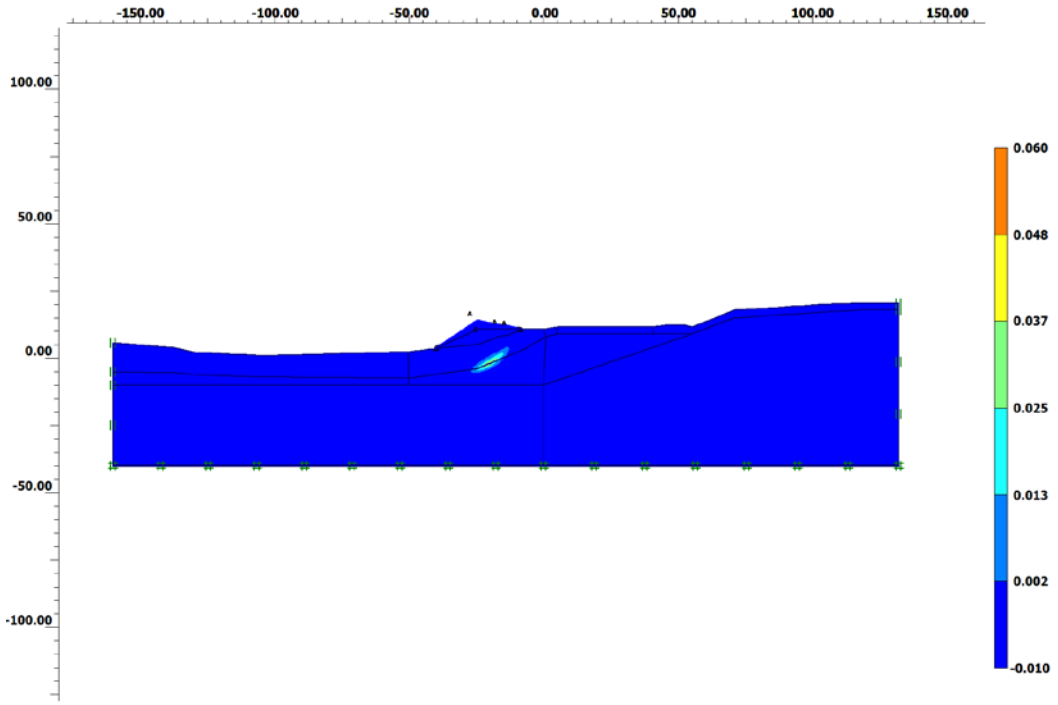

Figur 6.7 Konturer av κ_2 under peak last for nr. 12

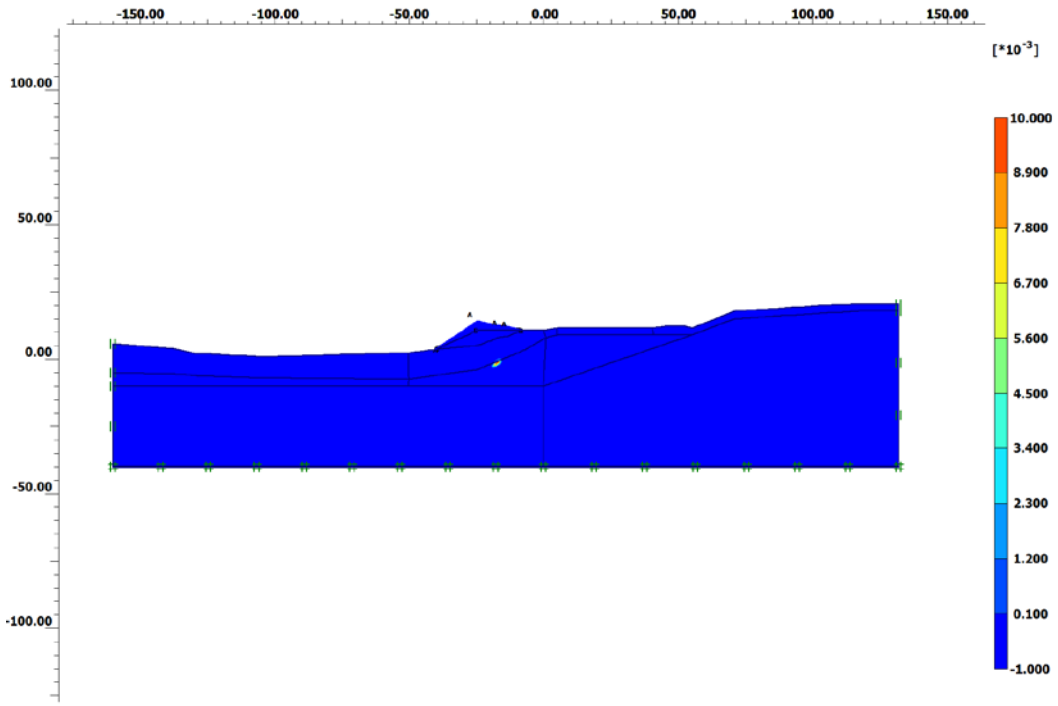

Figur 6.8 Konturer av κ_2 under maks last for nr. 15

7 Elementanalyser – Smårød

Skredet ved Smårød i Sverige i 2006 er tilbakeregnet i en mastergradsoppgave utført i samarbeid med NTNU (Bonadies, 2012), med progressiv bruddutvikling med materialmodellen NGI-ADPSoft i Plaxis og samme framgangsmåte som i seksjon 6. Arbeidet er ikke en del av dette prosjektet, men resultatene av tilbakeregningen presenteres her for å demonstrere enda et tilfelle hvor NGI-ADPSoft var velegnet. Oppgaven er gitt som Vedlegg A i denne rapporten.

I masteroppgaven er det tilbakeregnet et kritisk profil fra området hvor skredet først ble utløst, vist på Figur 7.1. Trolig var det en 7 m høy fylling i toppen av området A som forårsaket et lokalt brudd som forplantet seg videre med progressiv bruddutvikling (Vägverkets oberoende utredningsgrupp, 2007). Figur 7.2 viser glideflaten til skredet basert på sonderinger utført i etterkant av skredet.

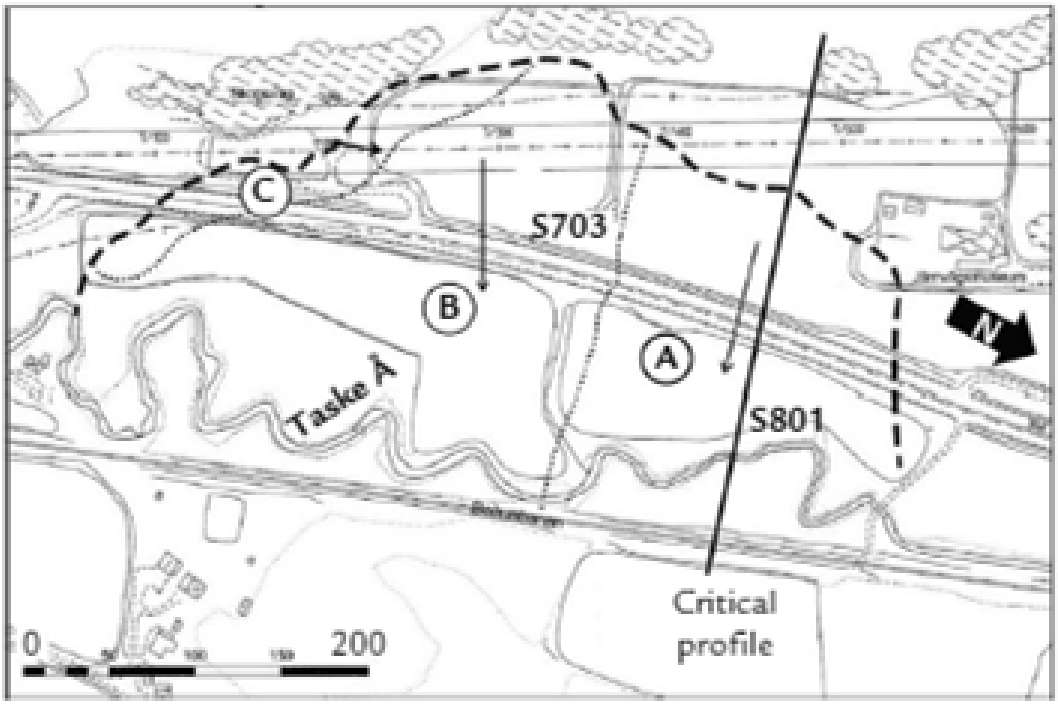

Figur 7.1 Kritisk profil i skredet ved Smårød (Bonadies 2012)

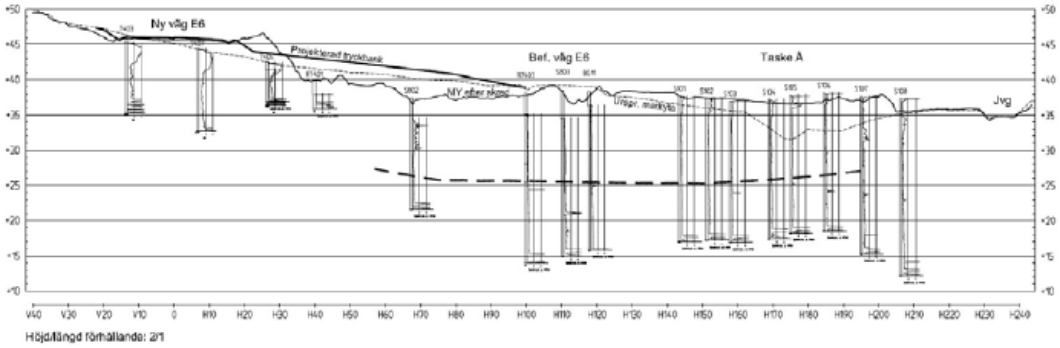

Figur 7.2 *Glideflate basert på sonderinger utført etter skredet (Vägverkets oberoende utredningsgrupp, 2007)*

Styrkeprofilet brukt i tilbakeregningen er vist på Figur 7.3. Anisotropiforhold er basert på Shansep-metoden etter Karlsrud et al. (2012).

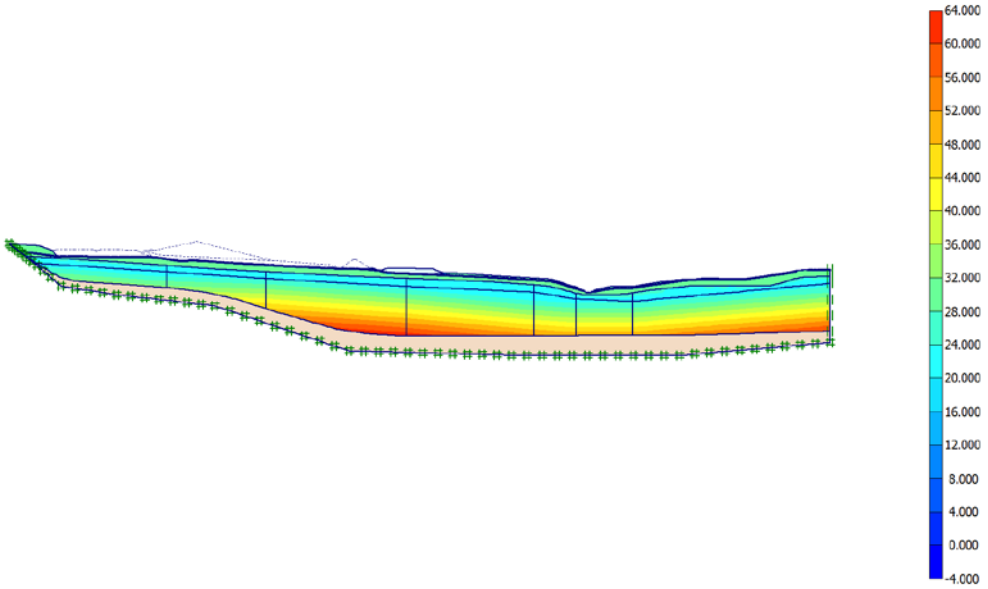

Figur 7.3 *s_u^A benyttet ved tilbakeregning av Smårød (Bonadies 2012)*

I beregningene ble lokalt brudd oppnådd ved å laste opp fyllingen til omtrent 7 m høyde, hvilket stemmer godt med den antatte bruddårsaken. Skjærtøyninger ved bruddlast er vist på Figur 7.4. Ved deretter å holde lasten konstant forplanter bruddet seg progressivt videre. Figur 7.5 viser de inkrementelle skjærtøyningene ved fullt utviklet progressivt brudd, og den endelige glideflaten stemmer godt med det observerte i skredet ved Smårød. Bonadies utførte også et sensitivitetsstudie av den interne lengden. Denne parameteren styrer skjærbåndtykkelsen, men så ut til å påvirke bruddlasten lite.

Ved å benytte NGI-ADPSoft er hele den progressive bruddutviklingen i skredet ved Smårød tilbakeregnet. Det viser at denne materialmodellen er egnet til å modellere skredoppførsel i sensitive leirer.

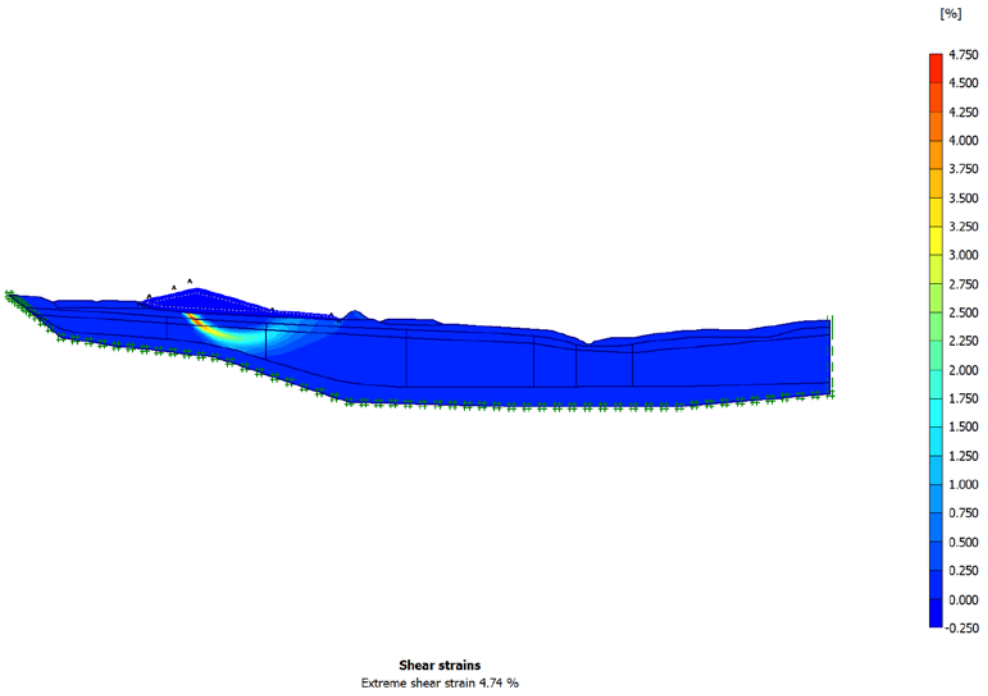

Figur 7.4 Skjærtøyninger ved bruddlast (Bonadies 2012)

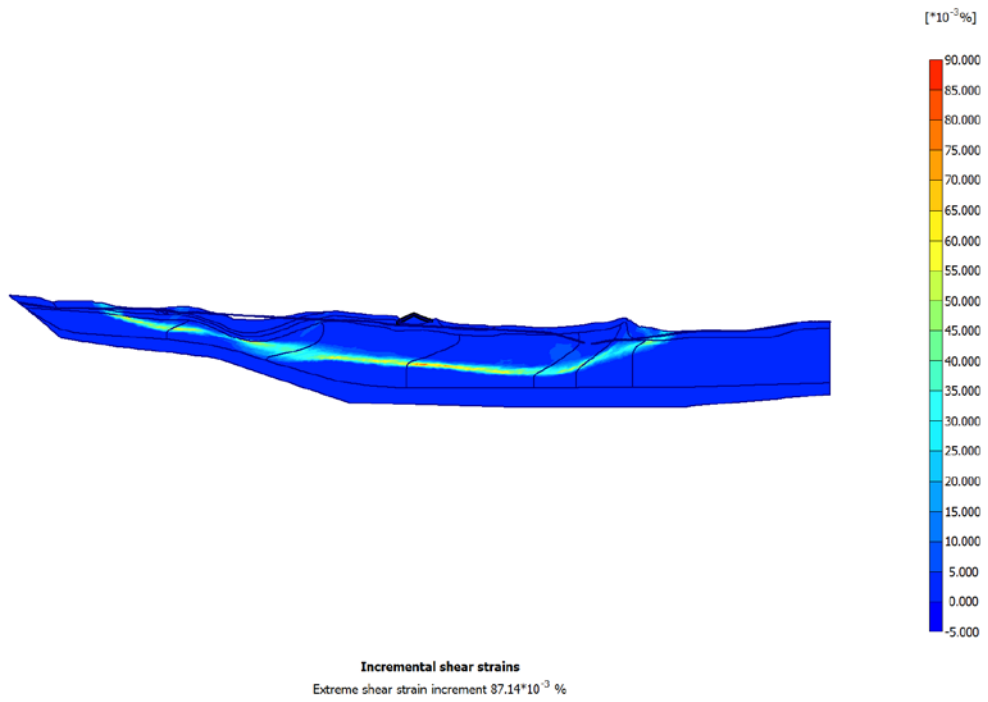

Figur 7.5 Inkrementelle skjærtøyninger ved progressivt brudd (Bonadies 2012)

8 Konklusjoner

Denne rapporten viser bruken av modellen NGI-ADPSoft med ikke-lokal tøyning i forbindelse med tilbakeregning av Vestfossenskredet i 1984 og Smårødskredet i 2006. Vestfossenskredet ble initiert av en fylling nederst i skråningen og forplantet seg omtrent 100 meter i nesten horisontalt terreng noe som må skyldes en gradvis reduksjon i skjærstyrken (softening).

Hovedkonklusjonene fra dette studiet er:

- Et realistisk valg av input parametere og antagelser gir en bruddlast som er tilnærmet lik aktuell oppfylling.
- Input parameterne er basert på målt vanninnhold i et profil, estimering av opprinnelig (historisk) terrengnivå fra vingeborforsøk, skjærspenning-tøyningskurver inkludert softening fra udrenerte skjærforsøk på prøver tatt i et profil og ekstrapolering av skjærstyrkene basert på NGIs forslag til SHANSEP parametere fra udrenerte forsøk på leire tatt med blokkprøvetaker.
- Bruddlasten fører til en progressiv bruddutvikling som (under konstant last) forplanter seg helt fram til den andre siden av Vestfosselva tilsvarende skredet i 1984.
- Likevekt under den progressive bruddutviklingen er oppnådd ved geometriendringer (setning av fyllingen og en progressiv heving av den passive sonen).
- Størrelsen på geometriendringen er i dette tilfellet delvis styrt av sprøheten til tørrskorpen. Geometriendringer på slutten av analysen samsvarer meget godt med innmålt topografi etter skredet.
- Effekten av softening ved initiering av bruddet er i dette tilfellet funnet til å være mindre enn ca. 10 %.
- Området med softening er kun lokalisert i et lite område under fyllingen idet bruddet blir initiert.
- Effekten av den indre lengden og sprøheten til kvikkleira er i størrelsen lik effekten av usikkerhetene til de andre input parametrene. Resultatene kan derfor ikke benyttes til si noe om forventet skjærbåndtykkelse idet bruddet initieres.
- I grenselikevektsbetraktningene er det vist at effekten av tøyningskompatibilitet er mindre enn 10 % i form av reduksjon av sikkerhetsfaktor.

Videre analyser i de påfølgende delprosjektene i dette prosjektet vil prøve å etablere et statistisk grunnlag for en ”korreksjonsfaktor” til bruk i design. Der ulike initialtilstander og parametere tas hensyn til.

9 Referanser

Andresen, L., Jostad, H.P. og Høeg, K. (2002), ”Numerical Procedure for Assessing the Capacity of Anisotropic and Strain-Softening Clay”, Proc. 5th World Congr. Comp. Mech. - WCCM V, Wien, Østerrike

Andresen, L. og Jostad, H.P. (2004), “Analyses of progressive failure in long natural slopes”, In G. Pande and S. Pieruszczak (Eds.), Proceedings of NUMOG IX. Int. Synp. On Num. Mod. In Geomech., Ottawa, Canada, pp. 603–608.

Andresen, L. og Jostad, H.P. (2007), “Numerical modeling of failure mechanisms in sensitive soft clay – application to offshore geohazards”, Offshore Technology Conference, 37. Houston 2007, Proceedings paper 18650

Bernander, S. (2000), “Progressive Landslides in Long Natural Slopes”, Licentiate Thesis, Luleå University of Technology, Sverige

Bernander, S. (2011), “Progressive Landslides in Long Natural Slopes: Formation, potential extensions and configuration of finished slides in strain-softening soils”, Doctor Thesis, Luleå University of Technology, Sverige

Berre, T., Lunne, T, Andersen, K.H., Strandvik, S., Sjursen, M. (2007), ”Potensial Improvements of Design Parameters by Taking Block Samples of Soft Marine Norwegian Clays”. Canadian Geotechnical Journal, No. 44, pp. 698-716

Bonadies, F. (2012), ”Modelling the progressive failure in natural slopes of sensitive clay”, Master Thesis, Università degli Studi di Salerno

Eide, O. (1955), ” Skredet ved Bekkelaget i Oslo 7. oktober 1953”, NGI publikasjon 011

Eide, O. og Bjerrum, L. (1955), ”The slide at Bekkelaget”, Geotechnique, No 5. pp. 88 -100

Gylland, A. (2009): ”Progressiv bruddutvikling i sensitive leire”. Geoteknikkdagen 27. november 2009

Grimstad, G., Andresen, L. and Jostad, H.P. (2011), “NGI ADP: Anisotropic Shear Strength Model for Clay”, International Journal for Numerical and Analytical Methods in Geomechanics, DOI: 10.1002/nag.1016

Grimstad, G., Jostad, H.P. og Andresen, L. (2010), ”Undrained capacity analyses of sensitive clays using the nonlocal strain approach”, 9th HSTAM International Congress on Mechanics Vardoulakis mini-symposia, Limassol, Kypros, 12. – 14. Juli, 2010

Janbu, N. (1970), ”Grunnlag i geoteknikk”, Tapir Forlag, Trondheim

Jostad H. P., Andresen L. og Thakur V. (2006), "Calculation of shear band thickness in sensitive clays" European Conference on Numerical Methods in Geotechnical Engineering, 6. Graz, Østerrike 2006. Proceedings, side: 27-32

Jostad, H.P. og Grimstad, G. (2011), "Comparison of distribution functions for the non-local strain approach", Proc., Sec. Int. Symp. on Computational Geomechanics (ComGeo II), Cavtat-Dubrovnik, Kroatia

Karlsrud, K. (1984), "Geologic aspects of slope stability problems, Progressive failure in stiff overconsolidated and soft sensitive clays", Contribution to discussion session 9A – ICSMFE

Karlsrud, K. og Hernandez-Martinez, F.G. (2012). "Stress-strain-and strength characteristics of clays from high quality block samples". To be published Can. Geot. Journal.

Ladd, C.C. og Foot, R. (1974), "New Design Procedure for Stability of Soft Clays", Journal of Geotechnical Engineering Division, ASCE, Vol. 100, pp. 763-786

Mayne, P.W. og Kulhawy, F.H. (1982), "K_0-OCR relationships in soil", Journal of Geotechnical Engineering, Vol. 108 (GT6), 851-872

NGI (1974), "Geotechnical investigation of the Sem slide", NGI rapport

NGI (1982), "Stabilitetsvurdering for Strandajordet, Vestfossen", NGI rapport 82032-1

NGI (1982), "Stabilitetsvurdering for Strandajordet, Vestfossen, basert på supplerende boringer", NGI rapport 82032-2

NGI (1984), "Strandajordet, Vestfossen, Utredning vedrørende utglidningen den 11. september 1984, samt de stabilitetsmessige konsekvenser for idrettsanlegget", NGI rapport 82032-3

NGI (1985), "Stabilitetsforholdene på Strandajordet, Vestfossen etter utglidningen den 11. september 1984", NGI rapport 85002-1

NGI (2011), "Vurdering av utvidelse av driftsbygning Vålen, Geoteknisk vurdering av ny gjødselkum og utvidelse av driftsbygning Vålen", NGI rapport 20100823-00-1-R

NGI (2011), "Data base for tests on high quality block samples on clay. Summary of compressibility, strength and deformation parameters in relation to index properties". Report 20051014-1, 2011.

NGI (2012), ”Effekt av progressiv bruddutvikling for utbygging i områder med kvikkleire, A1 Numerisk metode for beregning av udrenert brudd i sensitive materialer”, NGI rapport 20092128-00-4-R

NVE (2011), ”Veileder: Vurdering av områdestabilitet ved utbygging på kvikkleire og andre jordarter med sprøbruddegenskaper”, Vedlegg 1 til NVEs retningslinjer: Flom- og skredfare i arealplaner

Plaxis BV (2009) Plaxis manuals. Plaxis BV. www.plaxis.nl.

Statens vegvesen (2010), “Håndbok 016 – Geoteknikk i vegbygging”, vegvesen.no, 6. utgave

Thakur, V. (2007): ”Strain lokalization in sensitive soft clays”.
Ph.D. Thesis ved NTNU.

Vägverkets oberoende utredningsgrupp, 2007, ”Skredet i Småröd december 2006.” Rapport 1, Analys av skredorsaken, Vägverket

Vedlegg A - "Modelling the progressive failure in natural slopes of sensitive clay"

Francesco Bonadies

Università degli Studi di Salerno

Facoltà di Ingegneria

Corso di Laurea Specialistica in Ingegneria per l'Ambiente ed il Territorio

TESI DI LAUREA

Modelling the progressive failure in natural slopes of sensitive clays

Relatore

Prof. Leonardo Cascini

Co-relatore NTNU

Prof. Steinar Nordal

Co-relatori

Dott. Sabatino Cuomo

PhD Anders Samstad Gylland

Candidato

Francesco Bonadies

Matr: 0620500204

Anno Accademico 2011/12

In cooperation with:

NTNU

NORGES TEKNISK-NATURVITENSKAPELIGE UNIVERSITET

Faculty of Engineering Science and Technology

Department of Civil and Transportation Engineering

Geotechnical Division

www.ntnu.no

Research work developed within:

Erasmus Project

Lifelong Learning Programme

Index

Index of figures

Acknowledgements

I wish to express my gratitude to all the Geotechnical Department at University of Salerno and, in particular, to Professor Leonardo Cascini and Eng. Sabatino Cuomo for their support and encouragement. They also gave me the possibility to do my research thesis in Norway within the Erasmus project at NTNU in Trondheim.

There I found very nice people and I have to thank especially Professor Steinar Nordal and PhD Anders Samstad Gylland for their patience and helpfulness. They taught me everything I know about sensitive clays and we worked hard on my thesis for the entire period I spent in Norway.

All the people I mentioned have always believed in me and it made me work intensely and with enthusiasm.

I would further like to thank Gustav Grimstad at HiOA for the intense period I spent in Oslo and for the contribution and all the advices he gave me for my thesis. I am also grateful to Hans Petter Jostad at NGI for letting me use the NGI-ADPsoft model for my work and for the advices he gave me during my Erasmus period.

Of course all my family, friends, and especially my parents are within the people I thank.

At the end of my work I found a special friend, Stefania, with whom we got over the problems we found, always having fun.

A special thank is for my girlfriend that always supported me and she has been and she is still very important for me.

Sommario

La rottura progressiva di pendii naturali costituiti da argille sensitive è un problema di grande rilevanza in quanto le frane che si innescano in tali terreni possono essere disastrose, come nel caso di Verdal (Norvegia, 1893), o di Rissa (Norvegia, 1978). Oltre che in Scandinavia, problematiche simili si verificano in alcune regioni del Canada e sono intimamente connesse al particolare comportamento meccanico delle argille conseguente all'asportazione, durante l'ultima glaciazione, del sale presente nel terreno saturo di acqua marina, che ha determinato il costituirsi di una struttura molto fragile a livello di elemento di volume.

I fattori innescanti i fenomeni franosi che hanno sede in questi materiali sono rappresentati dall'applicazione di un carico locale e/o da erosione localizzata al piede dei versanti. Generalmente, i fenomeni di primo distacco conseguenti alla applicazione di tali condizioni al contorno aumentano di dimensione, in modo retrogressivo anche in conseguenza di fenomeni di liquefazione dei terreni strettamente legati alla particolare struttura dei terreni alla quale si è fatto in precedenza cenno.

In considerazione dei caratteri di tali fenomeni, questo argomento risulta particolarmente complesso da affrontare sia in ambito di ricerca e sia in campo applicativo. Da questo punto di vista la tesi propone un approfondimento teorico ed alcune applicazioni a casi di studio.

In particolare, la tesi descrive prima il metodo alle differenze finite (FDM) che risulta efficace per la simulazione del fenomeno della rottura progressiva e poi si focalizza su un metodo fisicamente basato proposto da Nordal (2004), confrontando i risultati di quest'ultimo con i risultati conseguiti con metodo FDM per una applicazione reale.

Un'importante alternativa per la modellazione è rappresentata dal metodo agli elementi finiti (FEM) che, pur consentendo una adeguata schematizzazione del comportamento meccanico dei suddetti terreni, è di più difficile applicazione a problemi per la non unicità della soluzione e per la localizzazione delle deformazioni nella banda di taglio. L'utilizzo di tale metodo richiede, quindi, l'uso di avanzati modelli costitutivi quali, ad esempio, il modello NGI ADPsoft.

Nella presente tesi è stato utilizzato il metodo FEM e si è fatto ricorso al modello costitutivo NGI ADPsoft per l'analisi a ritroso della frana di Smaaroed occorsa in Svezia nel 2006. La procedura utilizzata ha reso possibile una soddisfacente simulazione del fenomeno di rottura progressiva che ha caratterizzato la frana in esame. È stata, infine, eseguita un'analisi di sensitività per valutare la capacità del modello di fornire indicazioni sullo stato limite ultimo del pendio in relazione allo spessore della banda di taglio.

Abstract

Progressive failures in natural slopes of sensitive clays is a challenge that many researchers have dealt with during the last decades because slides in quick clays can be extremely disastrous, as in Verdal, (Norway 1893) or Rissa (Norway 1978). Particularly, these phenomena occur in Scandinavia and in some regions of Canada, and they are strongly connected to the mechanical behaviour of quick clays due to the removal from the terrain of salt water, during the last glaciations, that has left a brittle soil structure.

The triggering factors of landslides in sensitive clays are local overloading, river erosion or similar and the slides can escalate in size in a retrogressive manner in which large volumes of clay finally may liquefy. The term progressive failure means that the failure zone develops progressively with a shear mobilization varying from the initial state via the peak value to the residual state during the failure process. The mechanical behaviour of sensitive clays, and in particular quick clays, is one of the difficulties to model failures in this kind of soil. It entails that usual LEM approach is not suitable as it considers the same shear mobilization among the slope at the same time.

The present MSc thesis proposes a theoretical investigation and some applications to real case studies. In particular the thesis illustrates FDM method, that is very useful to understand the progressive failure and its evolution and then it presents a simple model proposed by Nordal (2004) and further developed in this thesis. The model has been applied to a real case and the results are presented and compared with the ones got through FDM.

The thesis also presents an alternative for modelling the FEM (Finite Element Method), which has the potential of capturing complex mechanisms. However, because of the strain softening material behaviour, issues of non-uniqueness and localization must be treated by introducing some advanced devices. A back-analysis of Smaaroed slide (Sweden) has also been done through the advanced constitutive model “NGI ADPsoft”. The model has the capacity to capture the global failure introducing the anisotropy of the material and setting the thickness of the shear band through the internal length parameter. In addiction a brief sensitivity analyses of bearing capacity of the slope varying the internal length is presented. The global failure obtained makes possible to simulate the evolution of the progressive failure analyzed.

1. Introduction

Sensitive clays are a special class of soil due to their loss of strength when remoulded. They present a strain softening behaviour after the peak before reaching the residual shear strength. That is due to the fact that the salt pore water of these marine clays has been leached out since last glaciations and left a brittle mineral structure. Quick clay is the extreme case of a strain-softening material. If disturbed by shearing or overloading, the structure of a quick clay may collapse and the clay will then float in its own pore water.

This M.Sc. thesis is focused on the study of downwards progressive failure in sensitive clays. This kind of failures is due to a fill that may cause a progressive failure that means that the shear strength depends on the deformation and therefore the soil does not keep their maximum undrained strength upon further deformations. It entails that the usual analyses with Limit equilibrium Method (LEM) are not suitable as LEM does not take into account the deformation and so the variation of shear strength in the slope. In the thesis, the behaviour of this kind of soil is described and, after a brief review of the Finite Difference Method (FDM), a simple model proposed by Nordal (2004) has been developed. In addition, a back-analysis of the 2006 Smaaroed slide (Sweden) through FEM is reported; it has been done using NGI ADPsoft model.

In details, the thesis is organized as follows.

The chapter 2 describes the origin and the main features of this kind of soil; mechanical behaviour is also described, together with the strain localization features.

In the chapter 3 the progressive failure is analyzed with the description of some different cases that may happen in sensitive clays. In particular downwards and upwards retrogressive failures are described together with the main features and different situations.

The chapter 4 illustrates some available methods for modelling, describing also the method proposed by Bernarder (2000) based on Finite difference Method. It also presents the Limit Equilibrium Method and the differences between these two methods.

The chapter 5 illustrates a simple method to study downwards progressive failure. This method has been proposed by Nordal (2004) and here it has been developed and applied to the 1977 Tuve slide (Sweden). The results are compared with FDM results, and it also reported a sensitivity analysis of the model.

In the chapter 6, it is analyzed the modelling of downwards progressive failure through FEM. In particular, an advanced constitutive model developed by NGI has been used. A landslide occurred in Sweden is described, Smaaroed slide, and it has been studied through a procedure described in this chapter. This part of the thesis has been supervised, besides the supervisors, also by G. Grimstad from HIOA and H.P. Jostad from NGI. The results are presented and discussed.

The thesis proposes some conclusions reported in the chapter 7 of the present work.

2. *Sensitive clays: a special class of soil*

2.1. Origin and main features

Sensitive clays are a special class of soil due to their loss of strength when remoulded.
The term sensitivity (S_t) is related to the fact that this kind of clay loses shear strength when it is remoulded. Sensitivity is defined as the ratio between the unconfined compressive strength of a soil in an undisturbed condition and the unconfined compressive strength of a remoulded soil (Figure 2.1). In other words it represents the distance between the undrained peak and the residual shear strengths, and it is a measure of the strain-softening that we have to expect in a sensitive clay.

Strain-softening materials exhibit a decrease in shear resistance with an increasing strain after peak shear stress. The degree of sensitivity is different for different clays, and it may differ for the same clay at varying water contents.

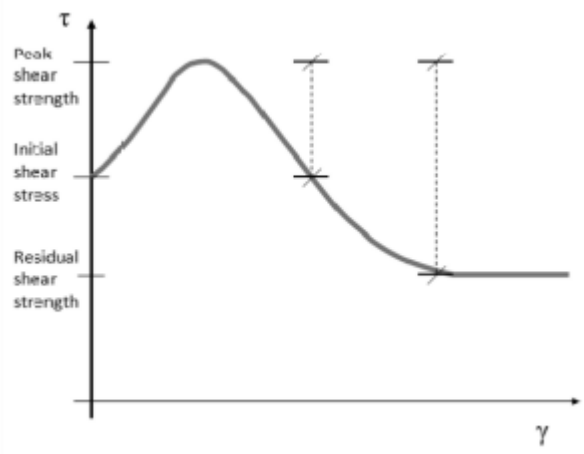

Figure 2.1 Constitutive relationship of a soft clay (Bernarder 2000)

Quick clay is the extreme case of a strain-softening material. In fact quick clay is a sensitive clay that has a sensitivity larger than 50 and a remoulded strength less than 0.5 kPa (Janbu 1970). It can lose its strength virtually instantaneously, and the remoulded shear strength below 0.5 kPa is so low that it is not easy to measure. This feature entails that a quick clay may turn liquid when overloaded.

Soft clays exhibit values of permeability ranging from $1.2x10^{-8}$ to $1.2x10^{-11}$ m/s.

Norwegian marine clays are rather silty (20-40% clay size fraction) and clay minerals are primarily of the illitic and chloritic type. (Karlsrund, 1985)

During the last glacial period, 10.000 years ago, there was a layer of ice with a thickness of several kilometres covering Scandinavia. A large amount of clay was eroded by the ice and deposited in the ocean, in stagnant water.

Clay deposited in this way obtained a loose structure held together by the attraction forces of ions in the salt water.

After the glaciation the land has been raised from the sea, somewhere even 200 m, and clay that was deposited in salt water was lifted above sea level. Consequently freshwater seeping through the clay has washed out the ions of salt, leaving the loose structure intact.

Normally, clay, having grain sizes below 0.002 mm, can settle under special conditions: in salt water. Sea water has a salt content of about 3.5 % (35 g/l), and the salt ions bind the grains in a structure as shown in Figure 2.2. This kind of structure is not strong enough so that a saturated clay has a water content above Attemberg liquid limit.

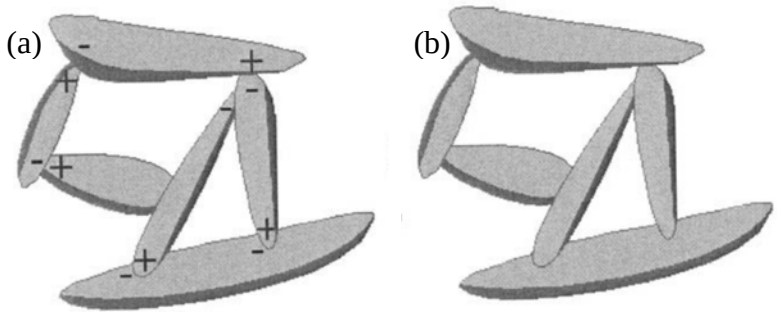

Figure 2.2 Marine clay (a) and soft clay (b), Thakur et all (2006)

Quick clay, instead, due to freshwater that has washed out salt ions from its structure shown in Figure 2.3, already presents in situ a water content above Attemberg limit liquid, because of falling down of Liquid limit decreasing NaCl content.

The Figure 2.3 represents the variation of the liquid and the plasticity limits with an increasing content of chloride of sodium.

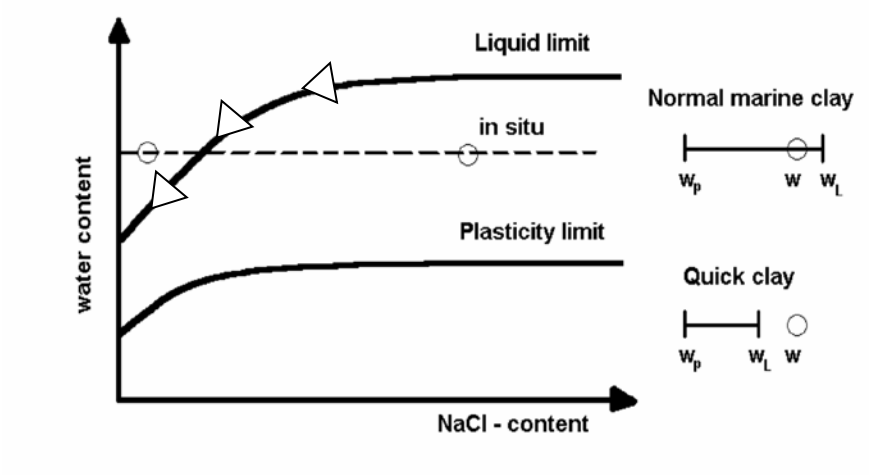

Figure 2.3 Variation of the liquid and plasticity limits with NaCl content, Thakur 2006

From the Figure 2.3 and Figure 2.4 can be seen that chloride of sodium is the most important parameter to have a soft clay as its characteristics are influenced by the content of sodium chloride [Bjerrum, 1954]. Figure 2.4 shows the variation of sensitivity and remoulded and undisturbed strengths for sodium chloride concentrations.

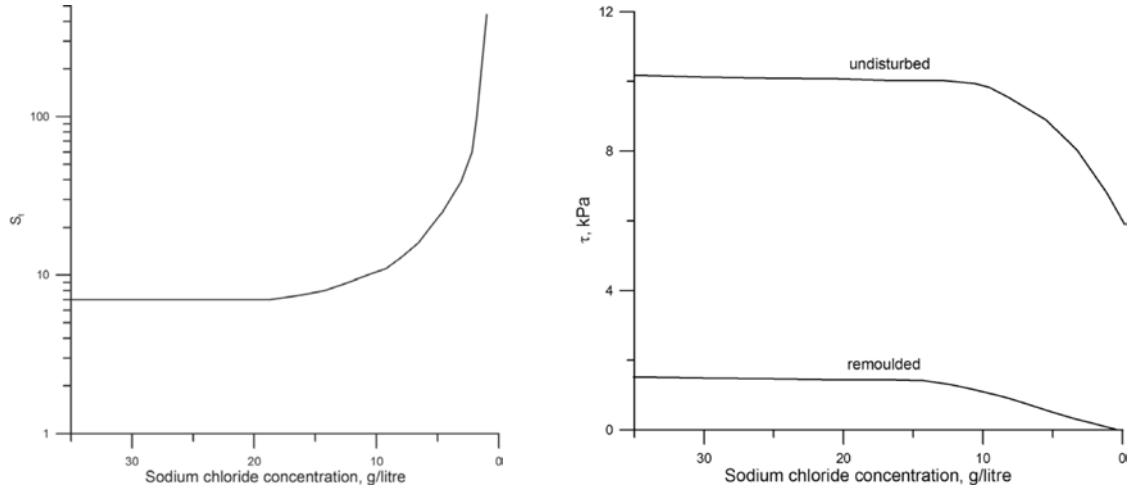

Figure 2.4 Variation of sensitivity and remoulded and undisturbed strengths for sodium chloride concentrations, Bjerrum 1954

The soft clay characteristics are constant for a decreasing of the sodium chloride content as long as the concentration is not too low. For a concentration less than 10 grams/litre the undisturbed strength shows a marked drop while the remoulded strength decreases slightly. The sensitivity presents a strong increase.

When the sodium chloride content in the pore water falls below 0.5 % (5 g/l) the clay becomes a quick clay and it acquires all the characteristics mentioned above.

If disturbed by shearing or overloading, the structure of a quick clay may collapse and the clay will then float in its own pore water [Wood, 2007].

As the structure collapses, the grains lose contact and the inter-granular stresses are reduced at the same time as the material contracts, the grains are dispersed in their own pore pressure. If salt is added, the clay can regain its bindings. Adding salt to quick clay in a large scale has been tried in order to reform the ionic bindings and stabilize it before it slides.

The presence of sensitive clay in the ground depends on leaching processes and then on hydraulic gradients. This arbitrariness of formation may be investigated only making soil borings. In Figure 2.5 an example is represented. Due to upward hydraulic gradients from the bedrock surface a pocket of quick clays has formed, while on the left hand, as the bedrock surface lies deeper, also the hydraulic gradient is smaller and then a non sensitive clay has formed.

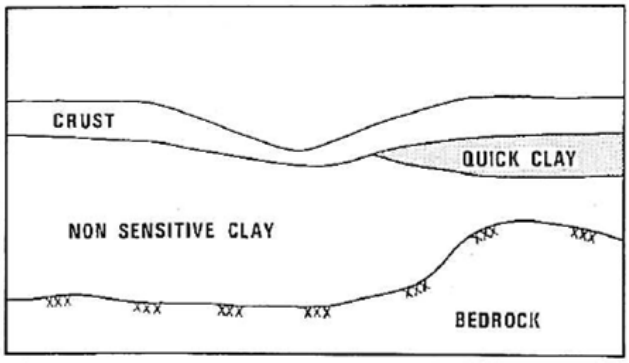

Figure 2.5 Localization of zone of quick clay along eroded stream valley. (Kalsrud 1985)

Moum et al. (1971) showed that a quick clay may turn into a non sensitive clay. This is because of the breakdown of the chlorites that causes the expulsion of magnesium ions. These ions adhere to the clay minerals similar to the original salt ions, which leads to a reduction of the sensitivity of the clay. This could have happened in the zone between the bedrock surface and quick clay in Figure 2.5; probably that clay was a quick clay, while actually it is completely leached (Karlsrud 1985).

Studying landslides occurring along the Namsen river valley, Jørstad and Hutchinson (1961) found out that landslides most frequently occur in the lower end of the river. The lower end of the river is the last to be exposed to leaching processes, so that it is easier to find deposits of quick clay close to the end of a river than inland.

The zone of sensitive clay at the ground surface that is in contact with weathering agents, like desiccation, chemical changes and frost action, presents different properties from the original sensitive clay.

In fact, due to desiccation and chemical changes the clay increases its strength considerably.

Furthermore, desiccation entails the formation of vertical cracks that can go far below the ground surface. Usually the distance between the cracks decreases with the depth.

Frost action breaks desiccated material into small fragments.

Vertical cracks allow water rich of oxygen to flow through the clay, disintegrating clay minerals and releasing cations. These are removed by leaching or are adsorbed at the surface of the clay particles acting as cementing agents (Karlsrud 1985).

2.2. Mechanical behaviour of sensitive clays

2.2.1. General features

Sensitive clays have a particular behaviour under undrained conditions. In fact they present a strain softening behaviour after the peak before reaching the residual shear strength. Other types of soil usually keep their maximum undrained strength upon further deformations.

As the maximum shear strength is reached, the structure starts to collapse and the clay behaves markedly contracting. Under undrained conditions this collapse leads to the development of excess pore pressures which in turn reduces the effective stresses.

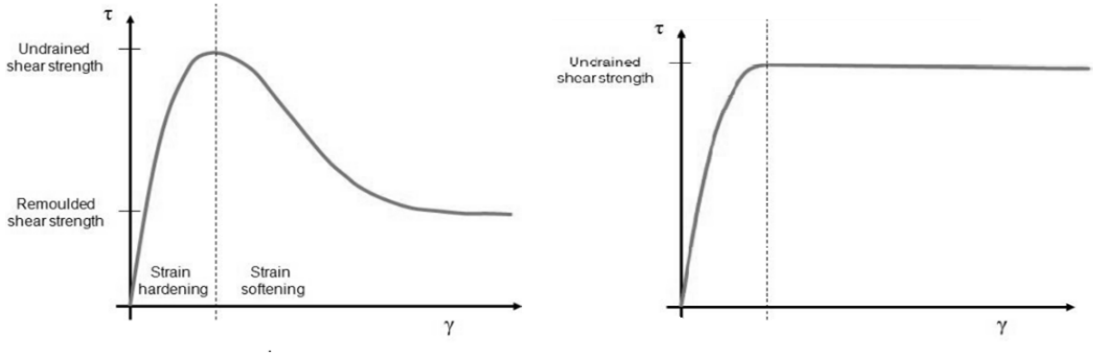

Figure 2.6 Stress-strain curve for typical sensitive clay and for typical non-sensitive clay (Hansenn 2010)

The Figure 2.7 represents a consolidated undrained triaxial test in a highly sensitive quick clay. The effective stress path and the pore pressure show that the clay is contractive in nature. Such laboratory results show that the pore pressure builds up due to collapse of microstructures, which is responsible for the post peak strain softening (Thakur 2007).

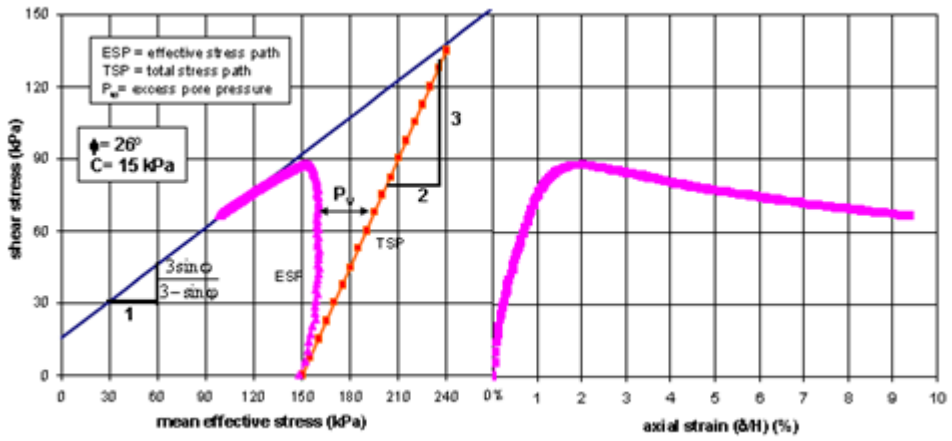

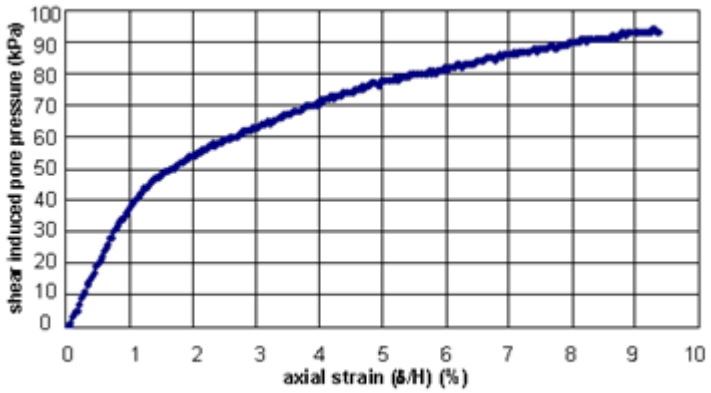

Figure 2.7 Consolidated undrained triaxial test in a highly sensitive quick clay, Thakur 2007

Strain softening behaviour depends on strain rate and over consolidation ratio (OCR).

In fact, as known from field vane tests, a higher strain rate and a higher over consolidation give higher peak strengths. But in sensitive clays, a higher over consolidation gives lower peak strength. This is due to the fact that the OCR set up in the lab should also give a similar trend if consolidation is done properly, but it might be that this process disturbs the clay to such an extent that the structure collapses and the strength is reduced.

Another important parameter is the limit shear strength. For lower strain rates it tends to be higher, whereas for higher strain rates it tends to be lower.

Hence in sensitive clays the peak shear strength and the limit state shear strength tend to increase with decreasing OCR.

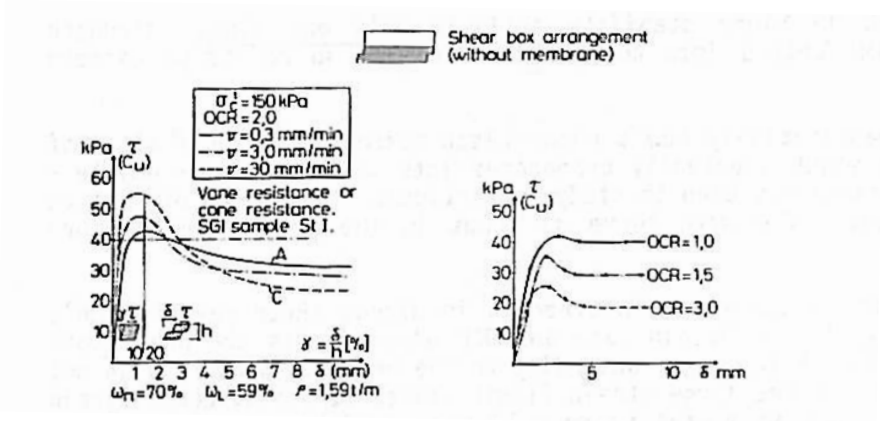

Figure 2.8 Typical test results from shear tests of some Swedish soft clays. (Bernarder 2011)

The rate dependency, which means that the strength and the stiffness are influenced by the strain rate, depends on two factors: the viscous inter-particle action of the soil and the time dependent dissipation of excess pore pressures during loading (Bernarder 1985). During a triaxial test the strain rate has been varied and the result is showed in Figure 2.9.

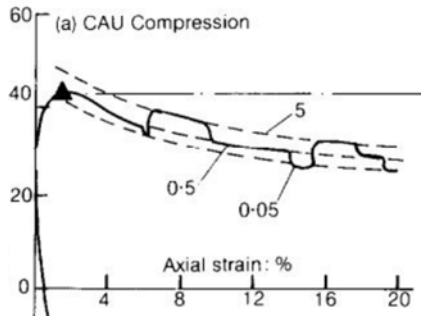

Figure 2.9 Dependency of soft clays on strain rate. Bernarder 2011

When analyzing the failure mechanism and the propagation, it is necessary to use appropriate undrained parameters. In fact, even in the case that a local failure starts under drained conditions, the subsequent rupture takes place under such strain rates that the conditions get undrained. Therefore, it is important to use strain rates in laboratory tests that are related to the actual timing of a slide to get adequate parameters.

Another problem related to sensitive clays is to get samples of high quality.
In fact, even the best tube techniques disturb the structure of a clay, which may result in significant differences in mechanical properties. The quality of samples generally increases with the diameter of the sampling equipment, so that it is better to use block samplers, that have a diameter of 300 mm, for a sensitive clay.

Lacasse et al. (1985) tested two Norwegian quick clays and a Norwegian sensitive clay to study the influence of sampling on the mechanical properties. Their results may be used to have an idea about mechanical properties of a quick clay and a sensitive clay.

In the Figure 2.10 there is a description of some parameters of clays. Emmerstad and Ellingsrud are quick clays, as their sensitivity is more than 50, whereas Onsøy is a sensitive clay.

Table 1. Description of three clays tested

Site	Emmerstad	Ellingsrud	Onsøy
Depth sampled (m)	3–8	7–13	3–10
Water content (%)	40–48	34–40	58–70
$\sigma'_0 > 60\ \mu$	10	9	0
$\sigma'_0 < 2\ \mu$	40	37	60
Liquid limit (%)	24–32	25–29	56–74
Plasticity index (%)	3–12	5– 8	30–44
Sensitivity (FV)	60–∞	60–∞	6–9
Overconsolidation ratio	5 at 4 m 3 at 7 m	2.4 at 7 m 1.4 at 13 m	3 at 3 m 1.5 at 10 m

Figure 2.10 Description of three clays tested (Lacasse et all 1985)

The Figure 2.11 gives some information about the water content, the undrained shear strength and the overburden stress for Emmerstad, a quick clay, and Onsøy, a sensitive clay. It is useful to note how the water content is always higher than the liquid limit, but in sensitive clays it is not as high as in quick clays.

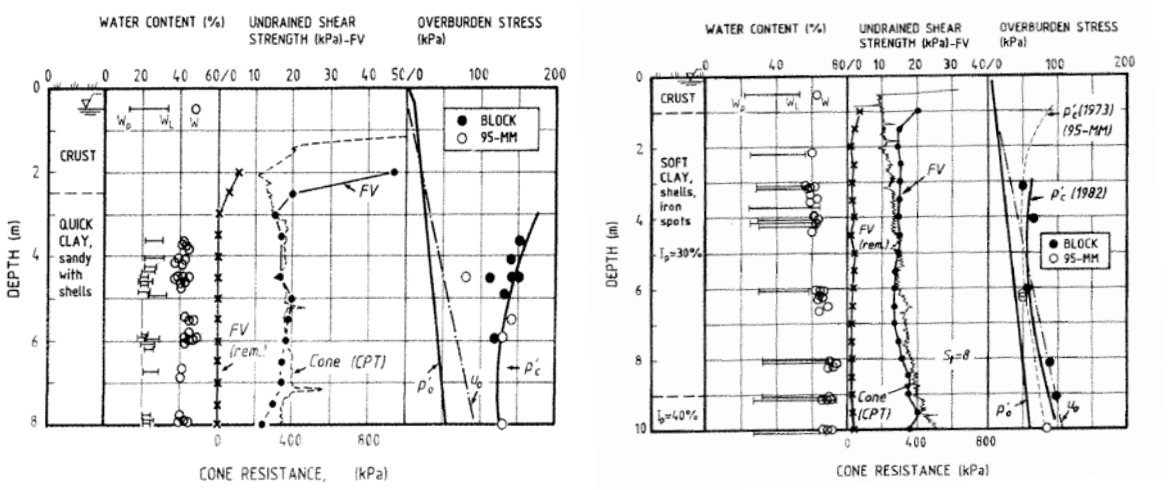

Figure 2.11 Soil profile at Emmerstad and Onsøy sites (Lacasse et all 1985)

2.2.2. Anisotropic behaviour

Sensitive and especially quick clays have a marked different anisotropic behaviour. In this chapter there will be a brief description of this behaviour using Lacasse (1985)'s studies based on the sensitive and quick clays presented in the last chapter. Additionally, the differences between two types of sampling will be explained.

The Figure 2.12 shows the results of triaxial compression and extension tests on all three types of clays.

The extension peak strength is lower than the compression peak strength. As well the brittle of the material is more pronounced in the compression undrained triaxial test, while the ratio between the peak and the residual strength is lower for the extensional test. Furthermore, the peak strain is reached for a lower value in the active triaxial test than in the extensional triaxial test. These differences are less marked for a sensitive clay than for a quick clay.

The specimens were anisotropically consolidated to the in situ effective stresses. There are some differences between the two kinds of sampling, especially for quick clays, since the undrained shear strengths for tests on block samples are 10 to 33 per cent higher than the strengths for tests on 95-mm samples. This involves that Young's modulus at 50 per cent of the peak shear stress can be larger by a factor of 4.

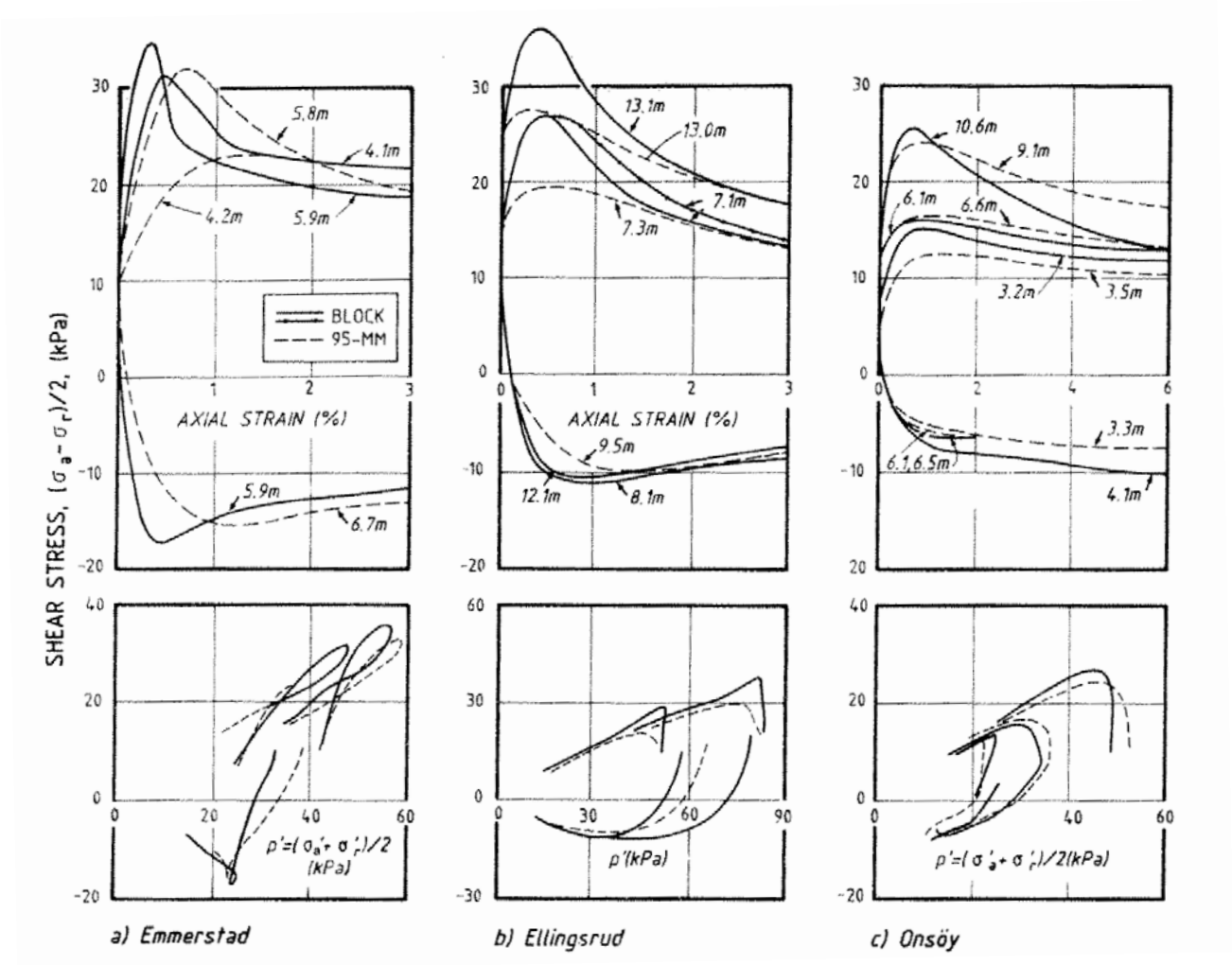

Figure 2.12 Results of a triaxial tests on block and 95-mm samples (Lacasse et all 1985)

As expected a triaxial undrained test and an unconfined compression test show different results, which is due to the high rate of imposed shear strain in the unconfined tests. In addiction

unconfined test does not represent the true effective stress level in the ground. Hence for low OCR samples the peak shear stress is lower than the confined triaxial tests. As shown in Figure 2.13, the undrained shear strength in the unconfined compression test is higher than the peak shear stress in consolidated undrained triaxial tests; this is due to the very high OCR of Emmerstad's clays. In this case there are important differences between the two types of sampling. Sometimes the peak shear stress varies with a factor of 2.

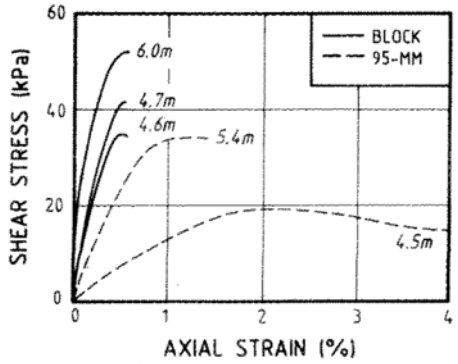

Figure 2.13 Unconfined compression tests on Emmerstad clay samples (Lacasse et al. 1985)

In different condition of stress strain system imposed, because of stress and strain concentrations, direct simple shear tests behaves differently from triaxial and unconfined compression tests. This is shown in Figure 2.14. For direct simple shear tests the soil shows a behaviour that is less brittle than for soils in active triaxial test. For a sensitive clay this behaviour is very slight.

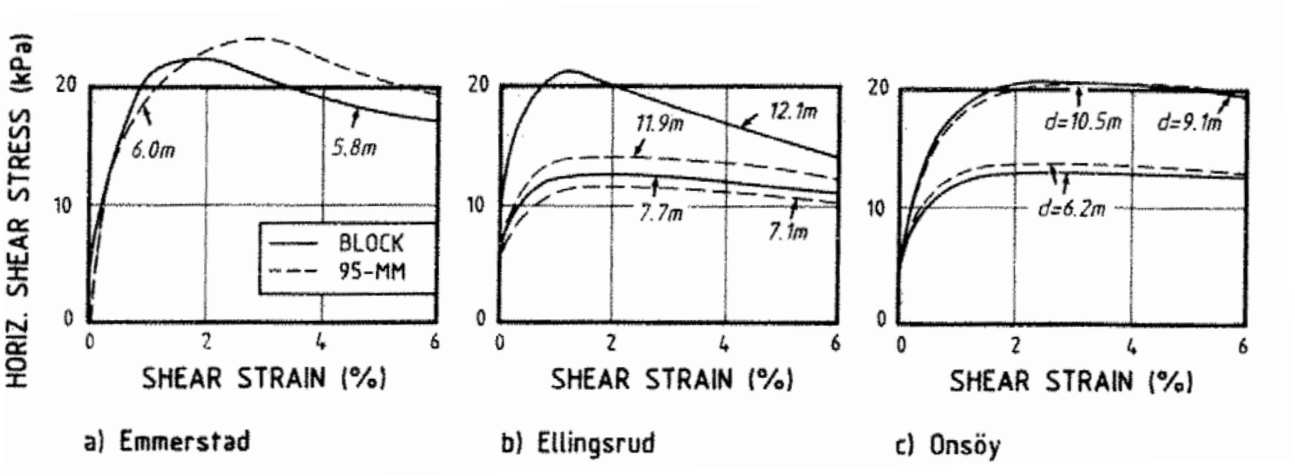

Figure 2.14 Results of direct simple shear tests on block and 95-mm samples. (Lacasse et all 1985)

2.2.3. Strain localization

Observing results from laboratory tests, provided the right conditions, it is noted that sensitive clays collapse in thin zones. In these zones the soil reaches its residual strength and large shear strains develop inside the zones. The soil around these zones presents only small local deformation and unloads elastically.

These zones are called shear bands and they are one of the most challenges to model, as the thickness depends on the particle size, deformation rate, local pore pressure dissipation and boundary condition.

The localization of strains into shear bands is then caused by instability in the behaviour of the material (Thakur 2007). In fact it entails a bifurcation of the continuing solution (load-displacement paths) and it means that there is more than one solution (Thakur 2007).

The Figure 2.15 illustrates the bifurcation problem, in which two different failure modes are shown.

The diffuse failure is when strain softening occurs in all the material points of the soil body, whereas in the localized failure strain softening it occurs only within shear band. As illustrated, the behaviour of the material depends on the thickness of shear bands, in fact thinner shear bands exhibit higher softening modulus in the post peak regime.

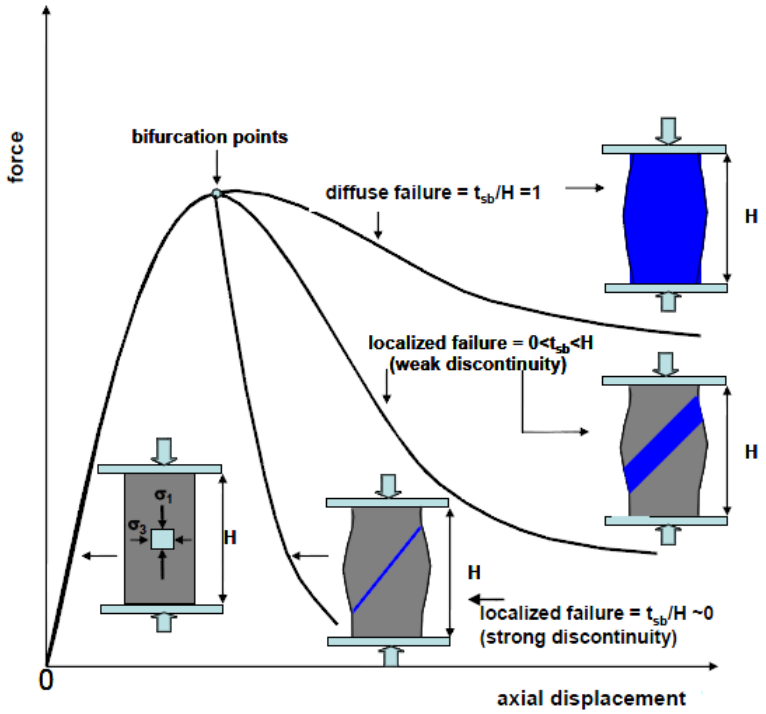

Figure 2.15 Shear band thickness dependent post peak behaviour. Thakur 2007.

Localization issue may be explained by a simple example shown in Figure 2.16.

A cube of soil is sheared and as strains tends to localize within shear band, one get a bifurcation into a softening part (shear band) and an unloading part. As the global response δ can be reached using infinitive thickness of the shear band ($0 \leq t_{sb} \leq H$) it means that there are infinite solutions of the same problem.

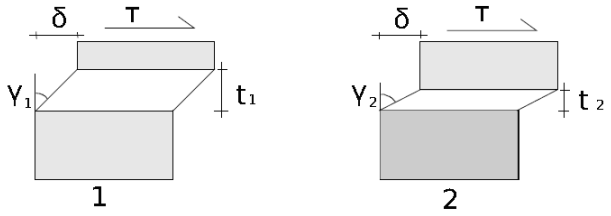

Figure 2.16 Localized shear strain for two cases where the shear bands are of different width (Brubakk and Smith, 2010)

In FEM the width is arbitrary and in principle infinitive solutions could exist, all satisfying global equilibrium; instead shear band shrinks to the minimum size possible and it entails that the results are mesh dependent. However there are some regularization techniques to control the shear band by the internal length parameter.

If the width of the shear band was known, it would be possible to have physical results. But shear band thickness is most of times unknown.

Thickness of shear band may vary from a few microns to several meters and it seems to be a continuous function of the shear band factors. The shear band factor is the ratio of a clay permeability to the applied rate of loading. It has to be noted that it is a numerical simulations. (Thakur 2007).

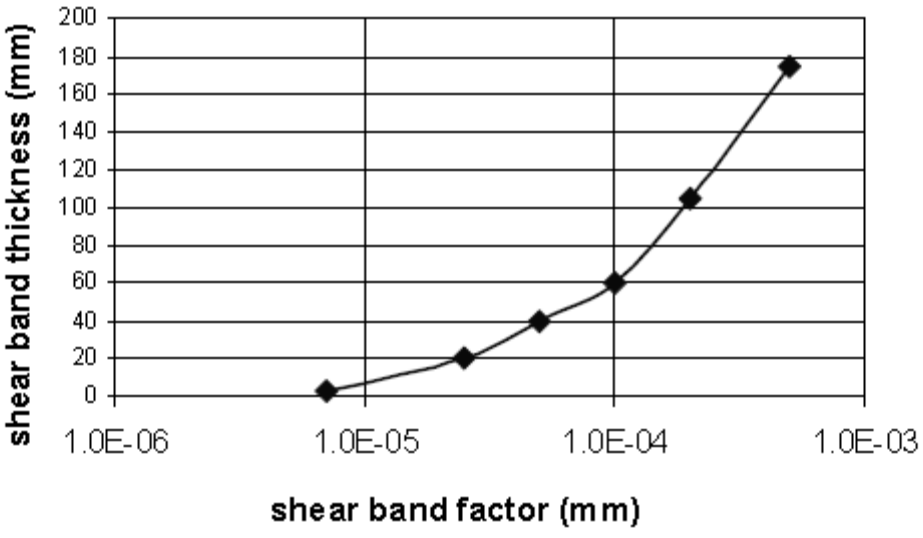

Figure 2.17 Shear band factor dependent thickness of shear band, Thakur 2007

Whether a discontinuity should be defined as weak or strong depends on the physical scale adopted during the study; for instance, shear band thickness of a few millimetres can be considerate as a strong discontinuity when long natural slopes are investigated, however this tiny thickness may play vital role while investigating laboratory test. Thakur (2007) shows a plot with permeability of clay and normalized deformation rates. Each combination of permeability and the normalized deformation rate indicates a specific thickness.

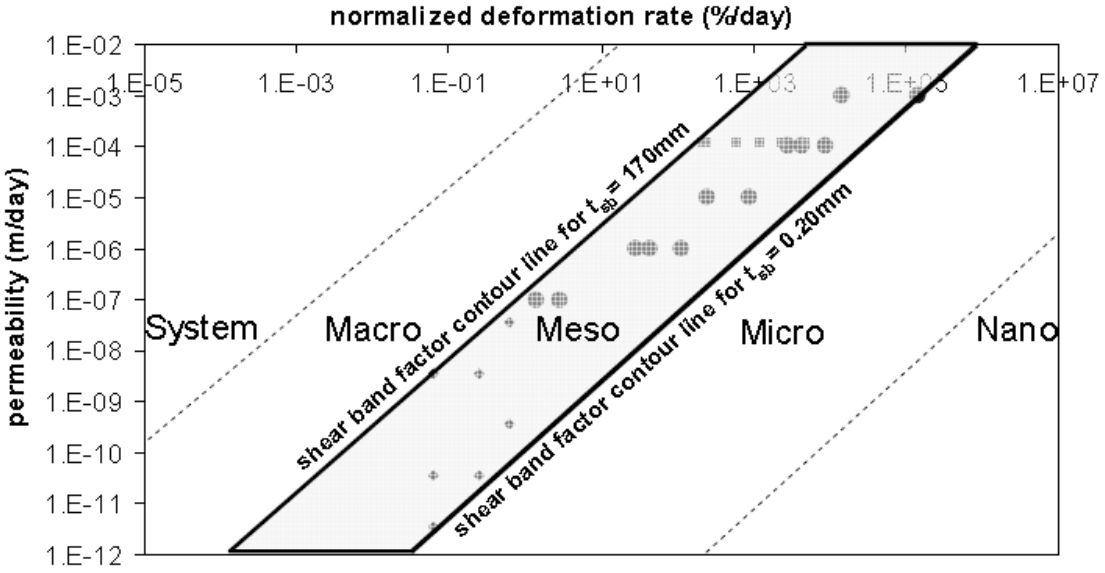

Figure 2.18 Contour lines for shear band factors, Thakur 2007

Meso-scale is the scale of the size of the specimens in laboratory for geotechnical investigations and based on this scale, the shear band factor may divide a problem in either of three categories:

- **Locally drained**: shear induced pore pressure gradient across the shear band becomes particularly zero. Size of model/specimen itself is a representative of the shear band. Strain softening becomes mesh independent and well-posed from a numerical point of view.
- **Locally undrained**: total volumetric strain at every material point may be zero. No dissipation of pore water pressure may occur across the shear band, which ultimately causes in severe strain softening. Shear bands thickness tends to go to zero and reduces with size of elements. This ultimately results in non-uniqueness in the solution.
- **Partial drained condition**: it is possible to have internal volumetric exchange. Volumetric compression in shear bands may be balanced by equal volumetric expansion in elastically unloading parts. A pore pressure gradient establishes across the shear band.

2.2.4. Two examples

Typical Norwegian quick clay values

Lean Norwegian normally consolidated quick clay presents typical undrained shear strength values:

- Triaxial compression $Su^{A} = (0.30 - 0.35)\sigma'_{ac}$;
- Triaxial extension $Su^{P} = (0.08 – 0.12)\sigma'_{ac}$;
- Direct simple shear $Su^{DSS} = (0.16 – 0.22)\sigma'_{ac}$

where σ'_{ac} is the applied axial vertical consolidation stress that corresponds to the in-situ vertical effective stress. This is for clays with Ip ≤ 20% and the results refer to a standard rate of shearing of 0.8% strain pr. hour. (Karlsrud 1985)

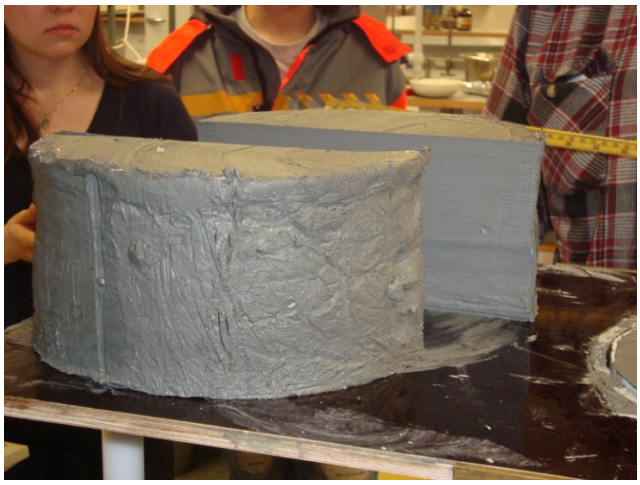

Figure 2.19 Sensitive clay

Typical crust strength values

The crust is formed by weathering agents explained in chapter 2.1.

It can show a very high undrained shear strength: from 50 to 200 kPa, with an apparent cohesion of intact clay that can be up to 20 kPa.

The zone that is affected by weathering agents reaches as deep as 4-6 m below the ground water table.

In boggy, or more in general in areas with upward hydraulic gradients, the crust may be smaller.

The crust may be analyzed in terms of drained parameters also for short term stability, as the cracks get rapid pore pressure equalization. In this case one should be careful using c' and ϕ' parameters as they have been estimated on intact material without taking fissures into account (Karlsrud 1985).

Figure 2.20 Weathering effects on soils (www.safeland.eu)

3. Progressive failure in slopes

3.1. General features

Sensitive clay is a strain-softening material which means that its strength depends on the corresponding strain value. After the peak, in fact, the strength falls down until it reaches a residual strength.

This kind of clay shows a strain-softening behaviour under undrained conditions. Therefore, if a sensitive soil is exposed to a load which is larger than its undrained shear capacity, it will distribute the overshooting load and what it has lost due to strain-softening to the neighbouring soil elements.

This kind of instability case will not be solved by a local failure, like the case of non-sensitive soil, but will propagate until it meets geometrical obstacles or non-sensitive soil. This can potentially result in a global type of failure where a large area can be involved. A failure mechanism like this is called a progressive type of failure.

The fact that the strength varies along the slip surface from the peak to the residual value, entails that it is not possible to integrate the maximum shear strength over the slip surface. It would overestimate the strength along the slip surface.

Bernarder (2000) defines the term progressive failure as:
"A failure propagating along the potential slip surface in strict accordance with a requirement for compatibility of displacements within and outside the potentially sliding body of soil."

Bjerrum (1967) listed three criteria for having a progressive failure:

1. such stress concentrations such that local shear stresses exceed the peak shear strength;
2. the failure zone has to obtain large enough strains so that the soil can approach its residual shear strength;
3. the residual shear strength must be considerably smaller than the peak shear strength (strain-softening behaviour).

For Bernarder (2000) the residual shear strength must be lower than the initial shear stress for a failure to propagate in an infinite long slope.

In Figure 3.1 a progressive failure is represented. It shows the shear stress distribution along a potential failure surface for a gently inclined slope. It can be seen that there are different stress strains and hence different shear stresses along the potential slip surface. When the curves go below the initial shear stress level, they add load to the following points.

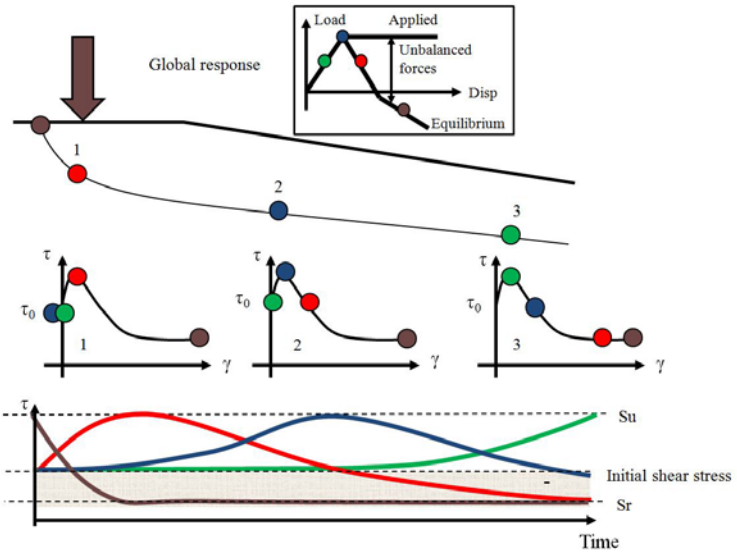

Figure 3.1 Progressive failure mechanism. After Gylland (2009)

According to Bernander (2011), a landslide that involves highly strain-softening soils has to be studied considering different phases and not just a single case of static loading.

A sensitive slope failure is of a different character depending on how the in situ stresses (τ_0) relate to the residual shear strengths (c_R). It depends on the magnitude and the rate of strain induced by an additional loading effect or by other triggering agents. There might be two different cases:

1. Case 1 $c_R < \tau_0$

If the residual shear stress is lower than the in situ stress and the deformations induced by the additional load are large enough that the stress falls below the in situ stress, a progressive failure of a dynamic character may be triggered at a critical value of the additional loading effect. In this case there are two possible scenarios:

1.1 A veritable landslide, if the down-slope earth pressures exceed the current passive resistance.

1.2 A moderate or insignificant displacement if the down-slope earth pressures do not exceed the passive resistance.

2. Case 2 $c_R > \tau_0$

If the residual shear stress is higher than the in situ stress throughout the duration of the impact of the additional load, the redistribution of earth pressures related to strain softening just entails an increasing down-slope displacement due to the additional load.

This condition probably represents the most frequent situation (Bernarder 2011).

Progressive failure can be divided into several subcategories dependent on the initial failure and geometry during the failure process:

1. Downwards progressive slides
2. Laterally progressive slides
3. Upwards progressive / retrogressive slides

3.2. Downwards/laterally progressive slides

Downwards progressive landslides are characterized by the fact that a local instability in the upper part of the slope propagates downwards and cause a global failure.
In this case the triggering agent could be a load. The failure mechanism is represented in Figure 3.2.

Downhill progressive landslides emerge from an initial local instability in the upper part of a slope, which propagates down the slope generating a major increase in horizontal earth pressures in less inclined ground further downhill. If the total pressure exceeds the current passive Rankine resistance in some parts, a global ground displacement takes place. Typically this involves large areas of inherently stable ground ahead of the foot of the slope. Downhill progressive landslides are characterized by a significant growth of the mean axial stress – i.e. in this context the normal stress acting in the downhill direction.

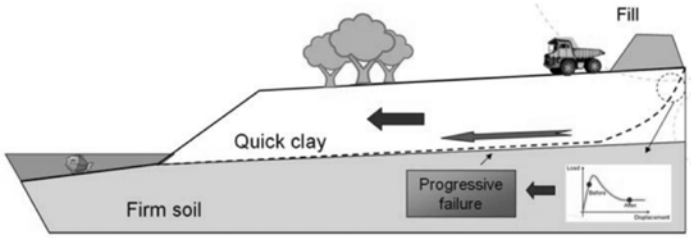

Figure 3.2 Downwards progressive slides. After Gylland (2009)

According to Bernarder (2011) a down-slope progressive failure presents six different phases.

- **Phase 1** The existing in situ stage
- **Phase 2** The disturbance phase, or the triggering mechanism, in which the soil element under the fill presents a post peak shear strength equal to the initial shear stress.
- **Phase 3** The virtual dynamic load transfer, in which there is a dynamic redistribution of forces in the slope. This is described as progressive failure.
- **Phase 4** Permanent or transitory static equilibrium, depending on whether the passive Rankine resistance is high enough or not to hold the maximum earth pressure, which is due to the additional load. If the passive Rankine resistance is higher than the maximum earth pressure, there will be a progressive failure but not a real slide.
- **Phase 5** The final breakdown, which is the main slide event. It happens if the passive Rankine resistance is lower than the maximum earth pressure.
- ***Phase 6*** Terminal state of equilibrium

The six phases are described in chapter 4.1.

To classify a slide as plastic or progressive failure, Bernarder (2000) states that only the final appearance of a landslide could give some indications.

In fact in an ideal-plastic failure (Figure 3.3) there is a short passive Rankine zone and then a heave over a short distance, whereas in a progressive failure (Figure 3.4) the passive Rankine zone as well as the heave is longer. It is well explained in the chapter 3.4.

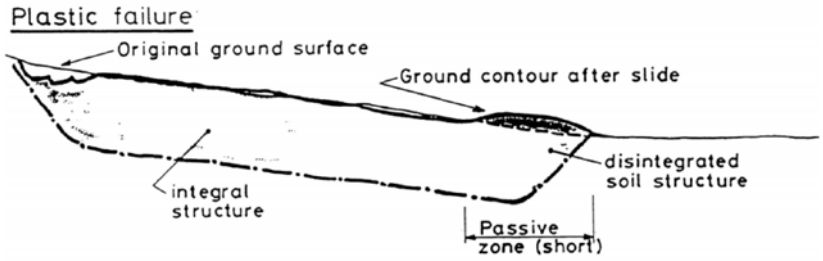

Figure 3.3 Plastic failure. After Bernarder 2011

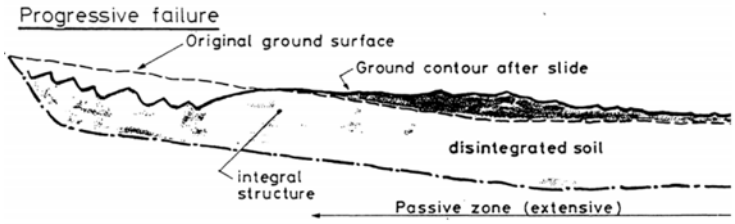

Figure 3.4 Progressive failure. After Bernarder 2011

Laterally progressive slides

Laterally progressive slides have a larger width than length in the sliding direction. In this case a local instability is transferred sideways until it finds stable soil masses.

For Bernarder (2011), this kind of slide can be controlled by ensuring an adequate safety factor for the most critical section in direction of the slope. An example of this mechanism is a slab avalanche in snow.

3.3. Upwards retrogressive slides

Upwards progressive slides are characterized by a down-slope initial failure, which propagates upwards along the slope, causing a global failure.

A premise to have a retrogressive failure is that the sliding material turns liquid and flows out of the slide foot (Grande and Janbu 1980).

Characteristic for a retrogressive failure is the reduction of the down-slope support as well as the tendency to develop active earth pressure instead of passive pressure, which is normally typical for a down-slope failure. In the end the whole slope may disintegrated in an active Rankine state. This is often denoted as a spread failure (Bernarder 2011).

The extension in the downhill direction resulting from the slide movement takes place along a continuous *preformed* failure surface. However, in some cases the disintegration of the soil mass takes place in form of a series of cylindrical active slides that do not derive from a continuous process (Bernarder 2011).

Retrogressive landslides develop as a result of failing or insufficient support in terms of passive earth pressure resistance in the lower parts of the slope. There exists as a rule no definable "post-dynamic" second state of equilibrium of the kind typical of downhill progressive slides, where predictable state of equilibrium are normally possible due to the build up of passive resistance over more level ground. (Bernarder 2011)

A potential retrogressive landslide can be divided into different phases:

- ***Phase 1*** The long time in situ shear stress and earth pressure conditions;
- ***Phase 2*** The disturbance condition, which depends on the kind of agents, and furthermore on the rate of loading and on the time (i.e. the analysis of uphill failure propagation set off by agents applied at varying rates of loading or acting during specifically shorter periods of time).
    1) *Disturbance generated by short-time effects* like seismic tremor or human activities such as excavation, vibratory compaction and pile driving. Man-made interference with the hydrological regime, resulting in higher peak pore water pressures than even before also belongs to this category.
    2) *Disturbance related to long-time degradation such* as weathering and loss of shear strength due to chemical change.

3) *Disturbance related to increased mobilization* of shear resistance due to erosion and permanent adverse changes of the down-slope support and/or of the hydrological regime.

- ***Phase 3*** Dynamic disintegration phase Due to insufficient passive earth pressure resistance at the foot of the slope a post dynamic state of is not defined in a retrogressive slide and it's not easy to predict the mode of dynamic disintegration features. (Bernarder 2011)

Upwards slides can exhibit different features, depending on the geometry of the slope, the firm bottom and the material involved.

1) Serial retrogressive slides

In this case the failure can be described as piece by piece failure (Hansen).

The disintegration of the soil mass takes place in the form of a series of cylindrical active slides generated by successively vanishing down-slope support. Like shown in Figure 3.5 this kind of slide occurs if there is a steep scarp formed in highly deformation-softening homogenous clay. An important prerequisite for serial retrogressive slides is that the disintegrated soil mass, involved in the preceding slide, moves away further downhill in a virtually liquid state, which results from extreme sensitivity and/or to specific slope geometry (Figure 3.8).

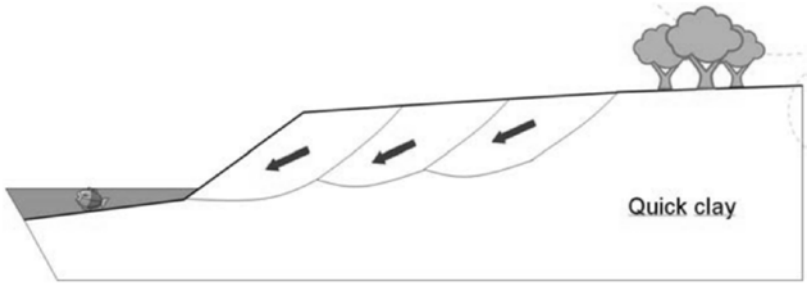

Figure 3.5 Upwards progressive mode. After Gylland 2009

Retrogressive landslides are triggered by the loss of support at the foot of the slope. This may be caused by the erosion of a riverbank, the degradation of the soil resistance due to decreasing effective stresses, a seismic tremor or by man-made activities like excavations, vibrator activities, pile driving and hydrological intervention.

Retrogressive slides normally occur in over-consolidated clay formations, because hard clay is a prerequisite for having high steep scarps and deep river canyons (Bernarder 2011).

Retrogressive sliding is not a continuous process: the slides take place in different moments, at random intervals. Therefore, the energies released in the individual slides are not contemporary or cumulative (Bernarder 2011).

2) Collapse of parts of the soil mass in brittle active failure –"column failure"

This progressive failure is owing to a significant reduction of the horizontal earth pressure in large portions of a slope. This is described by Janbu (1979), where a failure mechanism in quick clay due to the total loss of horizontal normal stress, which means a reduction of the ratio $\sigma_{hor}/\sigma_{vert}$ ($\approx\sigma_3/\sigma_1$), leaded to a vertical collapse of large sections of the soil mass. It was called "column failure".

Due to the insufficient or lacking horizontal stress, the sensitive soil mass left the site as a mudflow. The final phases of the Rissa slide exemplify a soil break-down of this kind (Bernarder 2011).

3) *Simultaneous collapse of the entire slope in active failure –"spreads"*

The slope in this case is of non-sensitive clay, except a deformation-softening layer in the soil profile. The failure progresses from the disturbance at the foot of the slope right up to the crest, which is followed by the disintegration in active failure. During this period the soil mass is an integral block until the down-slope displacements are high enough that the related horizontal earth pressure de-loading ends in general active failure.

The final appearance of the ground surface is like "horsts and grabens", and it extends all over the ground involved in the earth movement.

Slides of this kind are often denoted as "spreads" (Bernarder 2011).

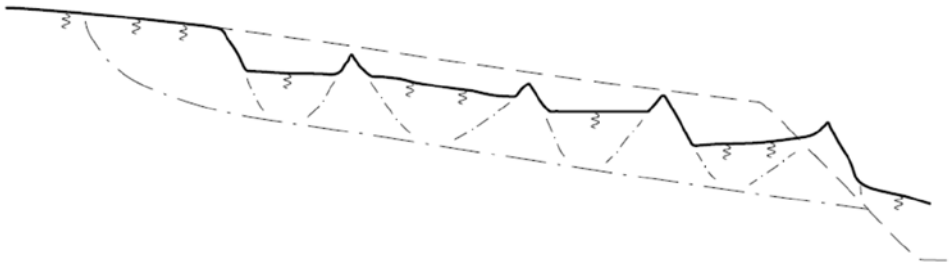

Figure 3.6 Spread failure (Bernarder 2011)

4) Flake type failure

Another kind of retrogressive failure is illustrated in Figure 3.7. It is typically caused by a collapse in a sensitive layer of clay beneath a layer of firm soil, causing a monolithic flake sliding on top of the liquefied clay.

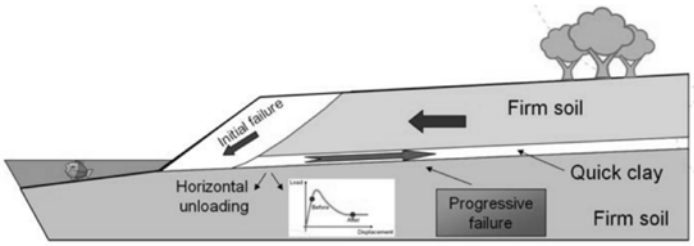

Figure 3.7 Flake-type failure mode (Gylland 2009)

5) Intrinsic deformation-induced retrogressive failure condition

Intrinsic long-time or "self-generating" failures occur in highly over-consolidated clay due to a deformation that entails a loss of shear resistance, which generates more deformations and so on.

The deformations are owed to creep and to the loss of down-slope supports because of erosion. This kind of active failure does not occur before the critical displacement (σ_{cr}) is reached (Bernarder 2011). The critical displacement (σ_{cr}) is explained in chapter 4.1.

Figure 3.8 The Rissa slide. NGI-2010

3.4. Some remarks

1 Shear strength and ductility of clays intimately depend on a number of ambient conditions in the soil structure. Such conditions are, for instance, the state and magnitude of principal stresses, the effective stress situation (*OCR*), and the level of shear strain and deformation. The time scale and the rate of loading are also of paramount importance to the strength characteristics of soft clays that are therefore often of a transitory nature. For instance, laboratory shear tests according to current practices are often carried out at strain rates in the range of 0.3 to 0.5 % per hour although the rate of strain (or deformation) may vary widely in different phases of a slide.

Reliable values of the residual shear strength c_R can only be established if the current rate of applying the additional load (or the disturbance) is considered. Moreover, the prevailing drainage conditions in the incipient failure zone have to be taken into account.

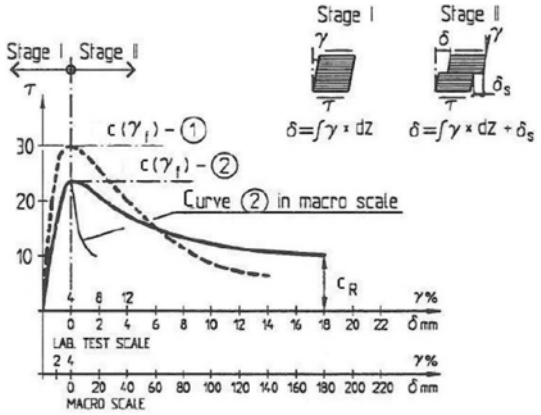

Figure 3.9 Assumed types of stress/deformation relationships τ (γ) and c_R (γ) of the soil in the example. Curves 1 and 2 exemplify such relationships at different rates of loading. c_R is the large deformation residual value of c_R(γ). After Bernarder 2011

2 Brittle progressive failure related to deformation-softening is possible if, in part of the slope, the residual shear strength (c_R) falls below the in situ shear stress (τ_0) : $c_R\ (x) < \tau_0\ (x)$. Progressive failure may then be generated by a virtually dynamic redistribution of unbalanced forces (earth pressures) resulting from gradually increasing deformations and associated strain softening.

If resulting down-slope earth pressures exceed current passive resistance causing a veritable landslide, otherwise displacement of earth masses will be moderate or insignificant.

On the other hand, if $c_R(x) > \tau_0(x)$ throughout the duration of the impact of additional loading, the redistribution of earth pressure will lead to increase the down-slope displacements, as the additional loading is increased.

3 It's very important to know the in-situ stress distribution because, for example, if τ_0 is close to the peak there will be little resistance that the slope could exhibit. In fact, under a little load the neighbouring elements will be subjected also to an overload due to strain softening.

4 Resistance against failure along planes essentially following firm bottom or sedimentary strata is, subject to the degree of deformation-softening, considerably less than the resistances based on shorter failure planes surfacing in the sloping ground closer to the applied local load, like ideal plastic approach.

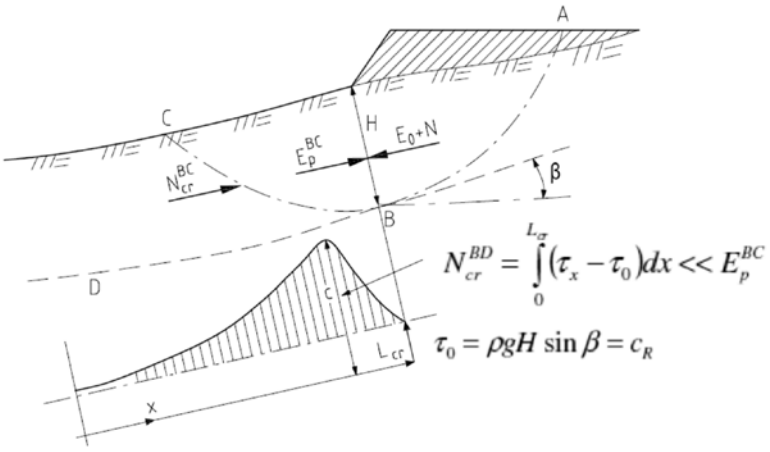

Figure 3.10 Maximum passive earth pressure that can be mobilized along the failure plane BD if deformations are considered. Note that $N_{cr} << E_P^{BC} - E_0$. After Bernarder 2011.

5 The ratio between L_{cr} and L offers an indication regarding the applicability of analyses based on ideal-plastic soil properties. In fact for low values of this ratio, ideal-plastic approach is not suitable. As L is the total length of the potential slide, it includes also a relevant portion of level ground beyond the foot of the slope. The critical length (L_{cr}) corresponding to the critical load N_{cr}, indicates in some measure the maximum length of a slide, that can be studied on the basis of 'ideal-plastic' soil properties with any prospect of attaining reasonable accuracy.

6 Another characteristic of the progressive failure is the final appearance of a landslide; in particular the final spread.

In an ideal-plastic failure, no significant build-up of earth pressures can take place down the slope, and the passive Rankine zone therefore is short. A short passive Rankine zone gives heave over a short distance in the lower end of the slide (Figure 3.3).

Progressive deformation mode can only be conceived over mildly sloping ground when considerably deformation-softening in the progressive phase of the slide comes in to play. This will then result in a long passive Rankine zone (Figure 3.4).

7 The failure zones and slip surfaces tend to develop into level ground far (i.e. hundreds of meters) beyond the foot of a slope and that *prior to* the incidence of the general extensive passive spread failure.

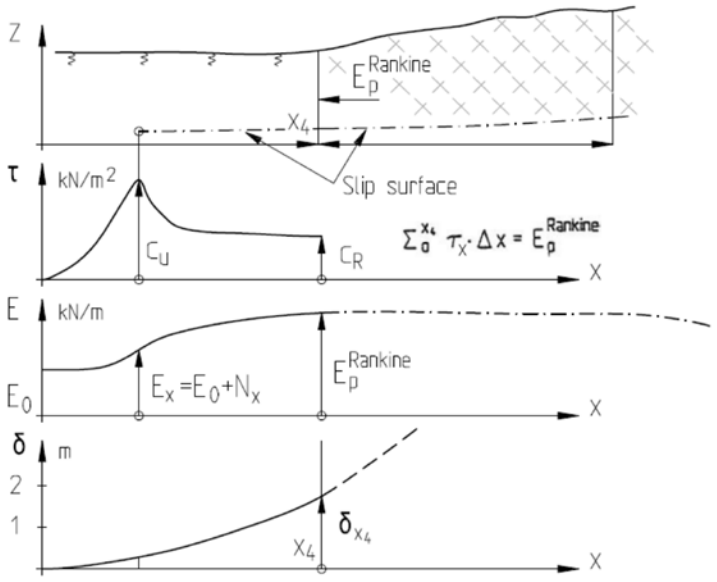

Figure 3.11 Conditions at the far end of a downward progressive landslide. Note displacement and considerable extension of failure zone and slip surface outside the limit of the slide proper. After Bernarder 2011

8 After the peak has been reached, the body above the slip surface unloads elastically. It means that all the deformations are concentrated into the shear band and also that this zone is characterized by a stress level lower than the peak.

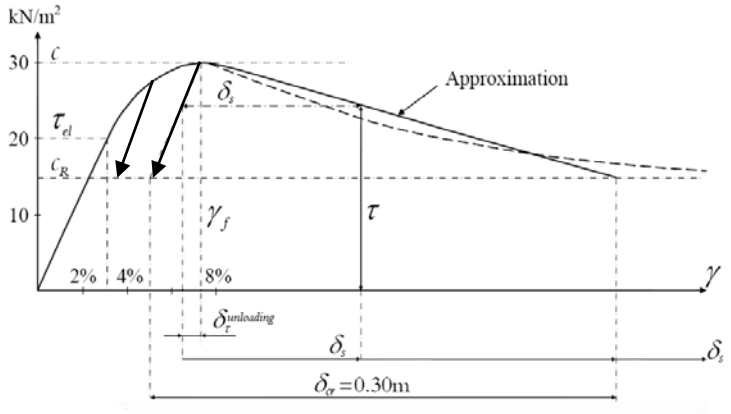

Figure 3.12 Body behaviour after the peak has been reached. After Bernarder 2011.

4. Available approaches for progressive slides

4.1. FDM: Finite Difference Method

The Bernarder's method (Bernarder 2011) is a way to study the progressive failure in soft clays, which are present in the Scandinavia's area and in part of Canada. The method is based on the congruency between the displacement owing to compression due to the earth pressure and the shear deformation.

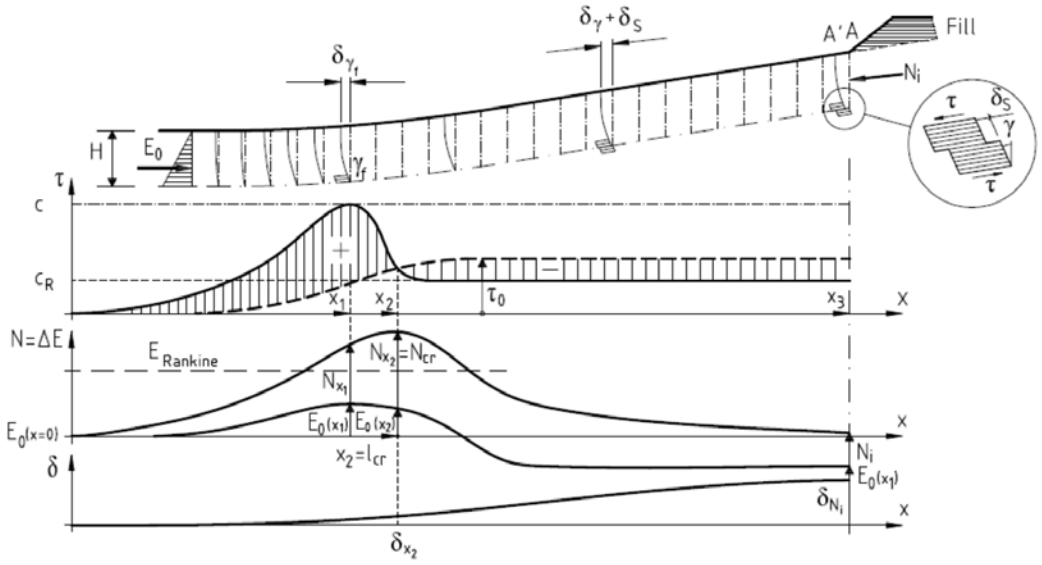

Figure 4.1 Possible new state of equilibrium (Phase 4) resulting from local up-slope failure and the ensuing earth pressure redistribution in Phase 3. Bernarder 2011

It is called FDM, finite difference method, because it uses finite difference instead of other numerical methods such as, for instance, the finite element (FEM).

The basic mathematical approach used is that of finite differences in a two-dimensional model, however it is possible to have any desired three-dimensional shape of the sliding body varying the width b(x).

The potentially sliding soil volume is subdivided into discrete vertical elements of length Δx with the coordinate (x) taken positive in the up-slope direction. Every element of length Δx is divided into discrete vertical elements of height Δz.

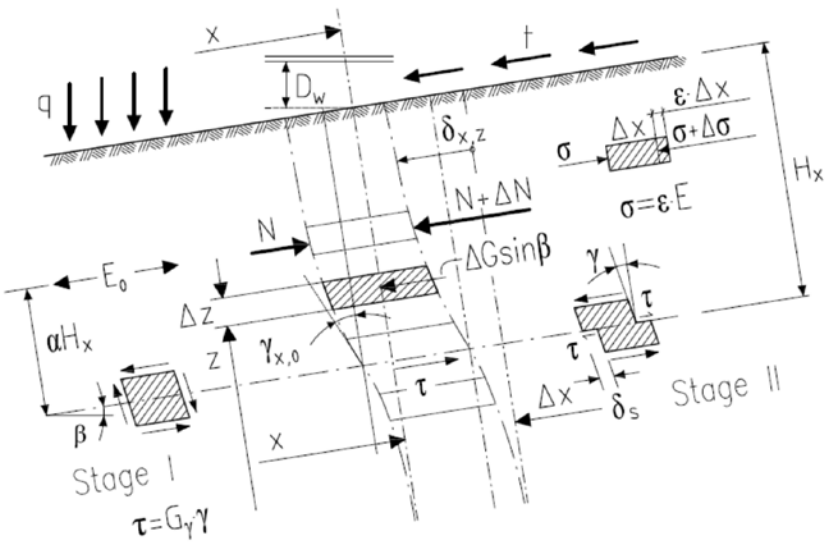

Figure 4.2 FDM - model – denotations. After Bernarder 2011

Bernarder considers the deformation of the only first third (α) of the whole height because here the resultant of the earth pressure is applied. α, in reality, varies along a slope, but, according to Bernarder, the variation is not so significant and it is assumed equal to 0.33 in all the slope.

A crucial feature in the FDM-approach is distinguishing between two radically different conditions of stress and deformation – i.e. the Stages I and II.

Stage I is before the peak is reached and the down-slope displacement corresponds to the accumulated deformation due to shear strain and the slip surface has not yet formed.

In Stage II, instead, the down-slope axial displacement corresponds to the accumulated deformation due to shear strain and slip in the failure surface.

The constitutive relationship is also divided into two stages (I and II) simulating the conditions before and after the formation of a slip surface.

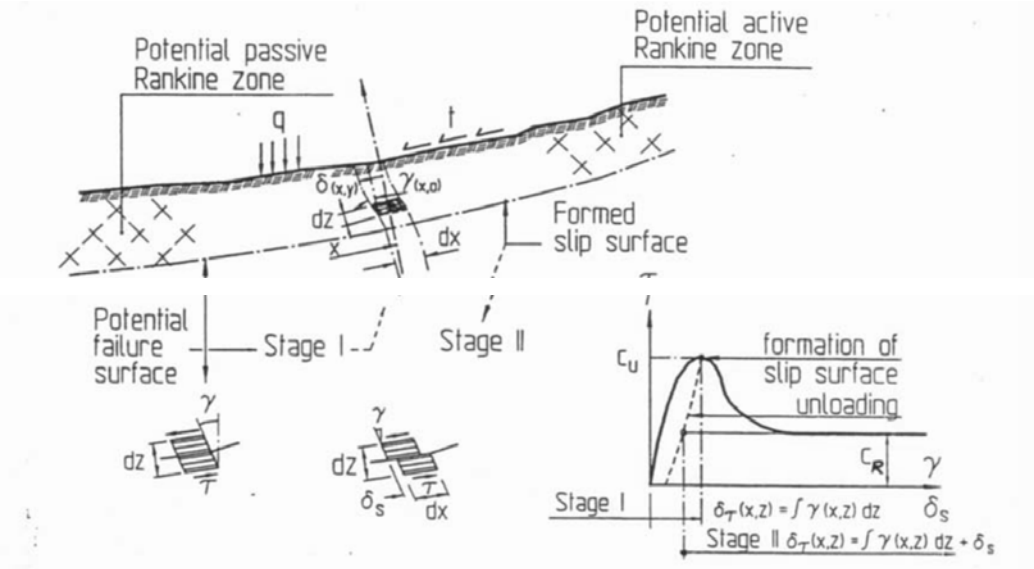

Figure 4.3 Structure and development of a down-slope progressive landslide – notations and principles. After Bernarder 2011

The FDM accounts of time effects, and it means that the slide events cannot be correctly studied as a *unique case* of *static* loading. This is related to the fact that progressive failure develops in successive distinct phases, where each phase is controlled by specific but highly varying conditions as regards rates of loading, residual shear resistance, time duration, drainage and geometry.

He distinguishes the progressive failure in six different phases, of which four are of a static nature:

- **Phase 1** The existing ***in situ stage***

- **Phase 2** The ***disturbance phase***, or **triggering mechanism**, subject to conditions relating to the agent triggering the slide. This is a state of static equilibrium as long as $\boldsymbol{N_i < N_{cr}}$ but which becomes critical if the initiating agent generates a force exceeding N_{cr},

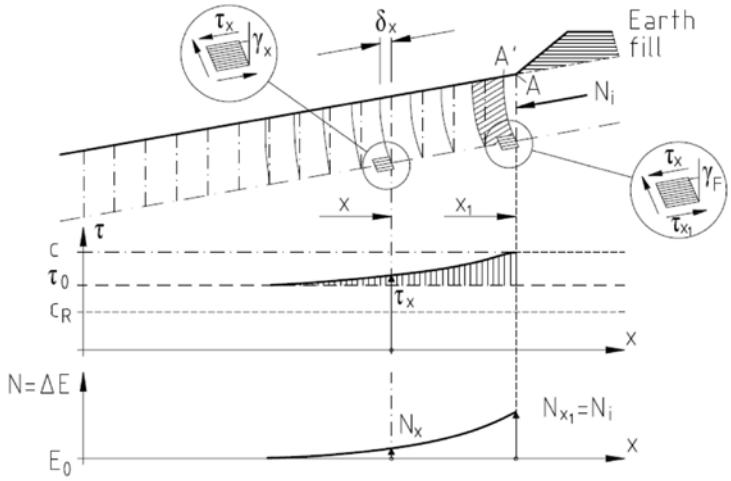

Figure 4.4 Stability situation prior to local failure. i.e. for $\gamma_x < \gamma_F$ and $\tau_x < c$. The figure illustrates the disturbing phase, when $N_i < N_{cr}$. N_x denotes the additional earth pressure force inducd by N_i – in this case caused by an earth fill. Bernarder 2011

N_{cr} is the maximum resistance or the critical load effect initiating local slope failure; it is reached when τ, after the peak c, is equal to τ_0.

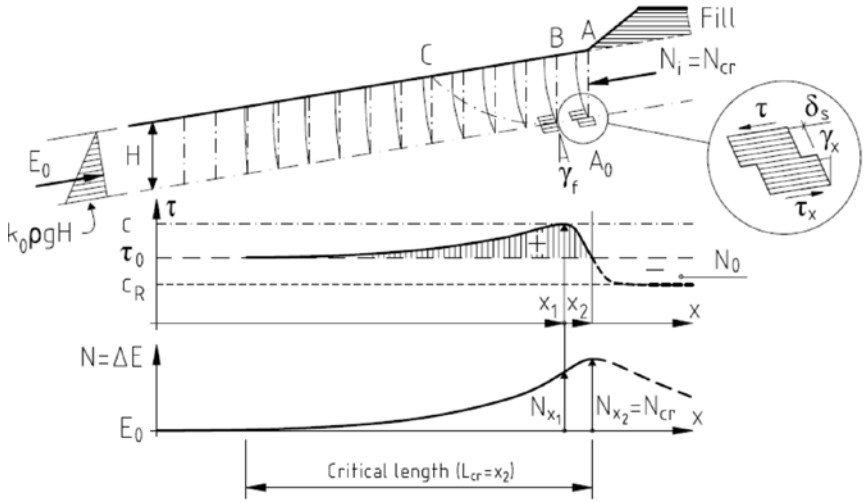

Figure 4.5 Effect of increasing the downhill active force (N_i) beyond the value corresponding to the peak shear strength at point A. When ($c_{R,x} - \tau_{0,x}$) = 0, the maximum resistance $N_{x2} = N_{cr}$ is reached. In the figure the critical length $L_{cr} = x_2$ is indicated. Bernarder 2011

- **Phase 3** The virtually ***dynamic load transfer***

  If N_i exceeds N_{cr} , i.e. $\boldsymbol{N_i > N_{cr}}$, a downward progressive failure generates a virtually dynamic transfer of unbalanced up-slope forces entailing significant increment of earth pressures in more stable ground further down the slope. The failure zone and slip surface may, already at the end of this phase, have developed far beyond the foot of the slope under the valley floor.

- **Phase 4** ***Permanent*** or ***transitory static equilibrium***
    - *Phase 4a* A possible state of static equilibrium may be reached if, subsequent to the downhill force transmission, the maximum earth pressures remain below current passive Rankine resistance, i.e. $\boldsymbol{E_{max} = [E_0(x) + N(x)]_{max} < E_p^{Rankine}}$. In this case, the progressive failure will only result in moderate cracking or a minor local active Rankine failure up-slope of the agent initiating the local failure.

    - *Phase 4b* On the other hand, the resulting maximum down-slope earth pressures exceed passive Rankine resistance, i.e. $\boldsymbol{E_{max} = [E_0(x) + N(x)]_{max} > E_p^{Rankine}}$.

      If this is the case, ground upheaval in passive failure will take place. Hence, Phase 4b is inherently of a transient nature. However, it defines in terms of static stability the length of the zone subject to passive Rankine failure before merging into the dynamic condition in Phase 5.

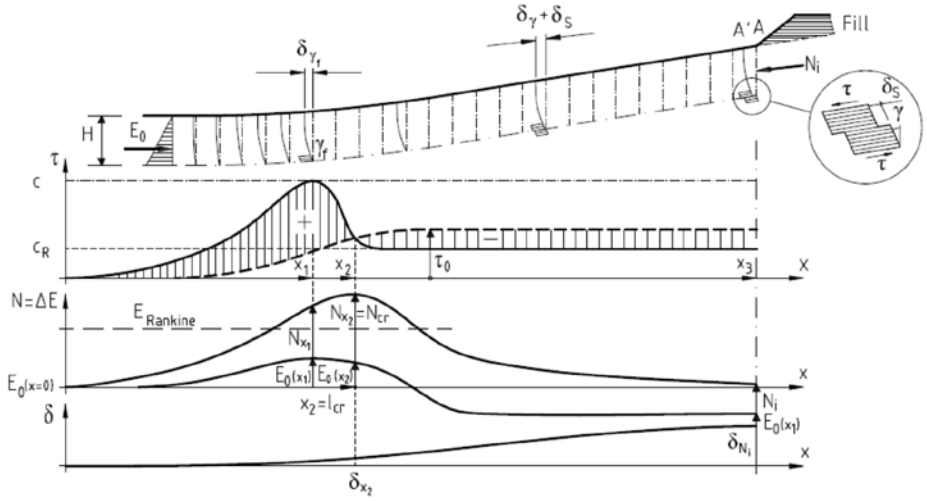

Figure 4.6 Possible new state of equilibrium (Phase 4) resulting from local up-slope failure and the ensuing earth pressure redistribution in Phase 3. Bernarder 2011

- **Phase 5** ***Final breakdown*** in passive Rankine failure if current passive resistance in the previous transitory state of equilibrium (Phase 4b) is exceeded. This is when the slide proper takes place, resulting in large displacements of soil masses down the slope, and massive heave of the ground surface - often extending over level ground far beyond the foot of the slope.

i.e. $\boldsymbol{N_i + N_D + N_{inertia} < E_p^{Rankine}}$ (heave), where N_D is the growing unbalanced down-slope driving force.

- ***Phase 6 Terminal state of equilibrium*** The foregoing phase is of a dynamic nature, and will end up in the final state of equilibrium of the finished slide provided sufficient passive resistance can be mobilized. This equilibrium is attained, when the static forces and forces of inertia are ultimately balanced by the passive resistance generated by ground upheaval and increase of earth pressure in the ground ahead of the visible slide limit.

The different phases are between themselves characterized by very different time scales related to the disturbance agent, to stress change under continued failure formation and to excess pore water pressure development.

Varying material properties, changing geometry and drainage conditions in the soil mass in the different phases of the slide movement are also of decisive importance to failure formation.

The soils of the entire slope profile are taken to be saturated. This means that the seepage pressures due to percolation of ground water down the slope are accounted for, even in cases with highly permeable soil strata.

If the slope is partially submerged, the stabilizing effect of horizontal hydraulic pressure can be considered in the model.

Local slope failure may lead to total collapse of not only the entire slope, but also of large areas of adjacent inherently stable ground subject to a number of factors such as:

- soil sensitivity;
- ground and slope morphology:
- profile of slip surface;
- distribution of incremental loads;
- type and synchronization of the agents initiating failure;
- hydrological conditions, etc.

Failure zones and slip surfaces tend to develop into level ground far (i.e. hundreds of meters) beyond the foot of a slope and that *prior to* the incidence of the general extensive passive spread failure.

FDM-analysis based on static loading can only predict minimum spread of the potential slide, since the dynamic effects are not included in the computations.

Bernarder method is an iterative method. The potential failure plane is initially presumed to be known; in fact it is often identifiable by the sedimentary structure of the ground; however the most critical condition may have to be found by “trial and error”.

Although the elevation of a potential failure plane is presumed to be known, the ultimate length of the failure plane and the extension of the passive zone, including the spread over level ground, emerge as results of the computation.

Hence, after a failure plane is assumed, the point x=0 has to be found so that, under the fill (q), N_i is equal to $q*H$.

X=0 is the point where the fill has not more effects on the earth pressure; then $E(x)$, down-slope earth pressure that is equal to $E_0(x)+N_i(x)$, is equal to the in situ earth pressure $E_0(x)$.

$N_i(x)$ denotes the additional earth pressure induced by the fill.

Then the integral computation begins at this point (x=0) further down the slope, where the conditions of stress and deformation are un-affected by the applied additional load (q). The parameters $E_{0,x} = 0$, $\tau_{0,x} = 0$, $N_x = 0$ and $\delta_x = 0$ constitute the down-slope boundary condition for the subsequent integral analysis. Correspondingly, the force $Nx_L = q \cdot H$ at $x = x_L$ is the up-slope boundary condition that, when satisfied, determines the associated values of $\tau_{x=x_L}$ and $\delta_{x=x_L}$.

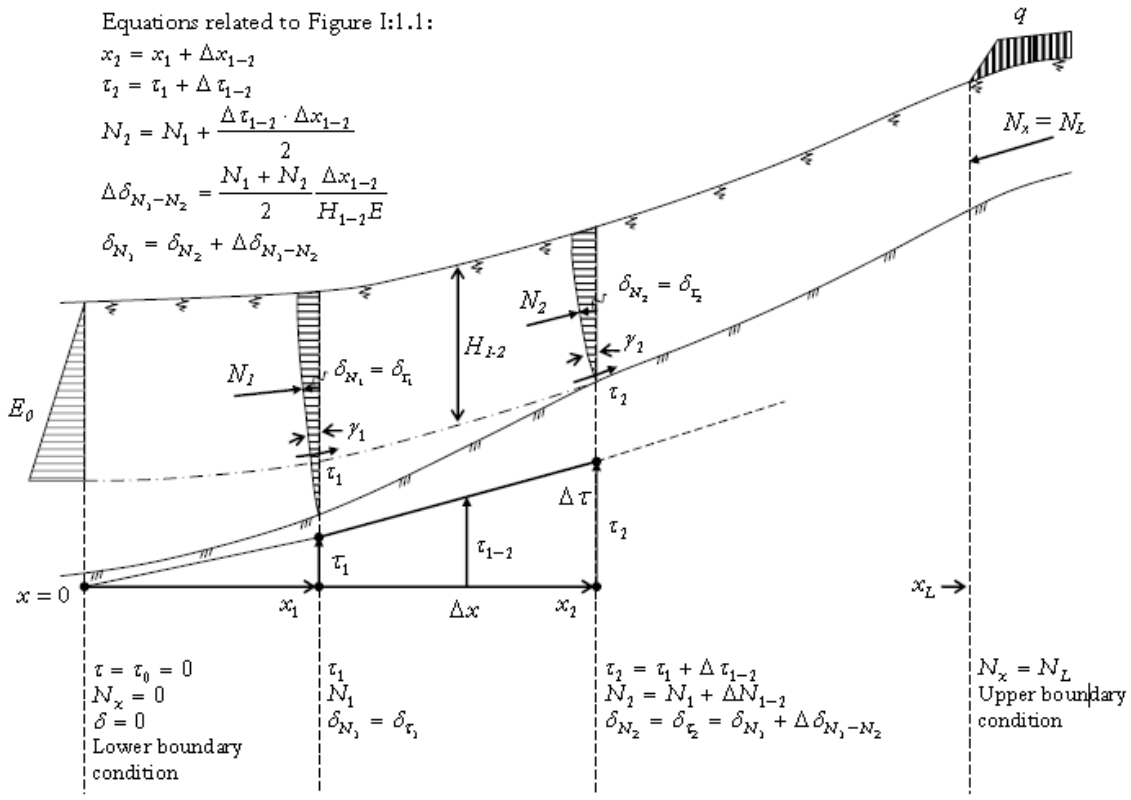

Figure 4.7 Section illustrating the calculation procedure. Bernarder 2011

The increment of *N* along x direction is obtained by an equilibrium of an element [*H(x)* b(x)*Δx*] in the down-slope direction:

Change of shear stress *Vertical load* *Down-slope load*

$$\Delta N = [\tau(x,0) - \tau_0(x,0)] * b(x) * \Delta x - q(x) * b(x) * sin\beta(x) * \Delta x - t(x) * b(x) * \Delta x \quad (4.1)$$

While the axial compression in x direction is

$$\Delta\delta_N = \left(N + \frac{\Delta N}{2}\right) * \frac{\Delta x}{[E_{el} * H(x) * b(x)]} \quad (4.3)$$

where $\Delta\delta_N$ is the incremental mean down-slope displacement due to the compression of an element.

The total mean down-slope displacement (δN), to which a vertical element is subjected, must be compatible with the shear deformation of the same element relative to the ground below the slip surface.

$$\delta_\tau(x) = \sum_0^{\alpha H(x)} [\gamma(x,z,\tau) - \gamma_0(x,z,\tau_0)] * \Delta z + \delta_S(x,0) \qquad (4.4a)$$

The calculation proceeds by advancing in steps of suitably chosen values of $\Delta\tau$ and Δx. As the values of δN and $\delta\tau$ can then be expressed in terms of the assumed values of the increments $\Delta\tau$ and Δx, the correlating values of Δx and $\Delta\tau$ in each step cycle have to be found by iteration so that the compatibility equation is satisfied, i.e.:

$$\delta_N(x) = \sum_0^x (\Delta\delta_N) = \delta_\tau(x) \qquad when\ \gamma(x,z) < \gamma_f\ , then\ \delta_S(x,0) = 0 \quad (4.5)$$

For uniform slopes with constant depth to the failure surface, working in steps of $\Delta\tau$ and finding the corresponding compatible value of Δx is most convenient. In slopes with arbitrary geometry, working in steps of Δx and determining the compatible value of $\Delta\tau$ is preferable.

As constitutive relationship he uses, for example, the following relation:

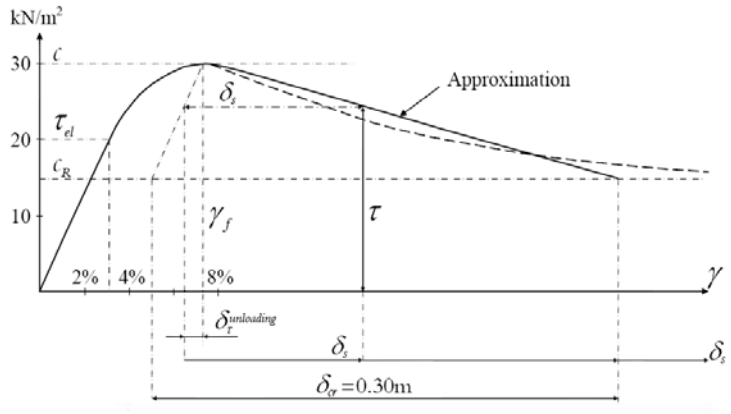

Figure 4.8 Constitutive shear stress/deformation relationships. It may be noted that the ratio of τ_{el}/c is here assumed to be constant as *c* varies with the coordinate (z). Bernarder 2011

The constitutive relationships of sensitive soils therefore have to be defined by special consideration of the rate of application of additional loads, time factors and drainage conditions in the incipient failure zone that is likely to initiate a progressive landslide.

In the Appendix 1th: FDM – constitutive relationships the constitutive relationships are described, for both stages.

Bernarder states that the conventional safety factor, commonly used in stability investigations, is not suitable in the context of progressive failure analyses in long slopes. He proposes $FS^{I} = N_{cr}/N = q_{cr}/q$ in respect of local triggering failure and $FS^{II} = E_{Rankine}/(E_{0x}+N_{max})$ in respect of global failure.

FDM involves iterative procedures, which make manual computations very laborious. However, this problem is readily overcome using computers, after entering data.

There is a program in *C++* but, although applicable to arbitrary slope conditions, this software is more practicable for slopes with simple geometry, i.e. with constant inclination and depth to the failure surface. An Excel sheet is well suited for educational purposes.

It is of course imperative that appropriate input data are introduced, which requires experience in geology and soil mechanics in general. So the method needs adequately detailed field investigations that often are not subject to routine investigation procedures.

Evaluation of the method

Bernarder's method does not care about what happens behind the fill, such as the distribution of shear stress. The method takes into account only the critic displacements but not how it is related to the soil behind the fill. In fact above the part of the slope that has moved it is not explained how the initial in-situ stress (τ_0) is related to the rest of the slope. Due to the movement of part of the slope, there will be an active Rankine state above the fill, and so the in-situ initial stress changes.

The method does not explain what happens due to the movement and also it should consider also the safety level of the upper part of the slope, because when the lower part moves it was a weight on the foot for the upper part.

The method does not explain how to have N_i value under the fill. So it is not clear how to obtain the additional earth pressure induced by the fill and it should be one of the main inputs of the model, as the method stops when N_i due to computation is equal to N_i due to the fill.

4.2. LEM: Limit equilibrium Method

The soil mass C is in limit equilibrium when, along the slip surface APB, the Mohr- Coulomb's criterion is valid:

$$\tau = \tau_f = c' + (\sigma - u)tg\varphi' \qquad Mohr - Coulomb's\ criterion$$

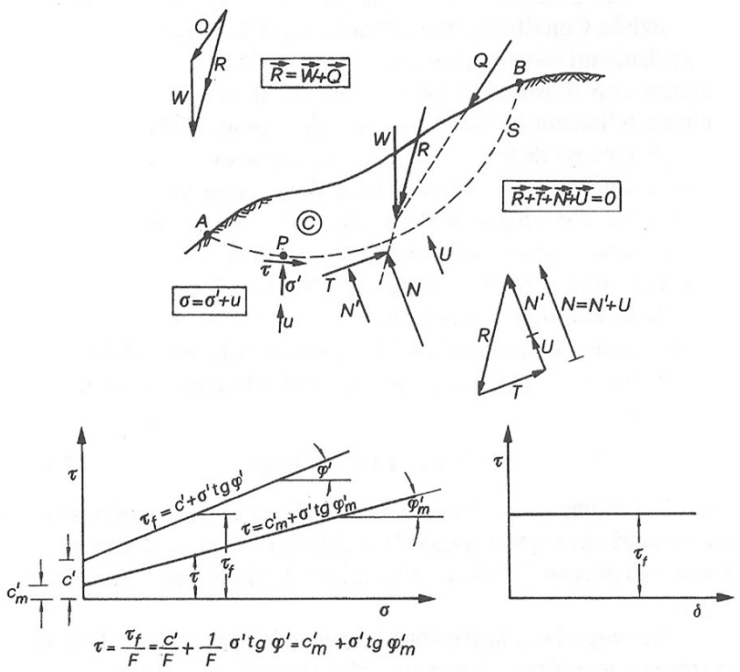

Figure 4.9 Basis of Limit equilibrium limit (Farulla 2001)

in which τ is the limiting (applied) shear stress required for equilibrium and τ_f is the maximum available shear strength that can be developed.

The shear stress (mobilized) τ, can be expressed by the relationship : $\tau = \frac{\tau_f}{F}$, in which F represents how far the soil mass is from the failure.

According to this method, the soil body is stable with respect to sliding when, for any potential slip surface, the resultant of the applied shear stresses required for equilibrium is smaller than the maximum shear strength that can be developed.

For slope stability analysis, the limit equilibrium method (LEM) is widely used by engineers and researchers. Although the LEM does not consider the stress–strain relation of soil, it can provide an estimate of the factor of safety of a slope without the knowledge of the initial conditions. The LEM is well known to be a statically indeterminate problem and assumptions on the distributions of internal forces are required for the solution of the factor of safety.

Analysis of the stability of natural slopes is in engineering practice normally based on the supposition of unlimited plastic properties of the soil material. The equilibrium of the potentially sliding mass is at failure determined assuming:

a) the potential sliding mass is regarded as a rigid body;

b) fully mobilized shear strength along the slip surfaces confining the moving soil mass;

c) the factor of safety assumes a unique value although it varies along the potential slip surface.

Limit equilibrium method requires the imposition of certain simplifying assumptions:

- conventional limit equilibrium solutions for assessing sliding stability incorporate the linear Mohr-Coulomb failure criterion for estimating the maximum available shear strength *(τf)*. Imposition of a linear criterion for failure requires experience and judgment in selecting appropriate shear strength parameters.
- The method is two-dimensional in nature, but can be expanded to 3D by including a width of the slice and shear on the side of the slice.
- Equations for assessing stability were developed by resolving applied and available resisting stresses into forces. Because only forces are considered, the effects of stress concentrations are unknown.
- Considerations regarding displacements are excluded from the limit equilibrium approach.

From a mechanical point of view, this methodology is highly simplified, since the deformations within (and outside) the sliding body are not considered. This means that the way in which the distribution of load, in situ stresses, stiffness properties and geometry affect the stress distribution in the potential failure zone (and slip surface) cannot be accounted for. Neither can the different phases of progressive slide development be identified or studied appropriately. For instance, the important impact of the in situ earth pressure distribution along the slope does not affect the results of stability analysis based on unlimited plasticity.

4.3. Difference between FDM and LEM

There are some differences between FDM and LEM:

- FDM focuses on the equilibrium of each individual vertical element into which the body of soil is subdivided. The ideal-plastic failure approach considers the equilibrium of the entire potentially sliding body of soil.
- FDM considers the main deformations within and outside the potentially sliding soil mass and it allows defining the distribution of shear stress induced by local concentrated loading as well as the extent to which shear resistance can be mobilized along a potential failure plane. LEM does not consider the deformations and it's not possible to define the distribution of shear stress within the soil's body.
- Bernarder's method considers the *entire* incipient failure zone as a thick structural layer, and not just as a discrete failure surface (or shear band), like LEM considers.
- For FDM the shearing properties of the soil are defined by a full non-linear 'stress-deformation' relationship; for LEM there is only a discrete shear strength parameter as is the case in normal limit equilibrium calculations.
- In FDM Local horizontal or vertical loads as well as local features in slope geometry that may be conducive to progressive failure formation can be taken into account. It's not the same for LEM.
- FDM results affected from geometric sensitivity, whereas LEM does not.

  Figure 4.10 depicts two slopes having different geometry; in slope A the potential failure surface is linear, whereas in slope B it varies as a 2^{nd} degree parabola. However, all relevant data, such as the mean slope angle from the crest to foot, the depth of the slip surface below ground level and all material parameters, are identical.

  In the following tables, some results are reported. In Table 4-1ideal-plastic analyses show the same safety factor for both slopes, while for the global failure condition (Table 4-2) having used FDM, it is shown that the slope A can sustain a crest load of q_{cr} = 34.5 kN/m^2 corresponding to about 2 meters of earth fill, whereas slope B cannot carry any additional load at all on its crest, i.e. q_{cr} = 0 kN/m^2.

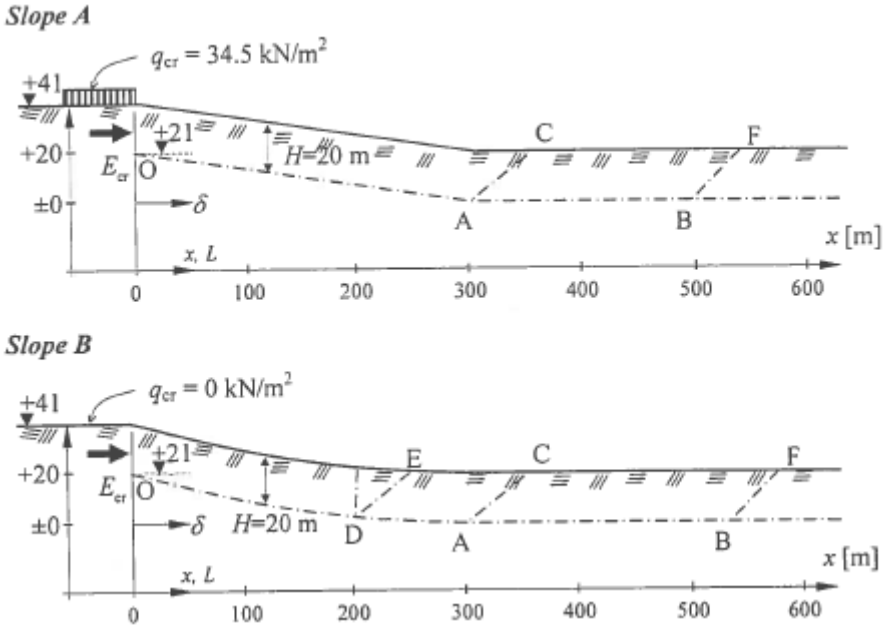

Figure 4.10 Two slopes with varying geometry. Slope A is a linearly descending surface. Slope B is a parabolically descending surface (Bernarder 2008).

In Table 4-1and Table 4-2 the results of LEM and FDM are reported for both slopes.

Slope A	F_s^{OAC} = 1.64	N_{cr} = 1537 kN/m	q_{cr} = 77 kN/m²
Slope B	F_s^{OAC} = 1.64	N_{cr} = 1537 kN/m	q_{cr} = 77 kN/m²
"	(F_s^{ODE} = 1.43)	(N_{cr} = 1030 kN/m)	q_{cr} = 52 kN/m²

Table 4-1 Results according to LEM, Bernarder 2008

	E_0	N_{cr}	E_{cr}	q_{cr}	E_x^{max}	E_R^P/E_x^{max}	L_{cr}	$\delta_{x=0}^*$
	kN/m	kN/m	kN/m	kN/m²	kN/m	1	m	m
Slope A	2400	690	3090	34.5	5305	0.83	540	3.52
Slope B	2400	0	2400	0	5376	0.82	490	2.86

Table 4-2 Failure condition (un-drained) according to FDM with Su_R/Su=0.6 Su=30 kN/m² E_R^P=4400 kN/m, Bernarder 2008

5. Modelling downwards progressive failure with a physical approach

5.1. General features

A progressive failure is similar to the process of falling dominos and a model proposed by Nordal (2004) is represented in Figure 5.1, in which a series of blocks are connected with the springs.

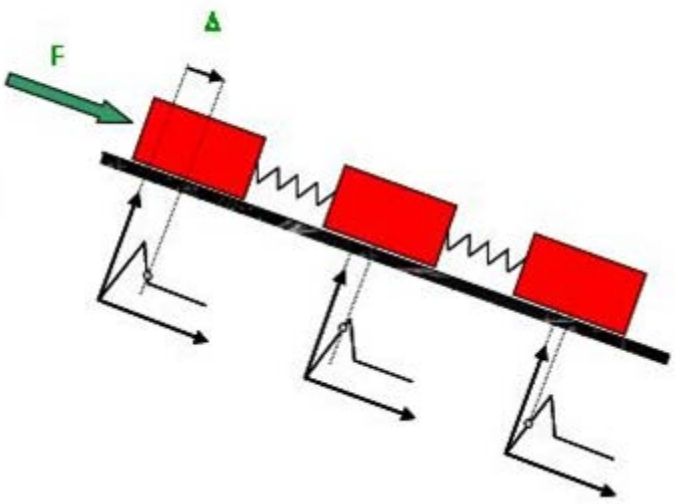

Figure 5.1 Progressive failure from Nordal 2004

This scheme shows what happens when a slope, which is made by material with strain-softening behaviour, is subject to a load represented by the force F.

The strain-softening materials exhibit the decrease in shear resistance with the increasing strain after peak shear stress, hence after the peak is reached they will distribute to neighbouring soil elements the overshooting load and what they have lost due to strain-softening.

The displacements of every block represent soil displacements, while the spring between two blocks depends on soil stiffness.

It is possible to calculate the force that two blocks exchange each others, and it depends on the stiffness and on the relative movements.

As shown in Figure 5.1 the three blocks do not have the same displacements, as there is a spring between them, but if springs are rigid then there is no progressive failure as all the blocks have equal stress.

Using only the local static equilibrium equations, and taking into account strain-softening material behaviour, that is the shear force that the block can exhibit, it is possible to calculate the displacements of all the blocks, and the global response F.

The global response F is the sum of the three forces that every block can exhibit, as the spring's forces are internal forces; this is the global equilibrium equation.

The shear force, that a block can exhibit, depends on the displacement because of the strain softening behaviour. In Figure 5.2 this behaviour is represented.

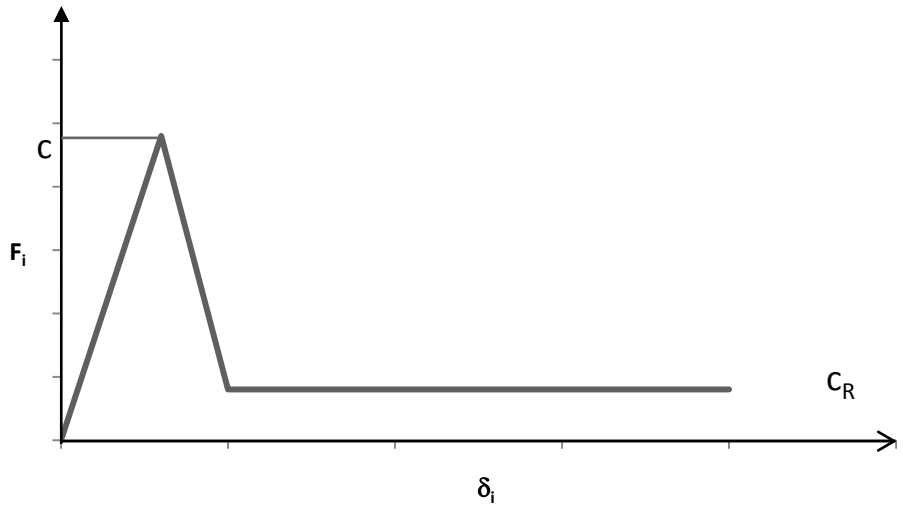

Figure 5.2 Example of mechanical behaviour for a strain-softening material

The material behaviour used like input for the analysis is a simplified version of real one, while in the chapter 5.3.3 a real behaviour is described. It is important to note that the results depend on the material behaviour, in particular on the ratio c/c_R, where c is the peak and c_R is the residual shear strength, and on the value of the elastic constants of the springs.

A model has been built considering, instead of three blocks, ten blocks to reproduce a real slope.

The purpose of this model is to study the *disturbance phase*, according to Bernarder (2011).

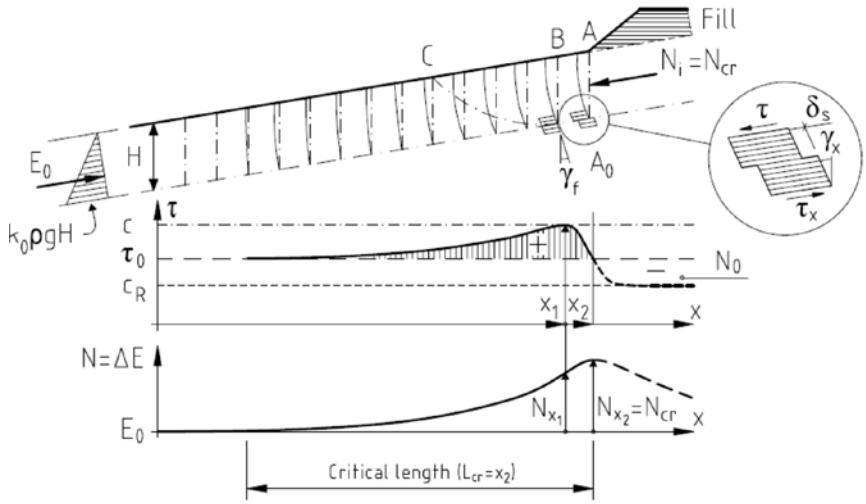

Figure 5.3 Triggering phase from Bernarder 2011

In this case the model finds the destabilizing displacement (δ_{inst}), or rather the displacement that is the trigger of the failure, and the maximum capacity N_{cr} is a result of the model.

From the model it is shown that the destabilizing displacement (δ_{inst}) is reached when the blocks are not in the residual line but still in strain-softening line.

The blocks are of different lengths because, as shown in Figure 5.3, the compression, which the slope is subjected, is not constant but varies along the slope. In particular it is maximum in the upper part and zero at the bottom. Then for catching better this behaviour the blocks are smaller in the upper part and bigger in the lower part. A proportion of the blocks compared to the total length has been chosen.

This model considers an average value of the stress beneath the blocks and, as there is an equilibrium, the force is made by the multiplication of the stress with the length of the block.

As explained in the last chapters the results are the displacements and the average stress of every block.

In this way it is possible to have an idea about the stress distribution along the slip surface, and also about the forces that blocks exchange (in Bernarder those forces are expressed by the symbol N_i, as that is the additional local load effect).

The inputs of the model are:

- the constitutive relationship, that is common for each block. It is a simplified relationship and it is made by two points in the plane τ-δ: the peak (c) and the corresponding displacement (δ_f) and the residual value (c_R) and the corresponding displacement (δ_R);

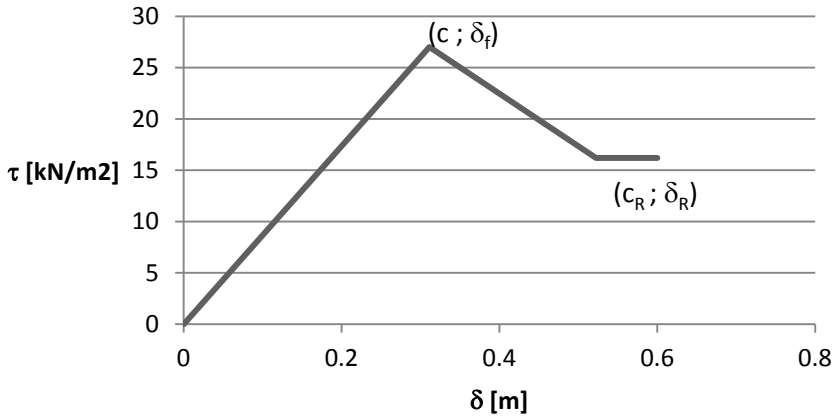

Figure 5.4 Constitutive relationship

- the total length of the potential slide L_{TOT};
- the geometry of every block: then the height H and the length b (it could be changed if it does not look good);
- the initial in situ stress (τ_0), also taking into account the presence of a preformed slip surface;
- Young's Modulus could be changed but it is got from the elastic theory: $E_{el} = G * 2 * (1 + \nu)$, in which G is the Shear's Modulus and it is $G = \frac{\tau}{\gamma} = \frac{\tau}{\delta} * \frac{H}{3} = \frac{c*H}{3*\delta_f}$;
- the elastic constant of the springs, that represented what the blocks exchange and then N_i, they are got by the same relationship in the last chapter $k = \frac{E_{el}*H}{2*b}$, but it is possible to change its value, also for take into account less blocks. In this case E_{el}, H and b are an average value between two blocks;

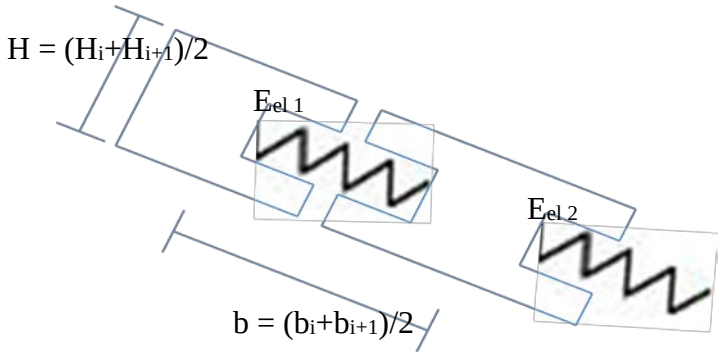

Figure 5.5 Geometric features of the model

- Some numbers that let the convergence go on in a better way.

As one of the outputs of the model is the maximum capacity N_{cr}. according to Bernarder (2011) it is possible to define a safety factor of the triggering phase: $FS' = N_{cr}/N_{load}$. This formulation can be applied if the value of N_{load} is known.

To simplify the understanding of the model the mathematical equations and some results have been calculated for three blocks, while in the chapter 5.4 the whole model is used.

5.2. Governing equations

Considering three blocks on an inclined plane and using the static equations represented in the figures below,

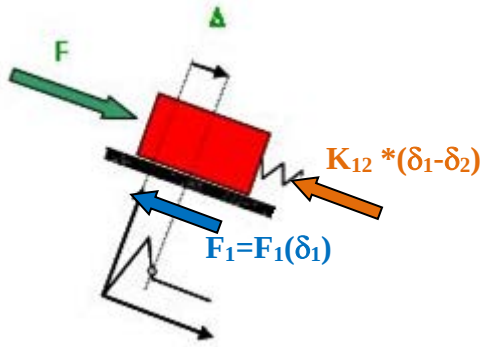

I local static equation $F = F_1(\delta_1) + k_{12} * (\delta_1 - \delta_2)$

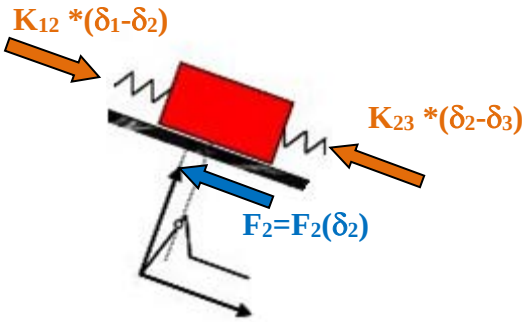

II local static equation $k_{12} * (\delta_1 - \delta_2) \quad = F_2(\delta_2) + k_{23} * (\delta_2 - \delta_3)$

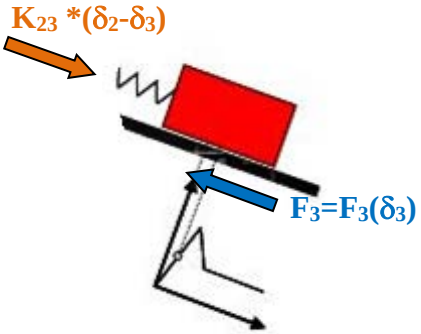

III local static equation $F_3(\delta_3) = k_{23} * (\delta_2 - \delta_3)$

The three local static equations can be written using a matrix:

$$\begin{bmatrix} F_1(\delta_1) - F \\ F_2(\delta_2) \\ F_3(\delta_3) \end{bmatrix} = \begin{bmatrix} -k_{12} & k_{23} & 0 \\ k_1 & -k_{12} - k_{23} & k_{23} \\ 0 & k_{23} & -k_{23} \end{bmatrix} \begin{bmatrix} \delta_1 \\ \delta_2 \\ \delta_3 \end{bmatrix}$$

As the forces that blocks can exhibit have that behaviour depending on the displacement, it is possible to know the value of the force after having the value of the displacement.

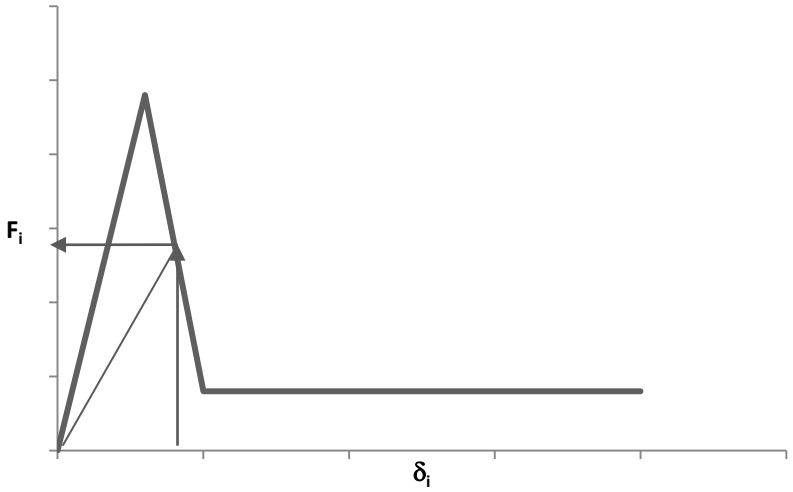

Figure 5.6 Model relationship

As the total displacement δ, the input of the model, is equal to δ_1 then the matrix becomes:

$$\begin{bmatrix} F_1(\delta_1) + k_{12} * \delta_1 \\ F_2(\delta_2) - k_{12} * \delta_1 \\ F_3(\delta_3) \end{bmatrix} = \begin{bmatrix} 1 & k_{12} & 0 \\ 0 & -k_{12} - k_{23} & k_{23} \\ 0 & k_{23} & -k_{23} \end{bmatrix} \begin{bmatrix} F \\ \delta_2 \\ \delta_3 \end{bmatrix}$$

In which the unknowns are F, δ_2 and δ_3, as δ_1 is the input of the model.

The global response is $F = F_1(\delta_1) + F_2(\delta_2) + F_3(\delta_3)$.

5.3. The case of three blocks

5.3.1. Results without initial in-situ stress (t_0)

In this paragraph it is shown how the global response (F) changes varying the elastic constants of the springs, and also the relative displacements of the three blocks. Later it is also shown what happens if there is already an initial shear stress (τ_0), and the results for a sensitive clay.

With this mathematical approach it is possible to see what happens varying the elastic constants of the springs. In particular, it is possible to calculate the three displacements and the relative forces that blocks can develop taking into account the strain-softening.

The results depend on the constitutive relationship and on the elastic constants of the springs. Afterwards, in the chapter 5.3.2, it is shown that they depend also on the initial in-situ stress. Hence the results shown in this paragraph have to be used only like an example, because they could vary for every change in these inputs.

When *k* is very rigid the three blocks show almost the same displacements and the total response is similar to the relationship of one block, but it is the sum of all values.

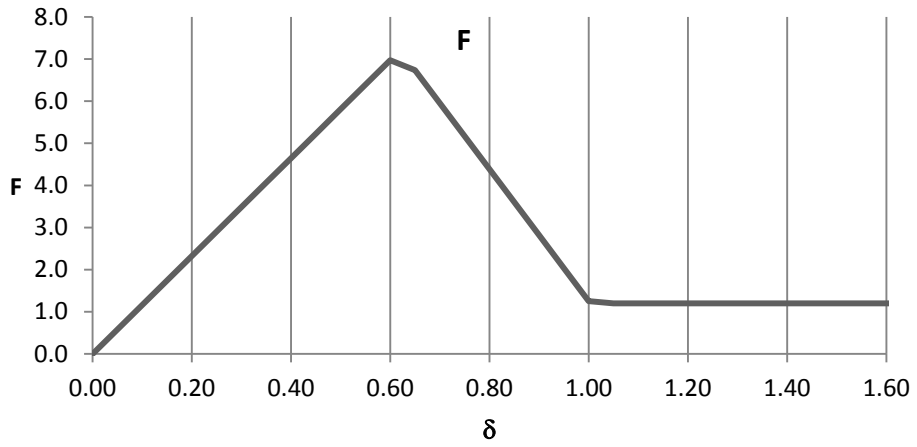

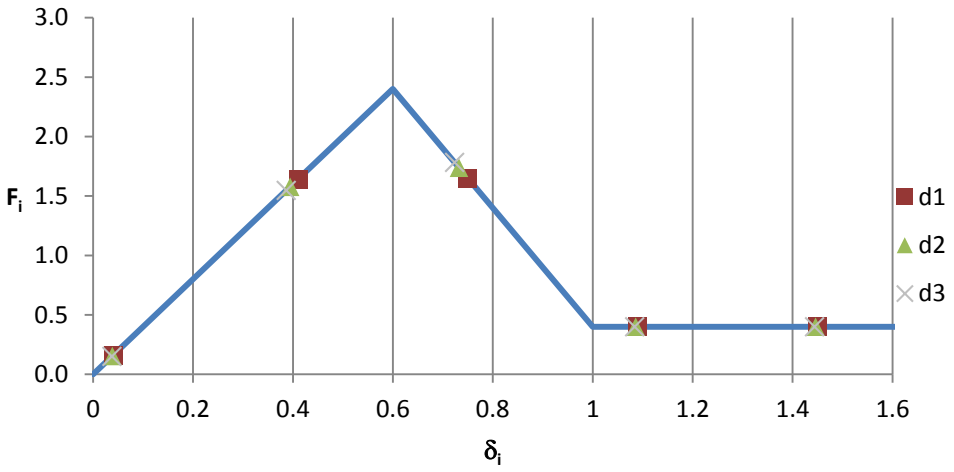

Figure 5.7 Results when *k* is rigid

As shown in Figure 5.7 the displacements of the three blocks are almost the same, and after the peak they became closer. The global response is the sum of the three forces F_i and as the displacements are so close its peak is reached when the three blocks reach the peak.

When K is soft, the total response presents a behaviour shown in Figure 5.8 below. The peak is lower than with rigid springs and the displacement of the three blocks are different, except when the third block has already passed the peak. In fact, in this condition, they present closer displacements.

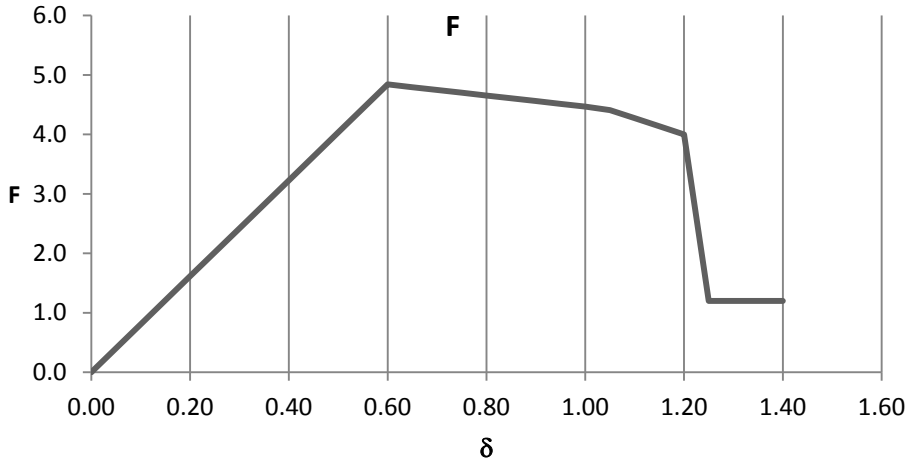

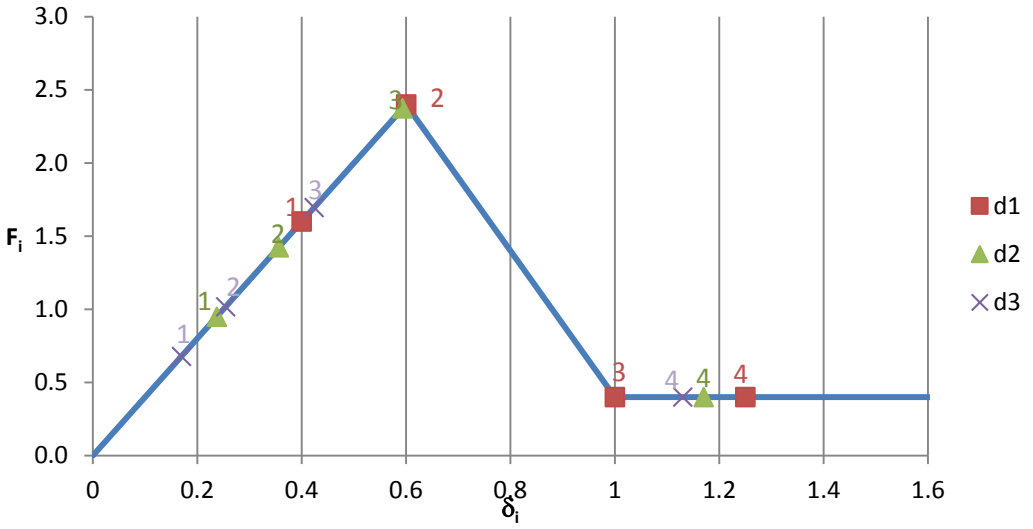

Figure 5.8 Results when *k* is soft

In this case the peak is reached when the first block presents its peak, but strain-softening behaviour is less pronounced until the third block reaches its peak. After there is a strong loss of strength and the global response became equal to the sum of the residual shear strength of the three blocks. This happens with a displacement δ higher than with rigid springs.

Finally, when K is very soft (Figure 5.9), the global response shows more peaks that are equal to the number of the blocks, because the displacements are so different that when one is overtaking the peak, the others are at the beginning of the linear part. But when the third has reached the peak, the displacements tend to be closer to reach an equilibrium.

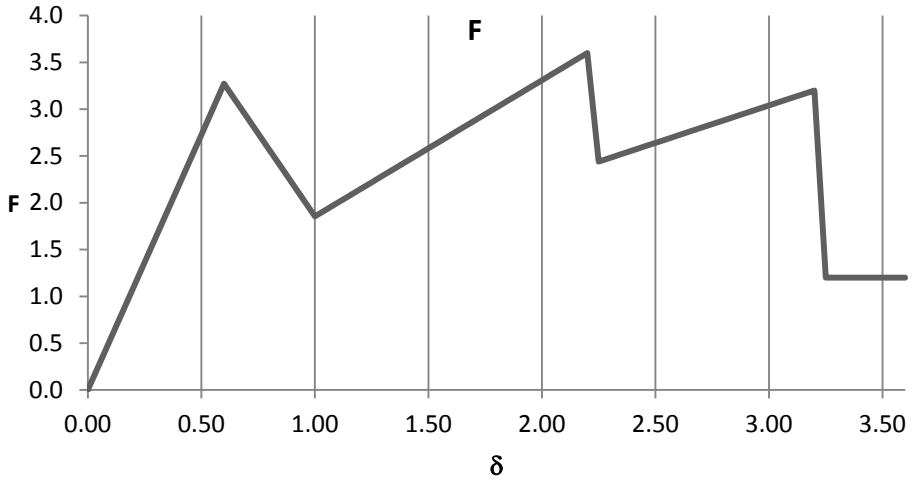

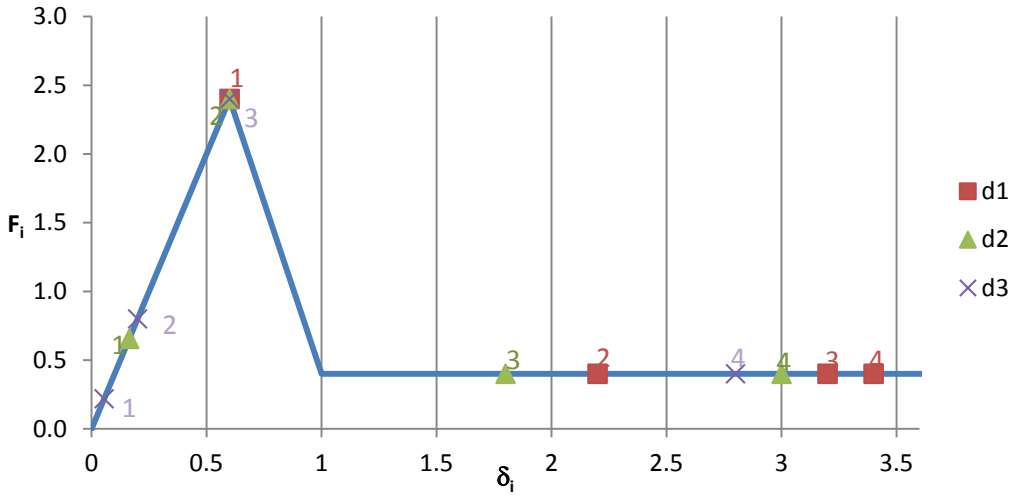

Figure 5.9 Results when *k* is very soft

The displacements in this case are very different because of the very low values of the stiffness/elastic constants of the springs and the peak is so low that it is not far from the peak of a single block.

At the end, when the second block has reached the peak, the total response is equal to the sum of the residual shear strength of the all blocks. It happens with a displacement δ very high.

The shape and the value of all peaks depend on the combination of the material behaviour and of the value of *k*.

5.3.2. Results with initial in-situ stress (τ_0)

Now the question is:" *What does it change if there is the initial in-situ stress*?"

The in-situ initial stress determinates that the blocks do not start from the origin of the axes (point 0;0), but they have already developed a displacement and then a force.

Hence they start from the point ($\delta_{init};\tau_0$), and they will show less resistance than without initial in-situ stress.

It's important to note the difference between when τ_0 is lower or higher than c_R, residual shear strength.

In fact brittle progressive failure can occur if τ_0 is higher than c_R, as there will a distribution of the unbalanced forces resulting from gradually increasing deformations and associated strain softening.

In other words, after every block has reached the peak and the stress is lower than in-situ stress, they will give a negative contribution of force to the other blocks. This negative contribution is due of strain softening and it depends on how much is the difference between τ_0 and c_R.

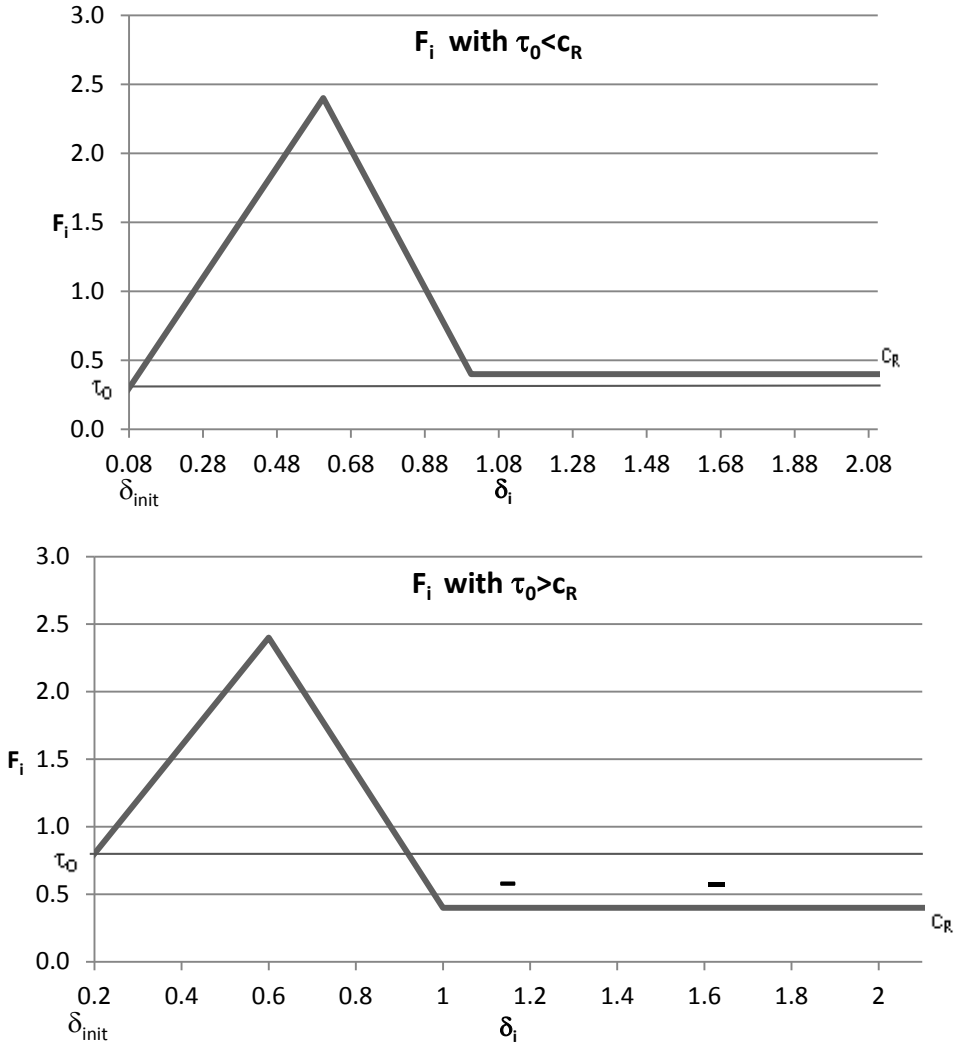

Figure 5.10 Differences when initial stress is lower or higher than residual strength

Hence if τ_0 is lower than c_R there will be always a low resistance that all the blocks can have.

Results when τ_0 is lower than c_R

In the following figures are shown the global response and the displacements of the three blocks when τ_0 is less than c_R, varying the elastic constants of the springs.

In figures $\delta_{i\ final}$ represents the sum of the in-situ displacement due to τ_0 and δ_i that is the displacement related to the force. The global displacement δ is equal to δ_1.

$F_{i\ final}$ is the amount of the initial in-situ stress and F_i, due to the additional displacement δ_i.

F is the sum of F_i of all the blocks.

The Figure 5.11 is very similar to those without in-situ stress; it looks like it is sufficient to shift the origin of the axis to the point (δ_{init} ; τ_0) especially for rigid springs because the displacements of the three blocks are close, but there are some slight differences.

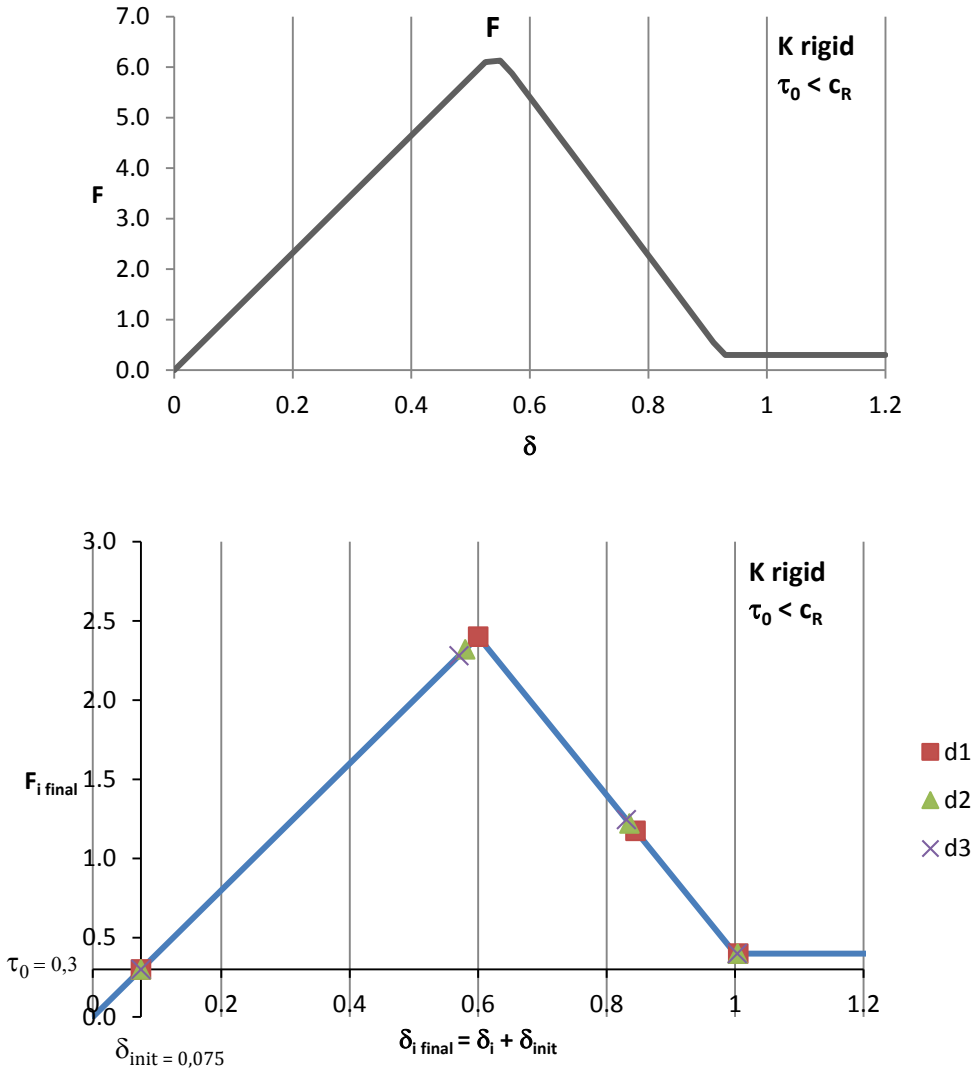

Figure 5.11 Results when *k* is rigid and initial stress lower than residual strength

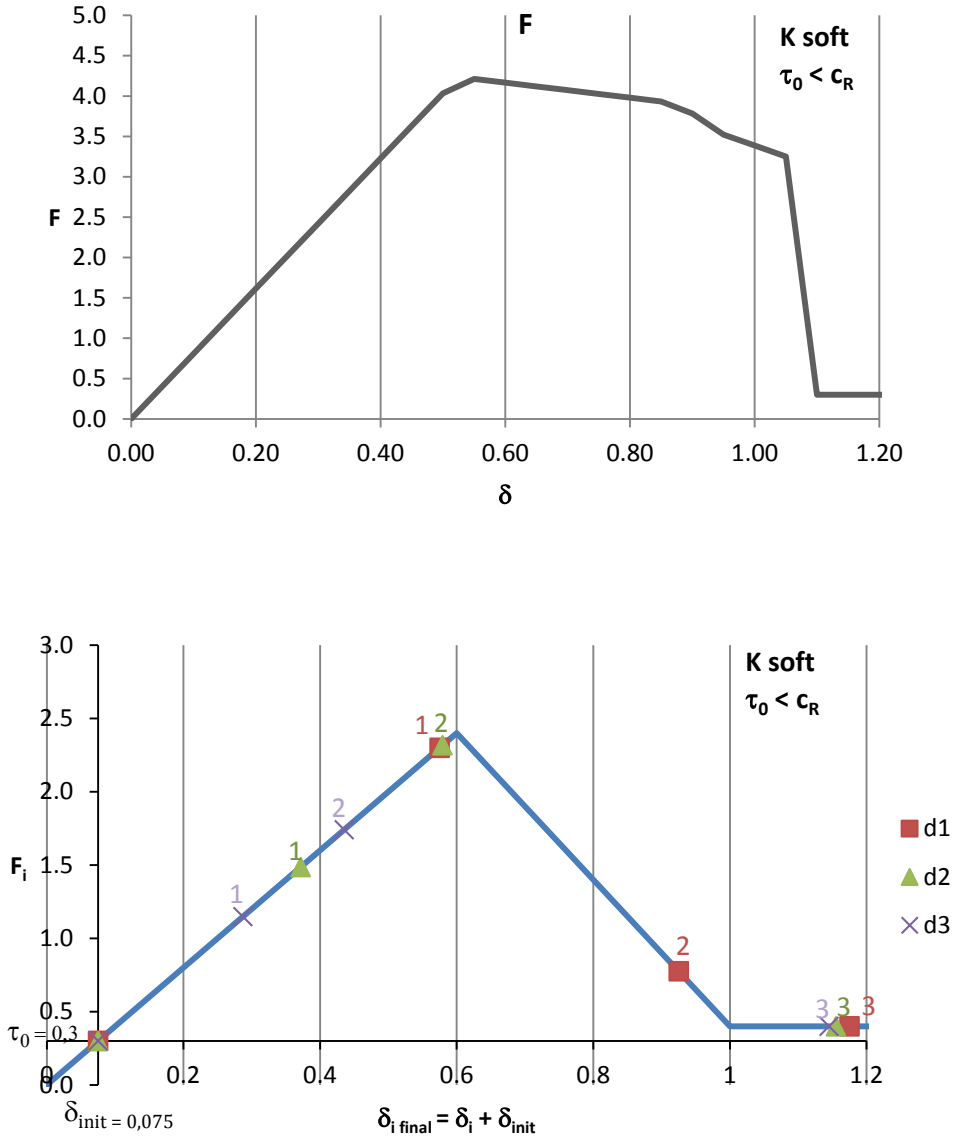

Figure 5.12 Results when *k* is soft and initial stress lower than residual strength

When k is soft the three displacements are different as shown in Figure 5.12, but after the third block has reached the peak, they get closer.

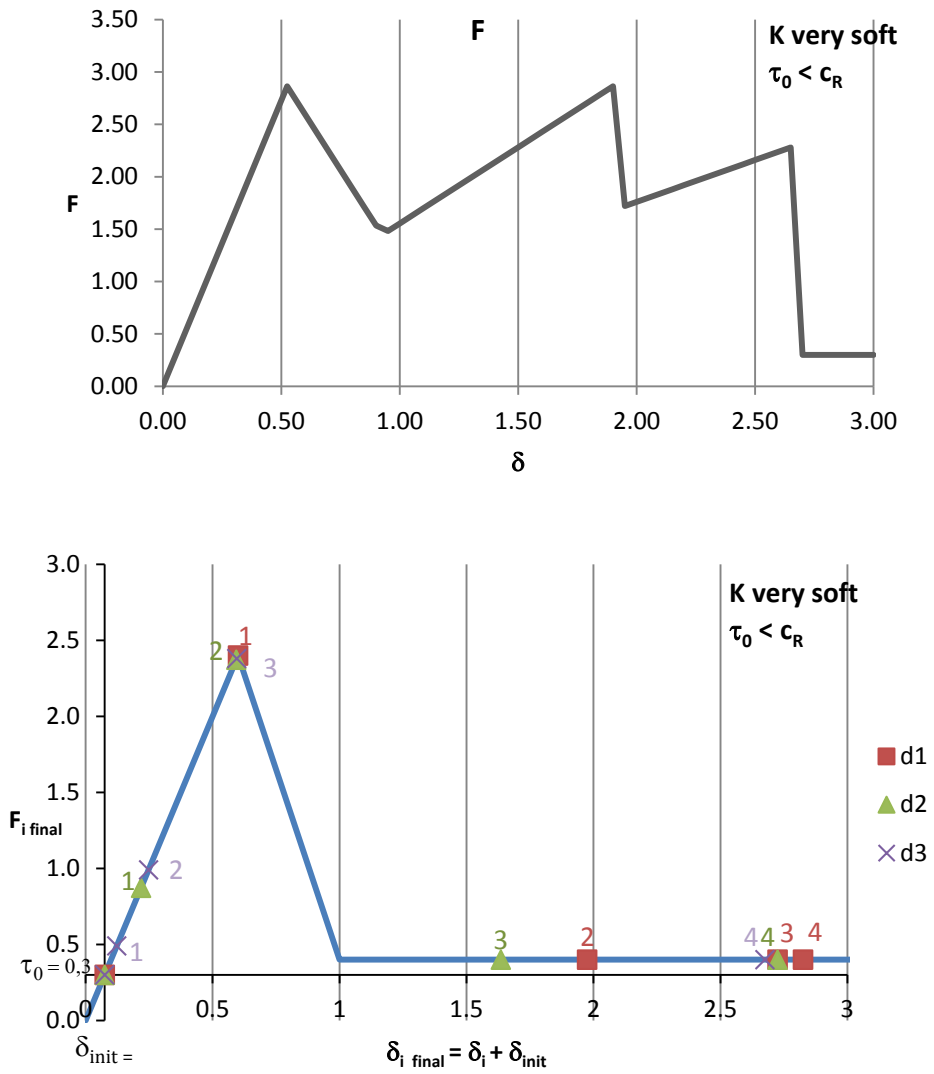

Figure 5.13 Results when *k* is very soft and initial stress lower than residual strength

With very soft elastic constant the distance among the three displacements is more evident. But after the third block has reached its peak the displacements get closer. We are again three peaks and then the loss of resistance that is equal to the sum of the difference between τ_0 and c_R for all the blocks.

Results when t_0 is higher than c_R

When τ_0 is higher than c_R a brittle failure is possible due to the strain softening that produce a negative contribute that a block can give to the following one.

In this case the brittle failure is reached when the third block overtakes its peak because there is no one other block that can support the force and the negative contributes of the other two blocks.

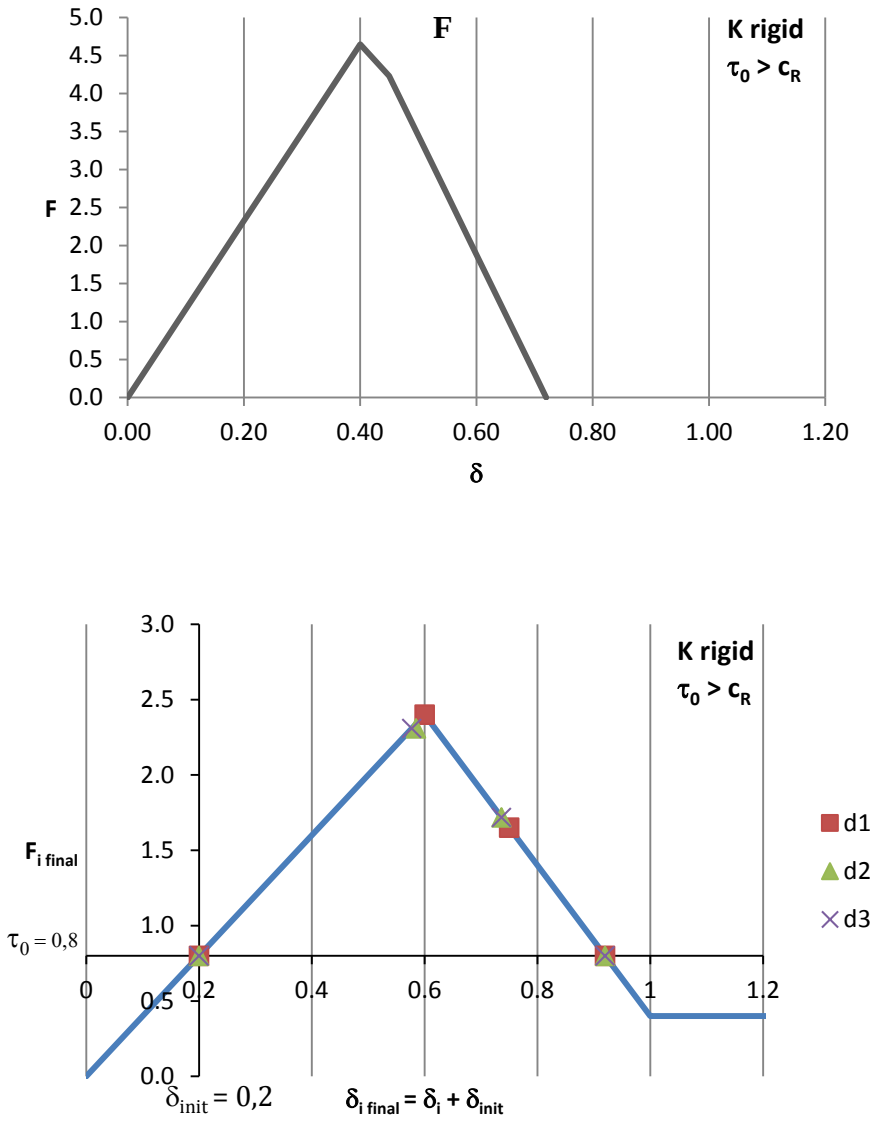

Figure 5.14 Results when *k* is rigid and initial stress higher than residual strength

When k is rigid the global response shows only a peak that is reached earlier because of the initial displacement. The maximum displacement that is possible to reach is when, after the peak, the three blocks have the initial in-situ stress. In fact after that value there would be negative contributes from all the blocks, and as the blocks show the same displacements, no other block could sustain them, i.e catastrophic failure.

No one block gives a negative contributes to the neighbours.

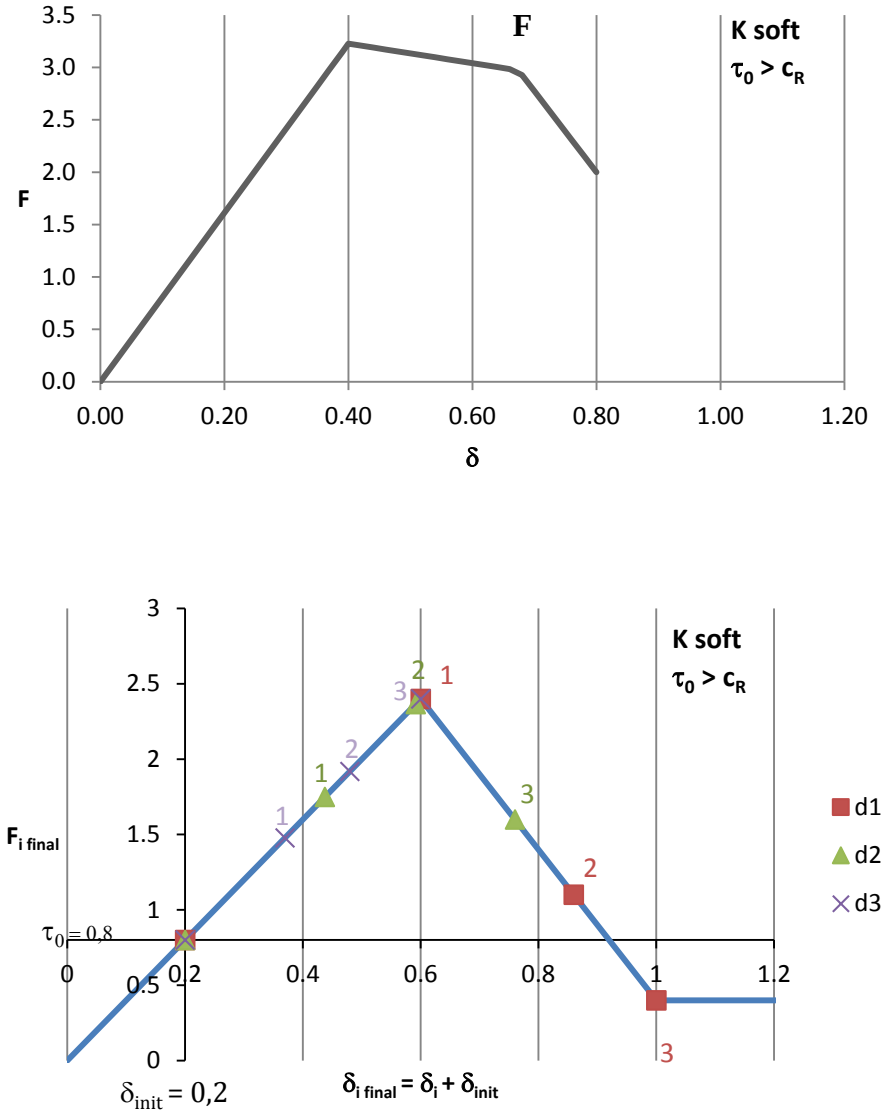

Figure 5.15 Results when *k* is soft and initial stress higher than residual strength

When *K* is soft the brittle failure is reached when the third block overtakes the peak. In this case no one other block can sustain the negative contributes of the other blocks.

Also Figure 5.15 presents a peak and a lower strain-softening behaviour than with rigid springs. The peak is lower than rigid springs and the failure is obtained for higher value of displacements.

In this case the first block gives, at the end, a negative contribute to the neighbours.

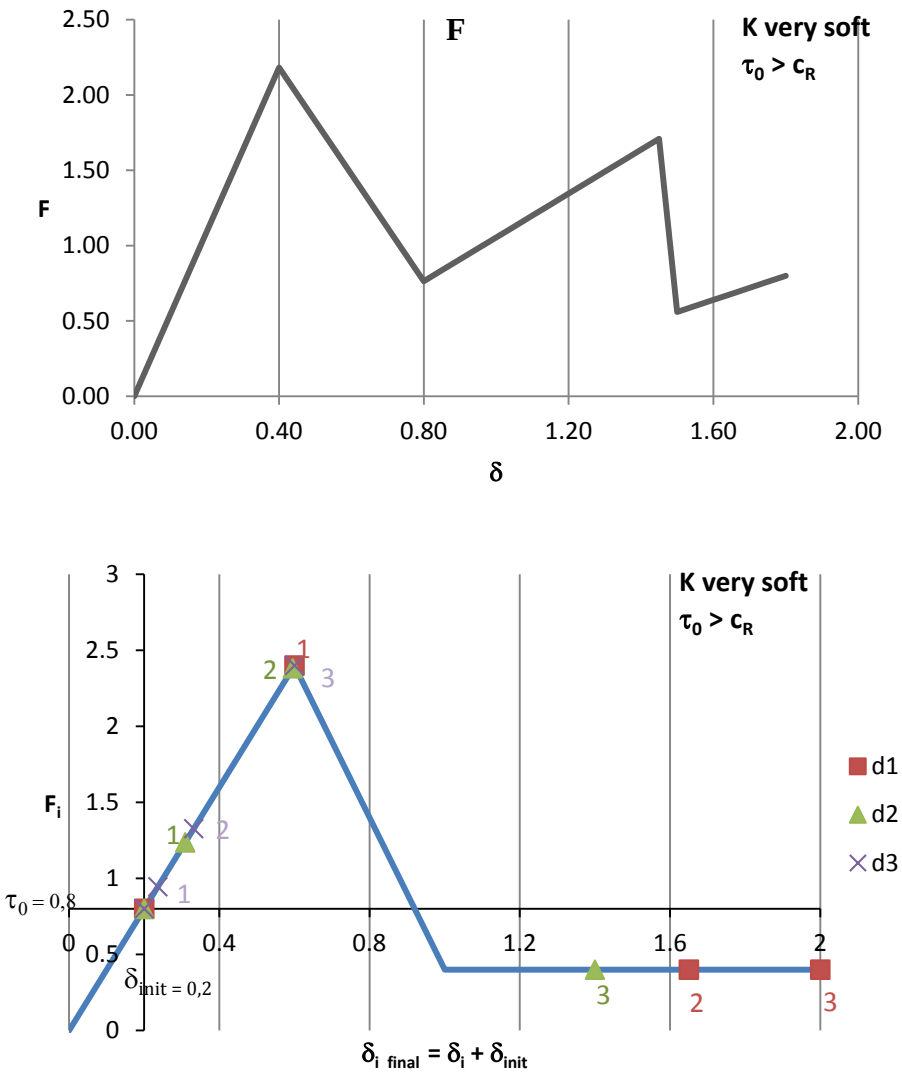

Figure 5.16 Results when *k* is very soft and initial stress higher than residual strength

At the end when k is very soft there are again three peaks, but after the last one there is a brittle failure.

The first two blocks give negative contributes and the global displacement is higher than with soft springs. However the last peak, and in this case the brittle failure, is reached for a value of the global displacement lower than without initial in-situ stress.

5.3.3. Results for a sensitive clay

A sensitive clay has a own constitutive relationship that depends on a lot of parameters like the rate of application of additional loads, time factors and drainage conditions in the incipient failure zone that is likely to initiate a progressive landslide.

A possible constitutive relationship for a block, with height and base equal to 1 m, is shown in figure, in which the peak is reached for a displacement equal to 0,016 m while the residual shear strength for a displacement of 0.05 m. These parameters have been taken from Bernarder studies.

In fact as the peak strain γ_p reported in the Tuve data is 4.67% (Bernarder 2011), the displacement has been calculated like it is centred on the last third of the height ($\delta = \gamma \frac{H}{3}$), whereas the residual strain γ_r is 15% and it entails a displacement of 0.05 m.

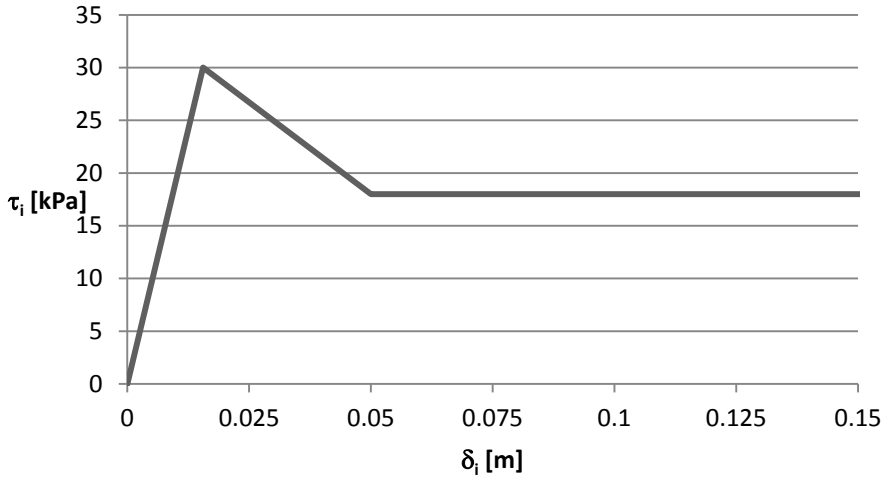

Figure 5.17 Constitutive relationship for a block with height and base equal to 1 m

The peak has been assumed equal to 30 kN/m^2 and the residual shear strength 18 kN/m^2.

A sensitive clay has a Young's Modulus value like about 2500 KN/m^2; as *k* could be related to E_{el} through the following expression $k = \frac{E_{el} * H}{2 * b}$, for *H*=*b*=1 m, *k* is equal to 1250 kN/m^2.

Hence for a sensitive clay, its behaviour is between rigid and soft springs, as shown in Figure 5.18.

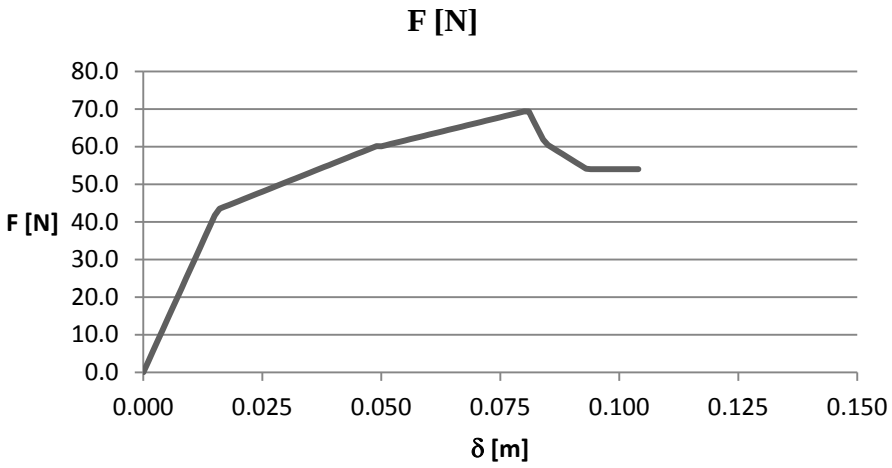

Figure 5.18 Result of the model for a sensitive clay

In fact the peak is reached for a value of δ (0,081 m) higher than the value of the constitutive relationship; it is not the sum of the three peaks and the residual is reached for a displacement equal to 0,094 m.

That relationship has been pulled out without taking into account the initial in-situ stress.

5.4. Application for a real slide

5.4.1. Features of landslide and results

The model has been tested on a real slide happened in Sweden: Tuve slide.

The landslide took place in Tuve, a community near Gothenburg in 1977, in which there were nine deaths and a change of the topography of about 270.000 m^2 of ground.

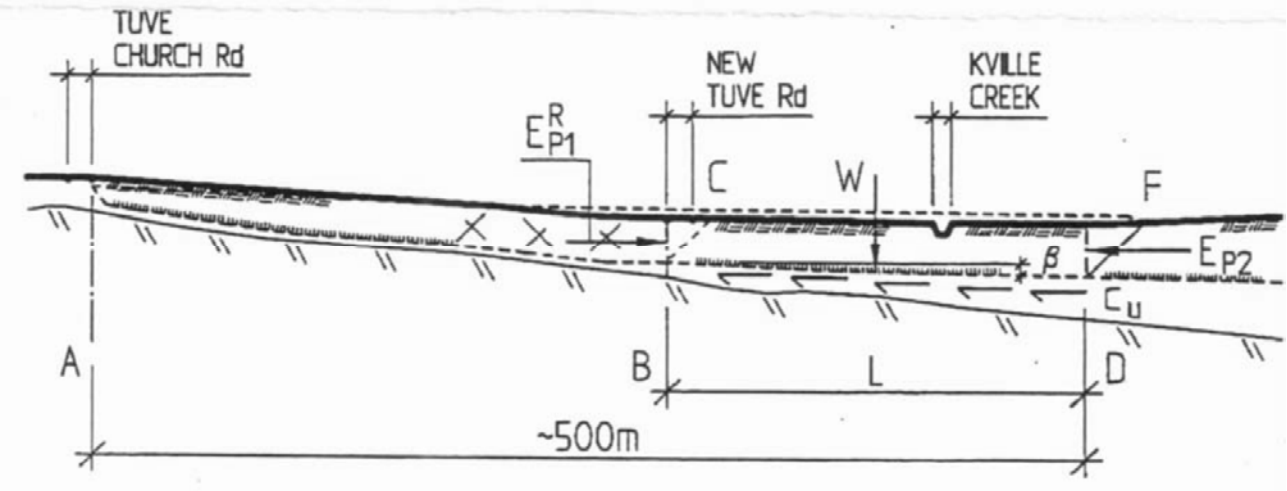

Figure 5.19 Tuve slide after Bernarder 2011

As shown in Figure 5.19 the slide is long about 500 m with a upheaval of 5 m in the passive zone of about 300 m.

The slide has been triggered by a local instability in the steepest portion of the slope, near the Tuve Church road. One of the features of this slide is that about 60% of the area consists in a passive upheaval and it happened in a zone almost horizontal.

Figure 5.20 Photography of Tuve slide, Bernarder 2011

The slip surface was at a depth of about 35 m in the lowest part, but in the steepest portion the depth varied between 17 and 25 m.

The results are $\delta = \delta_{rif}$ =0,1174 m and $N_{cr} = N_{cr\ rif}$ = 50,93 kN and the parameters reported in Table 5-1 have been used as reference sizes for parameter normalization afterwards.

L_{rif} [m]	130
$\tau_{0\ rif}$ [kPa]	24.9
c_{rif} [kPa]	27
$c_{R\ rif}$ [kPa]	16.2
$sr_{\ rif}$ [°]	-88.9

Table 5-1 Parameters used as references sizes

This results concern the *disturbance phase* (Bernarder 2011), or rather the triggering of the redistribution of the stress among the slope. For the physical model a depth of 20 m has been chosen.

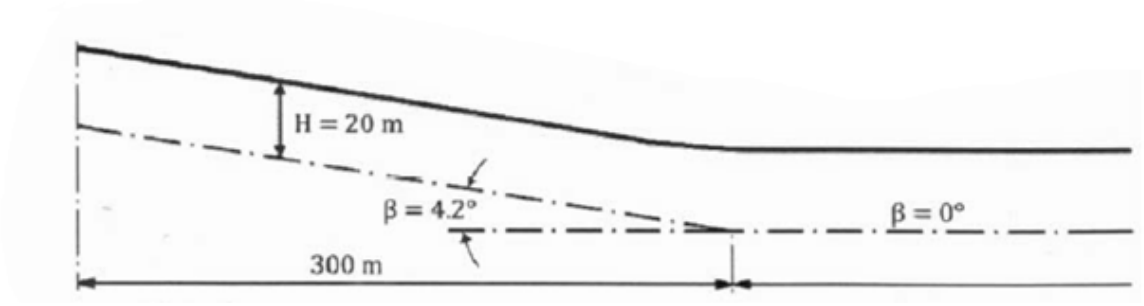

Figure 5.21Tuve scheme. After Bernarder 2011

The model finds the displacement (δ_{inst}), that is the ultimate displacement after that it is not possible to reach an equilibrium among the blocks.

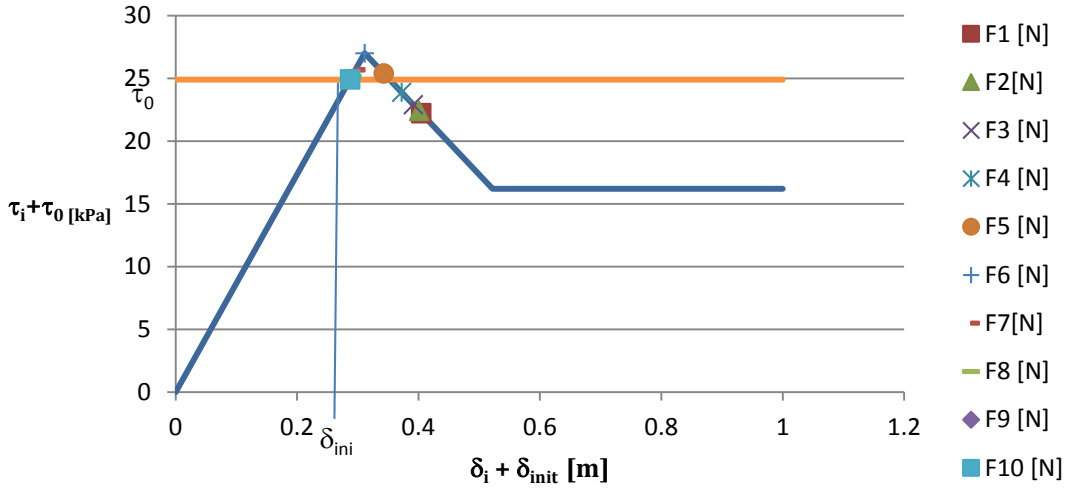

Figure 5.22 Final displacements of ten blocks in Tuve slide

In Figure 5.22 the displacements of all the blocks are represented. The first four blocks present a shear stress that is lower than the initial stress τ_0, so they give a negative contribute to the other blocks.

In Figure 5.23 the stress distribution and the exchange forces (N_i) are shown. The distribution is the same of the one in Bernarder (2011), but the residual value is not reached and the blocks are still on the strain softening line.

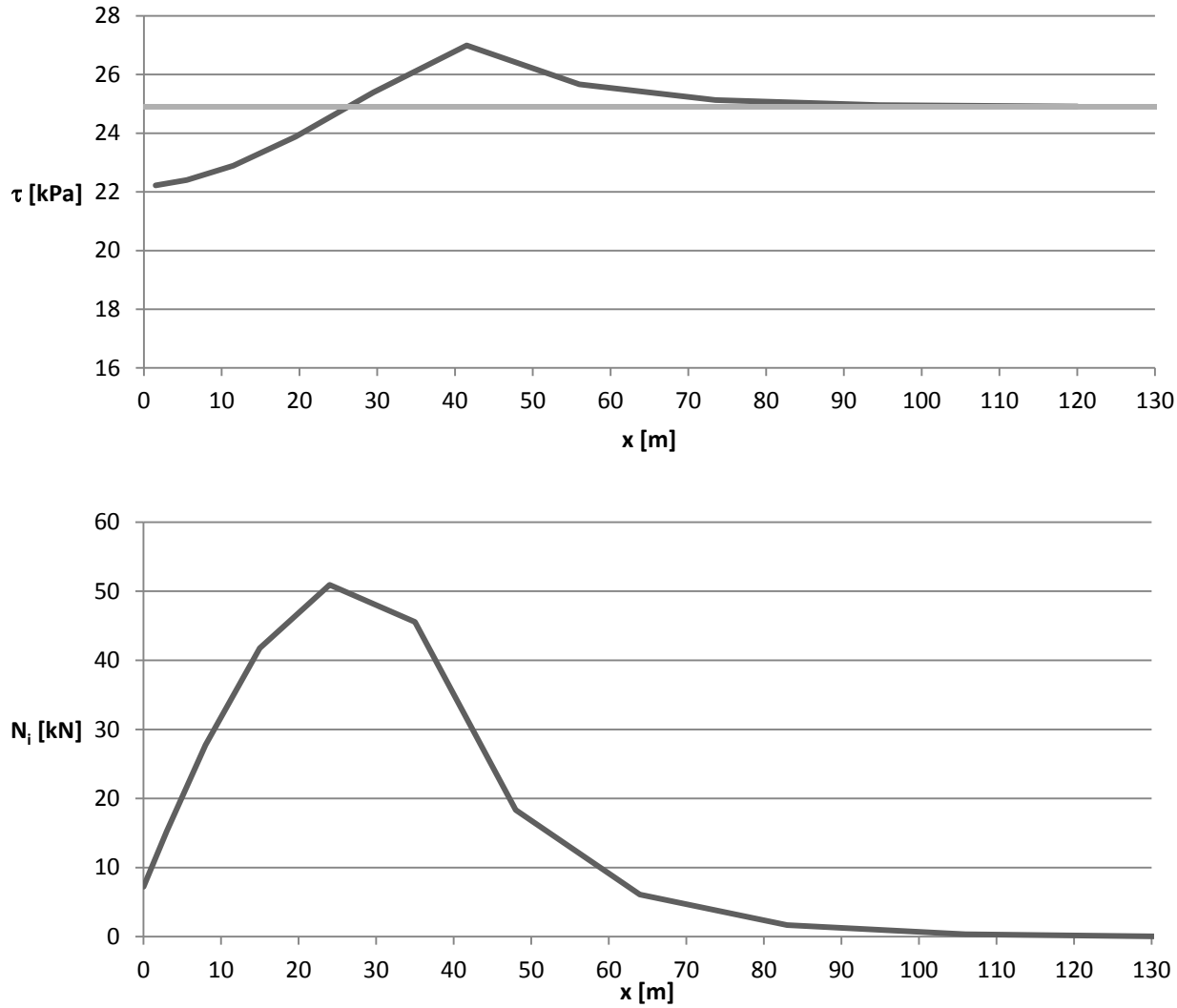

Figure 5.23 Stress and N_i distributions among the slope

As it is a punctual knowledge of distribution stress, also the maximum capacity is not perfectly reached when shear stress is equal to the in-situ initial stress and it entails lower value of N_{cr}.

5.4.2. Sensitivity Analysis

Using the results got for the Tuve slide, a sensitivity analysis has been done.

First analysis comes in useful to see if the model is sensitive of the length of the model.

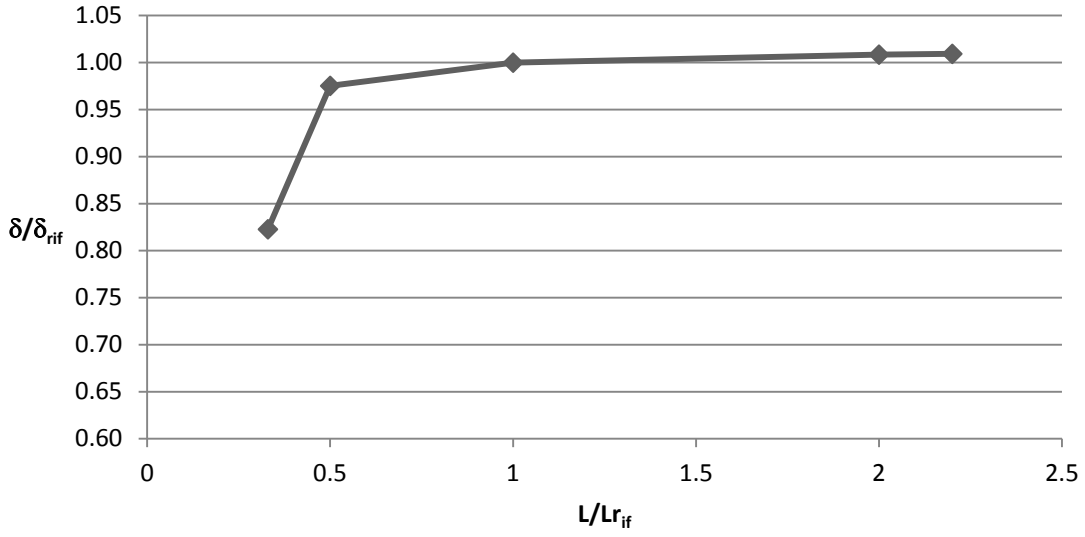

Figure 5.24 Displacement's sensitivity on the model's length

The results show that the model does not suffer of length variation, because it is almost constant but there are two limits:

- when the considered length is too long, the model cannot reach an equilibrium because the blocks are too long and cover all the negative length described in the precedent chapter;
- when the considered length is too short, the blocks do not cover all the length and so less resistance can be expressed. This happens when the considered length is less than an half of the reference length.

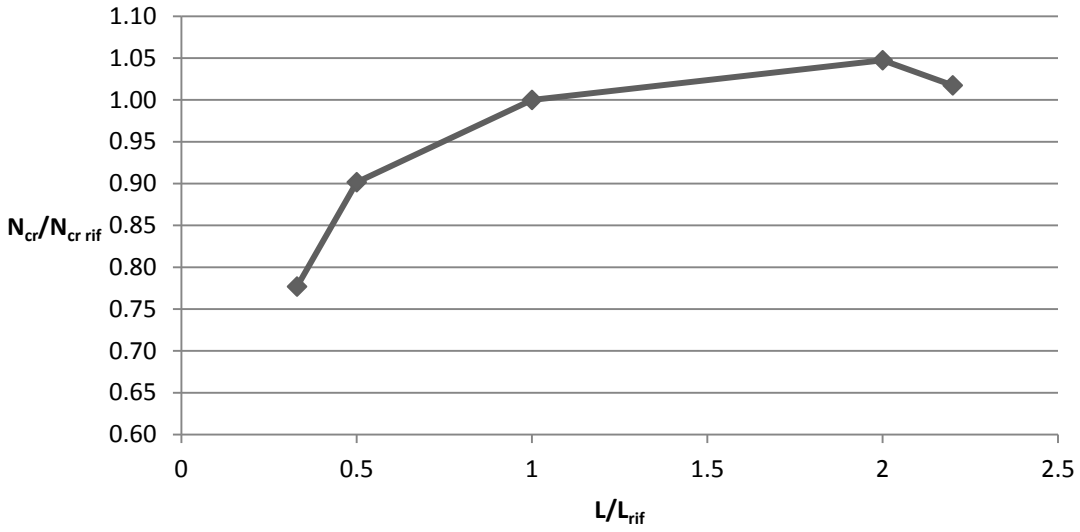

Figure 5.25 N_{cr}'s sensitivity on the model's length

N_{cr} is the maximum resistance or the critical load effect initiating local slope failure; it is reached when τ, after the peak c, is equal to τ_0. It does not vary a lot because when the length is twice the length of the slide the maximum resistance is 5% more while when length is an half, the maximum resistance is 10% less.

The following analyses have been made varying the inclination of the strain softening line (*sr*).

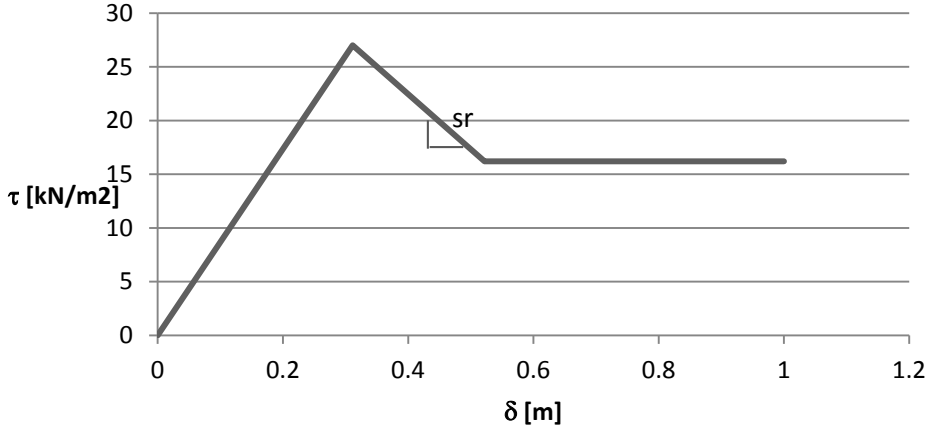

Figure 5.26 Inclination of the strain softening line

One of the most important parameter to take into account for studying progressive failure is the initial in-situ stress (τ_0), hence it is important to check how the model behaves varying this parameter.

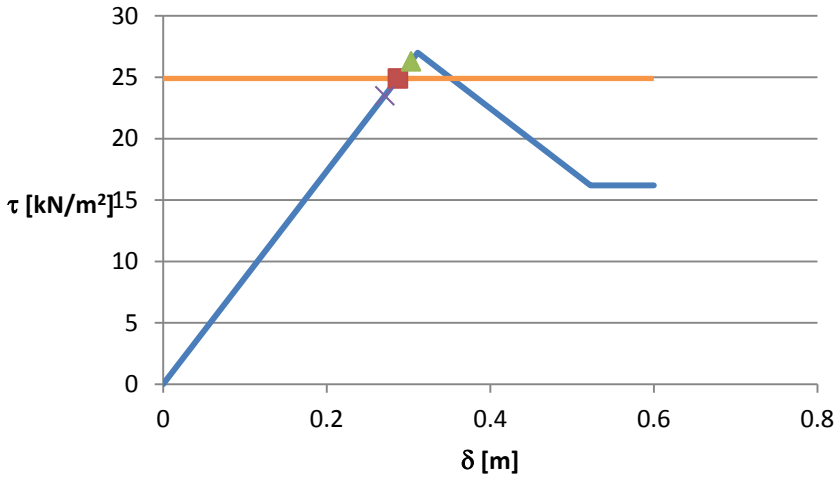

Figure 5.27 Variation of the in situ initial stress

The results, reported in Figure 5.28, show how the model is sensitive of the variation of τ_0 varying the inclination of the strain softening line. Higher inclination implies higher sensitivity and so a more brittle failure.

For the in situ initial stress equal to $\tau_{0\,rif}$ there is a difference of 68% of the critical displacement when *sr* is two times less inclined and 35% when is two times more inclined.

For $sr\ /sr_{ref}$ equal to 1 and for a variation of 28% of $\tau_0/\tau_{0\,ref}$ it entails that the solution compared to the reference solution varies of 33%.

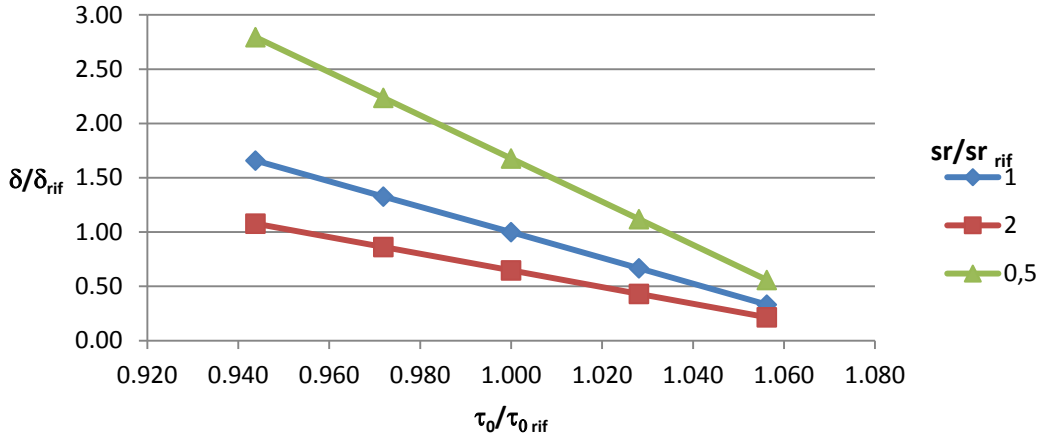

Figure 5.28 Displacement's sensitivity on the in situ initial stress

There are smaller differences for the maximum capacity: for the same initial in-situ stress there is a difference of 17% when is two times less inclined and of 19% when is two times more inclined for $\tau_0 = \tau_{0\,rif}$. In this case the curves are almost parallel and they do not diverge too much.

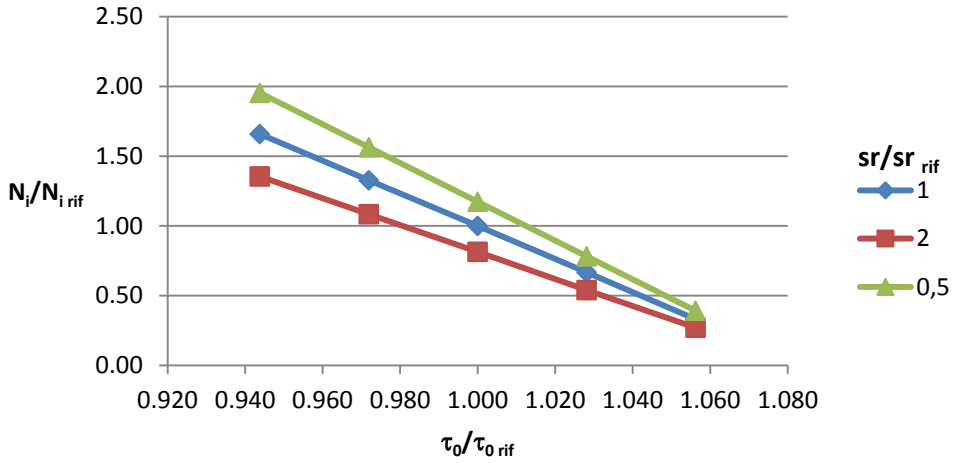

Figure 5.29 N_{cr}'s sensitivity on the in situ initial stress

Vary the peak *c*, keeping the same inclination of strain softening line *sr*, means that the point (δ_R) when the residual shear resistance is reached moves, like shown in Figure 5.30.

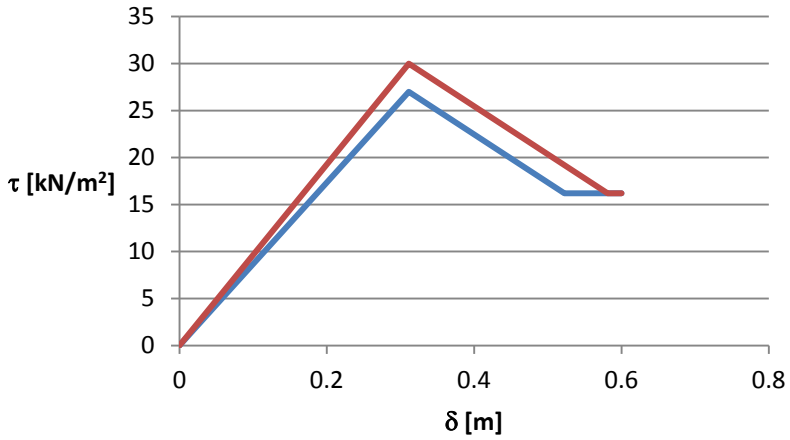

Figure 5.30 Variation of the peak *c*

Taking it in mind, the results of the analysis of peak sensitive are shown in the following figures.

When *sr* is twice the initial one, for c/c_{rif} equal to 1 there is a difference of 35%, while for *sr* equal to an half of the initial one the difference is 68%. In latter case the resistance increased because the positive area is bigger than before.

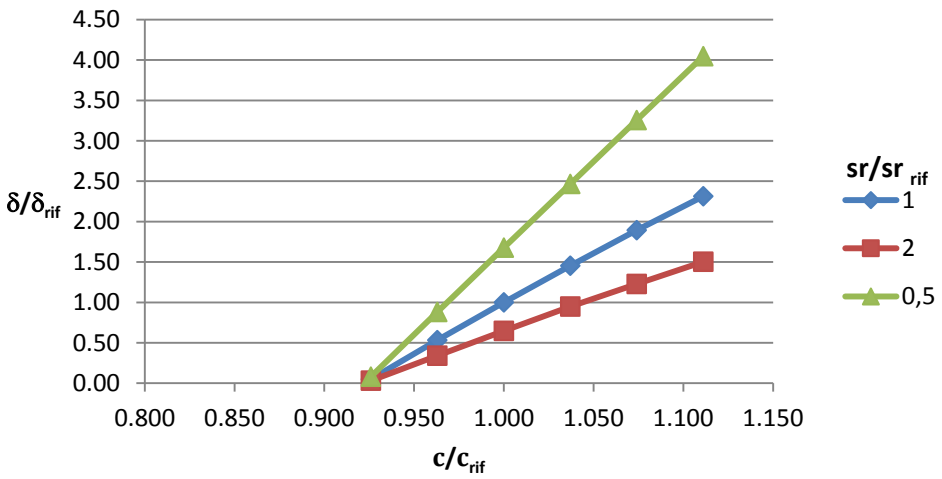

Figure 5.31 Displacement's sensitivity on the peak *c*

For the maximum capacity again the differences are smaller and the curves do not diverge much.

For the ratio between the peak and reference peak equal to 1 and for strain-softening line inclination two times more that the reference one there is a difference of 19%, while for *sr*/*sr* rif equal to 0,5 the difference is 18%. For a value of the peak 3.7% higher, the difference of the maximum capacity is 50%.

This means that it is more important to have the right value of the peak rather than the inclination of the strain-softening.

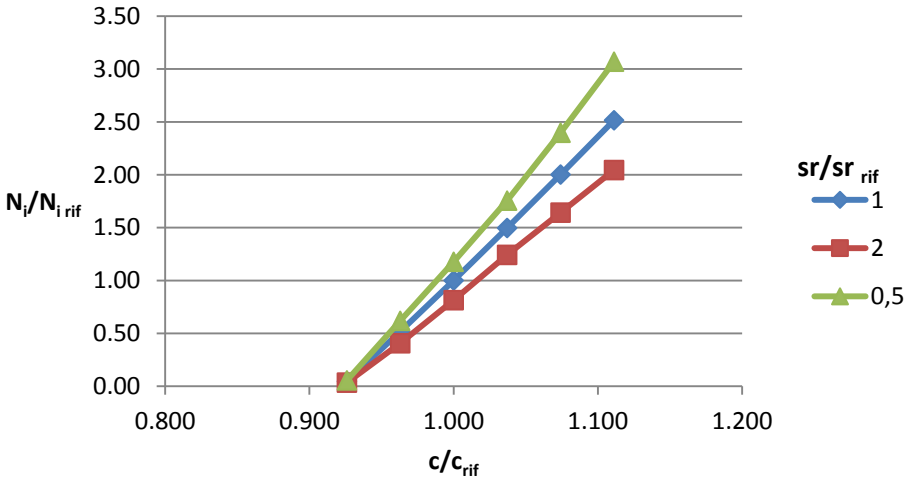

Figure 5.32 N_{cr}'s sensitivity on the peak *c*

The peak in this model has a determinant role; the model is very sensitive varying the peak and less varying the strain softening line inclination.

The last parameter taken into account is the residual shear resistance value.

Also in this case for keeping the same inclination the point δ_R has to move like shown in Figure 5.33.

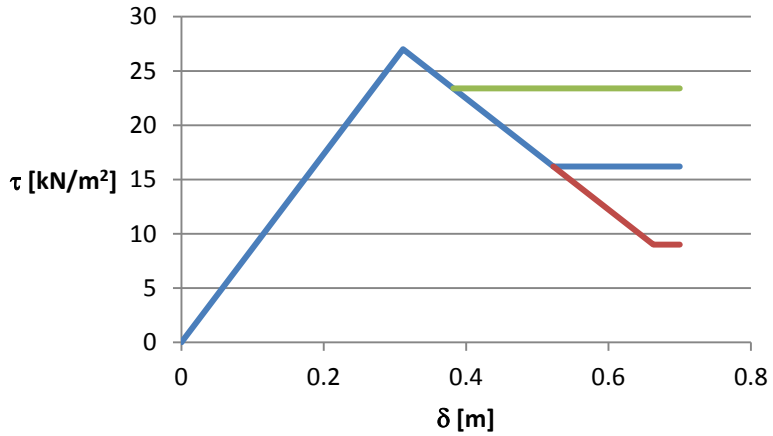

Figure 5.33 Variation of the residual value

As expected the model is insensitive of the value of c_R, here represented by the ratio between residual value and the reference peak (c_R/c_{rif}), until the value is so close to the peak than some blocks lie on the residual line. The model is insensitive of the value of c_R because the blocks do not reach the residual strength.

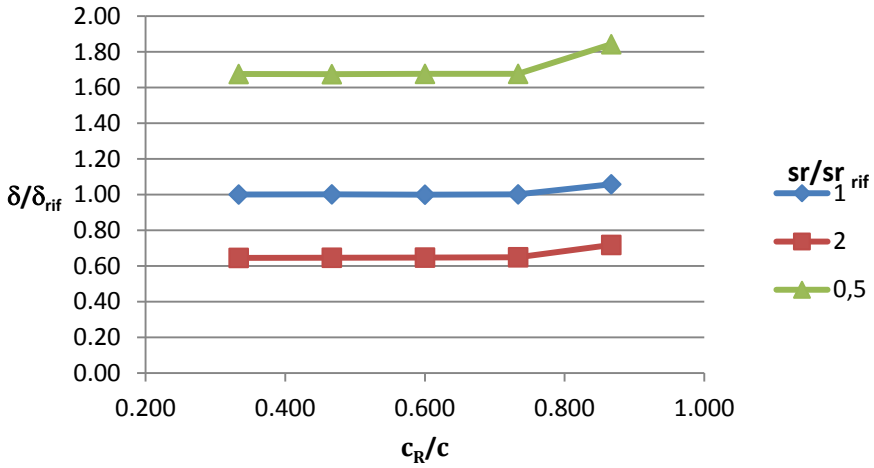

Figure 5.34 Displacement's sensitivity on the residual value c_R

Also the maximum capacity is not affected by the variation of the residual value in most of the analyzed cases.

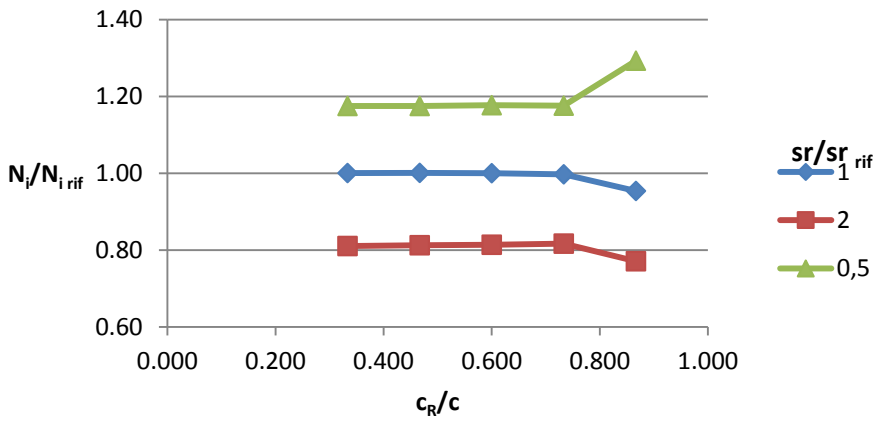

Figure 5.35 N_{cr}'s sensitivity on the residual value c_R

5.4.3. Comparison with FDM

Bernarder studied that slide in his PhD thesis and the results are inserted in it.

Using approximately the same constitutive relationship that Bernarder used for his studies, the physical model returned a result very close to Bernarder's one in terms of the triggering displacement.

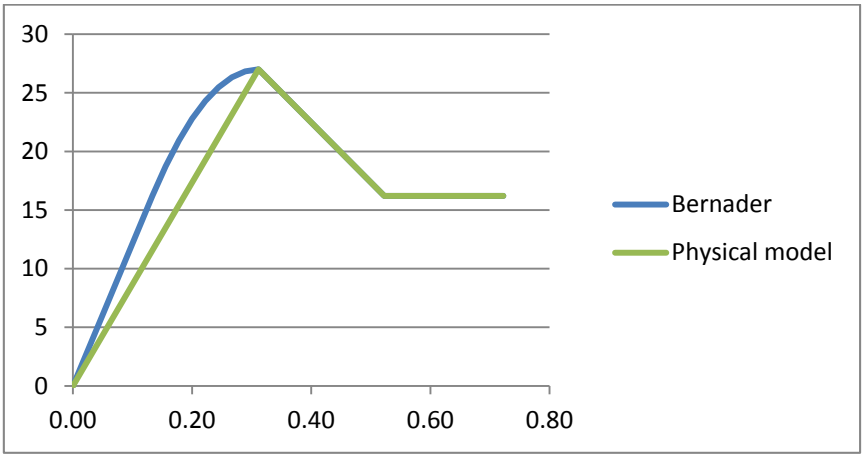

Figure 5.36 Differences between FDM and Physical model constitutive relationship

It has to be noted that the constitutive relationship in Bernarder varies along the surface, whereas it is the same in physical model as the one reported in Figure 5.36. The results of his studies and of the physical model are reported in the Table 5-2.

	FDM	Physical model	Difference
δ_{inst} [m]	0,105	0,117	11,8%
N_{cr} [kN]	75,8	50,93	48,8%

Table 5-2 Comparison of physical model and FDM

It has to be noticed that the difference in N_{cr} is high and this is due to the different constitutive relationships used and the fact that the model reported here considers big blocks while Bernarder used finite differences.

5.4.4. Some considerations

A small theoretical mistake is the triggering force that is shown in Figure 5.23. In fact, as the model can find only the destabilizing displacement, the force F should be equal to zero, but in this case there is still a little force and it entails some errors on the results.

Another error that probably affects the result of the maximum capacity is the constitutive relationship, because the model tries to find the physical features of the material behaviour, like the peak and the strain softening line, while Bernarder used the real behaviour testing some samples in a particular direct shear test (Bernarder 1985).

In addition Bernarder reproduced all the profile of the slide varying also the soil behaviour among the slope. Here, instead, an infinite slope has been considered with the same features among the entire slip surface.

So for the simplicity of the model compared to FDM, the results are very satisfactory.

5.5. Remarks on the model

When a strain-softening behaviour is present, the equilibrium is not so easy to reach. In fact if someone has a look at the iterations could see that when an equilibrium seems to be reached and the displacements are such that the peak is almost reached, after the peak the equilibrium became again far to be reached. The displacements, in fact, have to be higher, but in this way there is a loss of strength and so on.

The physical model is a simplified way to study the triggering phase of a local failure in sensitive clays. It is very simple from both a theoretical and practical points of view. It is also very flexible; in fact it is possible to change all the geometry of the slope, the constitutive relationship and the initial in situ conditions (initial stress and also the presence of a preformed slip surface)

The purpose of the present thesis was to use the model as a preliminary valuation of the safety of a slope. In fact, according to Bernarder (2011), a safety factor can be used and then the model can be useful for the valuation of the stability of a slope.

The results of comparison between FDM and physical model show that the latter approximates on the side of safety.

The model is sensitive to changes of constitutive relationship, so it is very important to choose the appropriate constitutive relationship to insert into the model.

Sometimes it suffers of convergence problems as it has been implemented in excel, but that kind of problems has been got over.

Further work

The model can be improved leaving its simplicity features.

In fact to have better results and a better representation of the slope it should be possible to have different soil behaviours for each block.

In addition more blocks could be implemented to have a better resolution of stress distribution along the potential slip surface and to reproduce the slope.

To avoid convergence problems and to have a lighter file, it should be better to improve the convergence algorithmic or it might be implemented in other programming software.

6. Modelling downwards progressive failure with FEM

6.1. An advanced constitutive model: NGI ADPsoft Model

6.1.1. General features

The NGI-ADPsoft model is the evolution of the NGI-ADP model (Grimstad and Jostad 2010), which is an anisotropic undrained shear strength model. It is an elasto-plastic model with anisotropic strain hardening/softening response and it incorporates a regularization technique.

The basis of the material model is:

- input parameters for undrained shear strength for three different stress paths/states (Active, Direct Simple Shear and Passive);
- input parameters for softening features for three different stress paths/states (Active, Direct Simple Shear and Passive);
- a yield criterion based on a translated approximated Tresca criterion;
- elliptical interpolation functions for plastic failure strains and for shear strengths in arbitrary stress paths;
- isotropic elasticity, given by the unloading/reloading shear modulus, G_{ur}.

NGI-ADPsoft derives from NGI-ADP and to incorporate the softening response a second hardening function k_2 has been included in addition to the original hardening function k_1.

$$\kappa_1 = 2 \cdot \frac{\sqrt{\gamma^p / \gamma_p^p}}{1 + \gamma^p / \gamma_p^p} \text{ when } \gamma^p < \gamma_p^p \text{ else } \kappa_1 = 1$$

$$\kappa_2 = \begin{cases} 0 & \text{when} \quad \gamma^{p^*} \le \gamma_p^p \\ \frac{1}{2} \cdot \left(1 - \cos\left(\pi \cdot \frac{\gamma^{p^*} - \gamma_p^p}{\gamma_r^p - \gamma_p^p} \right) \right) & \text{when} \quad \gamma_p^p < \gamma^{p^*} < \gamma_r^p \\ 1 & \text{when} \quad \gamma^{p^*} \ge \gamma_r^p \end{cases}$$

Equation 6-1 Hardening and softening functions in the NGI-ADPsoft model

where γ^P and γ^{P*} are local and non-local plastic shear strains (see chapter 2.2.2), $\gamma_P{}^P$ and $\gamma_r{}^P$ are stress state dependent plastic peak and residual shear strain.

The model presents a yield criterion based on a translated approximated Tresca criterion and the modified stress vector, which incorporates anisotropy in shear strength and hardening/softening response, is presented below:

$$\begin{bmatrix} \hat{s}_x \\ \hat{s}_y \\ \hat{s}_z \\ \hat{s}_{xy} \\ \hat{s}_{xz} \\ \hat{s}_{yz} \end{bmatrix} = \begin{bmatrix} \sigma_x - p + (1-\kappa_1)\cdot\frac{2}{3}\cdot\tau_0 + \kappa_1\cdot(1-\kappa_2)\cdot\frac{1}{3}\left(s_u^A - s_u^P\right) + \kappa_2\cdot\frac{1}{3}\left(s_{ur}^A - s_{ur}^P\right) \\ \sigma_y - p - (1-\kappa_1)\cdot\frac{4}{3}\cdot\tau_0 - \kappa_1\cdot(1-\kappa_2)\cdot\frac{2}{3}\left(s_u^A - s_u^P\right) - \kappa_2\cdot\frac{2}{3}\left(s_{ur}^A - s_{ur}^P\right) \\ \sigma_z - p + (1-\kappa_1)\cdot\frac{2}{3}\cdot\tau_0 + \kappa_1\cdot(1-\kappa_2)\cdot\frac{1}{3}\left(s_u^A - s_u^P\right) + \kappa_2\cdot\frac{1}{3}\left(s_{ur}^A - s_{ur}^P\right) \\ \tau_{xy}\cdot\left(\frac{s_u^A + s_u^P}{2\cdot s_u^{DSS}}\cdot(1-\kappa_2) + \kappa_2\cdot\frac{s_{ur}^A + s_{ur}^P}{2\cdot s_{ur}^{DSS}}\right) \\ \tau_{xz} \\ \tau_{yz}\cdot\left(\frac{s_u^A + s_u^P}{2\cdot s_u^{DSS}}\cdot(1-\kappa_2) + \kappa_2\cdot\frac{s_{ur}^A + s_{ur}^P}{2\cdot s_{ur}^{DSS}}\right) \end{bmatrix}$$

Where $\sigma_{x,y,z}$ and $\tau_{xy,xz,yz}$ are the Cartesian stresses and p is the mean stress.

The yield criterion is defined as:

$$F = \sqrt{\hat{J}_2}\cdot H\left(\hat{J}_2, \hat{J}_3\right) - \kappa_1\cdot(1-\kappa_2)\cdot\frac{s_u^A + s_u^P}{2} - \kappa_2\cdot\frac{s_{ur}^A + s_{ur}^P}{2} = 0$$

The invariants J_2 and J_3 are calculated from the modified stress vector. $H(J_2,J_3)$ is defined as:

$$H\left(\hat{J}_2, \hat{J}_3\right) = \left|\cos\left(\frac{1}{6}\arccos\left(1 - a_1\cdot\frac{27}{2}\cdot\frac{\hat{J}_3^{\,2}}{\hat{J}_2^{\,3}}\right)\right)\right|$$

The parameters of the model are 28 (see chapter 6.1.3), and most of them can be obtained from anisotropically consolidated undrained laboratory tests: triaxial compression and extension tests and undrained direct simple shear tests.

One of the main features of the model is that it takes into account the anisotropic soil behaviour. Typical strength and strain values are presented in sect. 2.2.4.

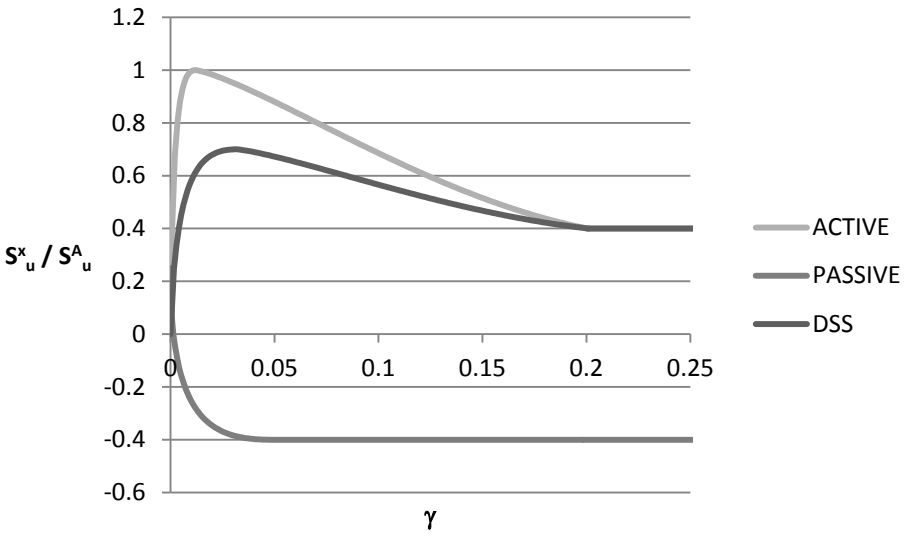

Figure 6.1 Anisotropy considered in the calculations

6.1.2. Regularization Over non-local Strain Approach

To model the post-peak strain softening response an internal length is needed as the response beyond the peak shear stress is not unique and the results become mesh dependent. In fact without a proper regularization technique the thickness and the orientation of the shear band depend on the adopted mesh.

The model uses a simple version of the non-local strain approach, because it can be implemented into a non-linear finite program without reformulating the governing finite element equations.

The non-local strain approach is implemented only at the material point level and this allows to be implemented in user-defined material models in Plaxis or in other commercial finite element programs.

The over non-local plastic strain approach derived from the classical non local strain formulation made by Eringen (1981).

The strain softening response in an integration point is governed by $\Delta\varepsilon^{p*}$ within a specific volume dependent on the internal length.

Brinkgreve (1994) found that, using the classical non local formulation, the strain may concentrate in central point of the localized zone and not spreading to the surrounding points and he proposed this approach in which it reduces the strain in the centre and increases the strain to the edge of the softening zone. This behaviour is controlled by the parameter α that has to be larger than one.

The over non-local strain formulation is:

$$\Delta\varepsilon^{p^*}(\mathbf{x}_i) = \Delta\varepsilon^{p}(\mathbf{x}_i) - \alpha \cdot \Delta\varepsilon^{p}(\mathbf{x}_i) + \frac{\alpha}{V}\int \left(w(\mathbf{x}) \cdot \Delta\varepsilon^{p}(\mathbf{x}) \right) dV$$

Where $V = \int w(\mathbf{x}) dV$ and $w(\mathbf{x}) = \int \frac{1}{l\sqrt{\pi}} \cdot e^{-\frac{(x-x_i)^T \cdot (x-x_i)}{l^2}} dV$ and x_i is the integration point coordinates and l is the internal length.

In this way the shear band thickness is controlled by α and internal length (l or l_{int}) parameters.

The shear band thickness can be calculated using the formula given by Brinkgreve (1984):

$$t_{sb} = \pi \cdot l_{\text{int}} \cdot \left(\ln\left(\frac{\alpha}{\alpha - 1} \right) \right)^{-\frac{1}{2}}$$

It entails that for $\alpha = 1{,}58$ t_{sb} is equal to $\pi \cdot l_{int}$, while for $\alpha = 2$ t_{sb} is equal to $3{,}77 \cdot l_{int.}$

The internal length sets the shear band thickness, but, as the model requires a mesh that must be finer than the specified internal length, the result is not directly mesh dependent but indirectly it is.

Furthermore the thickness of the shear band is unknown, especially for potentially slides, as the thickness is controlled by the particle size, deformation rate, local pore pressure dissipation and boundary condition.

6.1.3. Parameters

The model has 28 parameters that may be divided in four categories:

- Hardening parameters;
- Softening parameters;
- Geometric parameters;
- Others.

Most of them are refereed to active undrained strength.

	Number	Parameters	Explanation
Hardening parameters	1	G_{ur}/S_u^A	Ratio unloading/reloading shear modulus over active shear strength
	2	$S_u^A{}_{ref}$	Reference active shear strength
	3	$S_u^A{}_{incl}$	Increase of shear strength with depth
	4	S_u^{DSS}/S_u^A	Ratio of direct simple shear strength over active shear strength
	5	S_u^P/S_u^A	Ratio of passive shear strength over active shear strength
	6	τ_0/S_u^A	Initial mobilization
	7	ν	Poisson's ratio
	8	ν_u	Undrained
	9	$\gamma_P^{C,TX}$	Shear strain at failure in triaxial compression
	10	γ_P^{DSS}	Shear strain at failure in direct simple shear
	11	$\gamma_P^{E,TX}$	Shear strain at failure in triaxial extension
Softening parameters	12	S_{ur}^A/S_u^A	Ratio of residual active shear strength over active shear strength
	13	S_{ur}^{DSS}/S_u^A	Ratio of residual direct simple shear strength over active shear strength
	14	S_{ur}^P/S_u^A	Ratio of residual passive shear strength

			over active shear strength
	15	$\gamma_r^{C,TX}$	Shear strain at residual value in triaxial compression
	16	γ_r^{DSS}	Shear strain at residual value in direct simple shear
	17	$\gamma_r^{E,TX}$	Shear strain at residual value in triaxial extension
	18	c_1	Softening shape parameter 1
	19	c_2	Softening shape parameter 2
	20	α	Parameter for over non-local strain
	21	l_{int}	Internal length
Geometric parameters	22	x_{ref}	Position of y_{ref}
	23	y_{ref}	Reference depth of active undrained strength
	24	$\Delta y_{ref}/\Delta x$	Variation of y_{ref} with x
Others	25	1-l*/l	Parameter of scale
	26	INT.TYPE	Type of interpolation
	27	GS-pl/tot=0/1	
	28	DEBUG	

Table 6-1 List of all parameters of NGI-ADPsoft model

6.2. Different types of analyses

6.2.1. A simple case

The procedure can be divided into two macro phases: the local mode and the long global mode.

In the first the bearing capacity of the slope and the local failure have been found, while, in the latter, the global failure has been got.

As the procedure is not so easy to understand, in the following paragraphs a simple slope is used as an example, whereas in the paragraph 6.3 a real slope is dealt with.

In Figure 6.2 the geometry of the example is shown, in which beneath a dry crust there is a pocket of soft clay, divided into three clusters as the model needs to have different clusters because of its parameters.

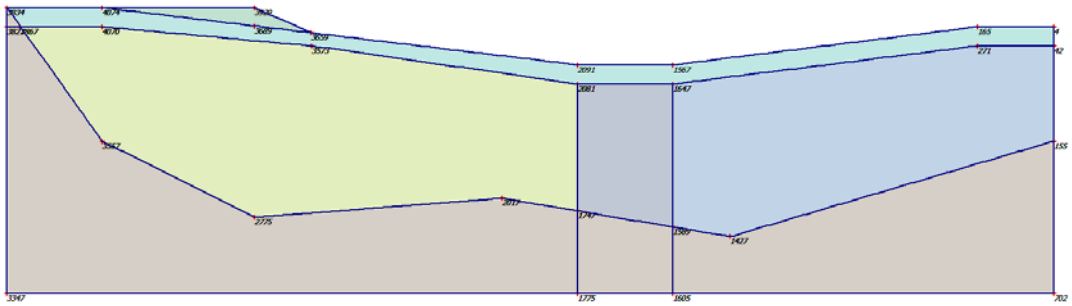

Figure 6.2 Plot of geometry model with significant nodes

The slide has been studied using different phases, reported in Table 6-2.

Phase	Ph-No.	Start phase	Calculation type	Load input	First step	Last step
Initial phase	0	0		-	0	0
Equilibrium	1	0	Plastic analysis	Staged construction	280	284
Load	2	1	Plastic analysis	Staged construction	277	279
Increasing load	3	2	Plastic analysis	Incremental multipliers	285	450
Applied load	4	2	Plastic analysis	Total multipliers	101	167
Increasing weight	5	4	Plastic analysis	Incremental multipliers	168	276

Table 6-2 Phases in the example's calculation

After the initial phase in which represents the initial situation of the project as defined in the initial conditions mode of the Input program. It is the starting point for further calculations. The initial stress condition using Mohr Coulomb and gravity loading is very dependent on ν and therefore it is difficult to get a good distribution with gravity loading. Hence a k_0 procedure has been used as the initial stress condition obtained with the NGI-ADP model is based on a stress condition that is unloaded from erosion with a drained ν.

The phase 1 is useful as an equilibrium step with “drained” NGI-ADP soft model. This is to obtain equilibrium between the initial stress generated by k_0 procedure and the strength parameters of NGI-ADP model. NGI-ADP is used as “drained” ignoring undrained behavior. The following phases will have the displacements reset to zero.

In Figure 6.3 the active undrained shear strength distribution, set in NGI-ADPsoft model, is shown.

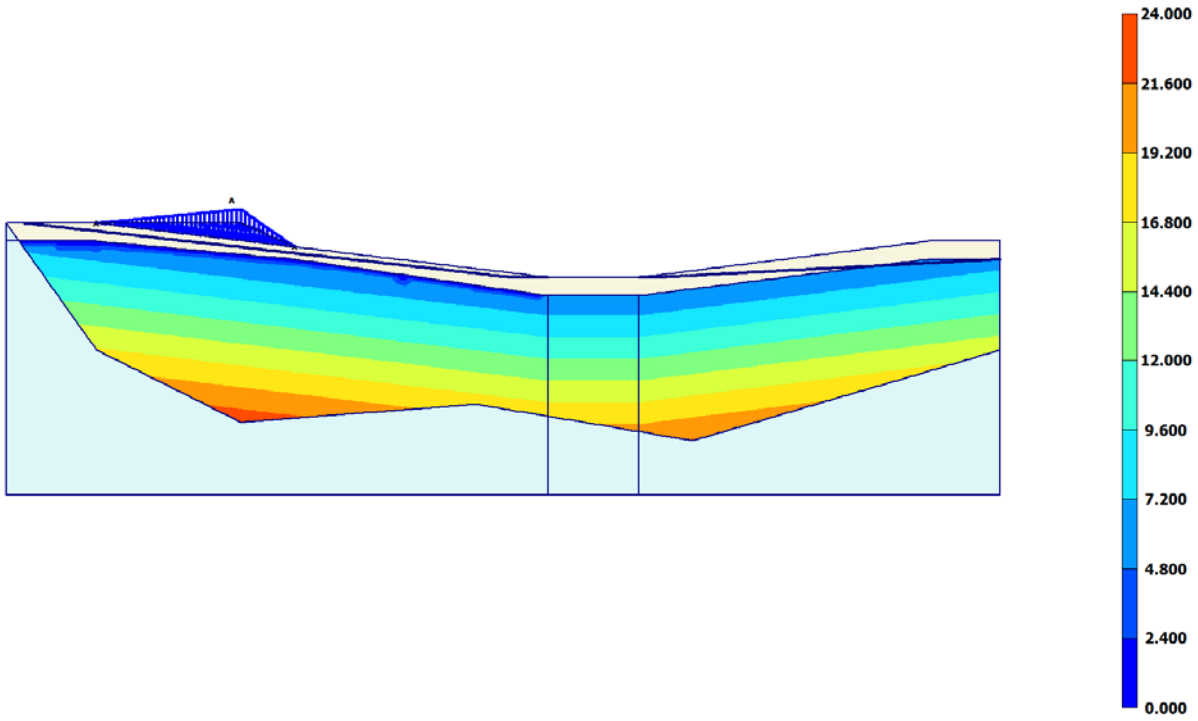

Figure 6.3 Su^A distribution within the slope

6.2.2. Local mode

The first three phases are used to get the bearing capacity of the slope and to get the local failure mode.

In the phase 2 the load is activated and in the phase 3 the load is incremented through incremental multiplier to get the maximum bearing capacity. After the peak the load decreases to get equilibrium as the slope cannot carry the same load than before.

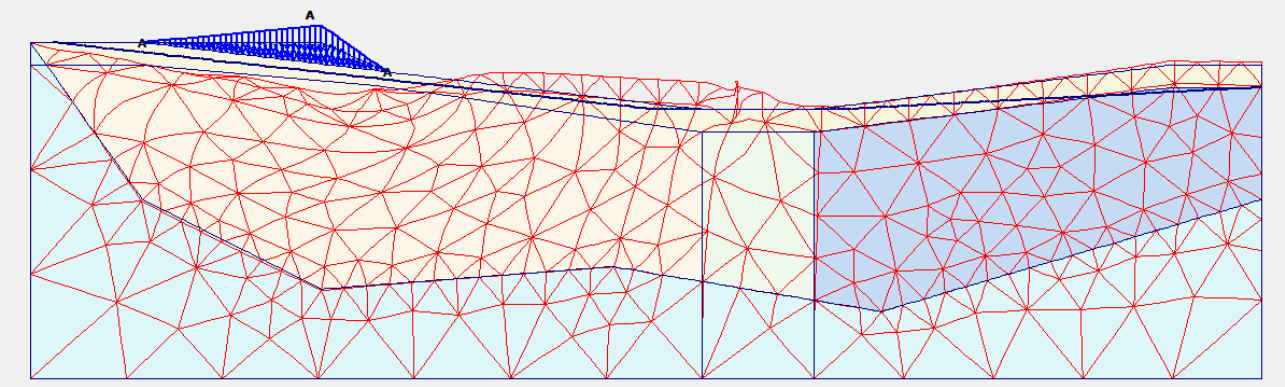

Figure 6.4 Deformed mesh in the example bearing capacity

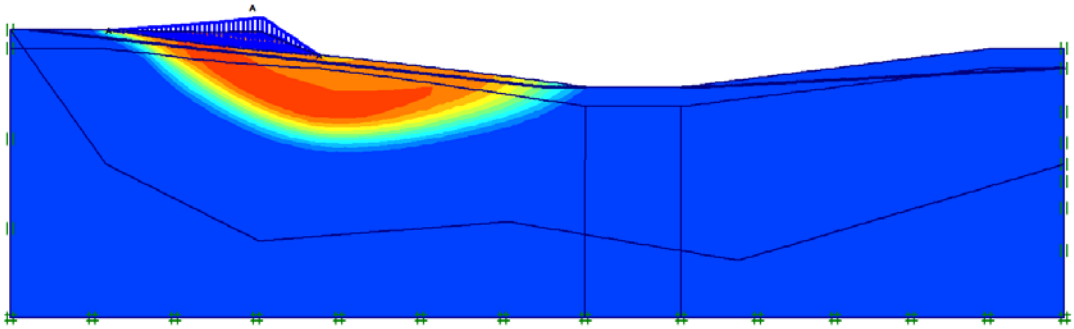

Figure 6.5 Total incremental displacements in the example bearing capacity

In Figure 6.5 the total incremental displacements, after that the slope reached the maximum capacity, are shown.

6.2.3. *Long global mode*

To get the progressive failure the procedure is to apply a load having the same value, or slightly lower, than the one got in the precedent phase. This is the phase 4 in which through total multiplier the load is applied and then the weight of the entire domain is increased. Incremental multiplier on weight with no arc length control, to ensure propagation with updated mesh, is useful to get equilibrium between softening and update mesh effects. In this case the load is kept constant for all the calculations.

In the ordinary calculations the load decreases due to softening behavior, whereas using this procedure the load is constant and the incremental multiplier on weight leads to a very small total increase in weight. In fact after a few iterations the weight reaches a value that is slightly higher than 1 (in this case 1.001) and then the calculations go on with this constant value. This check is very important otherwise for high value of weight it means that the calculation is far from reality.

The following chart shows what is explained above: the load, increasing the weight, is constant while using ordinary calculations it decreases. It is also present the effect of update mesh that entails that the load increases as the slope moved and so it needs more load to have more movement.

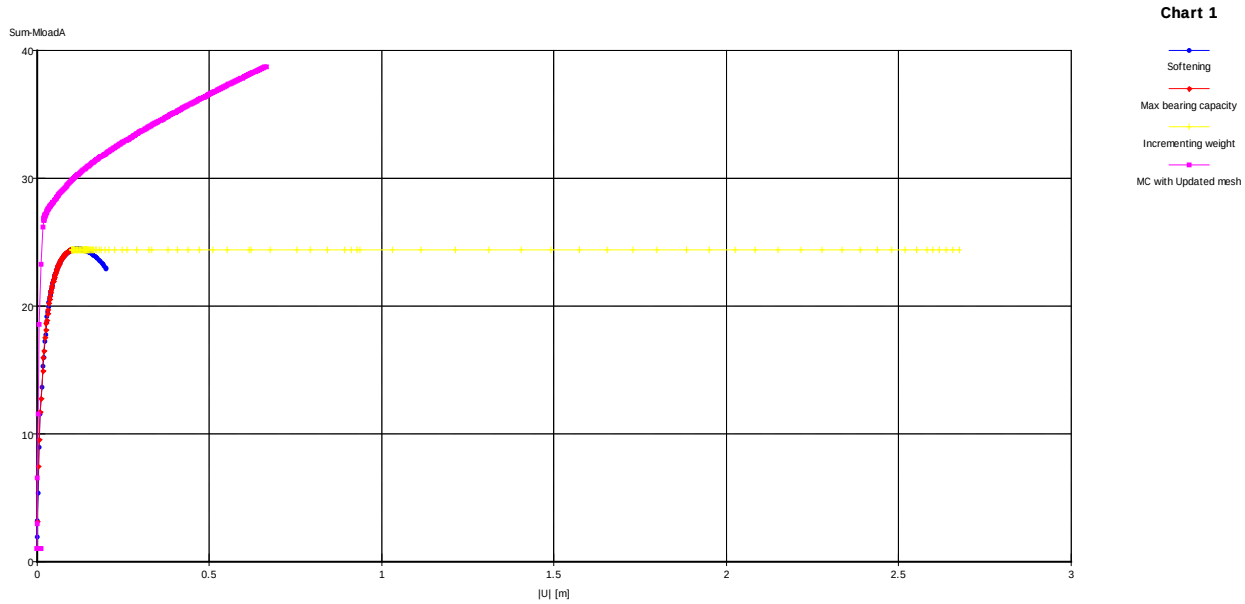

Figure 6.6 Procedure used taking into account softening and update mesh effects. After having applied a load slightly lower than the bearing capacity, the weight is increased and it entails that the load is constant during the calculations.

In the Figure 6.6 it is possible also to see the very high number of steps that the calculations need to get the equilibrium. In the Appendix 2nd: Plaxis - Manual settings all the manual settings are reported. They have been changed to avoid that calculations stop before reaching the equilibrium.

Step by step the portion of the slope involved in the landslide extends and in the Figure 6.7 the total incremental displacements of the last step is reported.

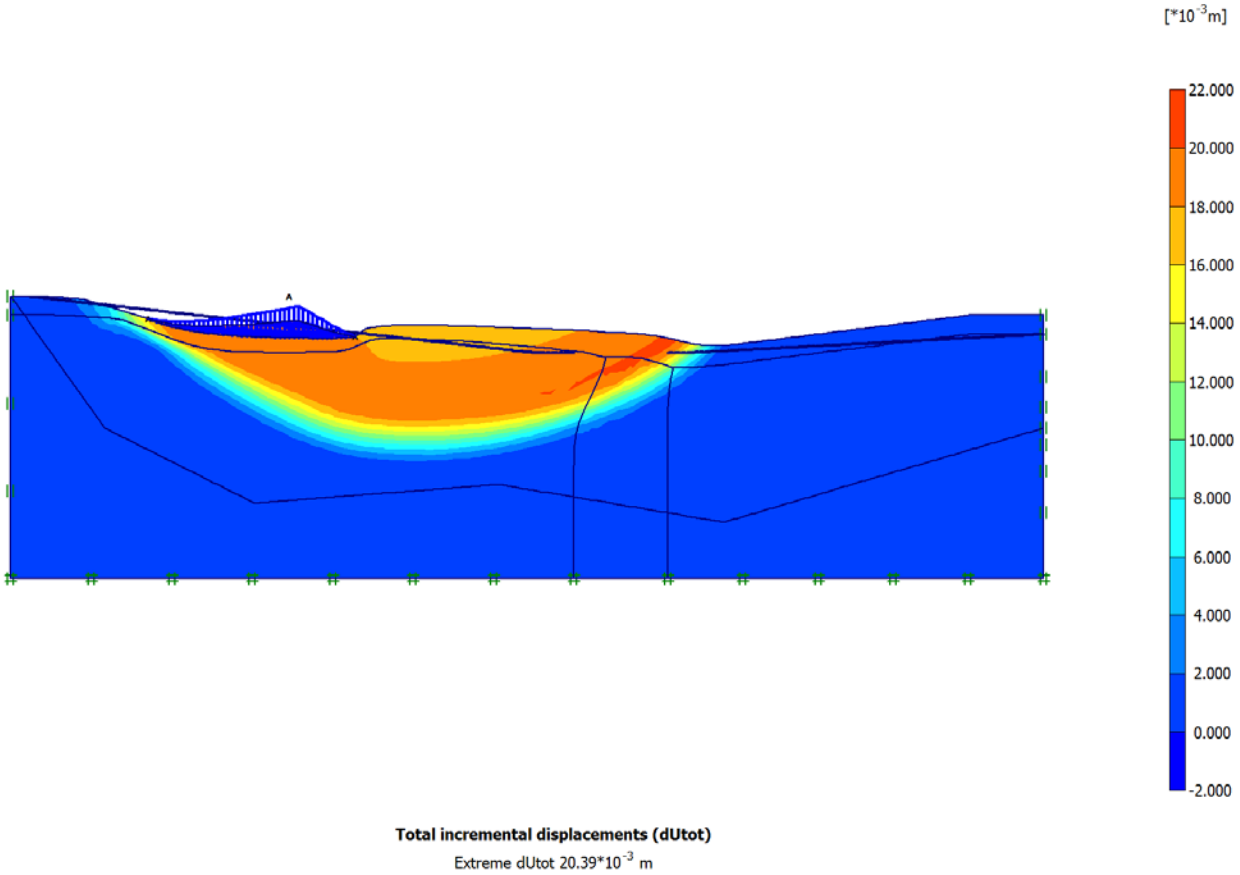

Figure 6.7Total incremental displacements in the example's progressive failure

6.3. An application to Smaaroed Slide

6.3.1. Features of the landslide

On 20th of December 2006, part of a major road in western Sweden has collapsed in a landslide.

The slide involved the E6 near Smaaroed, south of Munkedal during the evening, just before 8 pm.

Figure 6.8 Location of Smaaroed slide, after Google maps

Fortunately no deaths or serious injuries happened although cars were involved in the slide.

The volume of the slide was approximately 750.000 m^3 and it extended over a length of 200 m (east/west) and a width of 500 m (north/south).

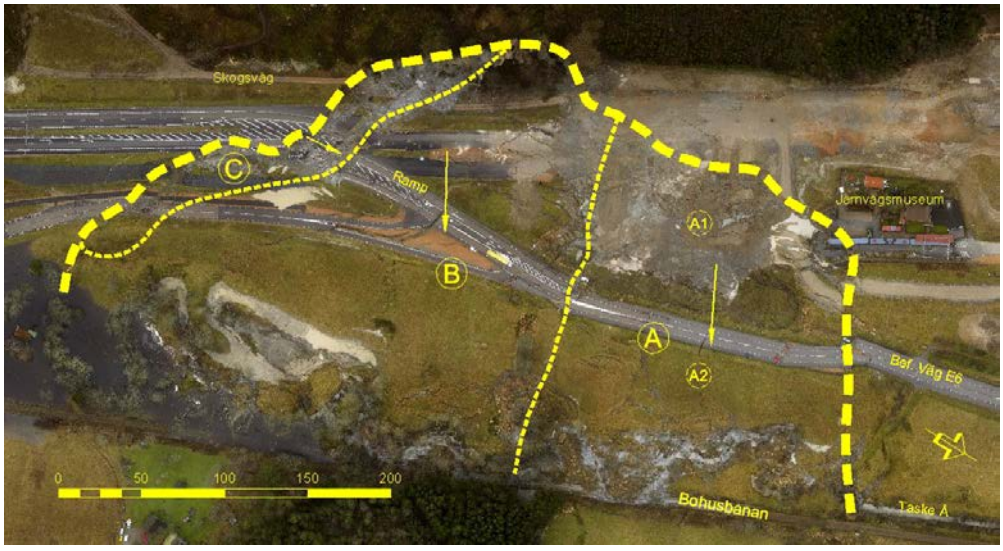

Figure 6.9 Smaaroed slide, Swedish Road Administrations Independent Investigation Committee. (2007).

The slide involved the old road E6, part of the under construction road E6 and the nearby railroad was damaged.

The ground consisted mainly of soft, sensitive clay over a firm layer believed to be till. Beneath the firm layer there is solid rock.

As reported in Figure 6.9 and by the Swedish Road Administrations Independent Investigation Committee (SRAIIC), the landslide can be divided into three main surfaces.

The first surface A is the initial failure, and it will be modelled in this chapter, then it followed by surface B and at the end by surface C.

Probably the trigger of the slide was a fill placed at top of the slope next to main road E6, approximately where the symbol A1 is placed. The height of the fill is unknown but due to witness and to the material found, it is believed to be as high as 7 meters. It is not established if the fill entailed a local failure and then a downward progressive failure or a global failure happened before the local failure as the conditions to trigger both failures are very close, but probably the slide started with the local failure.

6.3.2. Modelling the slope

The analyses have been performed choosing the critical profile reported in Figure 6.10.

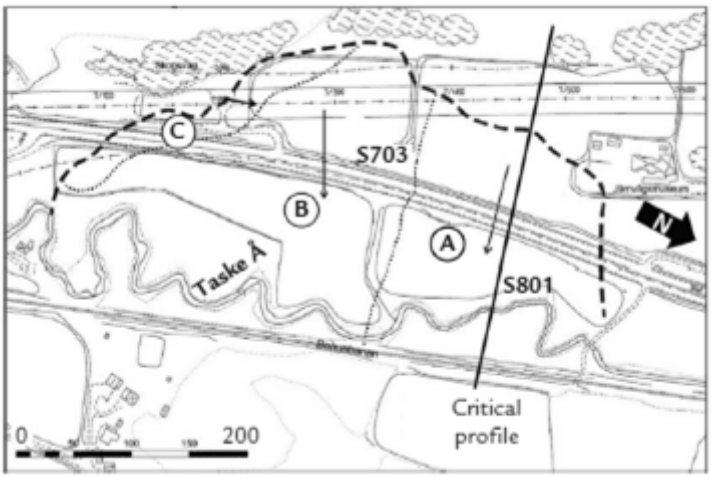

Figure 6.10 Critical profile in Smaaroed slide, Swedish Road Administrations(2007).

In this profile the slip surface is believed to be at 15 m below ground level and it is estimated on basis of sounding performed after the slide (Figure 6.11). This implies that severe earth volumes are affected by the landslide.

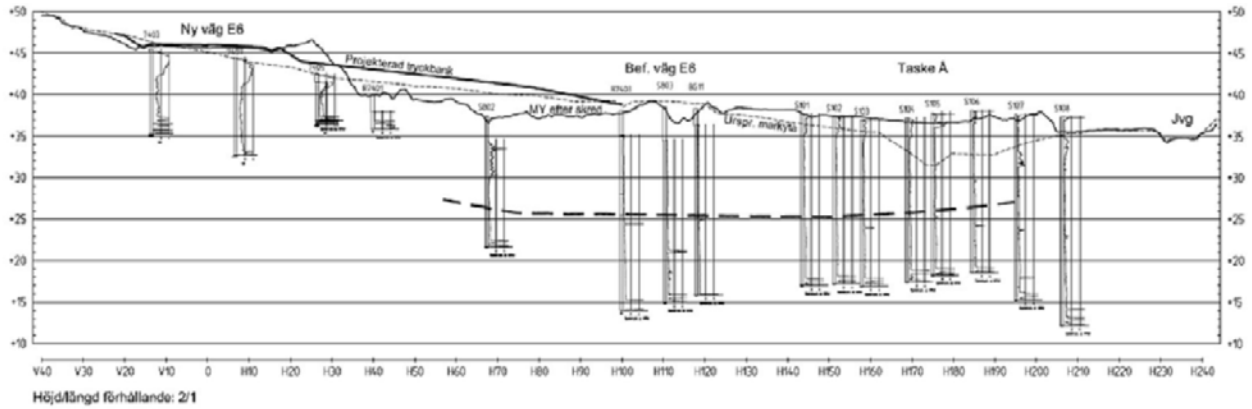

Figure 6.11 Slip surface based on soundings performed shortly after the slide. From Swedish Road Administrations (2007)

In this paragraph all the analyses made on Smaaroed slide are presented, in which it has been divided into two sub-chapters as the precedent one.

The clusters are shown in Figure 6.12 in which beneath a dry crust there are the clusters modelled with NGI-ADPsoft. At the lower part a firm bottom has been considered. The others clusters, excepted the ones modelled with NGI-ADPsoft model, are made by simplified models like Mohr-Coulomb and Elastic Linear.

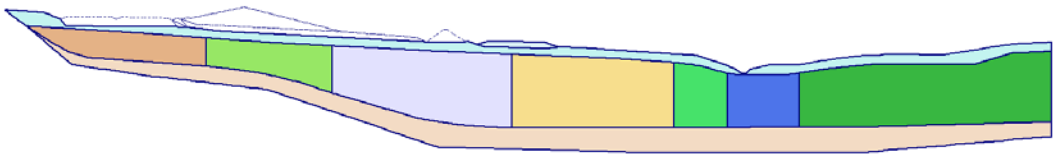

Figure 6.12 Clusters in Smaaroed simulations using NGI-ADPsoft model

As the model needs a mesh that is smaller than the internal length, the clusters involved in the progressive failure have a mesh smaller than 1 m, as reported in Figure 6.13. As the calculation time is very long the mesh has been reduced where it was necessary. The model used is plane-strain with 5917\6-noded elements.

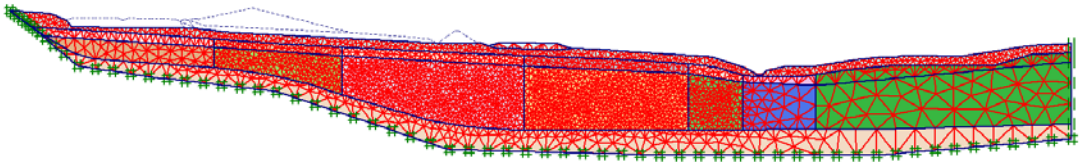

Figure 6.13 Mesh distribution

Through the choice of parameters reported in "Appendix 3rd: Smaaroed Slide - Steps to get Su^A distribution" the active undrained shear strength assumes the distribution shown in Figure 6.14. The upper part is kept constant, while in the lower part the active strength increases with depth.

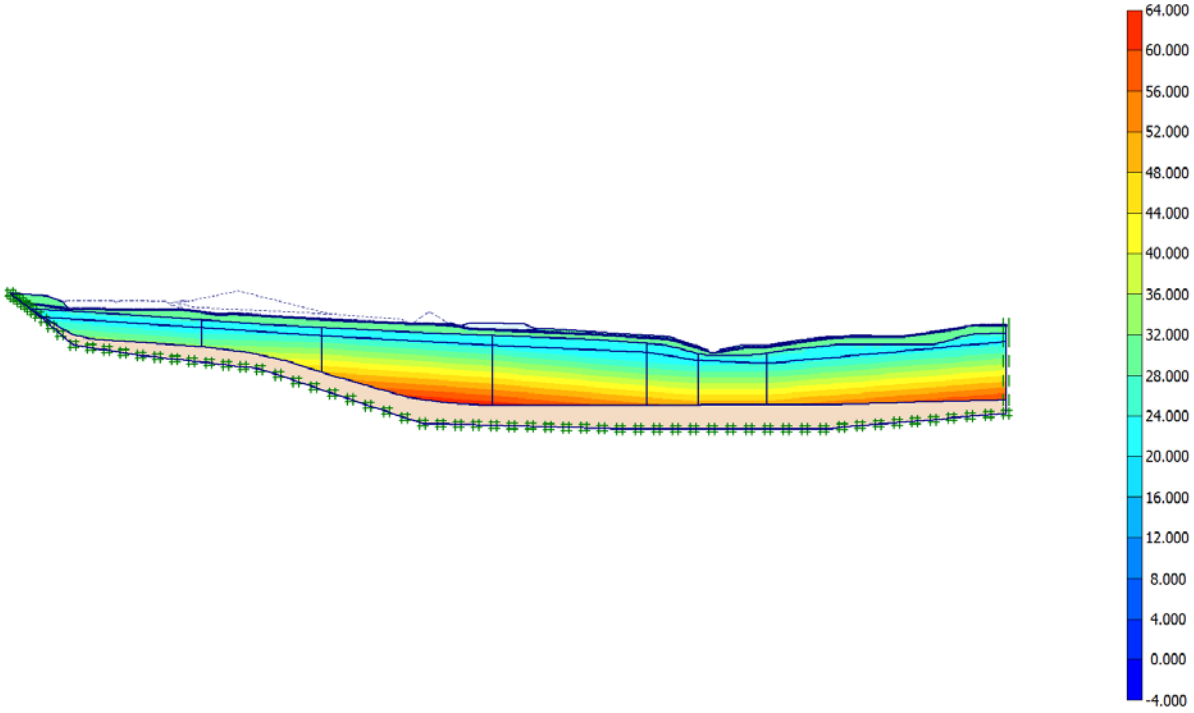

Figure 6.14 Undrained active strength assume din Smaaroed calculation

6.3.3. Soil properties and choice of parameters

The ground consists mainly of soft, sensitive clay with a sensitivity of 50-400 that permits to call it quick clay. The 1-2 topmost meters can be considered as dry crust.

The thickness of soft clay varies along the slide with the thickest part in the southern part of the sliding area (area B) with a thickness of 35 meters. In the area A the thickness is found to be about 10 meters in northwest and about 25 meters in north east.

The unit soil weight of the clay is about 17 kN/m3 up to 18 meters depth and an average value of 18 kN/m3 beneath 18 m depth.

The water content varies in the range 50%-80%, where lower values have been found for greater depth and the Attemberg limit varies between 20-45% but higher values have been found in the upper parts of the soil.

The choice of the parameters plays a fundamental role to get any results and to let the model work well.

In this work the slope has been studied in detail to get geometric and hardening parameters, while softening parameters have been got from laboratory tests and then modified.

The undrained strength may be related by the formula made by Kjell Karslrud.

$$S_u^{A,P,DSS} = s * OCR^m * \sigma'_{vo}$$

in which A,P,DSS referred to active, passive and direct simple shear, and s and m are coefficient that are functions of water content:

$s = 0{,}27 + 0{,}10 * w$ $m = 0{,}58 + 0{,}33 * w$	**Active**
$s = 0{,}0 + 0{,}26 * w$ $m = 0{,}86 - 0{,}30 * w$	**Passive**
$s = 0{,}14 + 0{,}18 * w$ $m = 0{,}35 + 0{,}77 * w$	**Direct Simple Shear**

Table 6-3 Undrained strength parameters proposed by Kjell Karslrud

To get the distribution of A, P, DSS undrained strengths, an excel sheet has been done in which the input are the effective weight, water content and friction angle. To realize this excel sheet the results have been compared with some laboratory tests made in the profile A (Figure 6.10).

The most important assumption made is that the deposition in the area was slightly inclined and not horizontal. That is because of comparing the results of the model with laboratory tests.

Taking into account the inclined deposition, OCR and τ_0 have been calculated and then all the coefficients needed to get strength distribution.

Knowing the distribution of undrained active strength, it has been possible to divide the slope into clusters as the ADPsoft model needs vertical clusters.

All the parameters needed are shown in the following Table 6-4

G_{ur}/Su^A	500.00	500.00	500.00	500.00	500.00	500.00	500.00
Su^A ref	19.50	19.50	19.50	19.50	19.50	19.50	19.50
Su^A incl	2.406	2.371	2.341	2.336	2.340	2.385	2.371
x ref	0.00	0.00	0.00	0.00	0.00	0.00	0.00
yref	42.00	37.00	36.00	32.00	30.00	28.00	28.00
Δyref/Δx	0.10	0.03	0.08	0.04	0.13	0.00	-0.08
Su^{DSS}/Su^A	0.715	0.715	0.717	0.717	0.717	0.715	0.716
Su^P/Su^A	0.398	0.399	0.402	0.403	0.402	0.399	0.400
τ_0/Su^A	0.310	0.373	0.514	0.548	0.525	0.358	0.389
Su_r^A/Su^A	0.40	0.40	0.40	0.40	0.40	0.40	0.40
Su_r^{DSS}/Su^A	0.40	0.40	0.40	0.40	0.40	0.40	0.40
Su_r^P/Su^A	0.40	0.40	0.40	0.40	0.40	0.40	0.40
$\gamma_P^{C,TX}$	0.010	0.010	0.010	0.010	0.010	0.010	0.010
γ_P^{DSS}	0.025	0.025	0.025	0.025	0.025	0.025	0.025
$\gamma_P^{E,TX}$	0.040	0.040	0.040	0.040	0.040	0.040	0.040
$\gamma_r^{C,TX}$	0.200	0.200	0.200	0.200	0.200	0.200	0.200
γ_r^{DSS}	0.200	0.200	0.200	0.200	0.200	0.200	0.200
$\gamma_r^{E,TX}$	0.200	0.200	0.200	0.200	0.200	0.200	0.200
c_1	1.3	1.3	1.3	1.3	1.3	1.3	1.3
c_2	0.8	0.8	0.8	0.8	0.8	0.8	0.8
ν	0.300	0.300	0.300	0.300	0.300	0.300	0.300
ν_u	0.495	0.495	0.495	0.495	0.495	0.495	0.495
α	2.00	2.000	2.000	2.000	2.000	2.000	2.000
l_{int}	1.00	1.000	1.000	1.000	1.000	1.000	1.000

Table 6-4 Values of NGI-ADPsoft model parameters assumed in the calculations

Softening parameters have been chosen using laboratory tests results, but they have been modified to get the global failure within the reasonable range of soft clay.

The internal length has been set to 1 m because of the speed of calculation, but it could have been used a smaller one. The sensitivity of this important parameter has been investigated in chapter 6.3.4

In the "Appendix 3rd: Smaaroed Slide - Steps to get Su^A distribution" all the steps are presented.

6.3.4. Local mode analyses - Sensitivity analyses of bearing capacity

The bearing capacity of the slope has been calculated through incremental multiplier of the load.

As previously there are the same phases reported in Table 6-5 in which after an equilibrium between the initial phase and NGI-ADPsoft the load is activated and then increased to get the bearing capacity of the slope and so the local failure.

Phase	Ph-No.	Start phase	Calculation type	Load input	First step	Last step
Initial phase	0	0		-	0	0
Equilibrium	4	0	Plastic analysis	Staged construction	1	13
ActivL	1	4	Plastic analysis	Staged construction	14	23
IncremL	2	1	Plastic analysis	Incremental multipliers	24	48
AppliL	3	1	Plastic analysis	Total multipliers	49	69
IncremWeight	5	3	Plastic analysis	Incremental multipliers	70	719

Table 6-5 Local mode phases

In this case the local failure has almost a circular shape as expected from theory. It is shown in Figure 6.15.

The calculations led to a load that is likely the one that has been the trigger of the slide that is a fill having a height of about 7 meters.

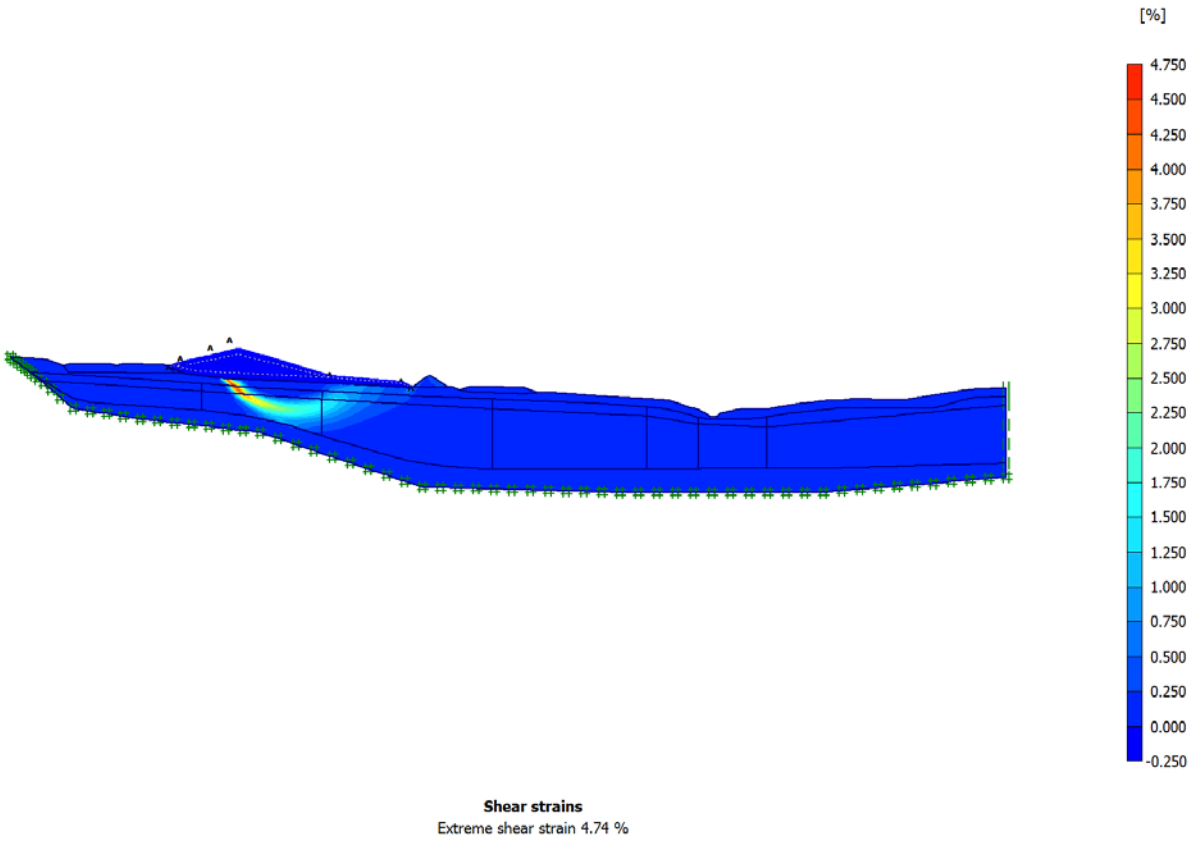

Figure 6.15 Shear strains after the bearing capacity is reached

To check the effect of the internal length on the bearing capacity a sensitivity analyses has been conducted.

The internal length has been made to vary from 1 meter to 2.5 meters and in addiction a fill, instead of a load, has been used. This fill has been modelled with Mohr-Coulomb having the same features of the real fill. As the load and the fill behave in different way, the results are different even for the same internal length. The results are shown in the Figure 6.16.

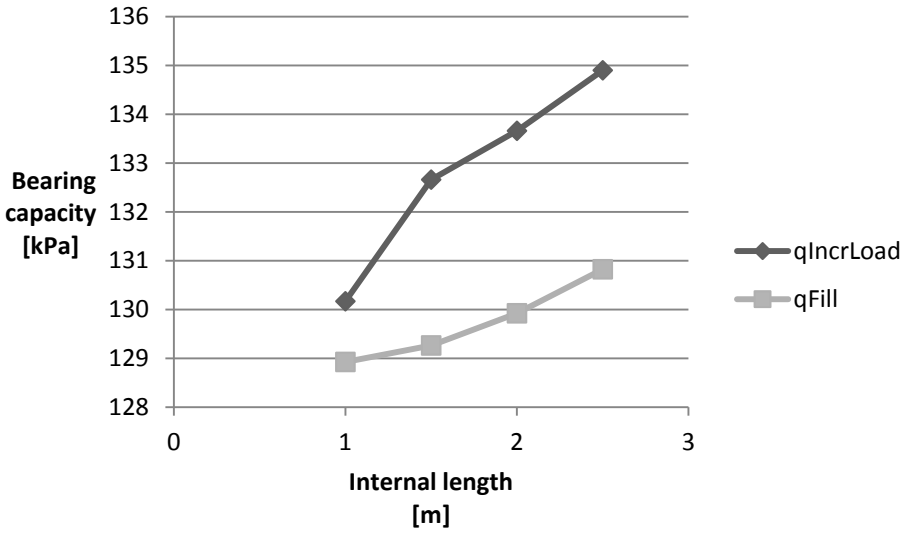

Figure 6.16 Differences in bearing capacity using different internal lengths

Increasing the internal length the bearing capacity increases but there is not so high difference.

This result is because a small internal length entails a more brittle behavior.

It is noticed that the internal length that should set the shear band of the slide do not control the thickness as expected from the theory of the model used. In fact the thickness of the shear band varies from the one given by the theory.

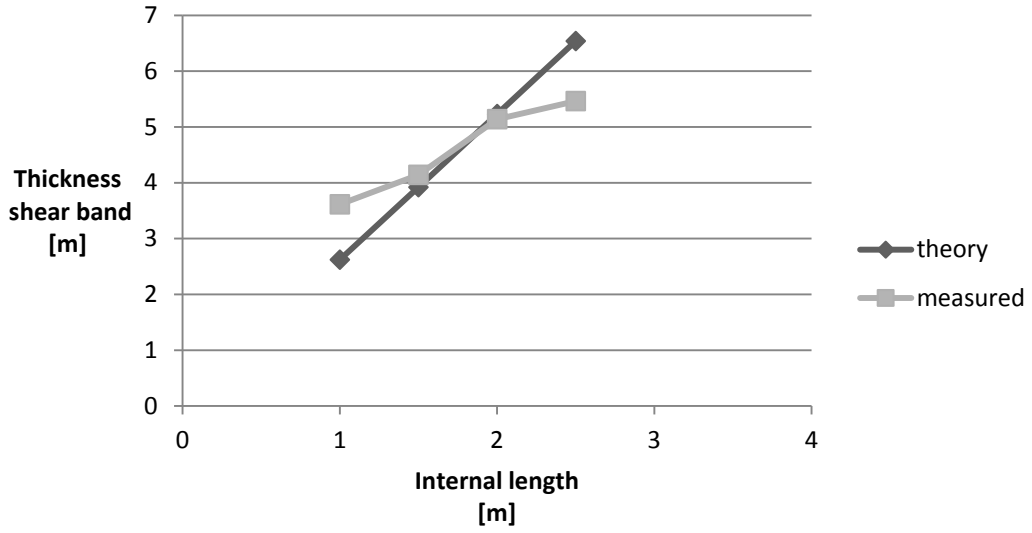

Figure 6.17 Differences in the thickness of shear band using different internal lengths. It is also reported the differences between the thickness measured and the one calculated from theory.

It has to be noted that the shear band thickness does not keep constant among the slope but it increases at end of the slip surface. This is due to the fact that strain softening is not taking place at the boundary of the failure surface. It is shown for all cases investigated in the following figures.

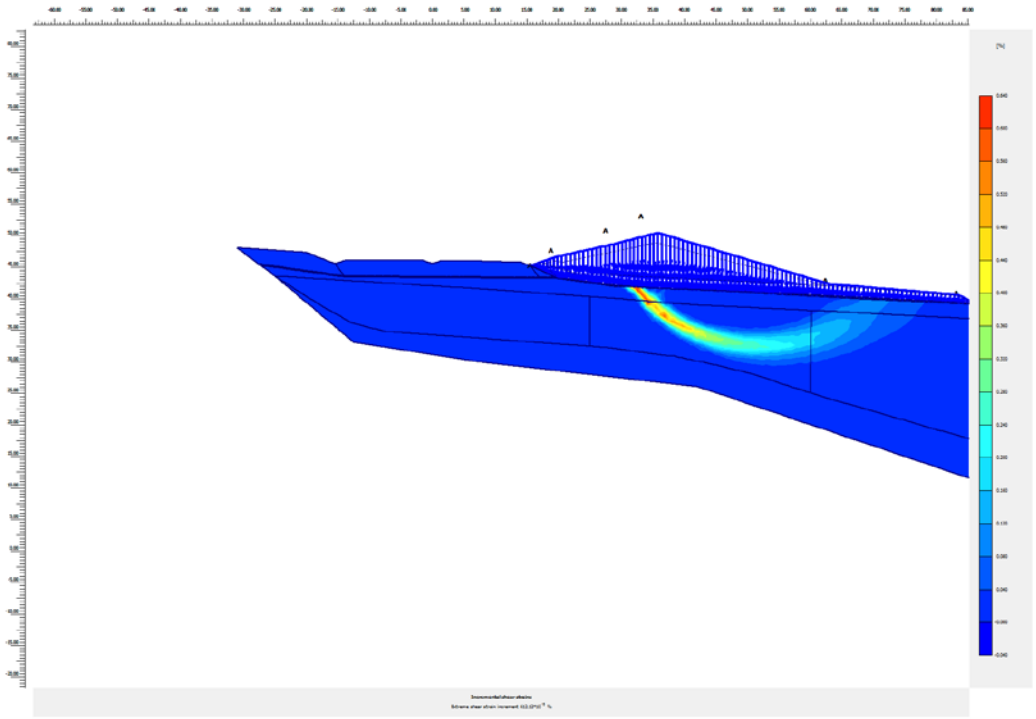

Figure 6.18 Shear band thickness with internal length of 1 m

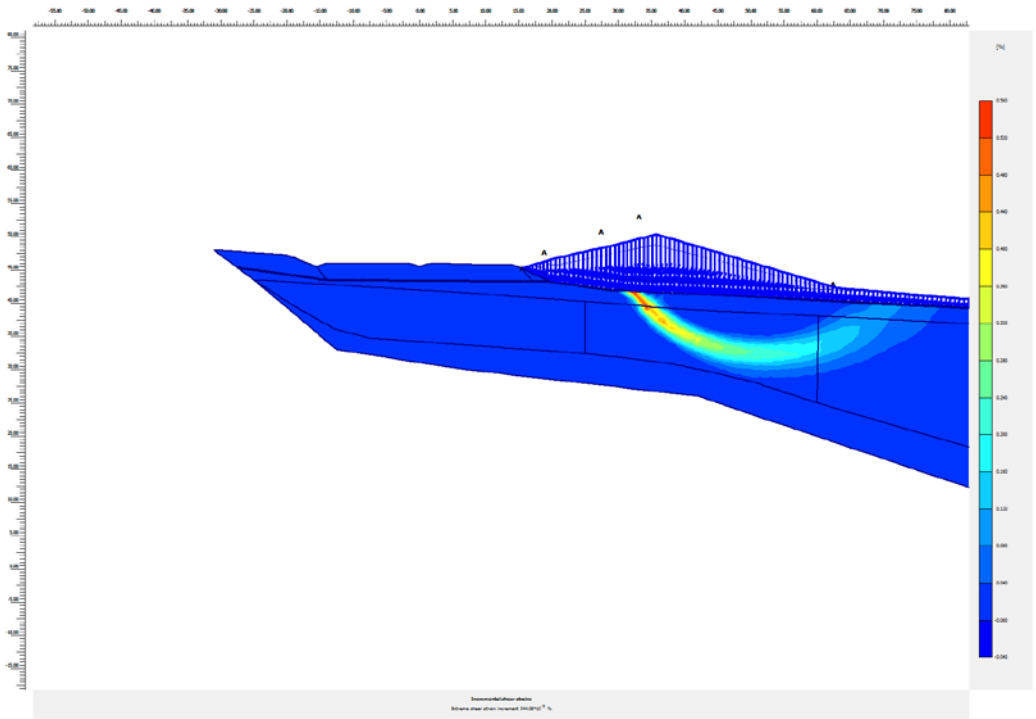

Figure 6.19 Shear band thickness with internal length of 1.5 m

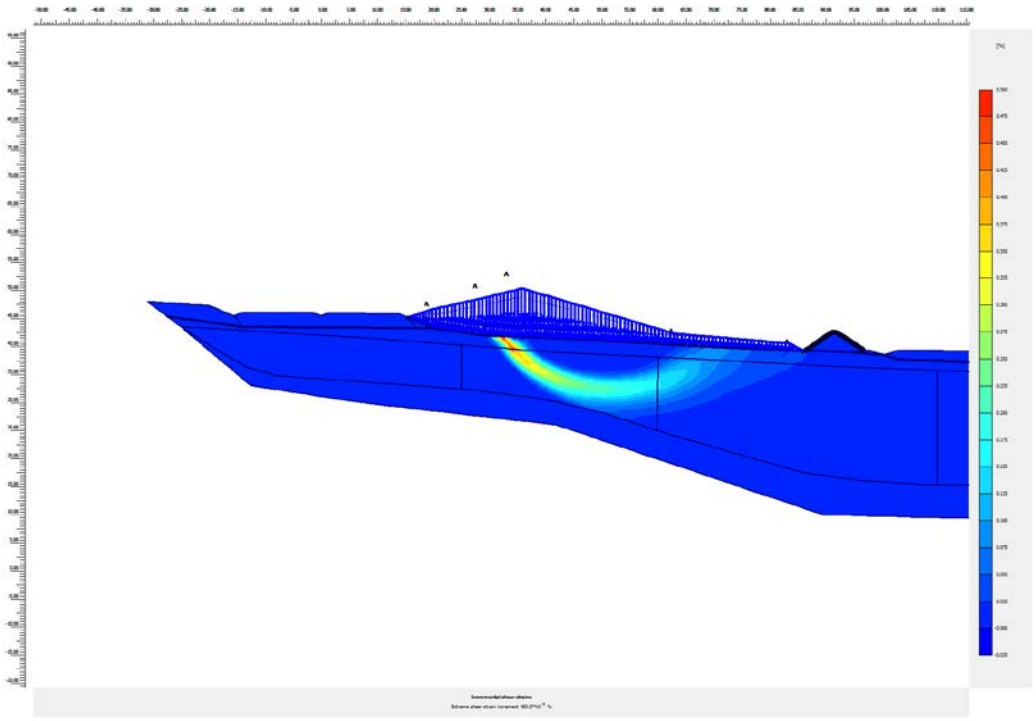

Figure 6.20 Shear band thickness with internal length of 2 m

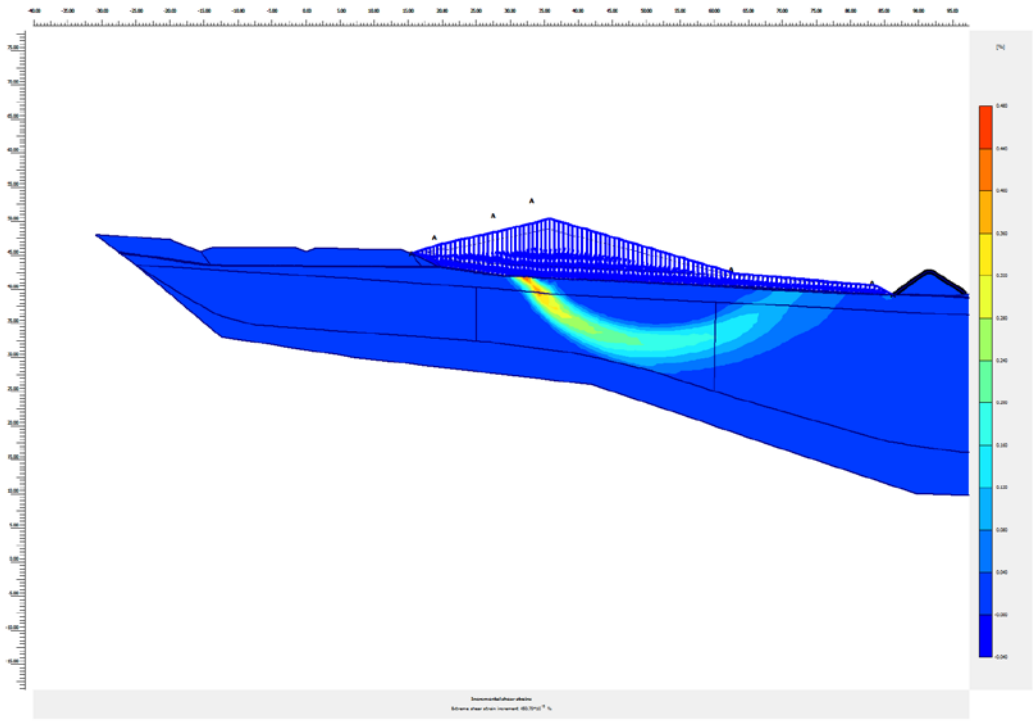

Figure 6.21 Shear band thickness with internal length of 2.5 m

The figures show the shear band thickness when the bearing capacity of the slope is reached. There are some slightly differences and one is that the shear band deepens as the internal length increases.

Another interesting thing is the differences of the points in the pre, post-peak and residual part of the constitutive relationship. From the Figure 6.22 it is noticed that the residual portion of the failure surface decreases increasing the internal length.

The reason the residual portion increases for smaller shear band thickness is that the global brittleness increases, i.e. the strain softening is more pronounced

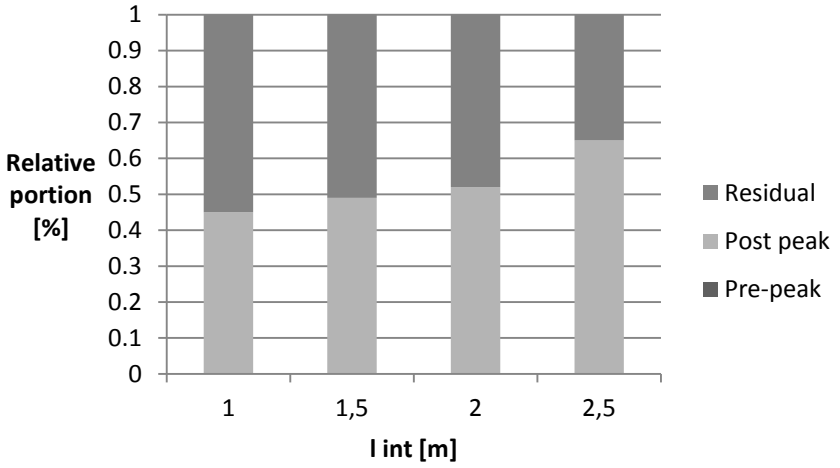

Figure 6.22 Relative portion of residual, post-peak and pre-peak state

6.3.5. Long global mode analyses

The progressive failure involved a very large mass of the slope and it arrives up to the river.

The slip surface pulled out from the model is shown in Figure 6.23 and it is very similar to the real one. It follows the initial steep part of the bedrock and then it is almost parallel to the ground.

To avoid convergence problems, after having calculated the triggering load, a fill with almost the same weight of the load was used. The weight of the entire domain has been increased to get the global failure.

The phases are reported in Table 6-6.

Phase	Ph-No.	Start phase	Calculation type	Load input	First step	Last step
Fill	6	4	Plastic analysis	Staged construction	49	69
IncremWeight	7	6	Plastic analysis	Incremental multipliers	70	719

Table 6-6 Long global mode phases

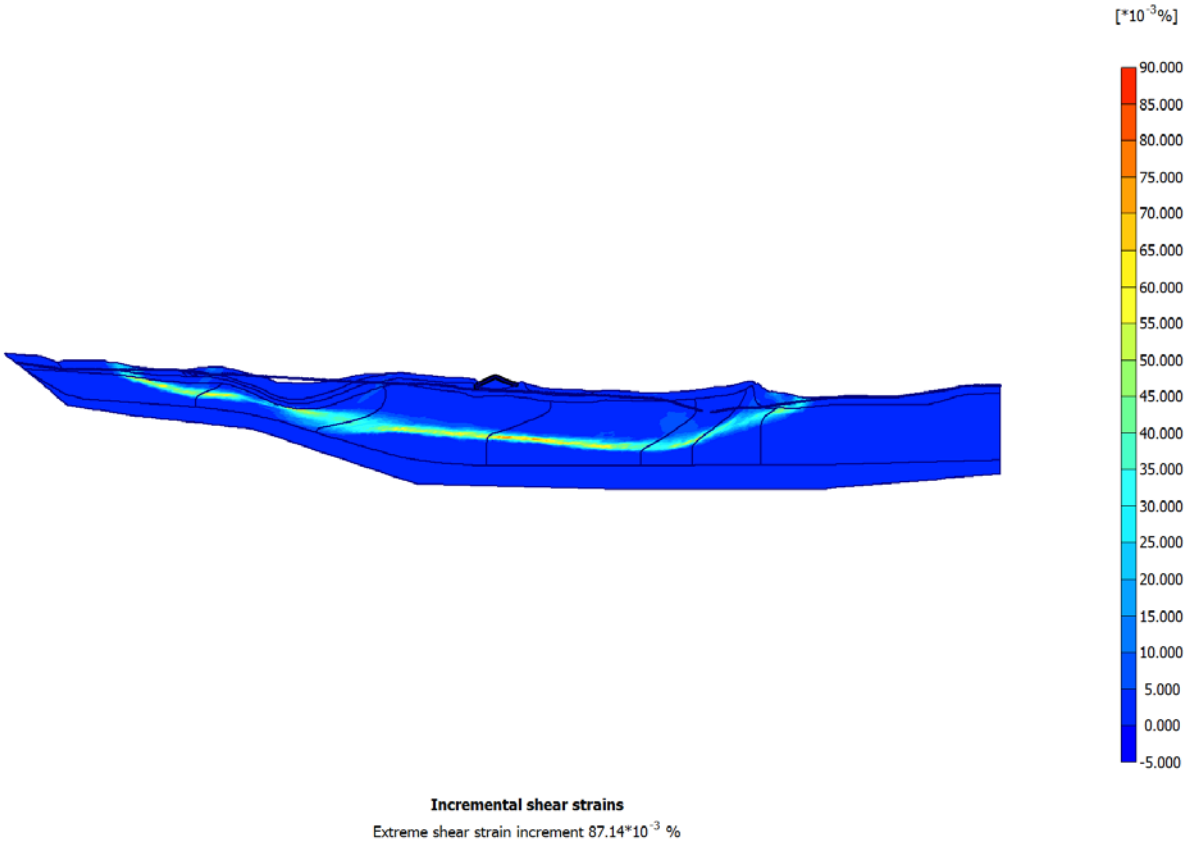

Figure 6.23 Incremental shear strains when progressive failure is got

The global failure shows a total displacement of more than 23 meters, close to the observed horizontal displacement.

As shown in the Figure 6.24 in the global failure it is also present the local failure.

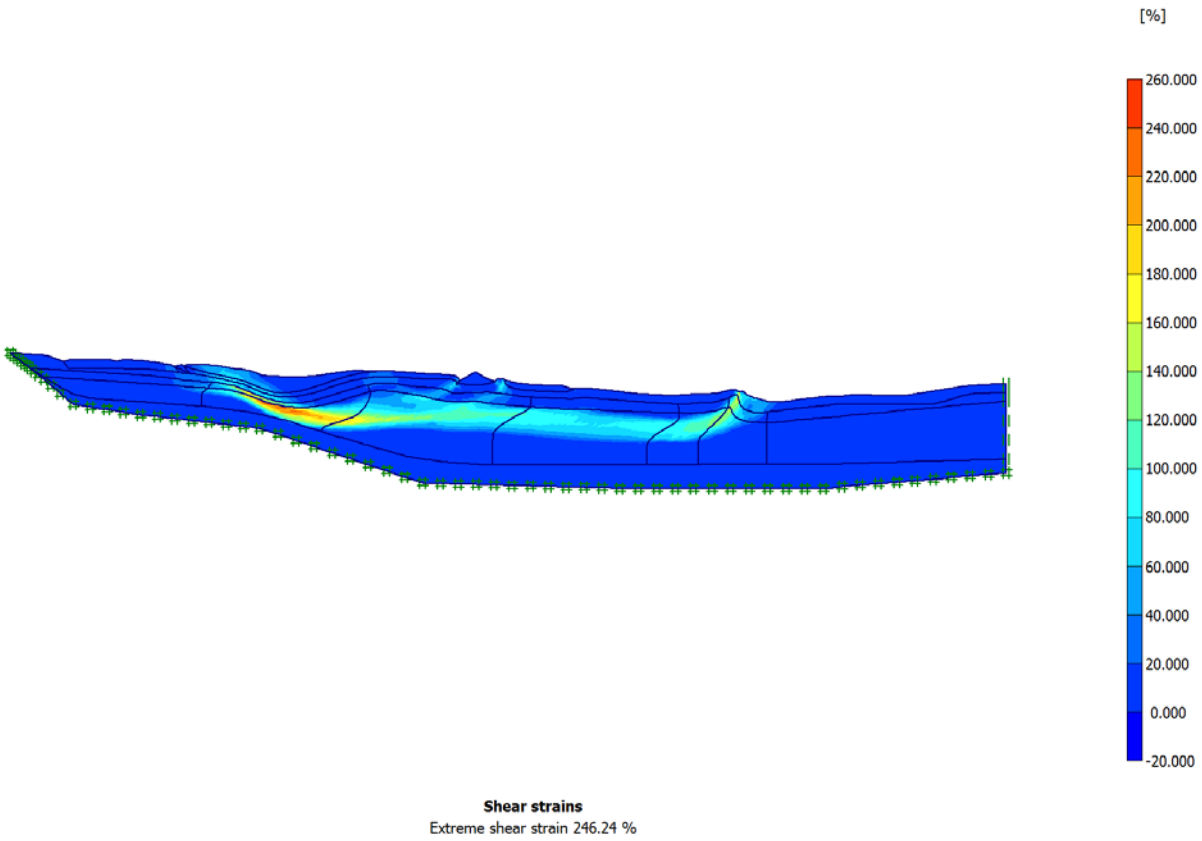

Figure 6.24 Shear strains when progressive failure is got

It is always very important to check the entity of the increase in weight to avoid having calculation far from reality. The Figure 6.25 shows the total displacement of a point placed beneath the fill. It is possible to see that sometimes the distance between two consecutive steps is bigger than others. In these steps the displacement is higher and it means that the mass of slide involved is accelerating and so the program tried to find a static equilibrium increasing the displacement. It entails a growth in the global error that, through this procedure, checks the entire domain and not only the slip surface. It means that it takes under control the global error that, through ordinary procedure, was very high. For the relevance of simulations a high error implies that the simulation is not realistic, and this procedure made the global error get reliable, but a bit higher than the standard tolerance.

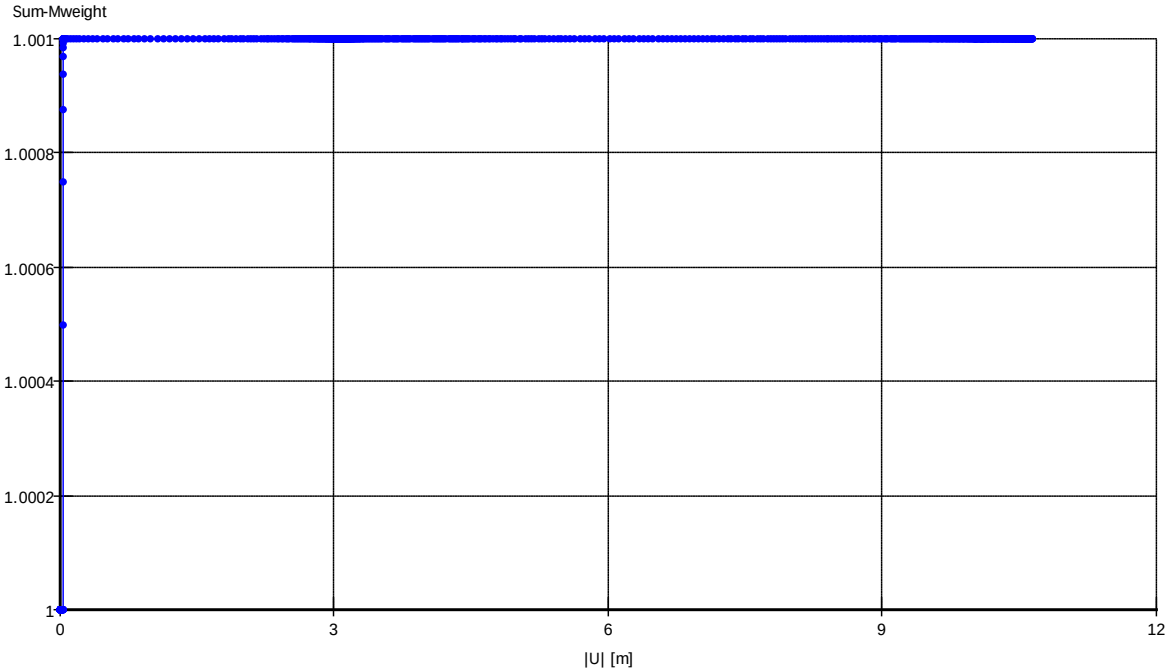

Figure 6.25 Value of the weight while incremental multiplier of it is used

Having a look at the steps it is possible to see the evolution of the progressive failure.

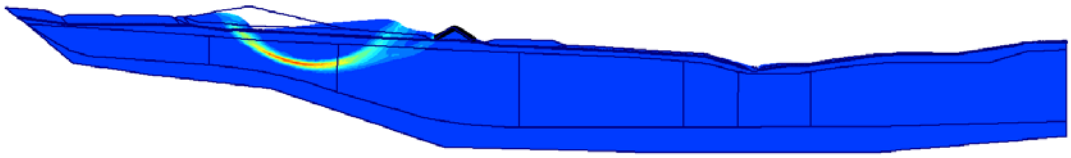

Figure 6.26 Incremental shear strains step 80

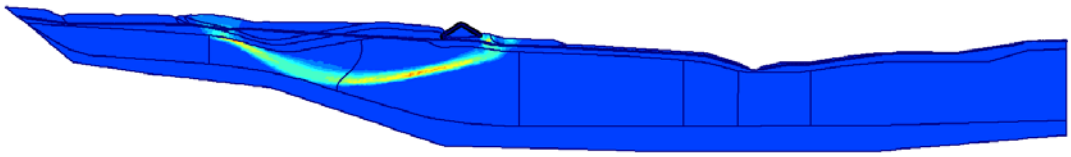

Figure 6.27 Incremental shear strains step 140

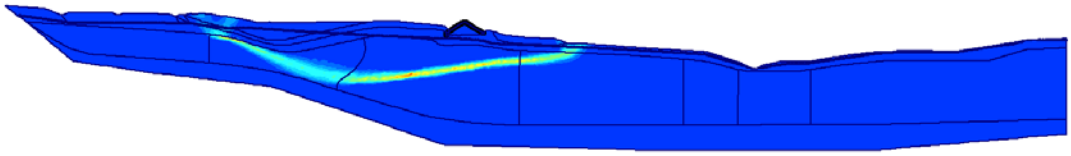

Figure 6.28 Incremental shear strains step 270

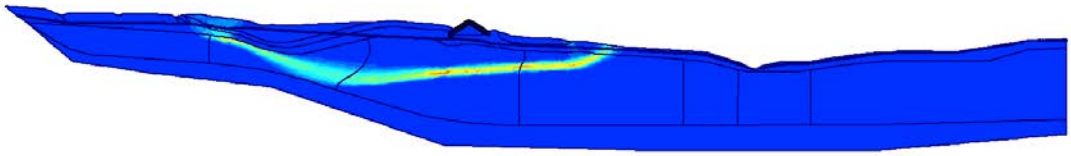

Figure 6.29 Incremental shear strains step 320

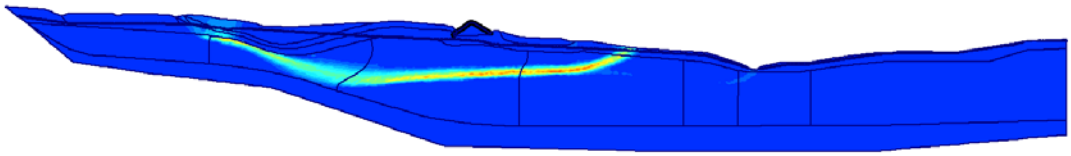

Figure 6.30 Incremental shear strains step 340

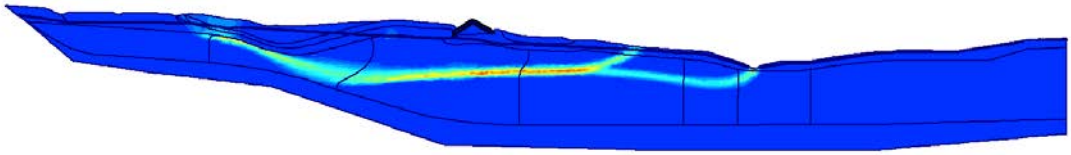

Figure 6.31 Incremental shear strains step 348

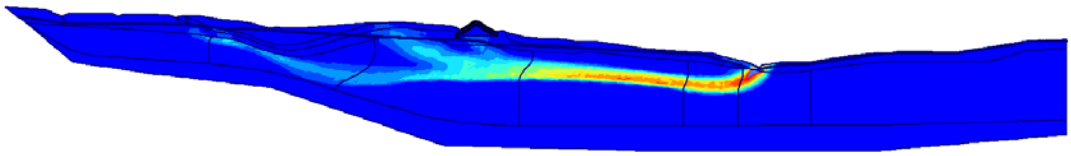

Figure 6.32 Incremental shear strains step 360

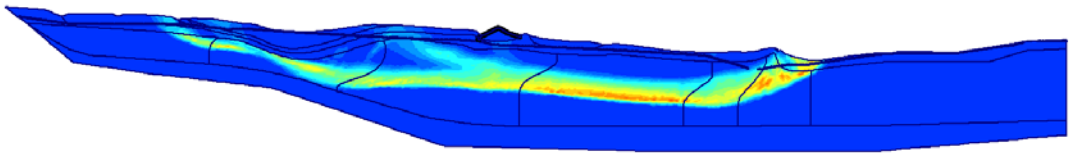

Figure 6.33 Incremental shear strains step 400

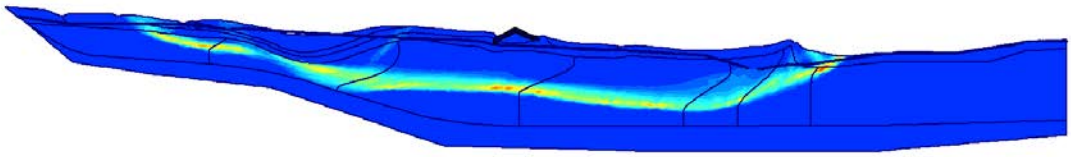

Figure 6.34 Incremental shear strains step 450

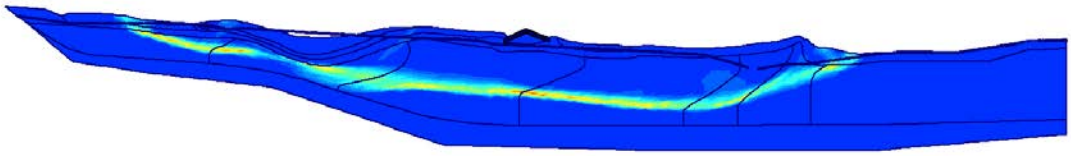

Figure 6.35 Incremental shear strains step 600

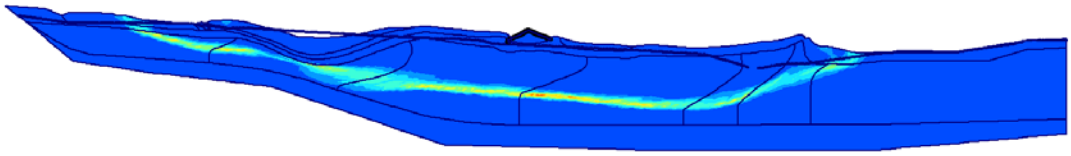

Figure 6.36 Incremental shear strains final step 719

Between step 340 and 348 the slip surface starts from the river and it links with the principal one. After that it becomes the slip surface and it involves more and more ample mass of the slope.

6.4. Remarks

Internal length: it is not as the one expected from theory but it is not so far from it.

Convergence: not always the program stops when the global error reaches the value set. Hence, often, the number of steps control the calculations and so the results. If the calculation is stopped it is not possible to continue but it has to be restarted from the beginning of the phase.

The model needs a powerful computer and a lot of time to finish the calculations; the mesh and so the internal length controls the time of calculation. As the internal length should be realistic, it entails a long time of running.

The shear band tends to get deeper as the calculations go on. It is reported in the precedent figures, in which different steps are shown.

As during the calculations the elements, due to the important displacements after the long global failure, became bigger than the internal length and so it may affect the results.

7. Conclusions

Modelling progressive failures in long natural slopes is a challenge that many researchers have dealt with. The mechanical behaviour of sensitive clays, and in particular quick clays, is the reason of the difficulty to model failures in this kind of soil. On the other hand, as sensitive clays may turn liquid if overloaded, it makes this failure very dangerous and often hard to prevent.

The thesis tries to face somehow the problem. In particular the work presents, in addition to some models already presented by other authors, a simple model proposed by Nordal (2004) and here applied to the Tuve slide (Sweden, 1977), close to the ones got by Bernarder's model that is based on Finite Difference Method (FDM). Both these models are explained in the work but, because of the difficulties of FDM in the application to real slopes, they should be used more in understanding the mechanism of progressive failure instead of in the analyses in engineering field.

It is shown that Limit Equilibrium Method, that is the most if not the only method used in engineering field, should not be used in studying progressive failures in sensitive clays. That is due to the fact that it does not take into account deformation among the slope and, as sensitive clays show a strain softening behaviour, it cannot catch the real process, the mobilized resistance and the evolution in these soils.

From this point of view, Finite Element method (FEM) could be a useful tool as it considers a realistic behaviour of a sensitive clay. It has to be considered that the real behaviour varies both in the slope and due to the evolution of the failure. It means that the constitutive relationship used in the calculation should consider all the factors that affect the behaviour.

In the thesis an advanced model (NGI ADPsoft) which has been used for the back-analysis of Smaaroed slide (Sweden, 2006). NGI ADPsoft has demonstrated to be a good model to get results close to the likely triggering factor and to catch the global failure happened.

The used procedure seems to be suitable to capture the global failure but it showed some problems and it needs some considerations. First of all, the calculation needs a lot of time that probably is far from engineering applications. It depends on the internal length adopted.

The choice of the internal length is very important as it entails the thickness of the shear band. However sensitivity analyses done in the present work showed that higher internal lengths do not entail significant differences in terms of bearing capacity of the slope.

Bibliography

G. Grimstad and L. Andresen and H.P. Jostad; "*Anisotropic shear strength model for clay*"; International Journal of Numerical and Analytical Methods in Geomechanics,2010.

N. Janbu. "*Grunnlag i geoteknikk*". Tapir Forlag, 1970.

K.Karlsrud, G. Aas, and O. Gregersen; "*Can we predict Landslide Hazards in soft Sensitive Clays*?"; Norwegian Geotechnical Institute, 1985

Vikas Thakur, Steinar Nordal, and Gustav Grimstad. "*Phenomenological issues related to strain localization in sensitive clays*". Geotechnical and Geological Engineering, 24: 1729‑1747, 2006

Stig Bernarder, "*Progressive Landslides in Long Natural Slopes*", PhD Thesis in Luleå University of Technology, 2000

Laurits Bjerrum. "*Geotechnical properties of Norwegian marine clays*". Geotechnique, 4, No. 2:49‑69, 1954

David Muir Wood. "*Soil Behaviour and Critical State Soil Mechanics"*. Cambidge University Press, 2007.

Moum, J.T. Løken and J.K. Torrance (1971). "*A geochemical investigation of the sensitivity of a normally consolidated clay from Drammen, Norway*". Géotechnique, (21),4,329-340. Norwegian Geotechnical Institute, Oslo. Publication, 96, 1973.

Jørstad and J.N. Hutchinson (1961). "Orienterende underøskelse av skredfaren i Namdalen". Norwegian Geotechnical Institute, Oslo. Report, 0.910.

Stian Baardsgaard Hanssen. "*On Numerical Simulations of Progressive Failure and Localized Deformation*". Master thesis, Norwegian University of Science and Technology. 2010.

M. H. Brubakk and V. B. Smith. "*Slope Stability Analysis in Soft Sensitive Clay at Heimdalsvegen*". Master thesis, Norwegian University of Science and Technology, 2010.

Vikas Thakur. "*Strain Localization in Sensitive Soft Clays*". PhD Thesis in Norwegian University Of Science and Technology, 2007.

Stig Bernarder, "*Progressive Landslides in Long Natural Slopes*", PhD Thesis in Luleå University of Technology, 2011.

Stig Bernarder et all. "*Shear strength and deformation properties of clays in direct shear tests at high strain rated*". 1985.

Lacasse et al (1985). "*Block sampling of sensitive clays*". XI Int. Conf. on Soil Mech. and Found. Eng. San Fransisc Vol. 2 887_892.

Laurits Bjerrum (1967). "*Progressive Failure in Slopes of Over-Consolidated Plastic Clay and Clay Shales*". The third Terzaghi Lecture. *NGI Publication 077.* Norwegian Geotechnical Institute, Oslo.

Anders Samstad Gylland, (2009). "*Progressive Failure in Soft Sensitive Clays*". *Fjellsprengningsdagen, Bergmekanikk- og Geoteknikkdagen 2009* (pp. 33.1 - 33.15). Oslo: Fjellsprengningsdagen Oslo 2009.

Grande, L. and Janbu, N. (1980). "*Retrogressiv bruddmekanisme i kvikkleire*", In Uppsala symposium.

N. Janbu, (1979). "*Failure Mechanism in Quick Clays*". *NGM-79, Nord. Geotekniker mötet, Helsinki.*

C. A. Farulla. "*Analisi di stabilità dei pendii, i metodi dell'equilibrio limite*". Hevelius edizioni, 2001

Stig Bernarder, "*Down-hill Progressive Landslides in Soft Clays*". Luleå University of Technology. Research report 11, 2008.

Nordal S. (2004) "*Geohazards: Major Challenges*" XVI NGM NordicGeotechnical meeting, pp 65-81.

Eringen, A.C. (1981), "*On non-local plasticity*", Int. J. Numer. Anal. Meth. Geomech. 26, pp. 1461-1474.

Brinkgreve, R.B.J (1994), "*Geomaterial Models and Numerical Analysis of Softening*", PhD Thesis, TU Delft, Delft, The Netherlands.

G.Grimstad, H.P. Jostad and L. Andresen. "*Undrained capacity analyses of sensitive clays using the non-local strain approach*". 9th HSTAM International Congress on Mechanics, Vardoulakis mini-symposia, Limassol, Cyprus, 12-14 July, 2010.

H.P. Jostad and G. Grimstad. "*Comparison of distribution functions for the non-local strain approach*".

Swedish Road Administrations Independent Investigation Committee. (2007). "*Skredet i Småröd december 2006"*. Rapport 1. Analys av skredorsaken. Vegvärket.

PLAXIS BV. (2009). "Plaxis Manuals v. 9.0".

A.S. Gylland AND M.S. Sayd, H.P. Jostad, S. Bernander. "*Investigation of soil property sensitivity in progressive failure"*, Numerical Methods in Geotechnical Engineering – Benz & Nordal (2010)

V.Thakur, S.Nordal and S.Hove, *"Short-term slope stability calculation according Eurocode 7"*, Numerical Methods in Geotechnical Engineering – Benz & Nordal (2010)

A.S. Gylland, H.P. Jostad. *"Effect of updated geometry in analyses of progressive failure"*. Numerical Methods in Geotechnical Engineering – Benz & Nordal (2010).

V.Thakur, S.Nordal and S.Hove. *"Phenomenological issues related to strain localization in sensitive clays"*. Geotechnical and Geological Engineering (2006) 24: 1729–1747. DOI 10.1007/s10706-005-5818-z

A.S. Gylland, S.Nordal, H.P.Jostad and M. Mehli. "*Pragmatic Approach for Estimation of Slope Capacity in Soft Sensitive Clay*"

Maj G. Bæverfjord and Vikas Thakur. *"The Verdal and Rissa Landslides -Application of case histories in education"*. 6th International Conference on Case Histories in Geotechnical engineering, Arlington, VA, August 11-16, 2008

Centre of Excellence – International Centre for Geohazards (ICG). *"Annual report 2010"*. 20031103-8, 31 March 2011.

S.B. Hanssen, A.S. Gylland & S. Nordal. *"Simulation of the Smaaroed Landslide in soft sensitive clay using a rate dependent, strain softening material model"*. 13th International Conference of the IACMAG 2011

Appendix 1th: FDM – constitutive relationships

Stage I

Stage I is divided into three sub-stages: stage Ia, Ib and Ic.

The stage Ia is the elastic range $0 < \gamma_{x,z} < \gamma el$ (for $0 < \tau_{xz} < \tau_{el}$) and so

$$\Delta\gamma_{x,z} = \frac{\Delta\tau_{xz}}{G} = \frac{\tau_{x(n+1),z} - \tau_{0\,x,z}}{G} \qquad eq\ I.1a$$

The stage Ib is a non-linear range $\gamma_{el} < \gamma_{x,z} < \gamma_f$ (for $t_{el} < t_{xz} < c_u$) The relationship is taken to be a 2nd power parabolic relationships with vertex in point (γ_f,c_u) and sloping τ_{el}/γ_{el} at the elastic limit.

$$\Delta\gamma_{x,z} = (\gamma_f - \gamma_{el}) * \left\{\left(1 - \frac{\tau_{0\,x(n),z} - \tau_{el}}{c_u - \tau_{el}}\right)^{1/2} - \left(1 - \frac{\tau_{x(n+1),z} - \tau_{el}}{c_u - \tau_{el}}\right)^{1/2}\right\} \qquad \ldots..eq\ I.4$$

The stage Ic is the transition range between linear and non-linear behavior from $\tau_{x(n),z} < \tau_{el}$ and $\tau_{x(n+1),z} < c$

$$\Delta\gamma_{x,z} = \frac{\tau_{el} - \tau_{0\,x(n),z}}{G} + (\gamma_f - \gamma_{el}) * \left(1 - \left[1 - \frac{\tau_{x(n+1),z} - \tau_{el}}{c_u - \tau_{el}}\right]^{\frac{1}{2}}\right) \qquad \ldots.eq\ I.4a$$

Stage II: post peak range

Stage II is divided into two stages: IIa and IIb.

Stage IIa for $c > t_z > c_R$ $(0 < \delta_{S,z} < \delta_{cR})$

The total deformation is the amount of displacement, rebound and slip deformation; it depends on τ.

if $\boldsymbol{\tau_0 > \tau_{el}}$

$$\delta_\tau = \sum_0^{\alpha H}\left[(\gamma_f - \gamma_{el}) * \left\{\left[1 - \frac{\tau_{0\,(x,z)} - \tau_{el}}{c_{x,z} - \tau_{el}}\right]^{1/2} - \left[1 - \frac{\tau_{max\,(x(n),z)} - \tau_{el}}{c_{x,z} - \tau_{el}}\right]^{1/2}\right\} - \frac{\tau_{max(x,z)} - \tau_{x,z}}{G}\right]$$
$$* \Delta z + \delta_{cR} * \frac{c - \tau_{x,0}}{c - c_R} \qquad \ldots\ldots eqI.5$$

Otherwise if $\boldsymbol{\tau_0 < \tau_{el}}$

$$\delta_\tau = \sum_0^{\alpha H} \left[\frac{\tau_{el} - \tau_{0\,x,z}}{G} + \left(\gamma_f - \gamma_{el}\right) * \left(1 - \left[1 - \frac{\tau_{max(x,z)} - \tau_{el}}{c_{x,z} - \tau_{el}} \right]^{\frac{1}{2}} \right) - \frac{\tau_{max(x,z)} - \tau_{x,z}}{G} \right] * \Delta z$$

$$+ \delta_{cR} * \frac{c - \tau_{x,0}}{c - c_R} \qquad \ldots\ldots eq\ I.5a$$

Stage IIb post residual shear stress stage when $\tau_{x,z} = c_R$ (residual) and $\delta_{slip} > \delta_{cr}$

The shear deformation at this stage is exclusively governed by the axial down-slope displacement (δ_N), and thus independent of $\tau_{x,z}$

For $\boldsymbol{\tau_0 > \tau_{el}}$ and $\tau_{x,0} = c_R$

$$\delta_\tau = \sum_0^{\alpha H} \left[\left(\gamma_f - \gamma_{el}\right) * \left\{ \left[1 - \frac{\tau_{0\,(x,z)} - \tau_{el}}{c_{x,z} - \tau_{el}} \right]^{1/2} - \left[1 - \frac{\tau_{max\,(x(n),z)} - \tau_{el}}{c_{x,z} - \tau_{el}} \right]^{1/2} \right\} - \frac{\tau_{max(x,z)} - \tau_{x,z}}{G} \right]$$

$$* \Delta z + \delta_{cR} + \delta_{slip} \qquad \ldots\ldots eqI.5b$$

Instead for $\boldsymbol{\tau_0 < \tau_{el}}$ and $\tau_{x,0} = c_R$

$$\delta_\tau = \sum_0^{\alpha H} \left[\frac{\tau_{el} - \tau_{0\,x,z}}{G} + \left(\gamma_f - \gamma_{el}\right) * \left(1 - \left[1 - \frac{\tau_{max(x,z)} - \tau_{el}}{c_{x,z} - \tau_{el}} \right]^{\frac{1}{2}} \right) - \frac{\tau_{max(x,z)} - \tau_{x,z}}{G} \right] * \Delta z$$

$$+ \delta_{cR} + \delta_{slip} \qquad \ldots\ldots eqI.5bc$$

Appendix 2nd: Plaxis - Manual settings

In Plaxis there are some control parameters that influence the iterative procedures and in particular the load advancement procedures. There are two available options for these parameters: *Standard setting* and *Manual setting*. As in this work Manual setting has been used, all control parameters are explained.

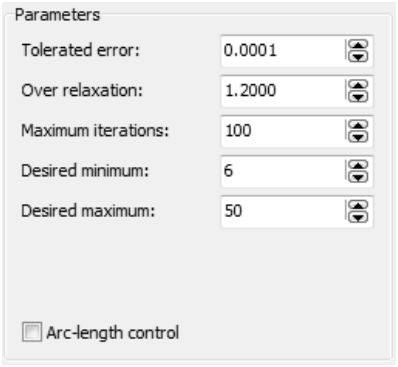

- *Tolerated error*

  When a non-linear analysis is carried out there will be some drift from the exact solution as shown in Figure 0.1.

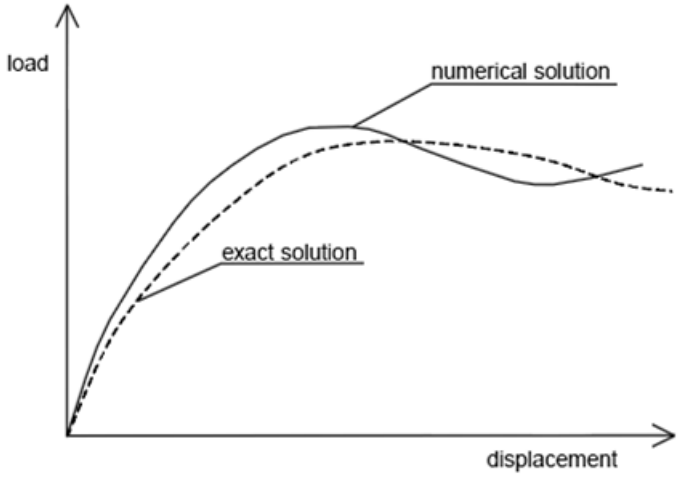

Figure 0.1 Computed solution versus exact solution, Plaxis v9

Within each step, the calculation program continues to carry out iteration until the calculated errors are smaller than the specified value.

The standard setting is set up to 0.01, while in this work for the last phase, the tolerated error is set up to 0.0001 to avoid that the program stops until it has reached an equilibrium. In this way the program is forced to find a solution enough accurate that it can be found when there is equilibrium between updated mesh and softening effects.

During the iteration is possible to see that of course the calculated error is higher when there are unbalanced forces and so when the slide mass is accelerating.

- *Over-relaxation*

This parameter reduces the number of iterations needed for convergence. The choice of the value of this parameter depends on soil friction angle. When the value is set up to 1 it means that the over-relaxation is not considered, whereas if it's set up to more than 1, it is considered. The explanation of this parameter is shown in Figure 0.2.

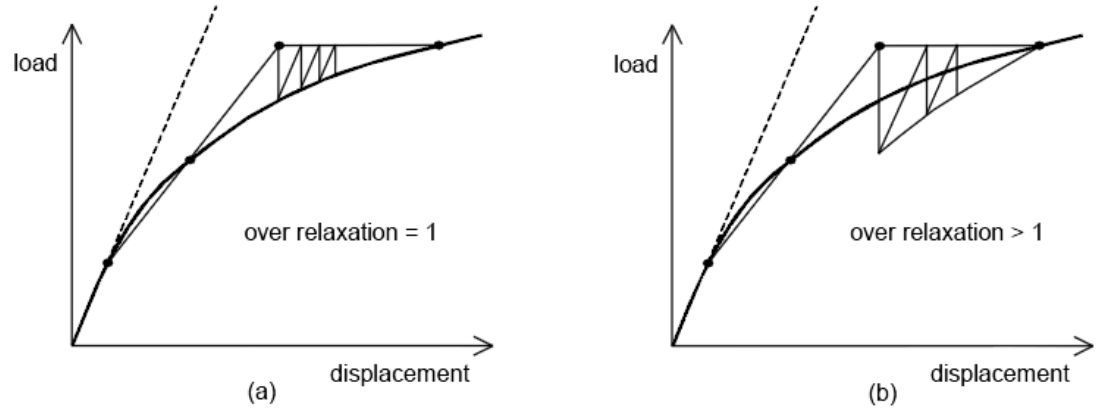

Figure 0.2 Iteration process with (a) and without (b) over-relaxation, Plaxis v9

In Standard setting this parameter is 1.2 and in this work it has been kept constant as in Standard setting.

- *Maximum iterations*

It represents the maximum allowable number of iterations within any calculation step.

It has effects on calculation time and on the accuracy of the convergence.

In Standard setting it is set up to 60, while it has been modified into 100 because, as the iterations are forced to find a solution, it has more iteration to reduce the global error.

- *Desired minimum and desired maximum*

These parameters control the automatic step size algorithm (*Load advancement ultimate level or Number of steps*). In fact when a load step is applied, a series of iterations are carries out to reach an equilibrium and the size of the load increment depends on when the solution reaches equilibrium. If the solution reaches equilibrium within a number of iterations that lies between desired maximum and desired minimum the load increment size is assumed to be satisfactory, otherwise the load increment size is multiplied or divided by a factor of two (it depends if number of iteration is lower than *desired minimum* or it is higher than *desired*

maximum) and further iterations are applied to reach equilibrium. These parameters can be changed when, for example, the automatic step size procedure generates steps that don't give a smooth load-displacement curve.

The standard values are respectively 6 and 15, but in this work they have been changed into 6 and 50. The last value has been chosen because of *Maximum iterations* value.

- *Arc-length control*

  It is useful to obtain reliable collapse for load-controlled calculations.

  The iterative procedure, when arc-length control is used or not, is shown in Figure 0.3, for the case where a collapse load is being approached.

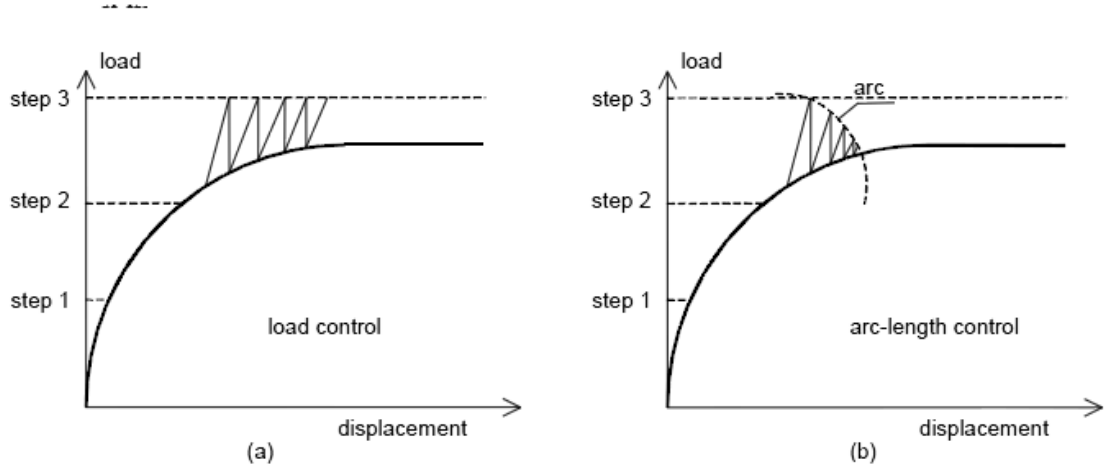

Figure 0.3 Iterative procedure for normal load control (a) and arc-length control (b), Plaxis v9

In this case (a) the algorithm will not convergence, while if arc-length is activated the program will automatically evaluate the portion of the external load that must be applied for collapse (b).

When using Incremental multipliers as loading input, arc-length control will influence the resulting load increments. As a result, the load increments applied during the calculation will generally be smaller than prescribed at the start of the analysis.

If the arc-length control is deselected and failure is approached, convergence problems may occur.

- Additional steps

  The number of steps has been increased to avoid the end of calculation before reaching the equilibrium

Appendix 3rd: Smaaroed Slide - Steps to get Su^A distribution

Gamma effective

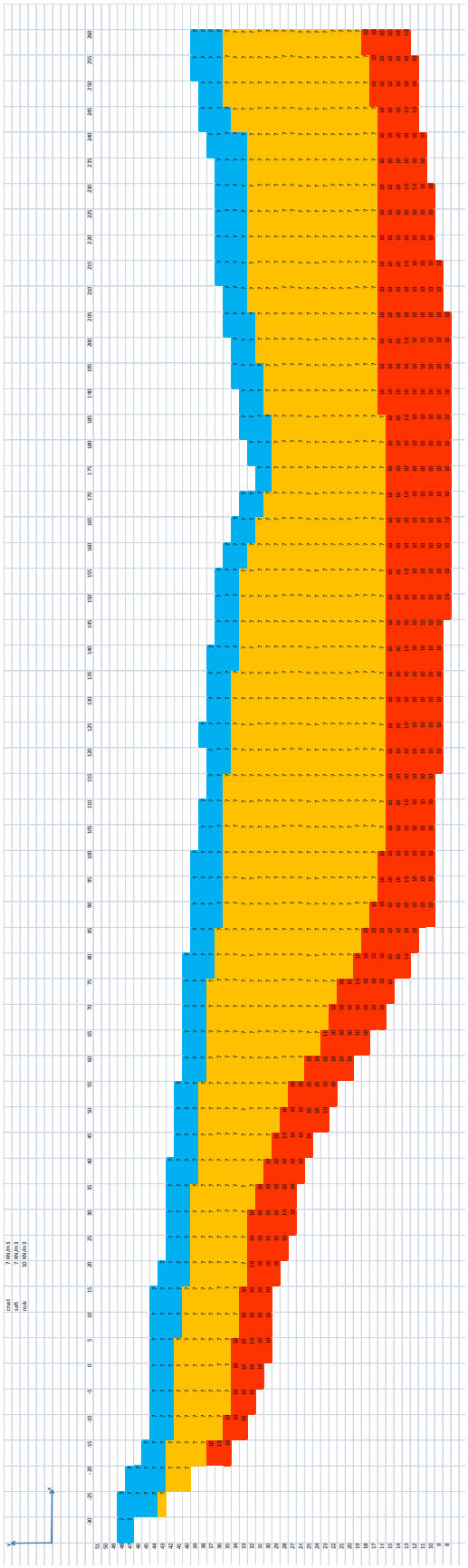

Water content

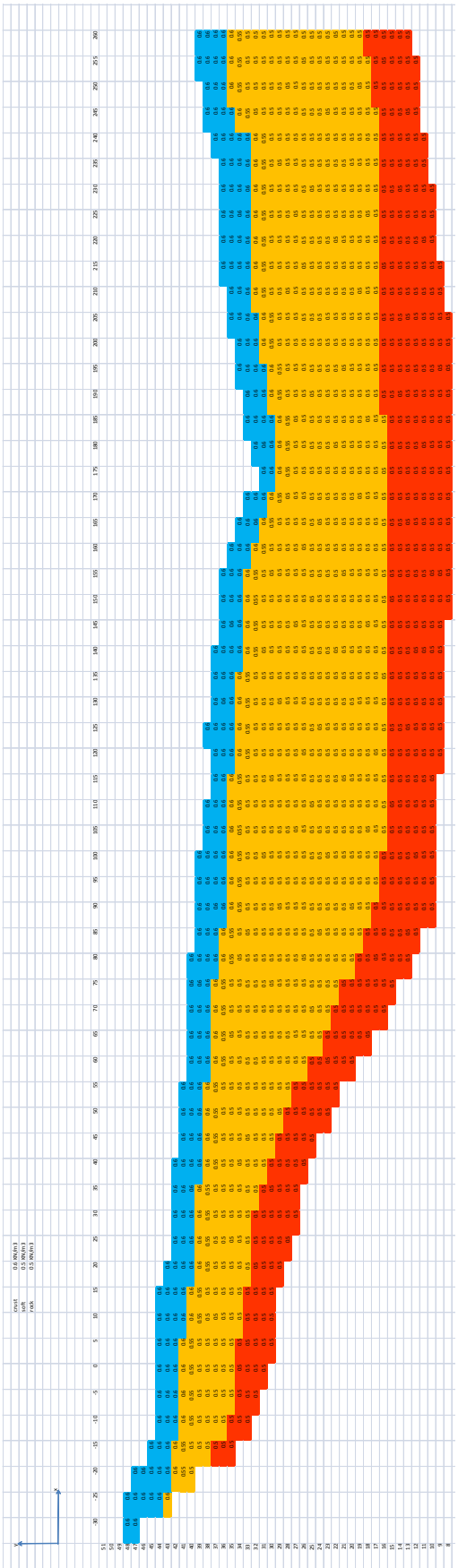

Friction angle

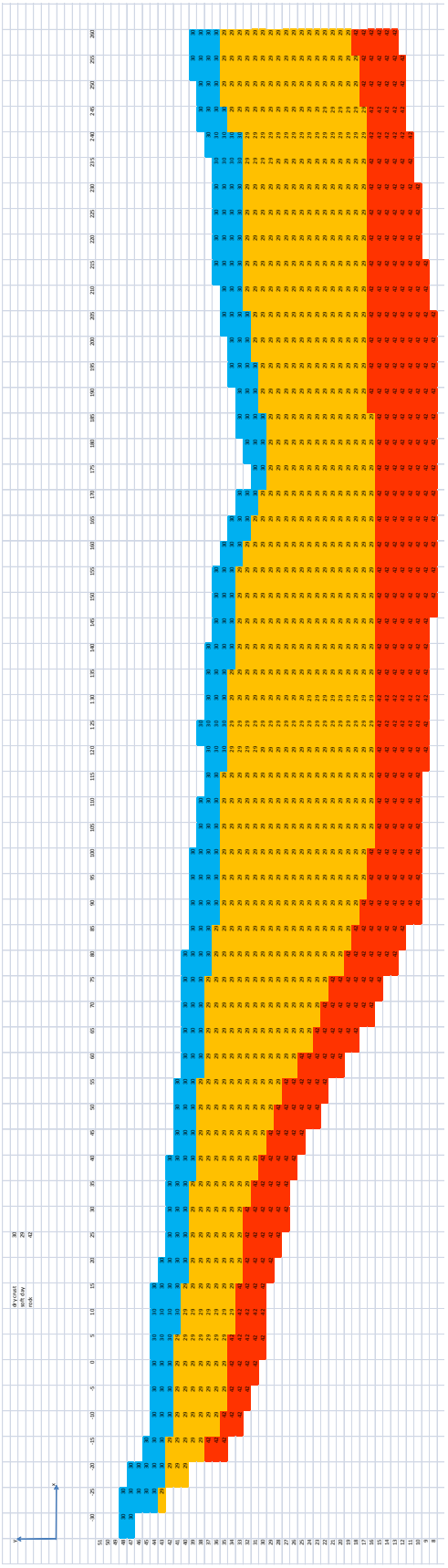

Sigma' v_0

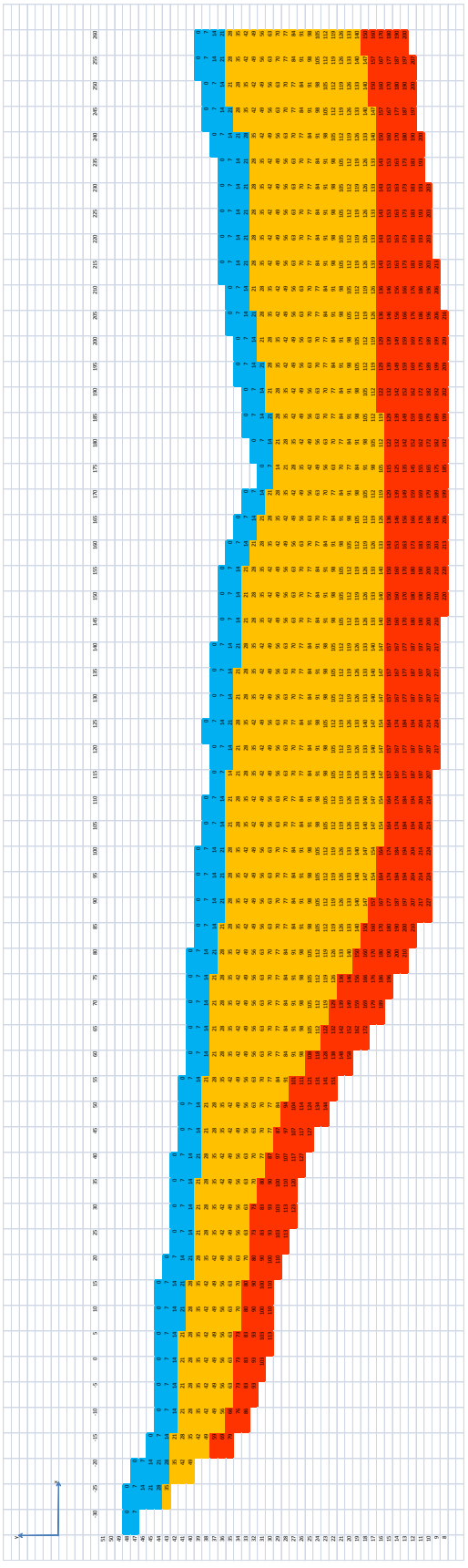

Sigma' v_P

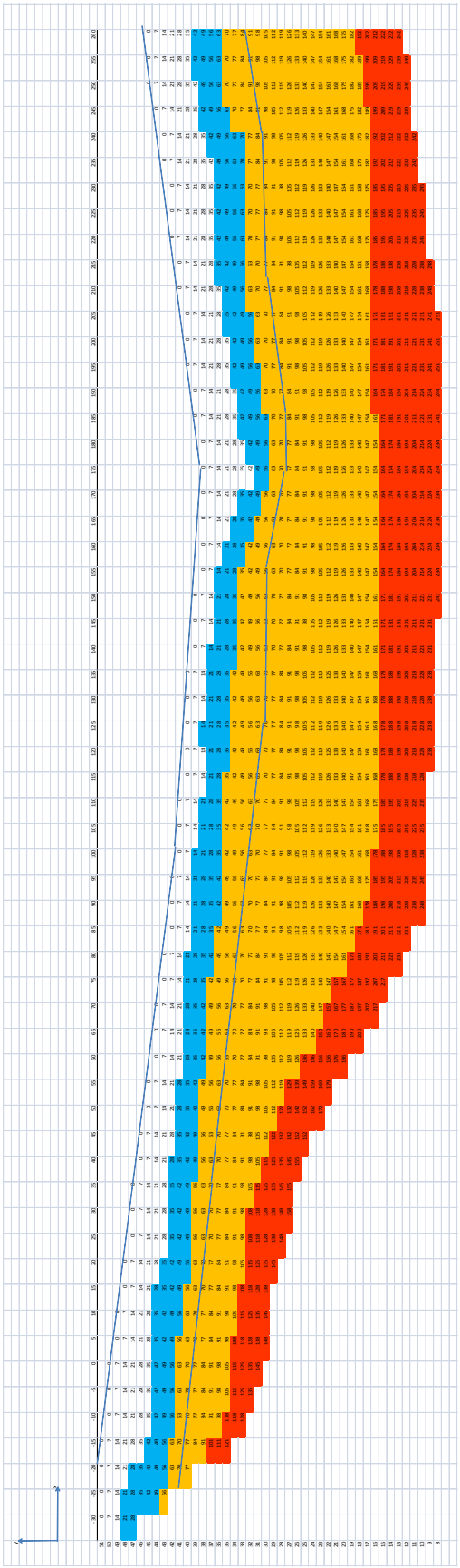

OCR

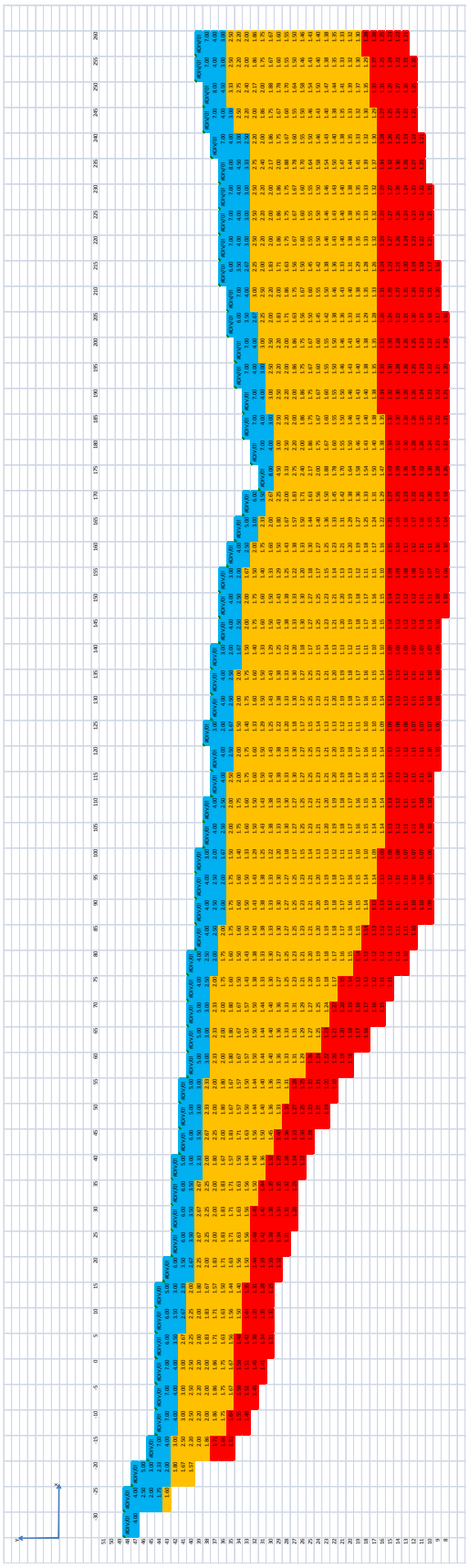

K_0

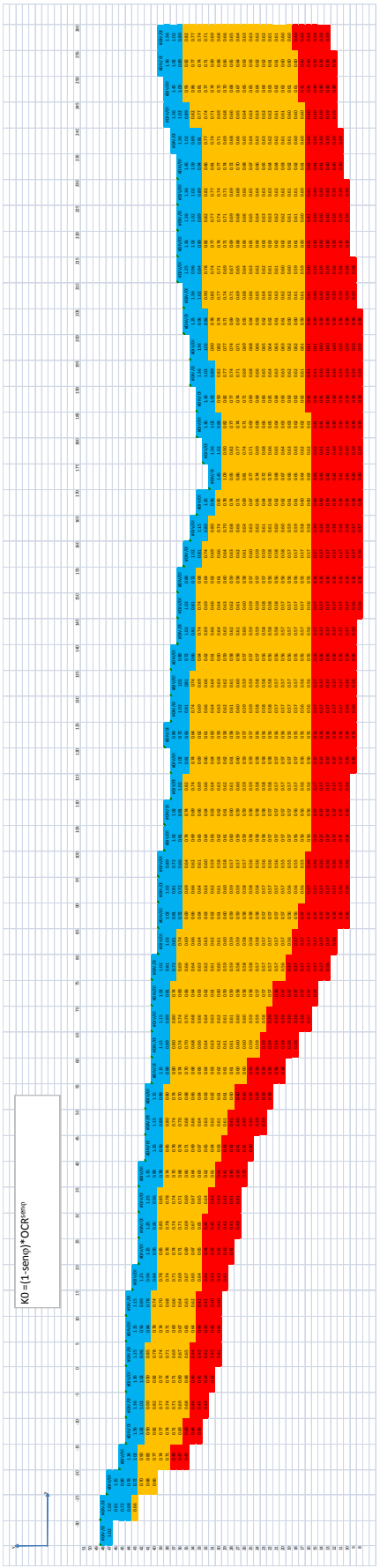

Tau0

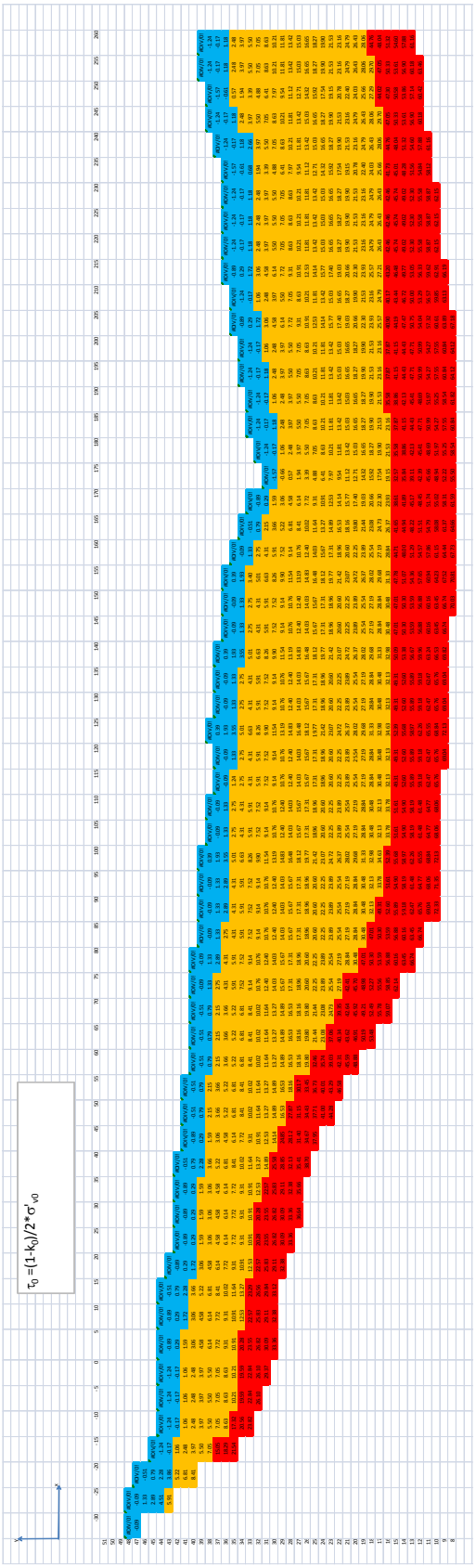

Active coefficient s

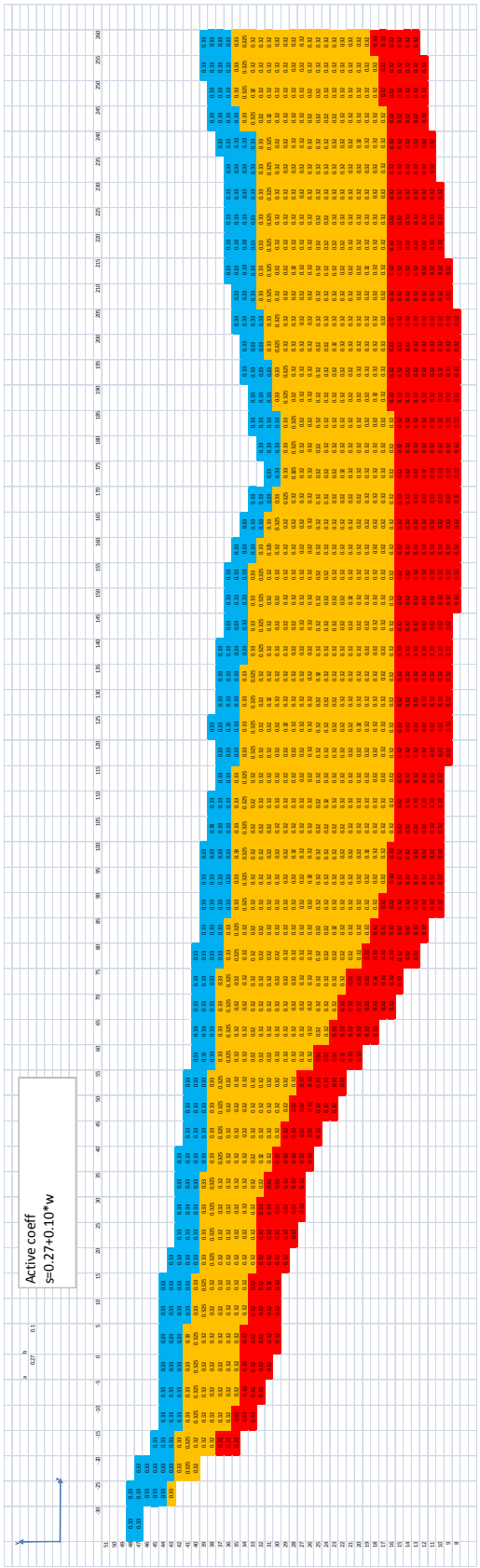

Active coefficient m

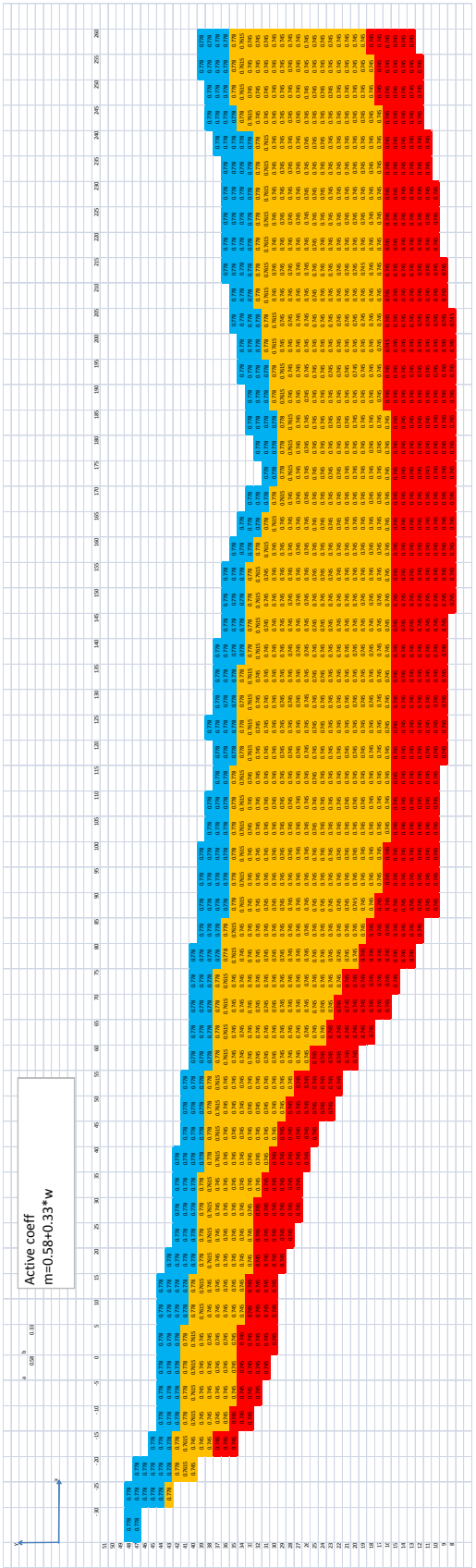

Passive coefficient s

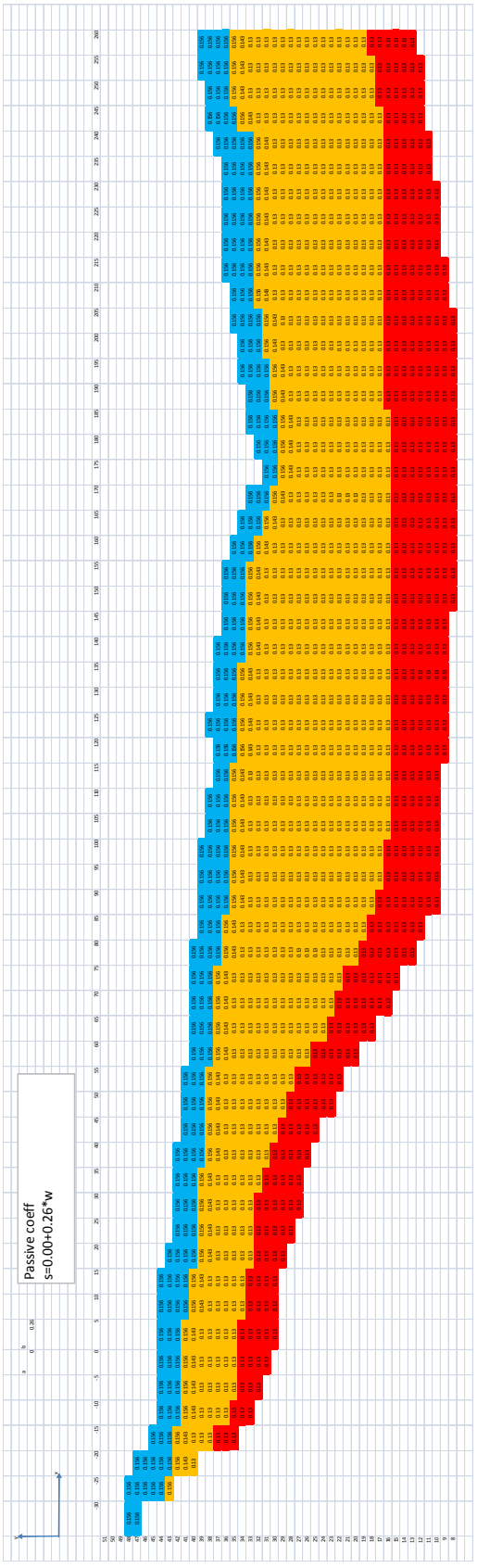

Passive coefficient m

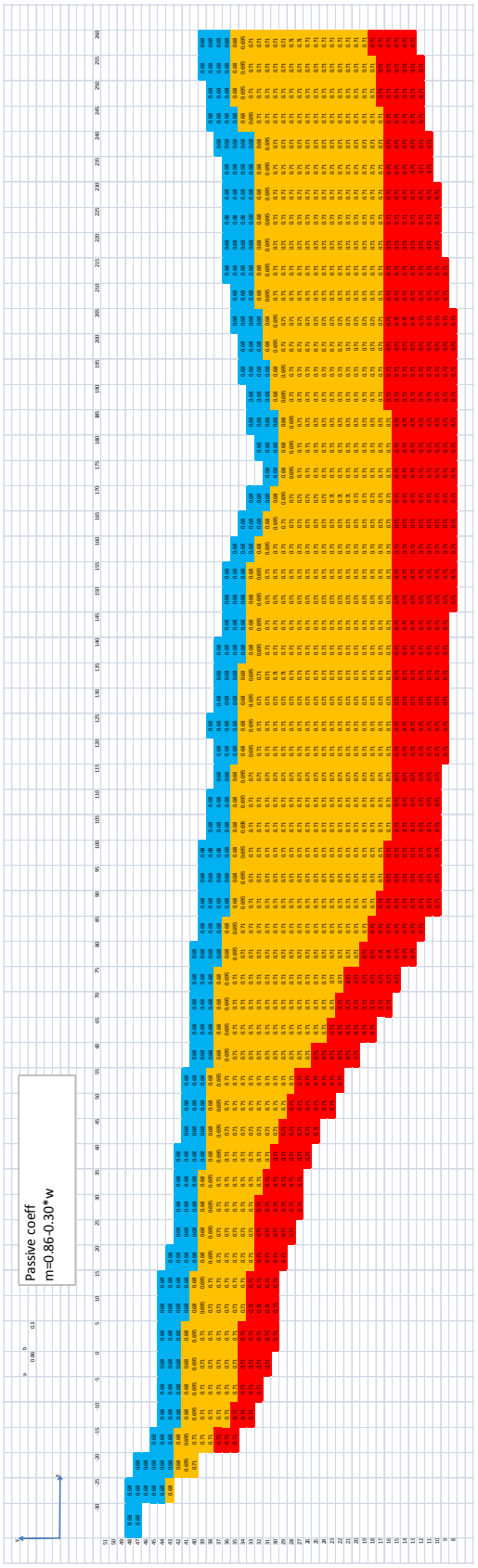

DSS coefficient s

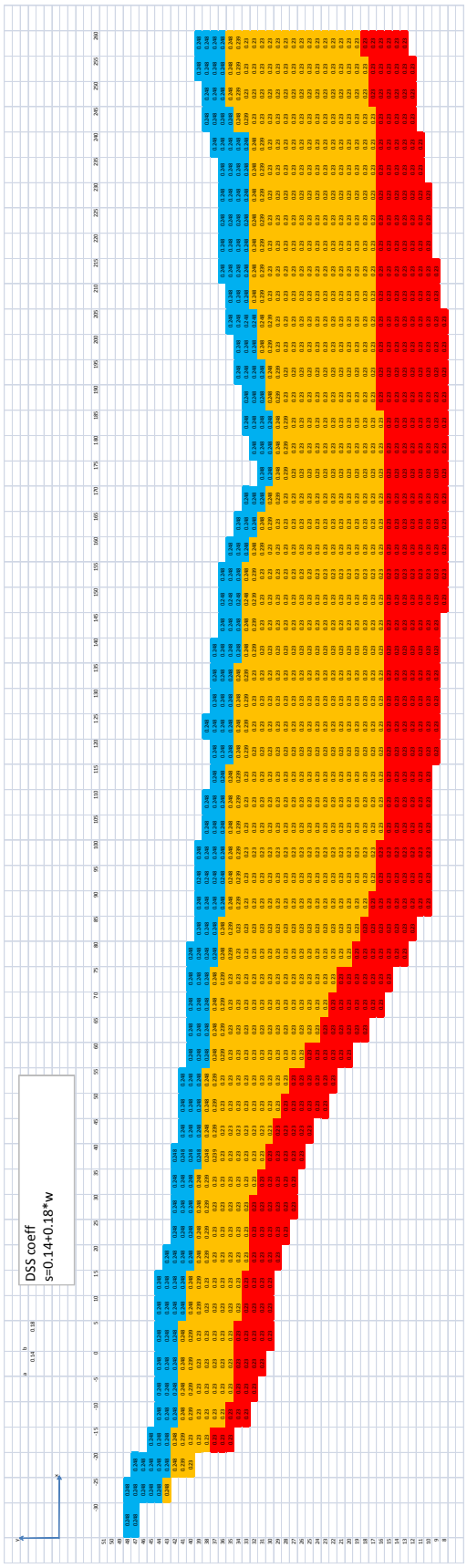

DSS coefficient m

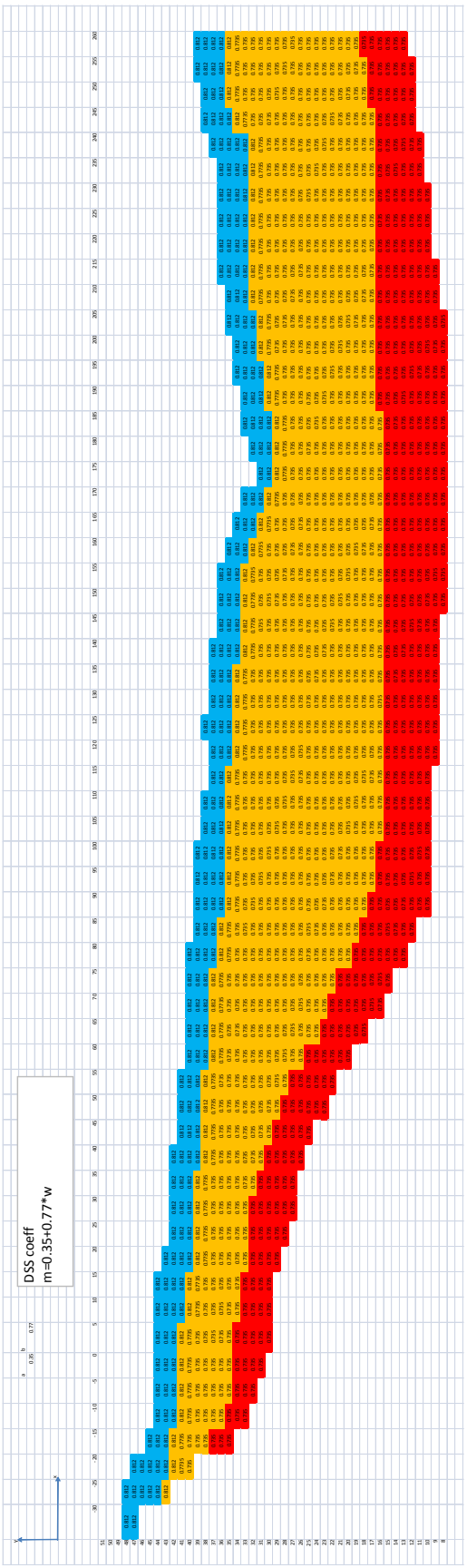

Active undrained shear strength

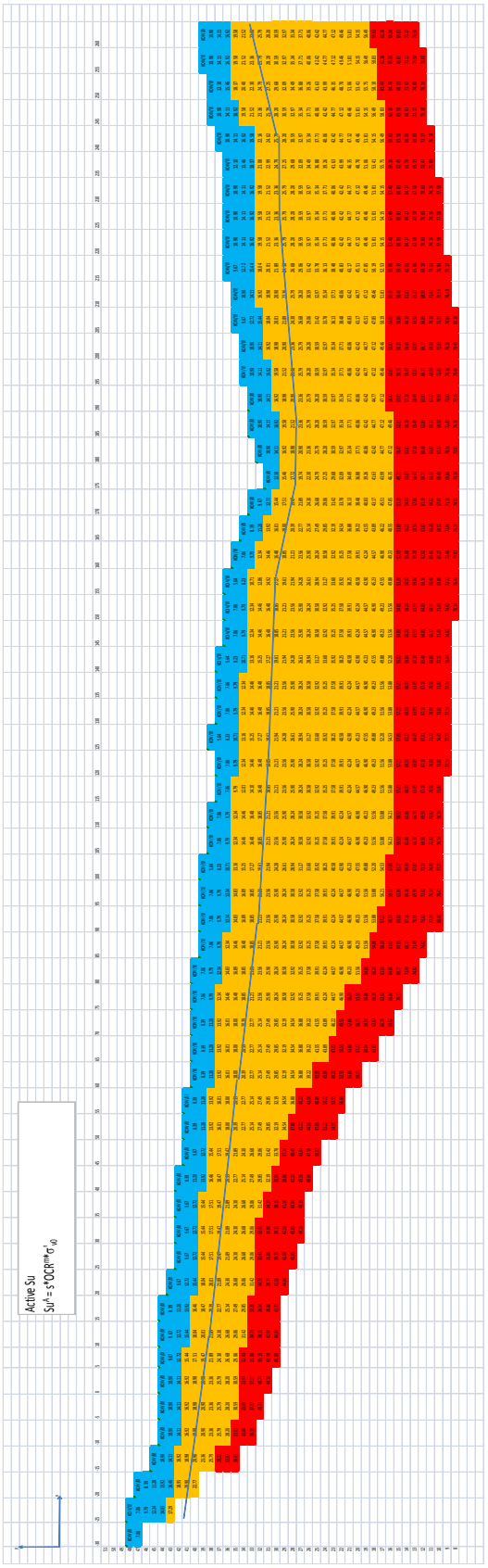

Passive undrained shear strength

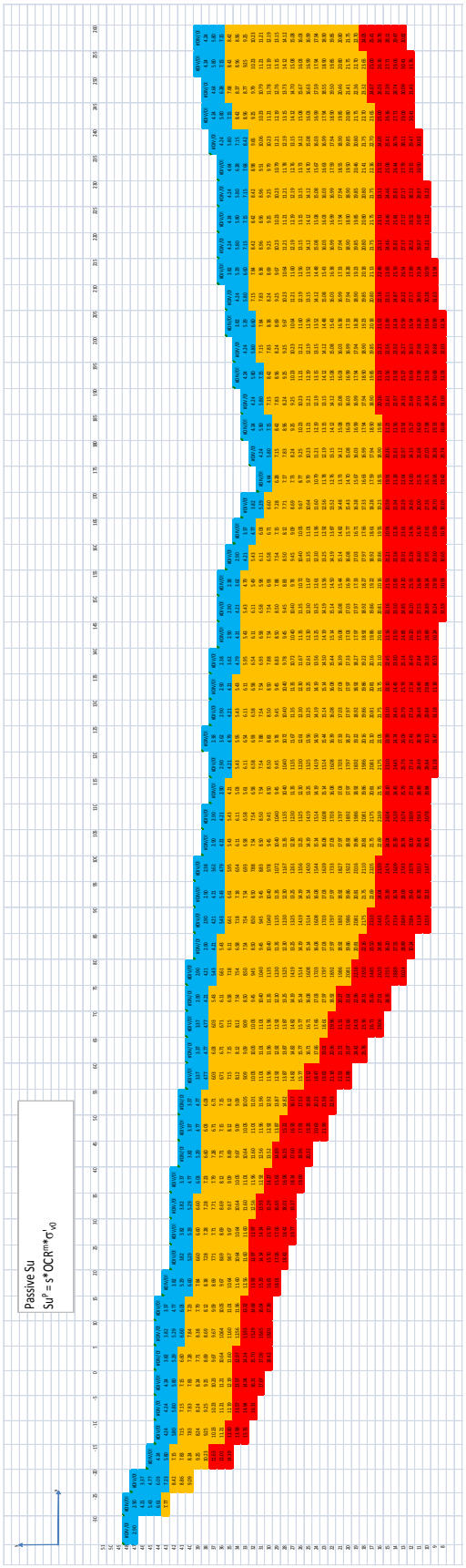

Direct shear strength

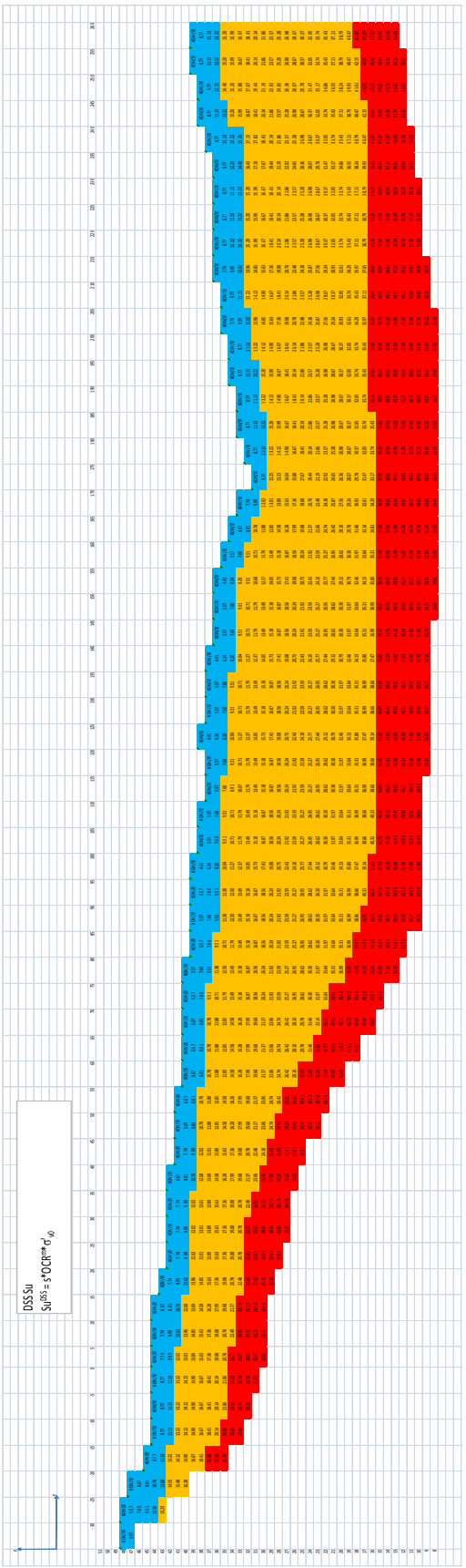

Passive Su / Active Su

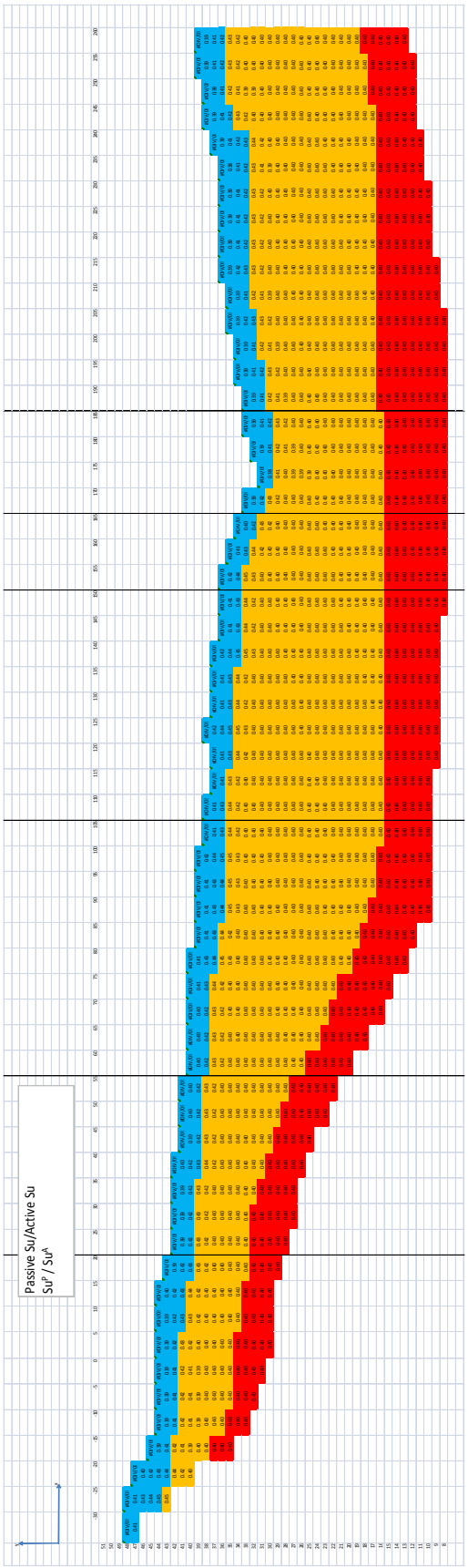

DSS Su / Active Su

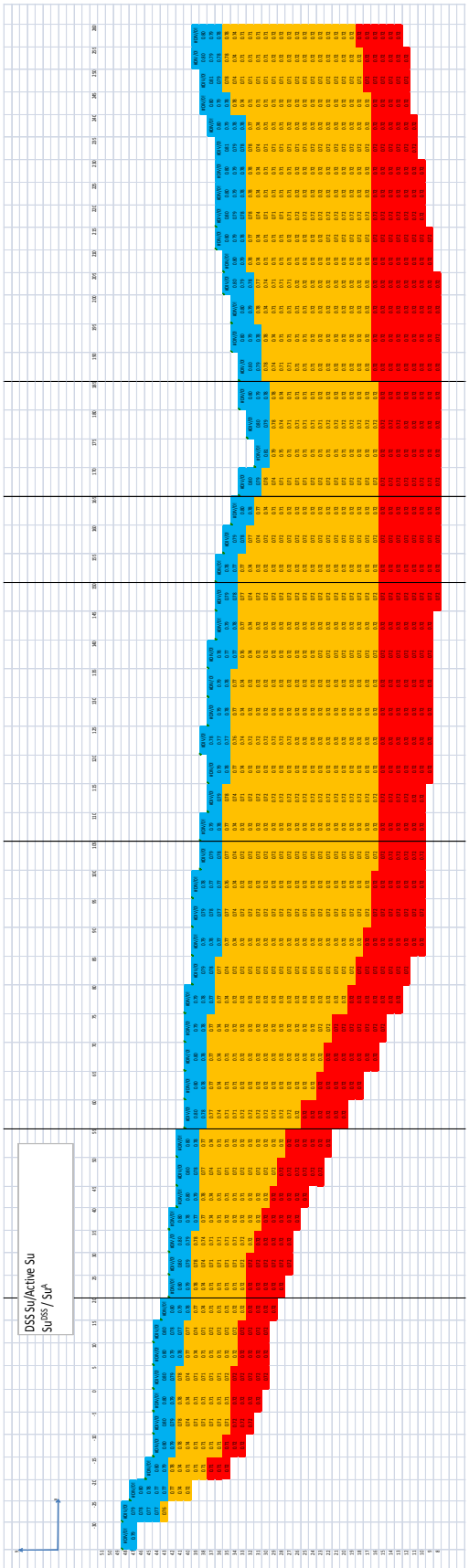

Tau0 / Active Su

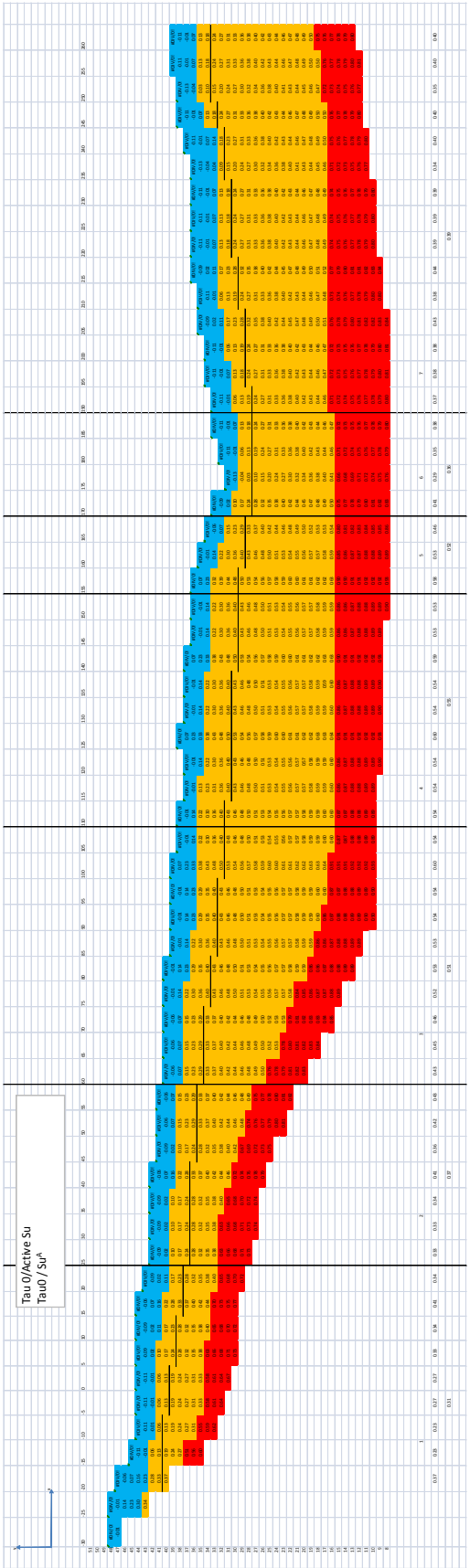

Su^A inclination

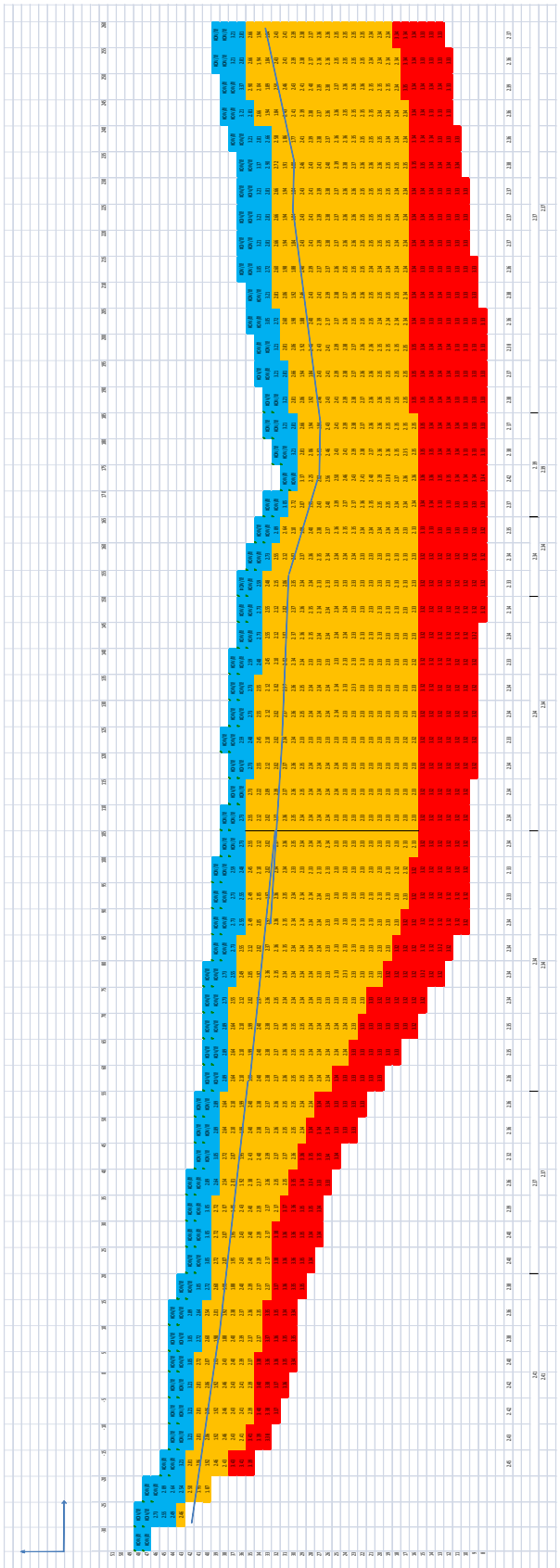

Su Active design

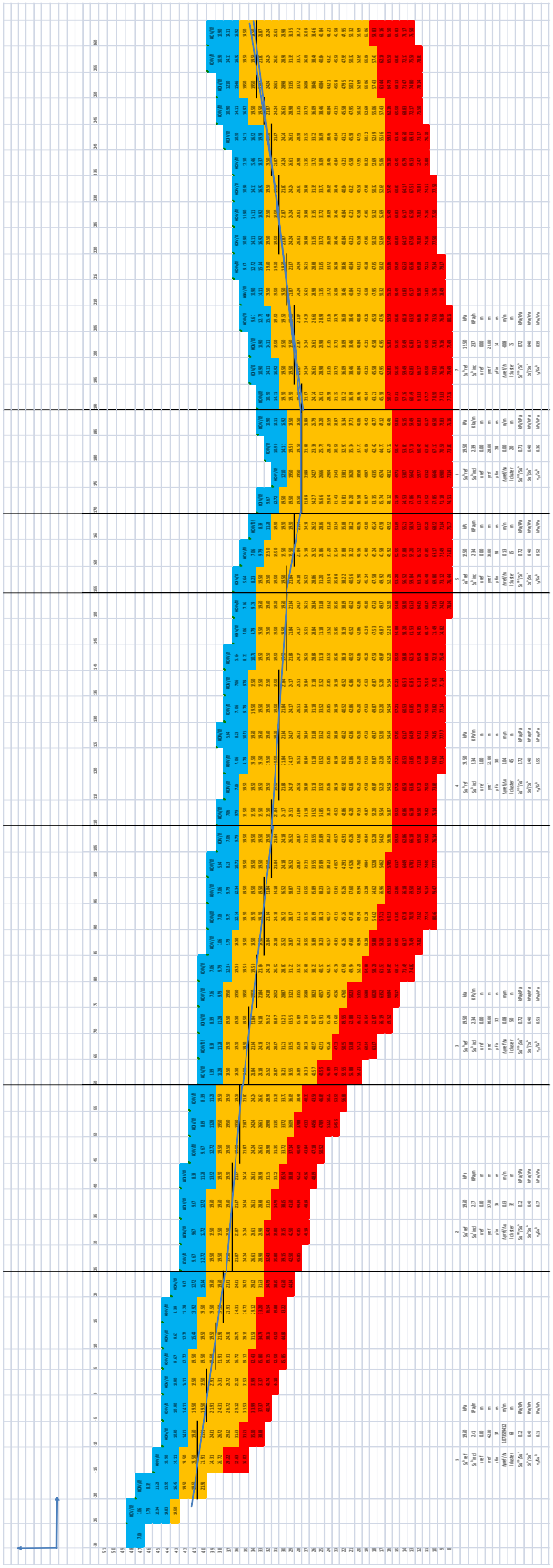

Kontroll- og referanseside/ *Review and reference page*

NGI

Dokumentinformasjon/*Document information*		
Dokumenttittel/*Document title* Effekt av progressiv bruddutvikling for utbygging i områder med kvikkleire. A2 Tilbakeregning av skred		**Dokumentnr./*Document No.*** 20092128-00-5-R
Dokumenttype/*Type of document* Rapport/Report	**Distribusjon/*Distribution*** Begrenset/Limited	**Dato/*Date*** 12. mai 2014 **Rev.nr.&dato/*Rev.No.&date*** 0
Oppdragsgiver/*Client* Statens Vegvesen Vegdirektoratet, Norges Vassdrags og Energidirektorat		
Emneord/*Keywords* Sensitiv leire, kvikkleire, softening, FEM, skred, progressivt brudd		

Stedfesting/*Geographical information*	
Land, fylke/*Country, County*	**Havområde/*Offshore area***
Kommune/*Municipality*	**Feltnavn/*Field name***
Sted/*Location*	**Sted/*Location***
Kartblad/*Map*	**Felt, blokknr./*Field, Block No.***
UTM-koordinater/*UTM-coordinates*	

Dokumentkontroll/*Document control*

Kvalitetssikring i henhold til/*Quality assurance according to* NS-EN ISO9001

Rev./ *Rev.*	**Revisjonsgrunnlag/*Reason for revision***	**Egen-kontroll/ *Self review* av/*by:***		**Sidemanns-kontroll/ *Colleague review* av/*by:***		**Uavhengig kontroll/ *Independent review* av/*by:***		**Tverrfaglig kontroll/ *Inter-disciplinary review* av/*by:***	
0	Originaldokument	PFo	PFo	HPJ	HPJ				

Dokument godkjent for utsendelse/ *Document approved for release*	**Dato/*Date***	**Sign. Prosjektleder/*Project Manager***
	12. mai 2014	Hans Petter Jostad

NGI (Norges Geotekniske Institutt) er et internasjonalt ledende senter for forskning og rådgivning innen geofagene. Vi utvikler optimale løsninger for samfunnet, og tilbyr ekspertise om jord, berg og snø og deres påvirkning på miljøet, konstruksjoner og anlegg.

Vi arbeider i følgende markeder: olje,gass og energi, bygg, anlegg og samferdsel, naturskade og miljøteknologi. NGI er en privat stiftelse med kontor og laboratorier i Oslo, avdelingskontor i Trondheim og datterselskap i Houston, Texas, USA.

NGI ble utnevnt til "Senter for fremragende forskning" (SFF) i 2002.

www.ngi.no

NGI (Norwegian Geotechnical Institute) is a leading international centre for research and consulting in the geosciences. NGI develops optimum solutions for society, and offers expertise on the behaviour of soil, rock and snow and their interaction with the natural and built environment.

NGI works within the oil, gas and energy, building and construction, transportation, natural hazards and environment sectors. NGI is a private foundation with office and laboratory in Oslo, branch office in Trondheim and daughter company in Houston, Texas, USA.

NGI was awarded Centre of Excellence status in 2002.

www.ngi.no

Hovedkontor/Main office:
PO Box 3930 Ullevål Stadion
NO-0806 Oslo
Norway

Besøksadresse/Street address:
Sognsveien 72, NO-0855 Oslo

Avd Trondheim/Trondheim office:
PO Box 1230 Pirsenteret
NO-7462 Trondheim
Norway

Besøksadresse/Street address:
Pirsenteret, Havnegata 9, NO-7010 Trondheim

T: (+47) 22 02 30 00
F: (+47) 22 23 04 48

ngi@ngi.no
www.ngi.no

Kontonr 5096 05 01281/IBAN NO26 5096 0501 281
Org. nr/Company No.: 958 254 318 MVA

BSI EN ISO 9001
Sertifisert av/Certified by BSI, Reg. No. FS 32989

Denne serien utgis av Norges vassdrags- og energidirektorat (NVE)

Utgitt i Rapportserien i 2014

Nr. 1 Analyse av energibruk i forretningsbygg. Formålsdeling. Trender og drivere

Nr. 2 Det høyspente distribusjonsnettet. Innsamling av geografiske og tekniske komponentdata

Nr. 3 Naturfareprosjektet Dp. 5 Flom og vann på avveie. Dimensjonerende korttidsnedbør for Telemark, Sørlandet og Vestlandet: Eirik Førland, Jostein Mamen, Karianne Ødemark,Hanne Heiberg, Steinar Myrabø

Nr. 4 Naturfareprosjektet: Delprosjekt 7. Skred og flomsikring. Sikringstiltak mot skred og flom Befaring i Troms og Finnmark høst 2013

Nr. 5 Kontrollstasjon: NVEs gjennomgang av elsertifikatordningen

Nr. 6 New version (v.1.1.1) of the seNorge snow model and snow maps for Norway. Tuomo Saloranta

Nr. 7 EBO Evaluering av modeller for klimajustering av energibruk

Nr. 8 Erfaringer fra ekstremværet Hilde, november 2013

Nr. 9 Erfaringer fra ekstremværet Ivar, desember 2013

Nr. 10 Kvartalsrapport for kraftmarknaden. 4. kvartal 2013. Ellen Skaansar (red.)

Nr. 11 Energibruksrapporten 2013

Nr. 12 Fjernvarmens rolle i energisystemet

Nr. 13 Naturfareprosjektet Dp. 5 Flom og vann på avveie. Karakterisering av flomregimer. Delprosjekt. 5.1.5

Nr. 14 Naturfareprosjektet Dp. 6 Kvikkleire. En omforent anbefaling for bruk av anisotropifaktorer i prosjektering i norske leirer

Nr. 15 Tilleggsrapport: Oppsummering av Energimyndighetens og NVEs gjennomgang av elsertifikatordningen

Nr. 16 Flomberegning for Nesttunvassdraget (056.3Z). Thomas Væringstad

Nr. 17 Årsrapport for tilsyn

Nr. 18 Verktøyprosjektet - hydrologi 2010-2013. En oppsummering av aktiviteter og resultater. Erik Holmqvist (red.)

Nr. 19 Flom og jordskred i Nordland og Trøndelag desember 2013. Elin Langsholt, Erik Holmqvist, Delia Welle Kejo

Nr. 20 Vindkraft i produksjon i 2013

Nr. 21 FoU-prosjekt 81072 Pilotstudie: Snøskredfarekartlegging med ATES (Avalanche Terrain Exposure Scale) Klassifisering av snøskredterreng for trygg ferdsel

Nr. 22 Naturfareprosjektet: Delprosjekt 3.1. Hvordan beregne ekstremverdier for gitte gjentaksintervaller? Manual for å beregne returverdier av nedbør for ulike gjentaksintervaller (for ikke-statistikker)

Nr. 23 Flomsonekart Delprosjekt Tuv. Kjartan Orvedal, Julio Pereira

Nr. 24 Summary of the review of the electricity certificates system by the Swedish Energy Agency and the Norwegian Water Resources and Energy Directorate (NVE)

Nr. 25 Landsomfattende mark- og grunnvannsnett. Drift og formidling 2011. Jonatan Haga Per Alve Glad

Nr. 26 Naturfareprosjektet: Delprosjekt 1 Naturskadestrategi. Sammenligning av risikoakseptkriterier for skred og flom. Utredning for Naturfareprogrammet (NIFS)

Nr. 27 Naturfareprosjektet Dp. 6 Kvikkleire. Skredfarekartlegging i strandsonen

Nr. 28 Naturfareprosjektet Dp. 5 Flom og vann på avveie. "Kvistdammer" i Slovakia. Små terskler laget av stedegent materiale, erfaringer fra studietur for mulig bruk i Norge

Nr. 29 Reestablishing vegetation on interventions along rivers. A compilation of methods and experiences from the Tana River valley

Nr. 30 Naturfareprosjektet Dp. 5 Flom og vann på avveie. Karakterisering av flomregimer

Nr. 31 Småkraftverk: Tetthet og reproduksjon av ørret på utbygde strekninger med krav om minstevannføring Svein Jakob Saltveit og Henning Pavels

Nr. 32 Kanalforvaltningen rundt 1814 – del av en fungerende statsadministrasjon for det norske selvstendighetsprosjektet. Grunnlovsjubileet 2014

Nr. 33 Museumsordningen 10 år

Nr. 34 Naturfareprosjektet Dp. 6 Kvikkleire. Skredfarekartlegging i strandsonen -videreføring

Nr. 35 Naturfareprosjektet Dp. 5 Flom og vann på avveie. Karakterisering av flomregimer Delprosjekt. 5.1.5. Revisjon av rapport 13-2014

Nr. 36 Kvartalsrapport for kraftmarknaden 1. kvartal 2014. Gudmund Bartnes (red.)

Nr. 37 Preliminary regionalization and susceptibility analysis for landslide early warning purposes in Norway

Nr. 38 Driften av kraftsystemet 2013

Nr. 39 Naturfareprosjektet Dp. 6 Kvikkleire. Effekt av progressivbruddutvikling for utbygging i områder med kvikkleire: Sensitivitetsanalyse basert på data fra grunnundersøkelser på vegstrekningen Sund-Bradden i Rissa

Nr. 40 Naturfareprosjektet DP. 6 Kvikkleire. Effekt av progressiv bruddutvikling for utbygging i områder med kvikkleire: Sensitivitetsanalyse-1

Nr. 41 Bioenergi i Norge

Nr. 42 Naturfareprosjektet Dp. 5 Flom og vann på avveie. Dimensjonerende korttidsnedbør for Møre og Romsdal, Trøndelag og Nord-Norge. Delprosjekt. 5.1.3

Nr. 43 Terskelstudier for utløsning av jordskred i Norge. Oppsummering av hydrometeorologiske terskelstudier ved NVE i perioden 2009 til 2013. Søren Boje, Hervé Colleuille og Graziella Devoli

Nr. 44 Regional varsling av jordskredfare: Analyse av historiske jordskred, flomskred og sørpeskred i Gudbrandsdalen og Ottadalen. Nils Arne K. Walberg, Graziella Devoli

Nr. 45 Flomsonekart. Delprosjekt Hemsedal, Martin Jespersen, Rengifo Ortega

Nr. 46 Naturfareprosjektet Dp. 6 Kvikkleire. Mulighetsstudie om utvikling av en nasjonal blokkprøvedatabase

Nr. 47 Naturfareprosjektet Dp. 6 Kvikkleire. Detektering av sprøbruddmateriale ved hjelp av R-CPTU

Nr. 48 En norsk-svensk elsertifikatmarknad. Årsrapport 2013

Nr. 49 Øvelse Østlandet 2013. Evalueringsrapport

Nr. 50 Et norsk-svensk elsertifikatmarked. Årsrapport 2013

Nr. 51 Forslag til nytt vektsystem i modellen for å fastsette kostnadsnormer i regionalnettene

Nr. 52 Jord- og sørpeskred i Sør-Norge mai 2013. Monica Sund

Nr. 53 Årsrapport for utførte sikrings- og miljøtiltak for 2013

Nr. 54 Naturfareprosjekt DP. 1 Naturskadestrategi Samarbeid og koordinering vedrørende naturfare. En ministudie av Fellesprosjektet E6-Dovrebanen og Follobanen

Nr. 55 Naturfareprosjektet DP.6 Kvikkleire. Effekt av progressiv bruddutvikling for utbygging i områder med kvikkleire: Numerisk metode for beregning av udrenert brudd i sensitive materialer

Nr. 56 Naturfareprosjektet DP.6 Kvikkleire. Effekt av progressiv bruddutvikling for utbygging i områder med kvikkleire: Tilbakeregning av Vestfossenskredet

Norges
vassdrags- og
energidirektorat

Norges vassdrags- og energidirektorat

Middelthunsgate 29
Postboks 5091 Majorstuen
0301 Oslo

Telefon: 09575
Internett: www.nve.no